UNIVERSITY OF TASMANIA

DEPARTMENT OF CHEMISTRY

ACTIVE SITES AND MORPHOLOGY OF MgO AND Li-DOPED MgO IN OXIDATIVE COUPLING OF METHANE

Supanee Pechsombut

A thesis submitted in fulfilment of the requirement for the degree of

DOCTOR OF PHILOSOPHY

January 1995

(Supanee Pechsombut)

DECLARATION

To the best of my knowledge this thesis contains no material which has been accepted for the award of any other degree or diploma in any university, and contains no material previously published or written by another person except where due reference is made.

Supanee Pechsombut

Department of Chemistry

University of Tasmania

January 1995

ACKNOWLEDGMENTS

I would firstly offer my sincere thanks to Dr. Barry O' Grady for his supervision and enthusiasm for every aspect of the work. His advice was always worthwhile and without him this work would not have been possible.

I cannot fail to thank my co-supervisor, Professor Frank P. Larkins. Professor Larkins provided me with many ideas when I encountered difficulties with the research. Further thanks also go to Professor Larkins for his efforts in proof reading this thesis.

Many thanks are also extended to Dr. Trevor Brown for his help in kinetic parameters determination and to Dr. Ashley Townsend for his assistance on proof reading, especially English.

For their friendship and encouragement for years I offer my thanks to Chatchawan Chayabutra, Scott Stark, Colin Hurley, Robert Fraser, Alison Featherstone.

Special thanks also go to the technical and professional staff, John Davis, Peter Dove, Michael Brandon and Marshall Hughes for their help with the experimental equipment.

I would also like to express my thanks to Professor David L. Trimm for the access to use many facilities at The Centre for Particle & Catalyst Technologies. Thanks are also extended to John Starling for his friendship and help in using the instruments at the Centre.

This work would not have been possible without financial support from IDP Scholarship.

Last but certainly not least I would express my deepest gratitude to my parents for their continual support and encouragement over the last four years.

Abstract

The relationship between morphology and catalytic performance in the oxidative coupling of methane over MgO and Li-doped MgO catalysts has been studied, and the active sites for methane coupling on the catalyst surface have been identified.

MgO catalysts of various morphologies were obtained from different Mg precursors using a variety of preparation methods. For Li-doped MgO catalysts, preparation techniques used included coprecipitation, hydrolysis, physical mixing and wet impregnation followed by calcination. All MgO and Li-doped MgO catalysts were characterised prior to the catalytic screening. Atomic absorption spectroscopy was used to determine the Li loading on Li/MgO catalysts. The morphologies of the catalysts, including surface area, particle profile/particle size distribution and pore structures were examined.

Temperature programmed desorption (TPD) of phenol on MgO was studied using several detection techniques including thermal conductivity, infrared spectroscopy and thermo-gravimetric analysis to explore the surface sites of the catalysts. A simple thermo-gravimetric technique was then developed and found to be effective in determination of the surface sites on MgO surfaces. The different surface sites of different basic strength can be distinguished via the desorption profiles obtained as phenol is desorbed with the increasing temperature. Two major surface sites were observed on MgO. They could be attributed to flat surface sites exposure {100} and surface sites of low coordination number (edges and corners).

For Li/MgO catalysts the TPD of phenol was also employed to examine the nature of the surface sites. The amount of phenol adsorbed was small due to the low surface area of the catalysts; however, a significant distinction between sites was still able to be observed. It was noted that apart from the desorption

temperature ranges attributed to the flat surfaces and to the surface sites of low coordination of MgO matrix, another desorption range at higher temperatures was also observed. This indicated the presence of a new site of higher basic strength, generated by the addition of Li to MgO. At low Li loadings ~ 0.1-0.2 % (wt % after calcination), this new site was observed at a very high concentration on the surface. As the Li loading was increased this new site was initially replaced by the surface sites of low coordination number. However, with further increased in the Li loading to greater than ~ 4.0-5.0 %, the number of low coordination sites also diminished.

Catalytic activities of all MgO and Li/MgO catalysts were determined using a conventional flow reactor operating at atmospheric pressure. The products were analysed at various times-on-stream during the reaction. Any change in the nature of the surface sites was investigated for most catalysts after catalytic testing. The correlation between sites and the catalytic activities of all catalysts was then conducted. It was likely that the methane activation and selectivity to C_2-hydrocarbon products arose from the high density of surface sites of low coordination.

It was found that catalyst morphology, catalyst surface sites of low coordination and catalytic performance for the oxidative coupling of methane are closely inter-related. The active surface sites of low coordination were presumed to originate from defects in the MgO crystal structure that result from the preparation methods and precursors used, along with the influence of the addition of Li. The presence of defects could be related to the physical characteristics of the catalysts such as surface area, particle size distribution profiles and pore structure.

TABLE OF CONTENTS

2.5 Results and discussion

CHAPTER 1

INTRODUCTION

1.1 Methane Utilization

Methane is the major component of natural gas. Gas reserves have been estimated to be as large as 10^{14} cubic metres (Mimoun, 1987) or three times larger than those of oil. It is anticipated that this hydrocarbon resource will last for around sixty years at current rates of consumption (Petroleum Gazette, 1988), while existing oil deposits will be irreversibly depleted in the near future. Natural gas reserves are typically found in remote areas and for economic reasons it is less desirable to transport natural gas to potential markets. A preferred option could be to manufacture liquid transportation fuels at the gas source. It is the use of methane as a feedstock for liquid fuel production coupled with the use of methane to manufacture ethylene that has promoted great interest in methane conversion using catalysts.

Two conversion processes that are only marginally economic have been developed to date. The first major advance in commercial liquid fuel production from methane, since the Fisher-Tropsch process was developed, was achieved by the Mobil Corporation and is called the Methanol-To-Gasoline (MTG) process using the ZSM-5 catalyst (Amenomiya et al., 1990). The process requires steam reforming of methane to produce synthesis gas (H_2 + CO), which is converted to methanol and then gasoline. The second established methane conversion route is the Shell Middle Distillate Synthesis (SMDS) process (Wechem, 1993). Desulphurized natural gas is converted into synthesis gas which is then converted into pure, long-chain paraffins. These long chain paraffins are then converted into very high quality gas-oil, kerosene and some naphtha via selective hydrocracking. However, both the MTG and SMDS processes are less than ideal from an economic viewpoint because the majority of the

costs are associated with synthesis gas generation (Amenomiya et al., 1990). Direct methane conversion to higher hydrocarbons seems to be an attractive way to overcome this economic problem.

1.2 Oxidative Coupling Approach

Since Keller and Bhasin (1982) published their work on the direct oxidative coupling of methane to produce ethylene, interest in this route has increased due to the possible further conversion of ethylene to either gasoline, distillates or other chemicals without any intermediate separation. In 1985 Lunsford and co-workers (Driscoll et al., 1985; Ito and Lunsford, 1985) demonstrated that lithium-doped magnesium oxide was an active and selective catalyst for the oxidative coupling reaction. Much research effort since then has been focused on the identification of suitable catalytic materials, as well as in gaining further understanding about the reaction mechanism.

Difficulties arise in the conversion of methane mainly due to its high thermodynamic stability. The dissociation energy of the first C-H bond is about 435 kJ/mol (Kerr, 1966); hence the dehydrogenation and coupling of methane has a large positive free energy change of 71 kJ/mol at 1000 K, equation [1.1] (Amenomiya et al., 1990). In order to effect practical conversions, temperatures higher than 800°C have to be employed. However, the thermodynamic disadvantage can be overcome by introducing an oxidant such as oxygen (see equation [1.2]).

$$2CH_4 \leftrightarrow C_2H_6 + H_2 \qquad \Delta G^\circ = 71 \text{ kJ/mol at } 1000 \text{ K} \quad [1.1]$$

$$2CH_4 + 1/2\, O_2 \leftrightarrow C_2H_6 + H_2O \qquad \Delta G^\circ = -122 \text{ kJ/mol at } 1000 \text{ K} \quad [1.2]$$

In theory the oxidative condensation reaction can progress further in the reactor to produce higher hydrocarbons. However, practically, the products are almost always limited to C_2-hydrocarbon compounds, as indicated by Amenomiya et

al. (1990). It should be noted that the complete oxidation of methane and hydrocarbon products to carbon dioxide and water, which is the thermodynamically favoured process, can also take place in the presence of oxygen. The selectivity to hydrocarbons is therefore an important issue in the successful development of the oxidative coupling of methane. The notion that a better selectivity control can be achieved by the use of a catalyst led several research groups to screen a number of catalysts as possible candidates.

1.3 Lithium-doped Magnesium Oxide Catalysts

A large number of compounds have been screened as suitable catalytic materials for the oxidative coupling of methane and virtually all oxides display some catalytic activity for this reaction. However, a combination of lithium and magnesium oxide is one of the most frequently used catalysts since it was first reported to be an effective catalyst for methane coupling by Lunsford and co-workers (Driscoll et al., 1985). Pure MgO is known as a very active catalyst for certain base-catalyzed reactions if properly activated (Tanabe et al., 1989). MgO has also been found to be active for the oxidative coupling of methane (Keller and Bhasin, 1982). Doping with lithium, however, improves the catalytic performance, in particular the selectivity. Although other alkali metals doped on MgO have been found to be highly effective catalysts, they are less selective than Li-based systems (Yingli et al., 1988; Iwamatsu et al., 1987).

Driscoll et al. (1985) have noted that the doped system designated Li/MgO is in fact not simply Li deposited on MgO. Since the radii of both cations are very close (0.68 Å for Li^+ and 0.66 Å for Mg^{2+}) the replacement of the alkaline earth metal by alkali metal can take place. Such substitution by monovalent ion for divalent ion in the oxide lattice to form a true mixed oxide requires that an equivalent number of O^- radical ions be formed to maintain electrical neutrality. Driscoll found a good correlation between the rate of methyl radical formation and the concentration of

[Li^+O^-] centres as the lithium content was varied. In addition, the fact that Na-doped MgO was less effective in generating active sites than Li-doped MgO also suggests the importance of substitutional defect sites. The radius of Na^+ is 0.97 Å, hence sodium is less effective in producing stable [Na^+O^-] centres in MgO. An analogy to the Li/MgO system is the Na-doped CaO system, which also acts as an effective catalyst (McCarty et al., 1988; Carreiro and Baerns, 1987). Both Na^+ and Ca^{2+} have similar radii of 0.97 and 0.99 Å respectively.

Although a number of studies have considered [Li^+O^-] to be the active sites of Li/MgO in generating the methyl radicals for the oxidative coupling of methane, the arguments about the nature of the active sites still persist (Mirodatos et al., 1987; Anpo et al., 1988; Wu et al., 1993). Hargreaves and co-workers (Hargreaves et al, 1990, 1991, 1992) have published a series of papers indicating the relationship between catalyst morphology and catalyst activity in the methane coupling reaction. More details about the active sites of Li/MgO catalysts will be presented in Chapter 5. In this study the active sites of Li/MgO catalysts will be studied using alternative approaches.

1.4 Project Objectives

The overall aim of the project was to make a systematic study of the behaviour of MgO as a catalyst from its preparation through to the catalytic reaction. The objectives and scope of the present work are as follows.

- To prepare and characterize MgO of different morphologies.
- To develop a reliable method for studying the active sites and basicity of MgO catalysts.

- To investigate the fundamental factors which influence the catalytic conversion of methane to higher hydrocarbons, especially C_2, via the oxidative coupling route, e.g. surface morphology and basicity of catalyst.
- To investigate the effect of dopant (Li), on the morphology and catalytic activity of magnesium oxide catalysts.

References

Amenomiya, Y., Birss, V.I., Goledzinowski, M., Galuszka, J., and Sanger, A.R. (1990), Catal. Rev. Sci. Eng., **32** (3) 163.

Anpo, M., Sunamoto, M., Doi, T., and Matsuura, I. (1988), Chem. Lett., 701.

Carreiro, J. A. S. P. and Baerns, M. (1987), React. Kin. Catal. Lett., **35**, 349.

Driscoll, D.J., Wilson, M., Wang, J-X, and Lunsford, J.H. (1985), J. Am. Chem. Soc., **107**, 58.

Hargreaves, J. S. J., Hutchings, G. J., and Joyner, R. W., Nature (London) **348**, 428 (1990).

Hargreaves, J. S. J., Hutchings, G. J., and Joyner, R. W., Stud. Surf. Sci. Catal., **61**, 155 (1991).

Hargreaves, J. S. J., Hutchings, G. J., Joyner, and Kiely, C. J., J. Catal., **135**, 576 (1992).

Ito, T. and Lunsford (1985), J.H., Nature, **314**, 721.

Iwamatsu, E., Moriyama, T., Takasaki, N., and Aika, K. (1987), J. Chem. Soc. Chem. Comm., 19.

Keller, G.E. and Bhasin (1982), M.M., J .Catal., **73**, 9.

Kerr, J.A. (1966), Chem. Rev., **66**, 465.

McCarty, J. G., Quinlan, M. A., and Sancier, K. M. (1988), ACS. Div. Fuel Chem. Preps., **33** (3), 363.

Mimoun, H. (1987), New J. Chem., **11**, 513.

Mirodatos, C., Perrichon, V., Durupty, H.C., and Moral, P. (1987), Stud. Surf. Sci. Catal., **34**, 183.

Petroleum Gazette (1988), Aust. Inst. of Petrol., **25** (8), p 17.

Tanabe, K., Misono, M., ONo, Y., and Hattori H. (1989), New Solid Acids and Bases, Kodansha, Tokyo, p 581.

Van Wechem, H.M.H. (1993), Proc. 3rd Natural Gas Conversion. Sym., pp 43-71.

Wu, M-C., Truong, C. M., and Coulter, K., J. Catal., **140**, 344 (1993).

Yingli, B., Kaiji, Z., Yutao, J., Chiwen, T., and Xiangguong, Y.(1988), Appl. Catal., **39**, 185.

CHAPTER 2

PREPARATION AND CHARACTERISATION OF MgO

2.1 Introduction

It has been reported that MgO is a useful support for many catalytic reactions due to its ability to stabilise added metals and to prevent sintering and volatilisation (Boudart et al., 1975, Tauster et al., 1977; Logan and Datye, 1988). MgO has also been widely used as a catalyst in many reactions, for example, (i) isomerization of alkenes, alkynes and unsaturated compound, (ii) amination and hydrogenation of alkenes and conjugated dienes, (iii) hydrogenation of CO and (iv) decomposition of alcohols, amines, and esters (Hattori, 1985; Tanabe et al, 1989) . However, in many cases the origin of the MgO catalytic performance and support effects are not well understood.

The most common way to prepare MgO catalyst is the dehydration of $Mg(OH)_2$ in the form of brucite. As a result much information about the transformation of hexagonal close-packed brucite into simple cubic MgO has been presented (Gregg and Razouk, 1949, Anderson and Horlock, 1962, Green, 1983). The effect of the temperature of calcination and the duration of heating at fixed temperatures on the activity of magnesium oxide prepared by the dehydration of brucite in the presence of air and under vacuum, was examined by Razouk and Mikhail (1957). Subsequent work investigated the calcination of magnesium carbonate and prepared hydroxide (Razouk and Mikhail, 1959). The results were interpreted as a consequence of the interaction of three rate processes, namely, decomposition, recrystallization and sintering. MgO prepared from precipitated $Mg(OH)_2$ or $MgCO_3$ behaves like that obtained from brucite, in that the maximum surface area is developed

on decomposition at 350°C, whereas the oxide prepared from magnesite at 650°C shows maximum surface area. The surface area then decreases at higher temperatures according to the extent of sintering.

Shastri et al (1985) investigated the influence of pretreatment time, temperature, gas environment (air vs argon/oxygen) and subsequent outgassing procedures on sample morphology and surface uniformity of various MgO surfaces prepared via dehydration of $Mg(OH)_2$. They concluded that impurities in the MgO have a significant influence on sample morphology and the extent of surface uniformity. Strong evidence of the effect of impurities on MgO morphology was presented by Holt et al. (1987). It was shown that the presence of any residual chloride ion from the catalyst precursor hinders the development of high surface areas. The effect of chloride ion on the surface area seems to be a post-dehydration process. More details about the effect of impurities on the thermal decomposition of $Mg(OH)_2$ have been given in a review by Green (1983).

It has been reported that the surface properties (viz surface area and basicity/base strength distribution) of MgO obtained from $Mg(OH)_2$ depend strongly upon the magnesium salt and precipitating agent used for the preparation of magnesium hydroxide (Choudhary and Pandit, 1991). The precipitation conditions (i.e. concentration of magnesium salt, pH, temperature, mode of mixing of the salt solution and precipitating agent), ageing period of precipitated magnesium hydroxide and its calcination temperature have also been found to influence MgO surface properties. Lopez et al. (1991) used the sol-gel method to prepare $Mg(OH)_2$. The method involves the hydrolysis of magnesium alkoxide in the presence of acid or basic catalysts, at a specific pH, followed by polycondensation. The $Mg(OH)_2$ samples were calcined at 300, 600 and 900°C for 72 h. The measured surface areas of the MgO samples were independent of pH.

Sidjabat et al. (1993) have shown that the surface area and porosity of MgO obtained from the calcination of $Mg(OH)_2$ at 400°C for 4 h depends on the pH of $Mg(OH)_2$ precipitation, ageing, washing and calcining. It was concluded that (i) the MgO surface area decreased, pore diameter decreased and pore volume first decreased and then increased as pH increased; (ii) as ageing time increased, the crystallinity of the deposit increased as did the particle size and the pore volume. However, the main pore radius remained unchanged; (iii) the calcining time had little effect, but the calcining temperature had a significant effect on the surface area and porosity of MgO samples; and (iv) washing the $Mg(OH)_2$ precipitate with organic solvents, such as methanol and acetone reduced the surface area but increased the pore volume of MgO (Sidjabat et al., 1993).

The morphology of MgO is known to be dependent on its method of preparation (Green, 1983). Many factors have been shown to affect the morphology, including precursors (Waida, 1941a, 1941b; Dell and Weller, 1959; Hattori et al., 1976; Hargreaves et al., 1990), precipitation conditions (Choudhary and Pandit, 1991), aging period and washing (Sidjabat et al., 1993), calcining conditions (Razouk and Mikhail, 1957, 1959; Anderson, 1905; Shastri et al., 1985), and storage time (Vinek et al.,1978). According to many research groups, the precursors and calcining temperatures appear to exhibit the largest effects (Hargreaves et al., 1990; Hattori et al., 1976; Choudhary et al., 1994).

The effect of temperature on the formation of MgO prepared by heating different magnesium carbonates sold by Merck as "heavy", "crystal" and "light" was investigated by Anderson (1905). It was found that the oxides preheated to different temperatures dissolved in water at different rates. The maximum dissolution was achieved when the oxides were heated at 810-865 ^{o}C. The rate of dissolution decreased as the temperature of preparation was increased, but the extent of this

decrease was not the same for oxides obtained from different sources. It was greatest in the case of the oxide obtained from a "heavy" carbonate, less marked in the product from "crystal" carbonate, and scarcely appreciable in that from "light" carbonate. Choudhary et al. (1994) showed that surface areas of MgO calcined from $Mg(OH)_2$, $MgCO_3$, $Mg(CH_3COO)_2$ and $Mg(NO_3)_2$ depended strongly on the calcining temperatures, the lower the calcining temperatures the higher the surface areas.

Dell and Weller (1959) showed that the thermal decomposition of $MgCO_3.(NH_4)_2\ CO_3.4H_2O$ and $MgCO_3.3H_2O$ produced MgO of different surface area. Waida (1941a, 1941b) reported that MgO derived from dehydration of $Mg(OH)_2$ and $MgCO_3.3H_2O$ showed different degrees of hydration when they were hydrated in a stream of saturated water vapour. The degree of hydration of MgO prepared from $MgCO_3.3H_2O$ is greater than the MgO prepared from $Mg(OH)_2$. Significant differences in surface properties have also been found for MgO prepared from $Mg(OH)_2$ and $4MgCO_3.Mg(OH)_2.5H_2O$ (Hattori et al.,1976). Electron microscopic studies on the morphology of MgO have shown that MgO prepared by burning magnesium metal in oxygen presents a cubic form which is different from that obtained by calcination of MgCO3 (Hargreaves, 1990). Choudhary et al. (1994) found that the surface area of MgO depends strongly upon the precursors (viz. $Mg(OH)_2$, $MgCO_3$, $Mg(CH_3COO)_2$ and $Mg(NO_3)_2$). MgO surface areas were found in order of $Mg(OH)_2 > MgCO_3 > Mg(CH_3COO)_2 > Mg(NO_3)_2$.

The effect of storage time on MgO samples was investigated by means of X-ray photoelectron spectroscopy (XPS), along with catalytic, desorption of H_2O and basicity measurements (Vinek et al., 1978). It was found from desorption measurements that only one H_2O peak at ~ 373 K was found with a freshly prepared MgO sample, whereas the samples which had been stored for some times showed two peaks, one at 373K, the other at 573K (Vinek et al.,1978). From this observation it

was inferred that a hydroxy layer was formed on MgO with increasing storage time. The effect of MgO on the dehydrogenation and dehydration of butan-2-ol was also investigated by Vinek et al. (1978). It was found that with increasing hydroxide layer (which means decreasing basicity) the selectivity changed from dehydrogenation to dehydration.

2.2 Scope of Work

In this Chapter MgO of different morphologies prepared from different preparation methods and precursors were characterized for their surface physical properties. Subsequent Chapters will report on their chemical surface properties and their use as catalysts for the oxidative coupling of methane. Three groups of MgO samples were prepared. The first set was obtained from the calcination of $Mg(OH)_2$ that had been precipitated from $Mg(NO_3)_2$ and NH_3 solution in the pH range 9.5 - 11.0. The second set was prepared by the calcination of $Mg(OH)_2$ precipitated at pH 10.0 at different temperatures, 400, 600 and 800°C for 4 h. The temperature programmed calcination (increased the temperature to 350°C, 350°C for 45 min, 5°C/min to 800°C and 800°C for 4 h) was also carried out. The last set of MgO samples was prepared by the calcination of different Mg salts, $Mg(OH)_2$ hydrolysed from $Mg(CH_3COO)_2$, $MgCO_3.H_2O$, $4MgCO_3.Mg(OH)_2.5H_2O$, and $MgC_2O_4.2H_2O$, at 800°C for 4 h. The limits in pH, temperature and precursor chosen were due to the capacity of practical techniques used in this work.

The samples were characterised by a number of techniques. Data obtained were the surface area, pore size/pore distribution and particle size distribution. It has been stated that the specific surface area of a solid catalyst is one of the first things that must be determined before any detailed physical or chemical interpretation of its

behaviour as an adsorbent is possible (Adamson, 1976a). The Brunauer, Emmett and Teller (BET) method was applied to analyse the surface area of MgO samples.

Pore structure is also an important factor because in a given catalyst preparation, the pore distribution may be such that some of the catalyst is completely inaccessible to large reactant molecules (Thomas and Thomas, 1981a). In addition, it may restrict the rate of conversion to products by impeding the diffusion of reactant in the internal pore structure. Mercury porosimetry was employed to characterise MgO pore size and pore distribution. Particle size distribution of the catalyst is another factor that sometimes has a significant effect on the rate of gas-solid reaction (Delannay, 1984). Therefore the particle size distribution of MgO samples were also determined by a light diffraction technique.

2.3 Experimental Procedures Used to Prepare MgO Samples

2.3.1 Preparation of MgO from $Mg(OH)_2$ precipitated at different pH

$Mg(OH)_2$ was prepared by slow addition of 2M $Mg(NO_3)_2$ solution ($Mg(NO_3)_2.6H_2O$ (BDH, AR grade) into 50 mL of ammonia solution (BDH, AR grade) of a known pH (NH_3 added dropwise to 50 mL of deionized water until the required pH was obtained) at a constant rate of 0.5 mL/min. A Metrohm Herisau Dosimat E535 and Potentiograph E536 were used for titrating $Mg(NO_3)_2$ solutions and recording the pH respectively. To maintain the pH, controlled addition of ammonia solution (6 % for pH 9-10, and 12 % for pH 11) was simultaneously added by a small pump (Iwaki Metering pump EX-A10) to the mixture which was mixed by a magnetic stirrer. The precipitate was separated by suction filtration and washed with deionized water, and then dried in a vacuum oven at 115°C for 3 h. This $Mg(OH)_2$ was ground and sieved (180 μm sieve) before calcination.

Approximately 0.5 g of $Mg(OH)_2$ were used for each calcination. The calcining temperature was held at 30°C for 2 min, then increased to 350°C at a rate of 15°C/min. This temperature was maintained for 45 min, and then increased to 850°C at a rate of 5°C/min and held at 850°C for 10 min. The calcination was performed in an atmosphere of high purity argon at a flow rate 10 mL/min. After cooling down, also under argon, the MgO was ground and sieved.

Another set of $Mg(OH)_2$ preparations were performed. The above procedure was repeated except the $Mg(OH)_2$ precipitate was boiled in deionized water for 4 h before drying. The preparation was repeated at least three times for each pH considered (pH = 9.5, 10.0 and 11.0).

The variation of $Mg(NO_3)_2$ addition rates was also carried out for $Mg(OH)_2$ precipitated at pH 11.0. The addition rate of 0.5 and 0.25 mL/min were used.

2.3.2 Preparation of MgO from $Mg(OH)_2$ calcined at different temperatures

The $Mg(OH)_2$ precipitated at pH 10.0 was filtered, washed with deionized water, boiled in deionized water for 4 hours, and dried in a vacuum oven at 115°C for 3 h. The dried precipitate was then ground and sieved (180 μm) before calcination. Four calcining conditions were chosen. Three samples were heated (approximately 20°C/min) up to 400°C, 600°C and 800°C respectively, then these three temperatures were held for 4 h. The fourth sample was calcined by increasing the temperature to 350°C and holding at this temperature for 45 min. The temperature was then ramped to 800°C with a rate of 5°C/min and held at 800°C for 4 h. Calcination of the $Mg(OH)_2$ was performed under a high purity argon atmosphere at a flow rate of 10 mL/min.

2.3.3 Preparation of MgO via different methods & compounds

2.3.3.1 The hydrolysis of $Mg(CH_3COO)_2 .4H_2O$ to $Mg(OH)_2$

A concentrated solution of $Mg(CH_3COO)_2$ (25.4 g of $Mg(CH_3COO)_2.4H_2O$ AR grade from Ajax chemicals and 50 mL of deionized water) was stirred and heated on a hot plate. A small amount of deionized water was continuously added to the mixture by a pump (mentioned in section 2.3.1) to sustain the reaction, and the acetic acid was removed from the mixture as a vapour. The reaction was very slow and at least one week was required to precipitate about 2-3 g of $Mg(OH)_2$.

$$Mg(CH_3COO)_2 + 2H_2O \rightarrow Mg(OH)_2 + 2CH_3COOH \qquad [2.1]$$

The precipitated $Mg(OH)_2$ was washed by stirring in deionized water twice, then filtered. It was then dried at 115°C in a vacuum oven for 3 h, ground and sieved (180 μm sieve). The sample was calcined under high purity argon atmosphere at 800°C for 4 h.

2.3.3.2 Precipitation of $MgCO_3.xH_2O$

A solution of 2M $Mg(NO_3)_2$ was reacted with saturated $(NH_4)_2CO_3$ solution (NH_4HCO_3 + $NH_2COO.NH_4$, LR grade from Ajax chemicals). The $MgCO_3.xH_2O$ formed was then treated as for the $Mg(OH)_2$ precipitate described in section 2.3.3.1.

Another solution of 70 mL of 2M $Mg(NO_3)_2$ was slowly added to a mixture of 12 mL of 25% NH_3 solution and 50 mL of saturated $(NH_4)_2CO_3$ solution. The precipitate was then treated in a similar fashion to the $Mg(OH)_2$ precipitate described in section 2.3.3.1.

2.3.3.3 Precipitation of $MgC_2O_4.2H_2O$

To 100 mL of $Mg(NO_3)_2$ solution, 5-10 drops of methyl red, 60 mL of $(NH_4)_2C_2O_4$ solution (20 g $(NH_4)_2C_2O_4$, 10 mL of concentrated HCl, made up with deionized water to 250 mL) and 25 g of solid urea were added. The container was then covered with a watchglass and boiled gently for about 30 min until the indicator turned yellow. After letting the solution cool down, the precipitate was treated in the same manner as the $Mg(OH)_2$ precipitate described in section 2.3.3.1.

2.4 Methods Used to Characterise MgO Samples

2.4.1 Generalisation of porous solids

According to Gregg (1982), the particles of a fine powder-*the primary particles*-will stick together more or less firmly under the action of surface forces to form the *secondary particles*. If the interaction between neighbouring particles are weak, the assemblage can be readily broken down again. This type of secondary particles is termed an *aggregate*. With elevated temperatures, or by application of mechanical pressure, the primary particles become strongly joined together, and the secondary particles are then called *agglomerates*. The voids between the primary particles within a secondary particle, together with those between a secondary particle and its neighbours, constitute a pore system in which the individual pores will tend to be related with both in shape and size to the primary or secondary particles (Figure 2.1).

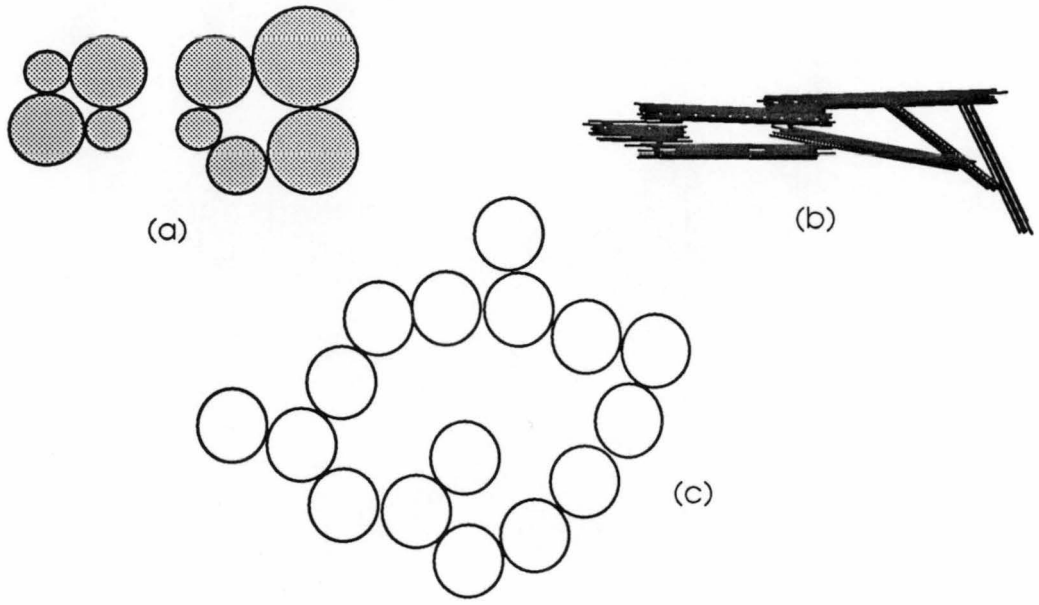

Figure 2.1 Pores produced by an aggregate of (a) spherical particles, (b) plate-like particles and (c) spherical particles, having a very open structure (Gregg, 1982).

A pore system can also be produced by a thermal decomposition of one solid which gives another solid and gas. For instance, the production of MgO by calcination of $MgCO_3$ or $Mg(OH)_2$, where the loss of volatile component leads to the development of a pore system with its associated surface area.

The pore systems of solids are of many different kinds. The individual pores may vary greatly both in size and shape within a given solid, and between one solid and another. A feature of particular interest for description purposes is the width of the pores, e.g. the diameter of a cylindrical pore, or distance between the sides of a slit-shaped pore. A convenient classification of pores according to their average width originally proposed by Dubinin (1960) and now officially adopted by the International Union of Pure and Applied Chemistry (1972) is displayed in Table 2.1.

Table 2.1 Classification of pores.

Type of pores	Width (Å)
Micropores	less than ~ 20
Mesopores	between ~ 20 and ~ 500
Macropores	more than ~ 500

Amongst solids as a whole, it has been noted (Gregg, 1982) that a wide and continuous range of pore size is to be found, from macropores through mesopores and micropores to sub-atomic pores in the form of cleavage planes, dislocations and point defects.

2.4.2 Surface Area Determination

The standard Brunauer, Emmett and Teller (BET) adsorption method using nitrogen at -196°C was applied to investigate the surface areas of MgO. The BET method is developed for multilayer physical adsorption by assuming that at equilibrium the surface is completely covered by at least one monolayer and that all layers beyond the first behave as a pure liquid (Thomas and Thomas, 1981b). This means that the heat of adsorption of each layer beyond the first is equal to the heat of liquefaction of the bulk adsorbate material and that the Van der Waals forces on the adsorbate are transmitted only into the first layer. At equilibrium the area of any given multilayer is constant, hence the rate of evaporation from a particular layer is equal to the rate of condensation on the preceding layer. With these assumptions the simple BET equation is

$$P/V(P_o - P) = 1/V_mC + (C-1)P/V_mCP_o \qquad [2.2]$$

where V is the volume adsorbed at pressure P, P_o is the saturation vapour pressure of the adsorbate at the temperature of adsorption, V_m is the monolayer volume in $mL.g^{-1}$ at s.t.p., and C is a constant which reflects the adsorption-desorption equilibrium. V_m was determined from a plot of $P/V(P_o - P)$ and P/P_o according to equation [2.2] over the P/P_o range 0.035 to 0.35. A single point surface area determination was also carried out. Similar values (± 3 %) of surface areas were obtained using both techniques.

2.4.3 Particle profile and particle size distribution

Sample texture and particle profile were examined by scanning electron microscope (SEM) technique using a Philips 505 Scanning Electron Microscope. The samples were mounted on sample holders in a powder form and then coated with gold prior to being studied. The sample surface was scanned by a focused electron beam, and the intensity of secondary electrons was monitored (Adamson, 1976b).

The particle size distribution profile of the samples was determined using a Mastersizer/ E Malvern instrument. Prior to determination samples were dispersed in ethanol by shaking in ultrasonic bath for 3-5 minutes. The coherent light from a low power laser source was passed through the suspended MgO sample and was diffracted. The energy diffraction pattern, a series of concentric rings is obtained in the form that the larger the particles, the closer the rings (Stone 1963). The particle size distribution profile is then derived by the analysis of energy distribution over various rings shown by the focal plane image of a lens system.

2.4.4 Mercury porosimetry

Mercury porosimetry using a Micromeritics Auto Pore 9200 was employed to investigate the pore size and pore distribution of the MgO samples. The pore diameter was measured directly as a function of applied pressure,

$$D = -(1/P)\, 4\, \gamma \cos \theta \qquad [2.3],$$

where D is the pore diameter, P is the applied pressure, γ is the surface tension of mercury and θ is the contact angle (Gregg, 1982). With this technique pore size distribution in the range from 36 to 4 x 10^6 Å corresponding to the applied pressure of ~ 50000 - 0.4 psia can be determined.

2.4.5 Thermo gravimetric analysis

Thermo-gravimetric analysis (TGA) was conducted to determine the formula of carbonate compounds prepared in section 2.3.3.2. The Setaram TGA 92 thermoanalyzer used comprises a thermobalance, a CS 92 controller, a PC 92 computer and a printer. Samples of about 10 mg were heated at a rate of 5°C/min to 300°C, and then further heating was carried out at a rate of 20°C/min to 700°C. It was assumed that the empirical structure of carbonate was in the form of basic carbonate, $mMgCO_3.nMg(OH)_2.xH_2O$ (Svehla, 1987). The amount of hydrated water was determined from the weight loss in the temperature range of 80-250°C, while the weight loss at higher temperatures belonged to CO_2 and H_2O from the carbonate and hydroxide. The values of m and n were estimated from the weight loss due to CO_2 and H_2O, and the number of moles of MgO was obtained as a final product as follows:

$$44m + 18n = \text{the weight loss due to } CO_2 \text{ and } H_2O \qquad [2.4]$$

$$m + n = \text{number of moles of MgO} \qquad [2.5].$$

The values of 44 and 18 are the molecular weight of CO_2 and H_2O respectively, and the number of moles of MgO can be estimated from the difference between the initial sample weight and the total weight loss.

2.5 Results and Discussion

2.5.1 Surface area and particle profile of MgO prepared from $Mg(OH)_2$ precipitated at different pH

Four samples of MgO were prepared under the same conditions to obtain statistically significant results. The determination of surface area for each sample was repeated several times and the average result is displayed in table 2.2.

Table 2.2 Surface area of MgO prepared at different conditions.

Sample No	pH of precipitation	rate of adding $Mg(NO)_3$ sol. (mL/min)	boiled in hot water	surface area (m^2/g) ± 5 m^2/g
1	9.5-9.6	0.50	yes	79 80 82 79
2	10.0-10.1	0.50	yes	82 84 82 81
3	10.9-11.0	0.50	yes	79 78 82 80
4	10.0-10.1	0.50	no	40 68 41 51
5	11.0-11.1	0.50	no	49 50 59 63
6	11.0-11.1	0.25	yes	82 80 78

It can be seen that the variation in pH and rate of $Mg(NO_3)_2$ addition does not result in a difference in surface area (samples 1-3, 6). However, removing of residual

NO_3^- from the precipitate seems to be important in maintaining the consistency of surface area. The decrease in surface areas of MgO samples obtained from the $Mg(OH)_2$ precipitate which were not digested (samples 4, 5) appears to be caused by the residual $NO3^-$ left in the precipitate. To clarify the effect of residual NO_3^- on the MgO morphology, three different MgO samples were prepared from different preparation treatments as shown in Figure 2.2.

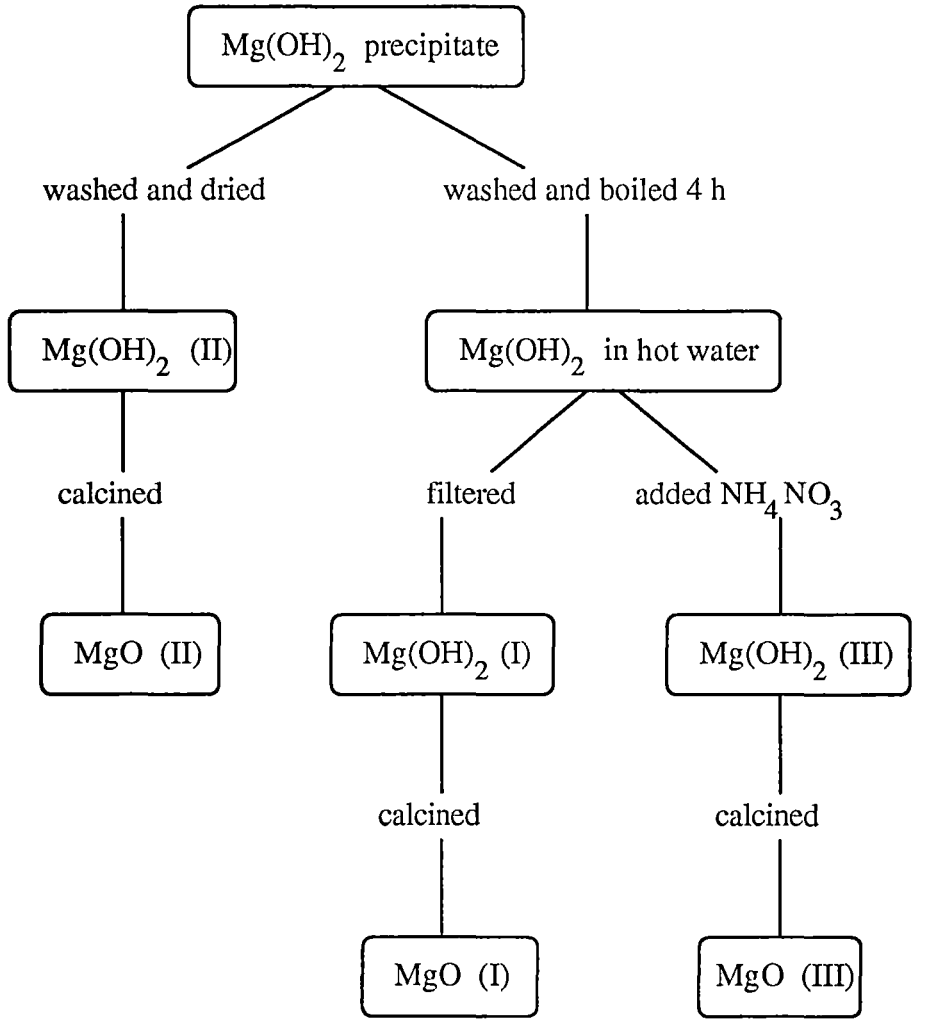

Figure 2.2 The procedure used in the preparation of three different MgO samples.

As shown in Figure 2.2, $Mg(OH)_2$ was precipitated from $Mg(NO_3)_2$ and NH_3 solution at pH 11.0 as described in section 2.3.1. After being filtered, the precipitate was divided into two portions. The first one was washed with deionised water and dried, ($Mg(OH)_2$ (II)), while the second portion was boiled in deionised water for 4 h. The digested $Mg(OH)_2$ was divided into two portions; one was filtered and then dried ($Mg(OH)_2$ (I)). The other portion had NO_3^- incorporated into the precipitate by adding a small amount (~ 0.3 g) of NH_4NO_3 into the slurry, after which it was filtered and dried ($Mg(OH)_2$ (III)).

After drying in a vacuum oven for 3 h, $Mg(OH)_2$ (I, II and III) were analysed for NO_3^- by UV spectroscopic 205-214 nm. Approximately 50 mg of samples were dissolved in 2 mL of 5 % HCl and made up with deionized water to 25 mL. The spectra were recorded in 1 cm cell between 190-250 nm (American Public Health Association, 1992) with a Varian DMS 100 UV Visible Spectrophotometer. The NO_3^- absorption at wavelengths 205-214 nm (Figure 2.3) was standardised by using three $Mg(NO_3)_2$ solutions of known concentration.

The surface area of the resulting MgO I, II and III was also determined and the results are shown in Table 2.3.

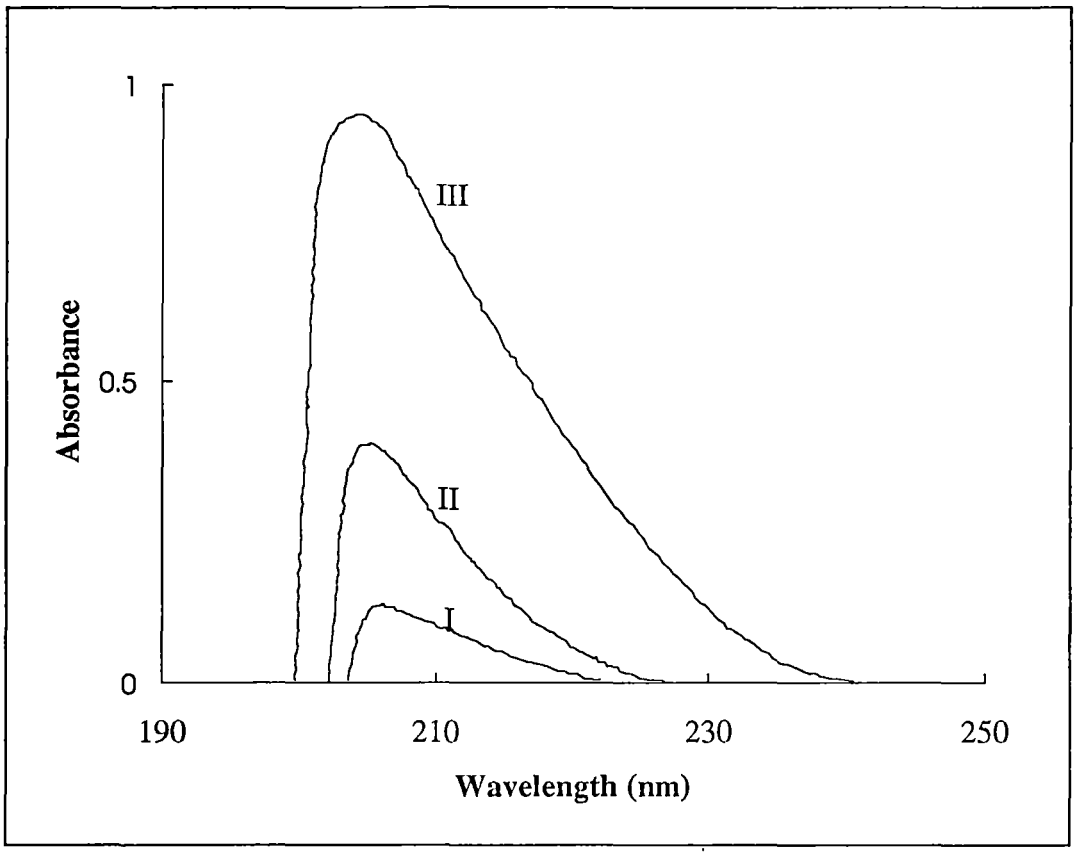

Figure 2.3 UV spectra of NO_3^- of $Mg(OH)_2$ (I), (II) and (III) samples.

Table 2.3 Surface area of MgO samples and the amount of NO_3^- left in the $Mg(OH)_2$ precursors.

MgO sample	% residual NO_3^-	MgO surface area (m^2/g)
I	0.1	79
II	0.4	68
III	1.2	40

From Figure 2.3 and Table 2.3 it can be seen that the digestion of the $Mg(OH)_2$ precipitate in water for 4 h has reduced the amount of residual NO_3^- that may be left in the form of $Mg(NO_3)_2$ and/or NO_3^- ion bound on the $Mg(OH)_2$ particle. $Mg(OH)_2$ (II) which was not boiled in water after washing was found to contain a higher amount of residual NO_3^- than that was found in $Mg(OH)_2$ (I). The MgO (II) derived from $Mg(OH)_2$ (II) shows a lower surface area than that of MgO (I) obtained from $Mg(OH)_2$ (I). It was observed that $Mg(OH)_2$ (III) contains the highest amount of NO_3^- due to the deliberate addition of NH_4NO_3, and MgO (III) calcined from this percusor possesses the lowest surface area. These results indicate that contamination of NO_3^- causes the reduction of MgO surface area.

Sidjabat et al. (1993) found that calcination (400°C 4 h) of $Mg(OH)_2$, precipitated from $Mg(NO_3)_2$ and NH_4OH solutions at different pH (and aging 1 day), resulted in MgO of slightly different surface areas (Figure 2.4). The slight difference in MgO surface area observed by Sidjabat may be due to the aging period of $Mg(OH)_2$ in that pH solution. When $Mg(OH)_2$ was allowed to stand in the solution for the longer time, the orientation of the plate-like $Mg(OH)_2$ crystals to form larger aggregates would be more affected by the pH of solution and would lead to small differences in MgO surface area. In the present work, $Mg(OH)_2$ precipitate was removed from its mother liquor and boiled in hot water for 4 h. With this procedure the effect of pH during $Mg(OH)_2$ precipitation on MgO surface area was not significant. These results indicate that pH during $Mg(OH)_2$ precipitation has no significant effect on MgO surface area provided $Mg(OH)_2$ has not been aged in the mother liquor.

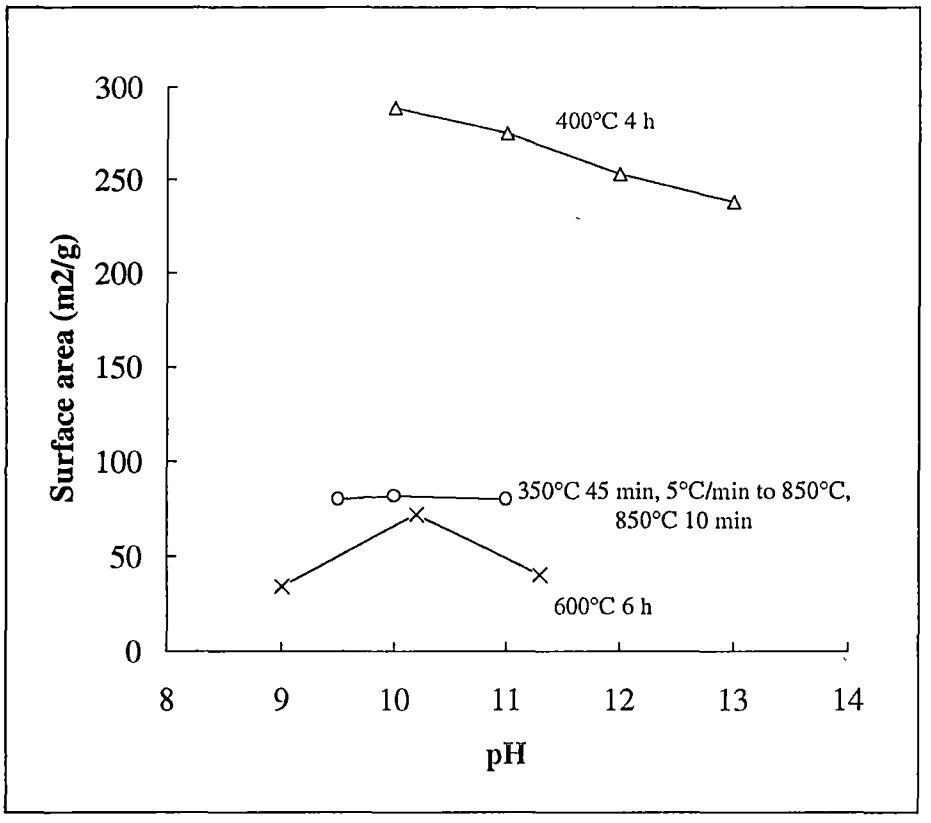

Figure 2.4 The relationship between pH of $Mg(OH)_2$ precipitation and MgO surface area; (Δ) Sidjabat et al. (1993), (o) the present work and (×) Choudhary and Pandit.

With similar reagents Choudhary and Pandit (1991), however, found that calcination (600°C 6 h) of $Mg(OH)_2$ precipitated at pH 9.0, 10.2 and 11.3 (aging period 30 min) resulted in MgO with surface areas of 34.0, 72.1 and 40.3 m^2/g respectively. The authors reported that $Mg(OH)_2$ precipitate was washed with deionized water until free from cations and anions. This was not likely to remove all the residual NO_3^- from $Mg(OH)_2$ precipitate, since it was found from this work that MgO samples with low surface areas (Table 2.2) were obtained when $Mg(OH)_2$ was not boiled in hot water eventhough it had been washed with deionized water several times. Recently, Choudhary et al. (1994) found that calcination (600°C 4 h) of $Mg(NO_3)_2$ resulted in a very low surface area MgO (8.7 m^2/g). This finding supports the assumption that the presence of NO_3^- causes the low surface area in MgO. The

low surface area MgO is thought to be due to the sintering of MgO acivated by NO_3^- during calcination.

2.5.2 Particle size distribution and pore size/pore distribution of MgO samples prepared from $Mg(OH)_2$ precipitated at different pH levels

To obtain more information on the morphology of MgO, the particle size distribution and the pore volume/pore distribution were determined. On the basis of the findings outlined in section 2.5.1 the investigation was divided into a consideration of two samples, (i) those precipitates that were contaminated by residual NO_3^- and (ii) those precipitates that were obtained at various pH without the interference from NO_3^-.

2.5.2.1 Effect of residual NO_3^- on the particle size and pore size distributions of MgO

The particle profiles of both $Mg(OH)_2$ and MgO were investigated by SEM technique and SEM micrographs of these samples are displayed in Figure 2.5. It was found from the micrographs that MgO formed by thermal decomposition of $Mg(OH)_2$ retains, on a microscale, the particle shape of the precursor. The plate-like structures of varying shapes and sizes were observed for both $Mg(OH)_2$ and MgO samples.

$Mg(OH)_2$ (I) % NO_3^- 0.1

MgO (I) surface area 79 m^2/g

$Mg(OH)_2$ (II) % NO_3^- 0.4

MgO (II) surface area 68 m^2/g

$Mg(OH)_2$ (III) % NO_3^- 1.2

MgO (III) surface area 40 m^2/g

Figure 2.5 The particle profiles of $Mg(OH)_2$ (I,II and III), and MgO (I, II and III).

It has been known (Green, 1983; Shastri et al., 1985; Lunsford et al., 1989) that MgO calcined from $Mg(OH)_2$ has the general plate-like morphology which reflects the relic structure of $Mg(OH)_2$. The relics or pseudomorphs consist of minute crystals of cubic MgO attached along their edges/corners to form a layer crystal aggregate defining the precursor crystal (Green, 1983) as shown in Figure 2.6.

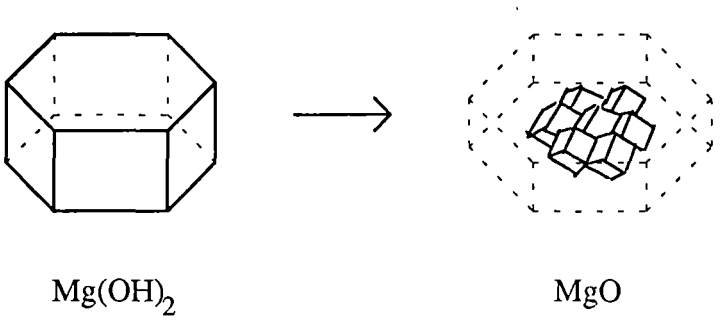

Figure 2.6 Precursor-product pseudomorphic relationships in $Mg(OH)_2$ and MgO (Green, 1983).

The formation of these highly orientated layers of MgO from thick $Mg(OH)_2$ crystals was explained (Rhodes and Wuensch, 1973; Copperthwaite and Brett, 1976) as the formation of a duplex microstructure. This type of microstructure consists of a few large grains of MgO, presumably formed from well orientated crystal layers, surrounded by a large number of smaller grains formed from less well orientated layers. An alternative form of this type of microstructure is large (up to millimetre dimensions) polycrystalline particles of high density surrounded by a porous matrix of small grains. It is thought (Green, 1983) that this latter phenomenon occurs because the plate-like $Mg(OH)_2$ crystals have a strong tendency to orientate themselves face to face during thickening/washing etc and thus give large multiple layer pseudomorphic aggregates, e.g. during calcination. Such microstructures are not noted in deadburned MgO produced from precursors where the decomposition does not occur

topotactically, for examples, MgO obtained from $MgCO_3$, MgC_2O_4 and $MgSO_4$ (Green, 1983).

Considering the SEM micrographs (Figure 2.5) of $Mg(OH)_2$ (I) and (III) which contain different amount of residual NO_3^-, it is noted that $Mg(OH)_2$ (III) which has a higher amount of NO_3^- exhibits a smaller plate-like particle than $Mg(OH)_2$ (I). This implies that contamination of NO_3^- interferes with the growth of $Mg(OH)_2$ particles and consequently the MgO particle. SEM micrographs of MgO samples show that MgO (I) calcined from $Mg(OH)_2$ (I) has a larger particle size than MgO (III) obtained from $Mg(OH)_2$ (III).

The effect of residual NO_3^- in $Mg(OH)_2$ on MgO particle structure was also observed from the particle size distribution. The particle size distribution of MgO samples calcined from $Mg(OH)_2$ (I), (II) and (III) containing various amount of NO_3^- are displayed in Figure 2.7.

From Figure 2.7 (next page) it can be seen that the higher the contamination of NO_3^- present in $Mg(OH)_2$ precursor, the smaller the average particle size. The existence of NO_3^- in $Mg(OH)_2$ may also interfere in the aggregation of plate-like particles to orientate themselves face to face and form a large multiple layer pseudomorphic aggregates during calcination. Hence, a smaller aggregate is found for MgO calcined from the $Mg(OH)_2$ that has a higher contamination of NO_3^-. Green (1983) has reported that impurities in the $Mg(OH)_2$ which negatively influence MgO crystal growth during low temperature calcination are Na^+, K^+, SO_3^- and possibly NO_3^- and NO_2^-. The evidence obtained here confirms that the presence of NO_3^- in $Mg(OH)_2$ has an influence on MgO morphology.

MgO	Particle sizes < 1 μm (%)	Particle sizes 1-10 μm (%)	Particle sizes > 10 μm (%)
I	5.8	60.7	33.5
II	2.7	72.8	24.5
III	4.6	75.6	19.8

standard deviation is 2-3 %

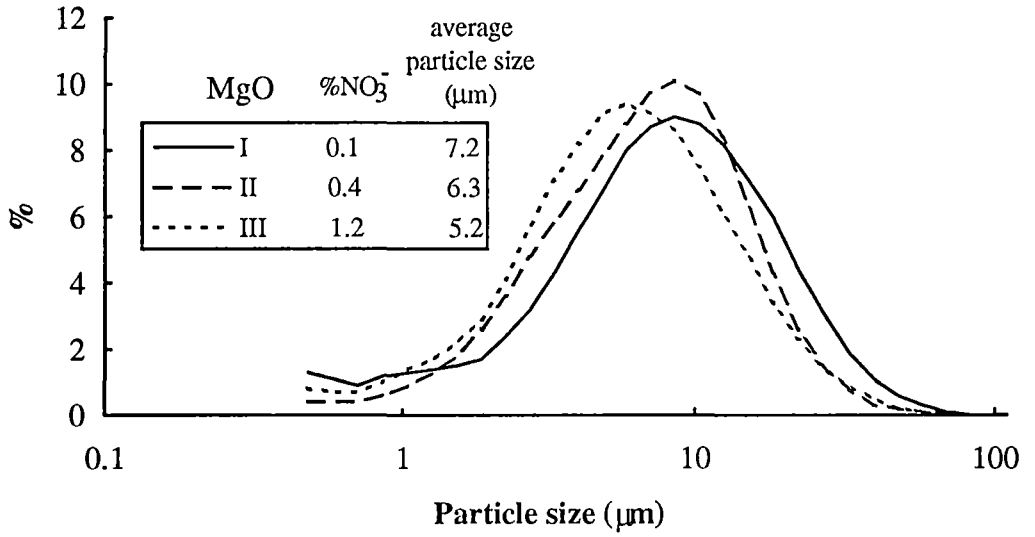

Figure 2.7 The effect of NO_3^- residual on particle size distribution of MgO calcined from $Mg(OH)_2$ precipitated at pH 11.0.

In mercury porosimetry the volume (V) of mercury taken up by the solid is measured as an applied pressure P is gradually increased (Gregg, 1987). The value V_i at any value of applied pressure P_i gives the volume of all pores having a radius equal to or greater than r_i and is termed the cumulative pore volume. The pore size distribution curves are obtained by differentiation of the curves of cumulative volume against r, giving curves of dV/dr vs r. In the present work pore size distribution curve is presented in terms of pore diameter.

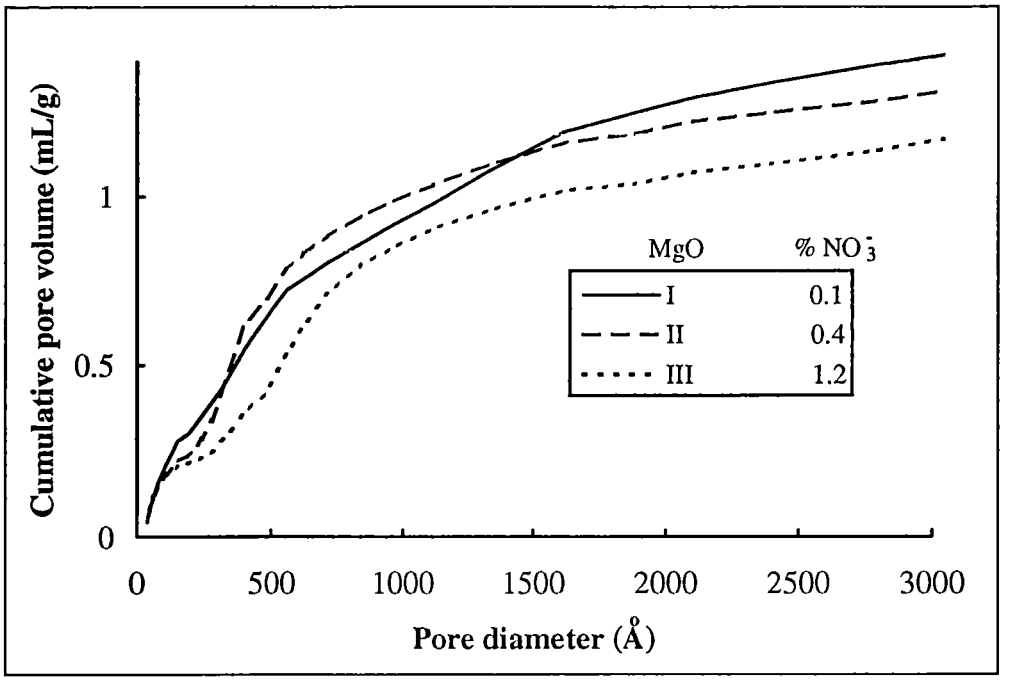

Figure 2.8 Effect of residual NO_3^- on cumulative pore volume of MgO.

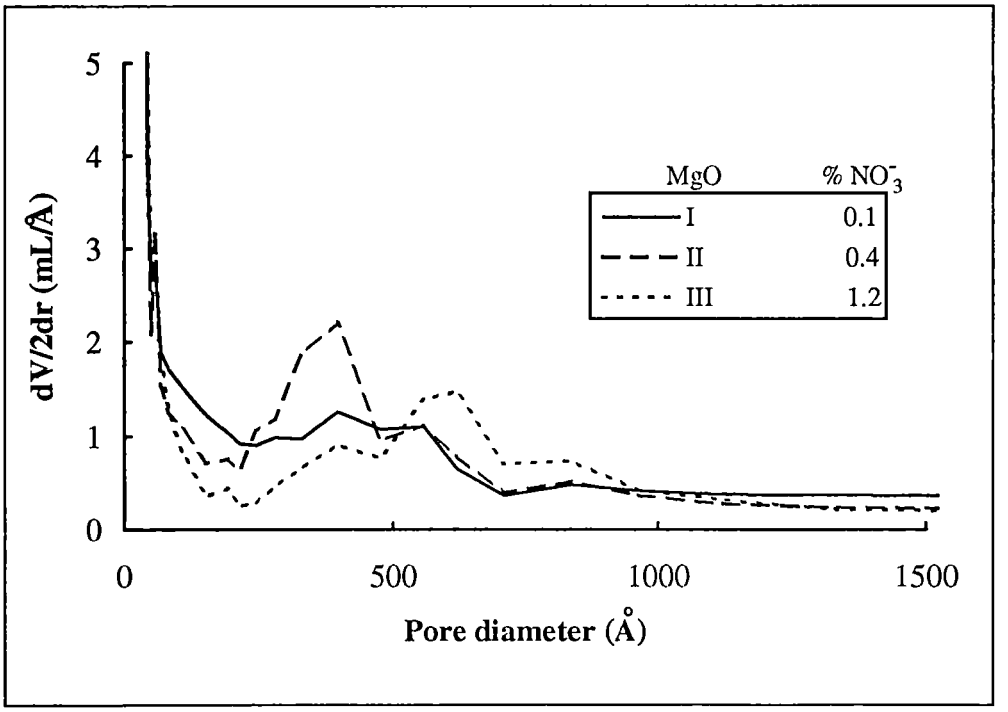

Figure 2.9 Effect of residual NO_3^- on pore size distribution of MgO.

In Figure 2.8 and Figure 2.9 it is likely that the higher the amount of NO_3^- left in $Mg(OH)_2$ the larger the pore size but the less the cumulative pore volume of MgO. The larger pore size which is due to the presence of NO_3^- is presumably because the size of NO_3^- (diameter 3.3 Å (Jenkins and Thakur, 1979)) is larger than the size of OH^- (diameter 2.38 Å (Jenkins and Thakur, 1979)). After calcination all NO_3^- ions and H_2O would be removed from the $Mg(OH)_2$ sample, and consequently spaces or pores would be created on the MgO. Pores derived from the removal of NO_3^- are therefore larger than pores obtained from the removal of H_2O. The loss in cumulative pore volume as a result of NO_3^- ions arises from the destruction of particle size and aggregation, and the long range structure of the MgO samples. An alternative explanation is that contamination of NO_3^- activates the sintering process during the calcination. Such a process results the lower surface area, larger pore size and lower cumulative pore volume.

2.5.2.2 Particle size and pore size distributions of MgO calcined from $Mg(OH)_2$ precipitated at different pH

It was assumed that there is no significant effect of residual NO_3^- since the precipitates were digested in boiling water for 4 h after precipitation so that most NO_3^- was removed. The particle size distribution of MgO calcined from $Mg(OH)_2$ precipitated at various pH is displayed in Figure 2.10.

pH	Particle sizes < 1 μm (%)	Particle sizes 1-10 μm (%)	Particle sizes > 10 μm (%)
9.5	4.8	56.2	39.0
10.0	1.3	71.3	28.7
11.0	5.8	60.7	33.5

standard deviation is 2-3 %

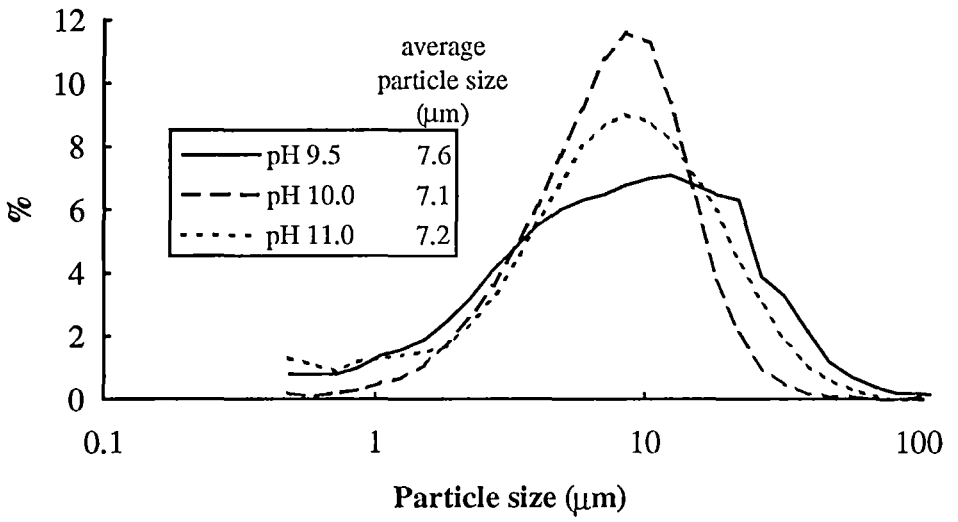

Figure 2.10 Particle size distribution of MgO calcined from $Mg(OH)_2$ precipitated at different pH.

From Figure 2.10 the particle size distributions of MgO obtained from $Mg(OH)_2$ precipitated at pH 9.5, 10.0 and 11.0 are observed to be slightly different. The particle size distribution profile of MgO that was obtained from $Mg(OH)_2$ precipitated at pH 10.0 was observed to have the narrowest distribution and smallest average particle size while the MgO sample derived from $Mg(OH)_2$ precipitated at pH 9.5 represents the broadest distribution shape and largest average particle size. These observations imply that the pH of $Mg(OH)_2$ precipitation may have an effect on the particle profiles of MgO in some aspects. The pH during the precipitation of $Mg(OH)_2$ would have an effect on the aggregation of $Mg(OH)_2$ (the orientation of

plate-like $Mg(OH)_2$ crystals face to face to form large multiple layer aggregates), and consequently on the MgO particles. At pH 10.0 the crystal growth of $Mg(OH)_2$ seems to have less ordering than at the other pH values. The less ordering of $Mg(OH)_2$ crystals leads to a small and loose aggregate and after sintering result in smaller particles. $Mg(OH)_2$ crystals precipitated at pH 9.5 have the best ordering so that the compact and large aggregate is formed and leads to the largest particle size.

The effect of the pH of $Mg(OH)_2$ precipitation on the MgO morphology was also determined from the mercury porosimetry characteristics displayed in Figure 2.11 and Figure 2.12.

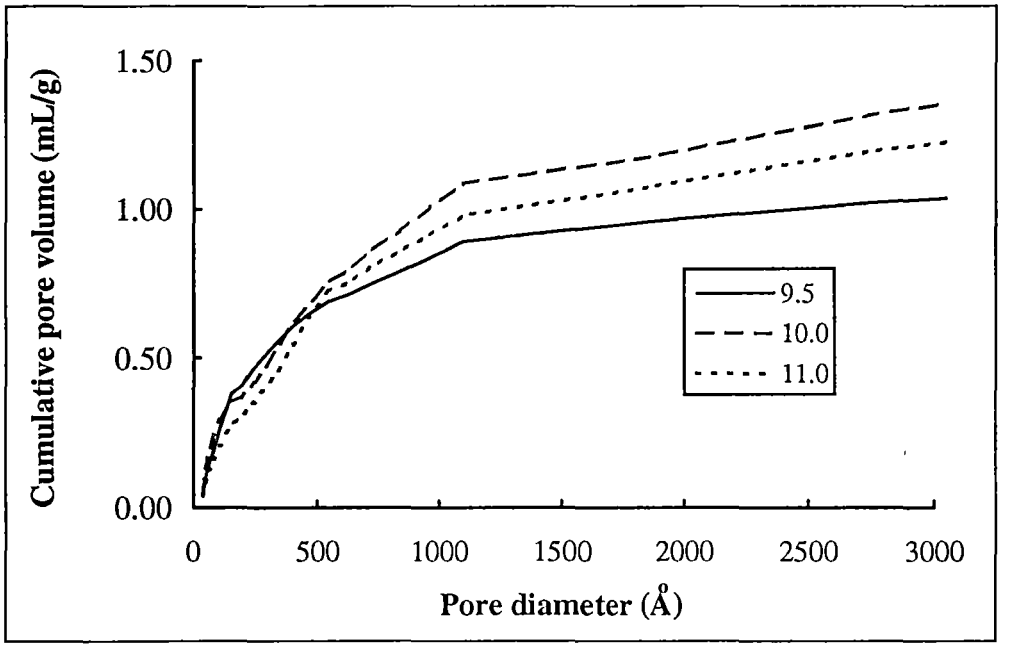

Figure 2.11 Cumulative pore volume of MgO calcined from $Mg(OH)_2$ precipitated at different pH.

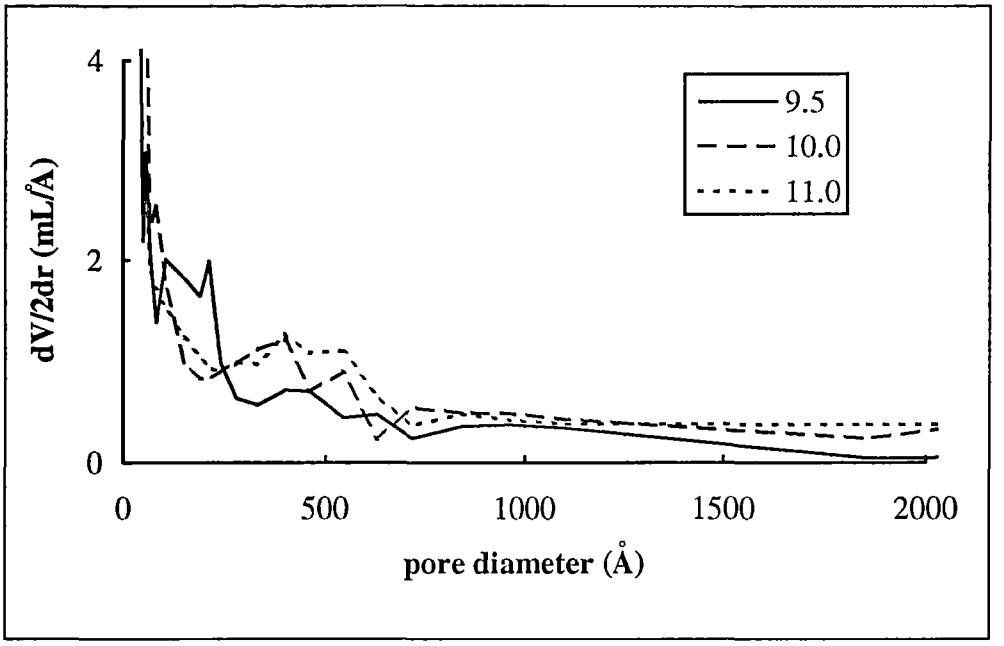

Figure 2.12 Pore size distribution of MgO calcined from $Mg(OH)_2$ precipitated at different pH.

The measurement of the cumulative pore volume of each of the MgO samples was repeated twice using a new sample for each pH value. Virtually the same cumulative pore volume profile was obtained. From Figure 2.11 and 2.12 it was observed that the MgO sample prepared from $Mg(OH)_2$ precipitated at pH 9.5 has a large number of small pores, while the sample obtained from the precipitation at pH 10.0 has a large number of both small and large pores so that its pore volume is highest. The differences in pore structures of these MgO samples are also attributed to the difference in aggregation of $Mg(OH)_2$ plate-like particles at different pH. As mentioned earlier at pH 10.0 the crystal growth of $Mg(OH)_2$ seems to have less ordering than at the other pH values. The less ordered $Mg(OH)_2$ crystals lead to larger pore diameter and higher pore volume in MgO (Sidjabat et al., 1993). $Mg(OH)_2$ crystals precipitated at pH 9.5 have the best ordering and consequently lead to the smallest pore diameter and lowest pore volume in MgO.

Sidjabat et al.(1993) found that average pore diameter and cumulative pore volume of MgO obtained from $Mg(OH)_2$ precipitated at pH 10.0 is lower than at pH 11.0. Such a result was the reverse of the result obtained in the present work. This may be attributed to the differences in precipitation process. Sidjabat reported that NH_3 solution was added to $Mg(NO_3)_2$ solution until the desired pH was obtained, while in the present work the desired pH was adjusted before the precipitation process and kept constant during the precipitation. As a result, the pH used in the present work was different from that used by Sidjabat. These results indicate that it is necessary to define the procedure used to obtain the desired pH if comparison of results between various investigations is carried out.

2.5.3 Surface area, particle size distribution and pore size/pore distribution of MgO calcined from $Mg(OH)_2$ at different temperatures

Five calcining conditions as described in section 2.3.2 were used. Three samples were calcined by increasing the temperature to 400°C, 600°C and 800°C, and holding at that temperature for 4 h. To explore the effect of the heating process, two $Mg(OH)_2$ samples were calcined by a temperature programming method- to 350°C at a rate of 15°C/min, holding at 350°C for 45 min, then heating up to 800°C at a ramp rate of 5°C/min and holding at 800°C for 4 h. Another MgO sample was calcined as above, but held at 850°C for 10 min.

2.5.3.1 MgO obtained at different calcining temperatures

The surface areas, particle size distributions, pore volumes and pore size distributions of MgO calcined from $Mg(OH)_2$ at 400, 600 and 800°C for 4 h are displayed in Table 2.4 and Figures 2.13, 2.14 and 2.15 respectively.

Table 2.4 Surface area of MgO obtained from thermal decomposition of $Mg(OH)_2$ at various temperatures for 4 h.

calcination temperature (°C)	400	600	800
surface area, BET (m^2/g)	210	95	49

Calcining T (°C)	Particle sizes < 1 μm (%)	Particle sizes 1-10 μm (%)	Particle sizes > 10 μm (%)	Average particle size (μm)
400	10.2	81.3	8.5	3.9 ± 0.1
600	9.6	83.5	6.9	4.2 ± 0.1
800	5.6	68.4	26.0	5.8 ± 0.2

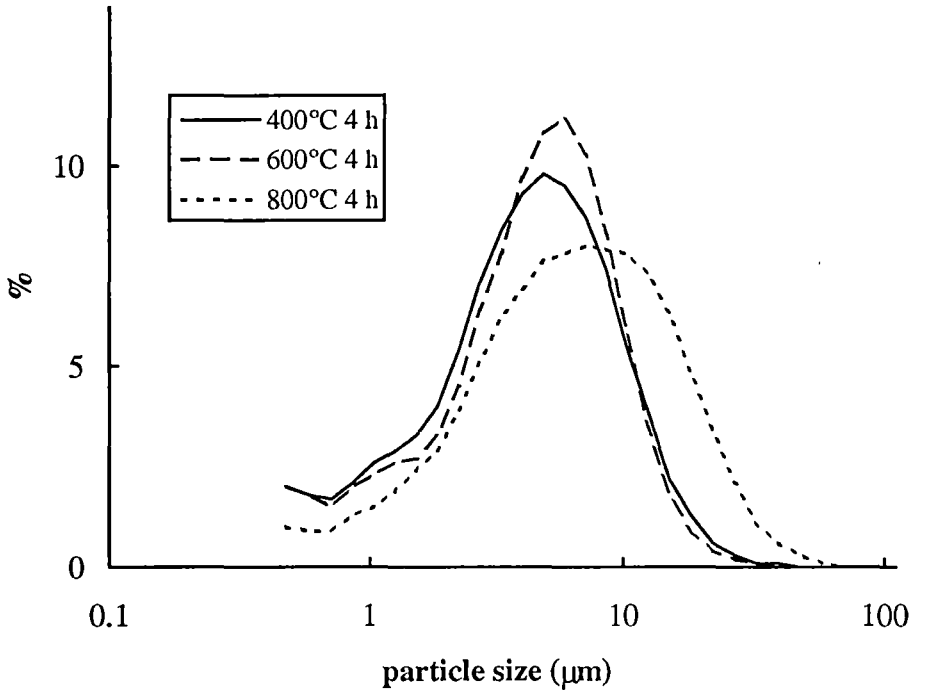

Figure 2.13 Particle size distribution of MgO calcined at different temperatures.

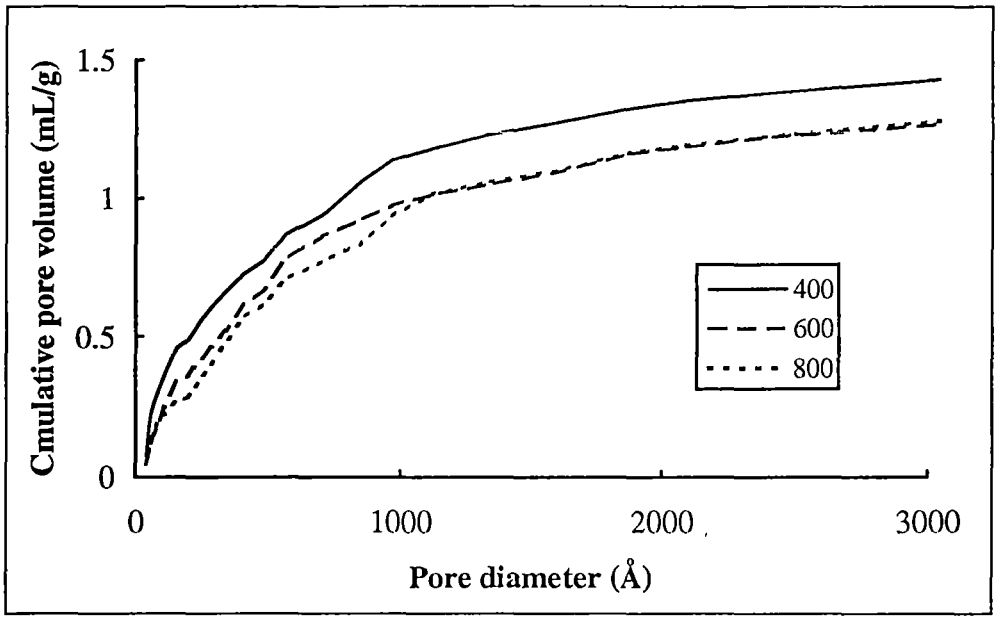

Figure 2.14 Cumulative pore volume of MgO calcined at different temperatures.

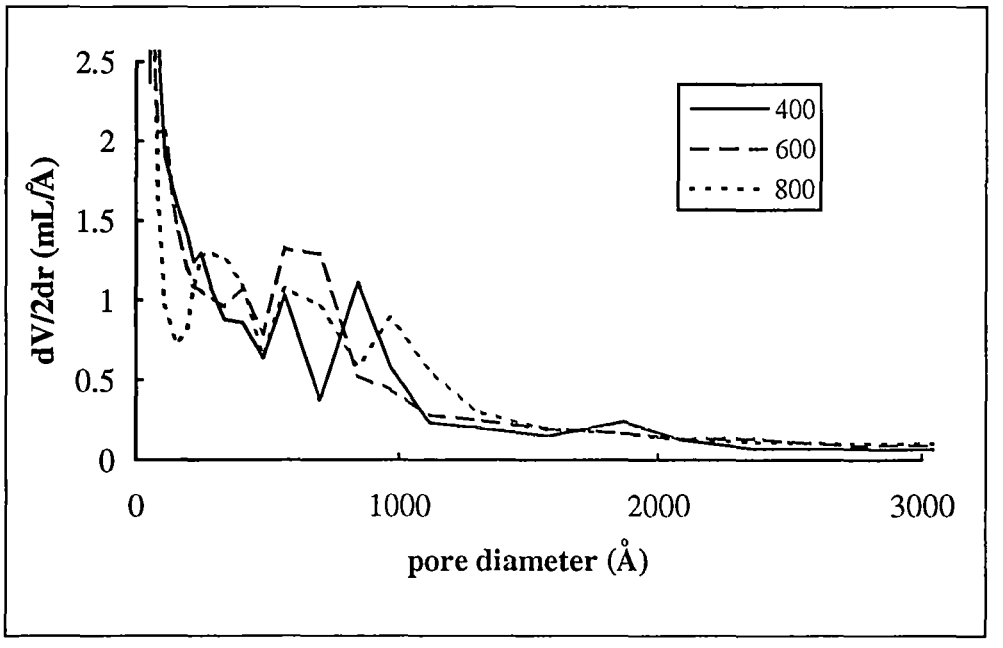

Figure 2.15 pore size distribution of MgO calcined from $Mg(OH)_2$ at different temperatures.

From Tables 2.4 and Figure 2.13 it can be seen that the higher the temperature of calcination, the lower the surface area and the larger the particle size. For the pore structures, Figure 2.14 and 2.15, it was observed that MgO, obtained from low temperature calcination at 400°C, exhibits a large number of small pores so that its cumulative pore volume is highest, in particular between pore diameter 36-1000 Å. On the other hand MgO calcined at 800°C shows the lowest number of small pores 36-1000 Å. This observation can be explained by the sintering of MgO at higher temperature. At calcination temperature of 400°C the high surface area of 210 m^2/g is attributed to the release of water from the hydroxide leading to the formation of small pores (Shastri et al., 1985). Further heating to 600°C caused a significant reduction in surface area to 95 m^2/g mainly due to the loss of small pores from sintering of plate-like particles together. Heating to 800°C increases the degree of sintering, with a corresponding lower surface area of 49 m^2/g and a reduction in the number of small pores.

The results obtained in the present work have the similar trend to that obtained by Sidjabat et al. (1993) that the higher the calcination temperatures (400, 600 and 800°C 4h) the lower the surface area (288, 95 and 39 m^2/g respectively). The values of cummulative pore volume obtained in this work for these MgO samples were also found to be similar as obtained by Sidjabat (about 1.1-1.3 mL/g in pore range 36-1000 Å). Sidjabat reported only the average particle size of MgO calcined at 400°C which was 3.5 μm (without aging of $Mg(OH)_2$ in the solution). In the present work the average particle of MgO calcined at 400°C 4 h was found to be 3.9 μm which is comparable to that obtained by Sidjabat.

Recent work carried out by Dunski et al. (1994) on dehydroxylation of the surface of MgO by temperature programmed desorption showed that not all the surface OH group can be removed at temperatures below 1200 K. This phenomenon

has also been reported by Coluccia et al. (1987) who found that at temperatures below 1073 K the OH stretching vibration in the IR spectra (3800-3200 cm^{-1}) of MgO was still readily observed. Hence it is likely that MgO obtained via calcination at temperatures lower than 800°C may retain some residual OH on the surface. The amount of residual OH remaining on the surface of MgO calcined at 400 and 600°C for 4 h was determined and will be presented in the next Chapter. The overall amount of OH may be negligible compared with the total OH removed from the original $Mg(OH)_2$, but it may be significant when it is considered that on the MgO surface it occupies about 20-40 % of the total surface area. Therefore we can conclude that the surface properties of MgO obtained from the calcination temperatures lower than 800°C do not only represent MgO, but Mg-OH species also. As a result MgO obtained from calcining temperatures of 400 and 600°C were not used as catalysts for the oxidative coupling of methane in the present work. The main objective of this work is to investigate the effect of morphology and identify the active sites and the basicity on the catalytic activity in methane coupling over MgO catalysts. The presence of residual OH on MgO surface may interfere with the relationship between these properties.

2.5.3.2 MgO calcined from $Mg(OH)_2$ by different heating procedures

Coluccia et al. (1987) reported that $Mg(OH)_2$ slowly decomposed at 220°C and finally outgassed at 850°C gives high surface area MgO samples (200 m^2/g). It was anticipated that varying calcination conditions would provide MgO samples with different surface structures. Results are displayed as follows.

Table 2.5 Surface areas of MgO calcined using different procedures.

Calcining T (°C), holding period at final temperature	800, 4 h	TP to 850, 10 min	TP to 800, 4 h
surface area, BET (m^2/g)	49	82	89

TP denotes temperature programmed calcination procedure.

Calcining condition (°C)	Particle sizes < 1 μm (%)	Particle sizes 1-10 μm (%)	Particle sizes > 10 μm (%)	Average particle size (μm)
800, 4 h	5.6	68.4	26.0	5.8 ± 0.2
TP to 850, 10 min	1.3	71.3	28.7	7.1 ± 0.3
TP to 800, 4 h	0.6	49.0	50.4	10.3 ± 0.4

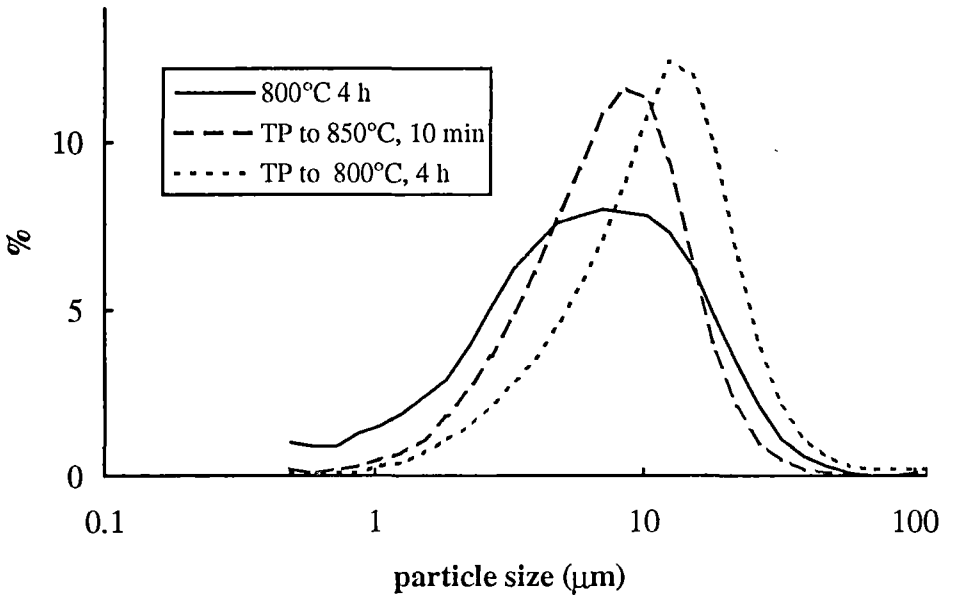

Figure 2.16 Particle size distribution of MgO calcined from $Mg(OH)_2$ using different calcining procedures.

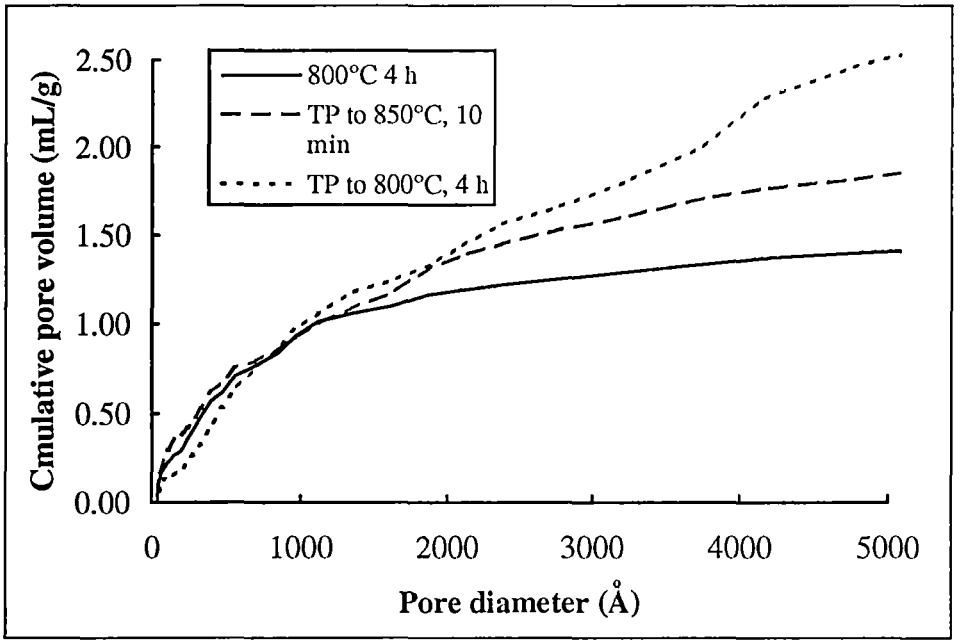

Figure 2.17 Cumulative pore volume of MgO calcined from $Mg(OH)_2$ using different calcining procedures.

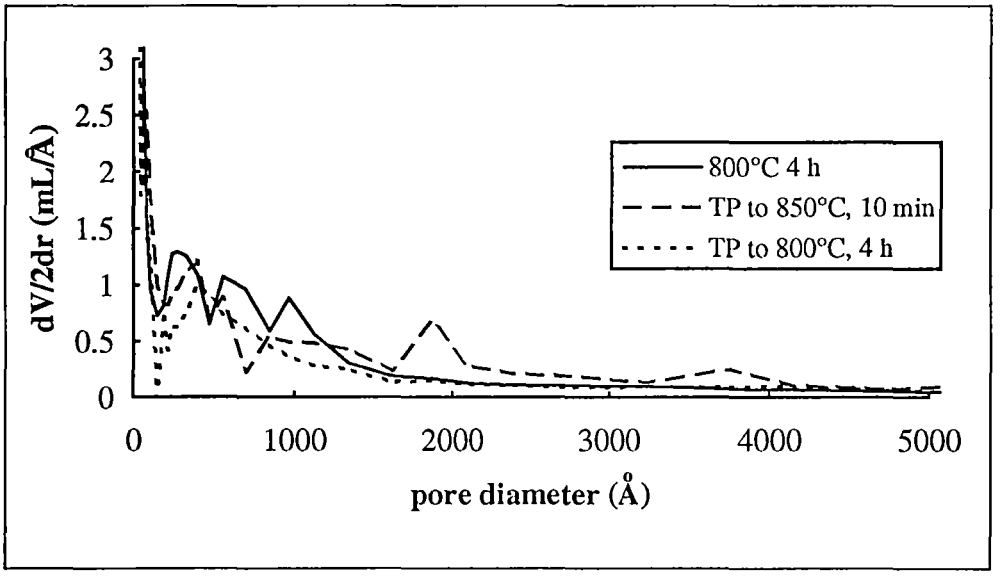

Figure 2.18 Pore size distribution of MgO calcined from $Mg(OH)_2$ using different calcining procedures.

The calcination conditions, especially allowing $Mg(OH)_2$ to slowly decompose at low temperature, have a very significant effect on the MgO morphology. MgO calcined by a temperature programmed ramp and held at 800°C for 4 h showed a higher surface area and higher pore volume than that of MgO calcined by increasing the temperature (about 20 °C/min) directly to 800°C and holding at this temperature for 4 h. For MgO samples calcined by the temperature programmed method, it was observed that the one which was held at 800°C for 4 hours has a larger particle size, larger average pore size and pore volume. However, the surface areas of these MgO were found to be similar. This means that the period of holding at 800°C for 4 h has virtually no effect on the surface area of MgO calcined using the temperature programmed method.

From these observations it is likely that different calcining procedures result in different agglomerations of MgO during the sintering process. With normal calcination (increasing directly to the final temperature), the small particles would be expected to aggregate together with only a small space created inside the larger particle. This leads to a significant reduction of surface area and cumulative pore volume. The process of slow decomposition of $Mg(OH)_2$ at low temperatures seems to allow the MgO crystals to agglomerate in the form that the external surface of the individual particles may be partially converted into an internal surface of a bigger particle as shown in Figure 2.19. This results in a slight reduction of surface area but higher cumulative pore volume. As a result, MgO calcined by the temperature programmed method had a higher surface area and cumulative pore volume than the sample calcined by the normal calcination procedure.

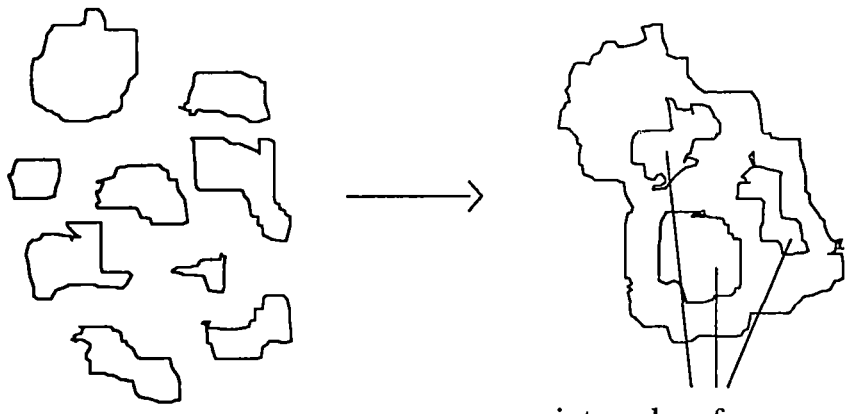

(a) (b)

Figure 2.19 The external surface area of individual particles (a) is partially converted into an internal surface (b) when the agglomerate is formed (Gregg, 1982).

2.5.4 Surface area, particle size and pore size of MgO obtained from different Mg salts calcined at 800°C for 4 h

Five MgO samples obtained from different Mg salts, namely $Mg(OH)_2$ prepared by either precipitation or hydrolysis, $MgCO_3.H_2O$, $4MgCO_3.Mg(OH)_2.5H_2O$ (basic carbonate) and $MgC_2O_4.2H_2O$, were analysed for their surface area, particle size and pore size. The results are shown in Table 2.6 and Figures 2.20, 2.21 and 2.22.

Table 2.6 Surface area of MgO prepared from different Mg salts calcined at 800°C for 4 h.

Precursor	$Mg(OH)_2$ precipitate	$Mg(OH)_2$ hydrolysis	$MgCO_3$ $.H_2O$	$4MgCO_3.Mg$ $(OH)_2.5H_2O$	$MgC_2O_4.$ $2H_2O$
Surface area, BET (m^2/g)	49	38	24	23	30

Precursor	Particle sizes < 1 μm (%)	Particle sizes 1-10 μm (%)	Particle sizes > 10 μm (%)	Average particle size (μm)
$Mg(OH)_2$ precipitate	5.6	68.4	26.0	5.8 ± 0.3
$Mg(OH)_2$ hydrolysis	6.1	82.8	11.1	4.3 ± 0.2
$MgCO_3.H_2O$	23.4	68.4	8.2	3.0 ± 0.5
$4MgCO_3.Mg(OH)_2.5H_2O$	11.9	48.8	39.3	8.2 ± 0.8
$MgC_2O_4.2H_2O$	5.7	93.7	0.6	3.5 ± 0.1

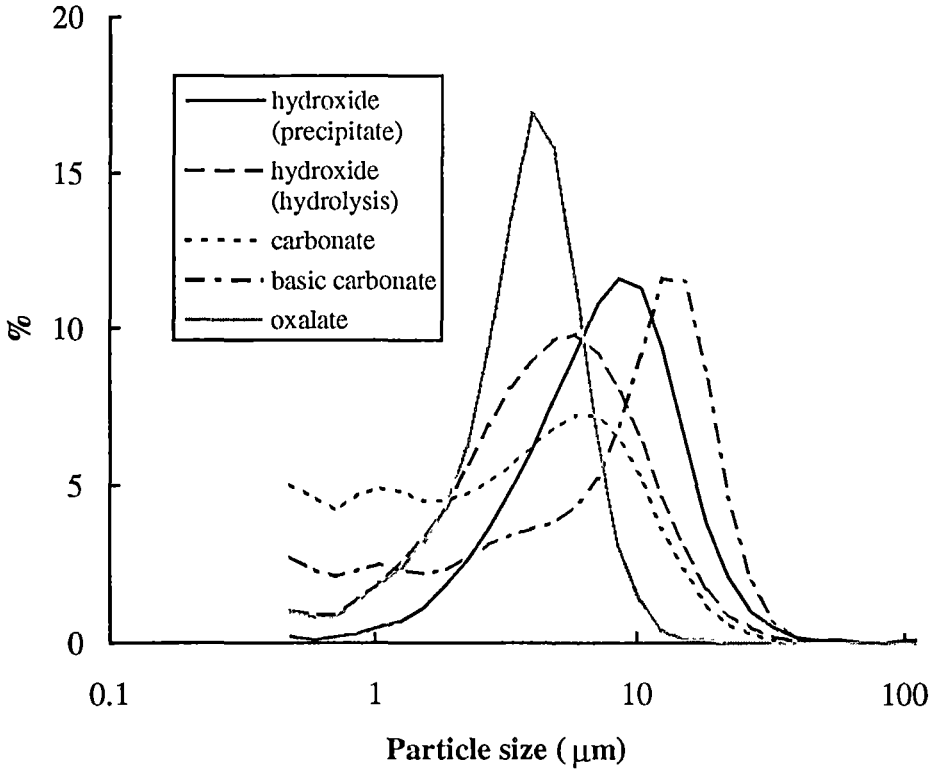

Figure 2.20 Particle size distribution of MgO calcined from different Mg salts.

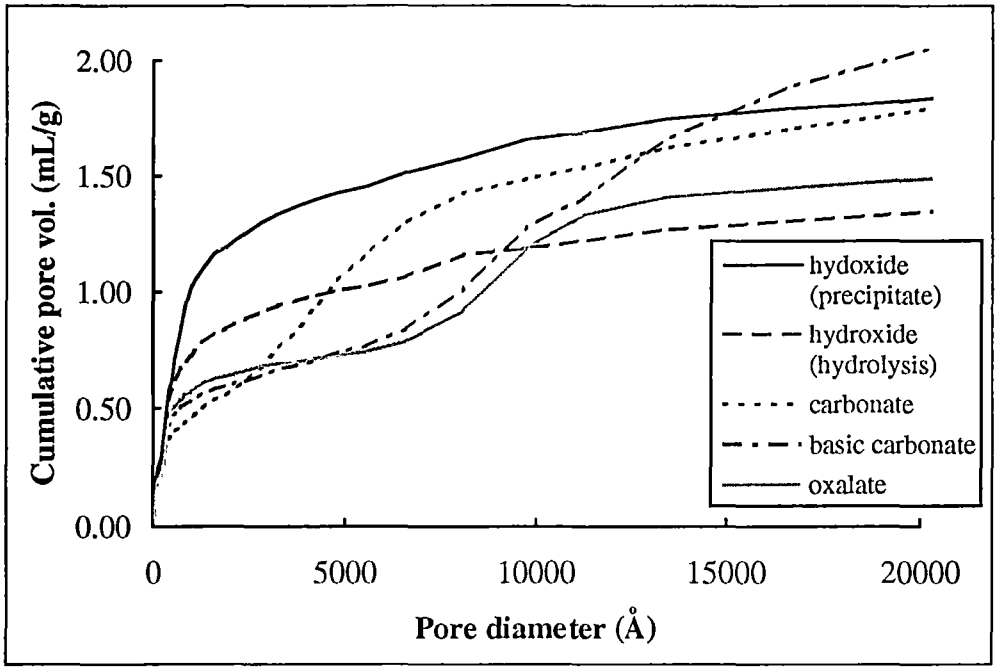

Figure 2.21 Cumulative pore volume of MgO calcined from different Mg salts.

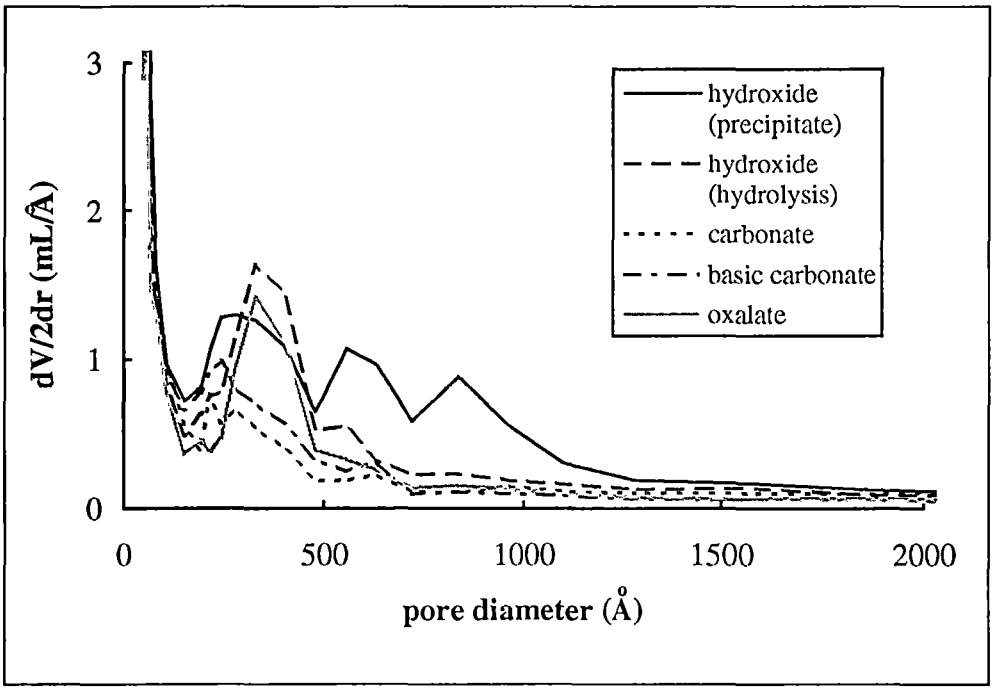

Figure 2.22 Pore size distribution of MgO calcined from different Mg salts.

For MgO obtained from $Mg(OH)_2$ it was observed that the sample prepared via the precipitation method has higher surface area (Table 2.6), larger particle size (Figure 2.10) and larger pore size and pore volume (Figures 2.21 and 2.22) than the MgO sample prepared via hydrolysis. The MgO prepared via the hydrolysis method was slightly gray. It was likely that there was some carbon deposited in the sample. The carbon impurity may arise from the decomposition of residual acetate which was not totally removed. Such contamination results in a low surface area, small particle size and small pore size with low pore volume.

Moodie and Warble (1971) and Hargreaves et al. (1992) found from the transmission electron micrographs (TEM) that MgO obtained from thermal decomposition of basic carbonate shows a smaller and less regular shape than that of MgO prepared from $Mg(OH)_2$. Similar results were obtained in the present work. Considering the particle size distribution of MgO samples calcined from different Mg salts (Figure 2.20), it was noted that MgO calcined from the carbonates ($MgCO_3.H_2O$ and $4MgCO_3.Mg(OH)_2.5H_2O$) have irregular particle size distribution profile with a high number of very fine particles (< 1 μm). The MgO samples obtained from the hydroxide and oxalate show regular particle size distribution; however, the hydroxide precursor gives MgO samples with larger average particle size.

According to Green (1983) MgO produced from the carbonate and oxalate does not show a topotactical particle formation (the formation of highly orientated layers of MgO due to the face-to-face orientation of precursor particles (Figure 2.5)) as MgO obtained from the hydroxide. This seems to indicate that MgO calcined from the hydroxide has a higher crystal ordering than that obtained from the other precursors. With respect to this assumption, coupled with the particle size distribution data, it could be deduced that the irregular particle size distribution arises from the many defects in the MgO microstructure. For the regular particle size distribution

profiles, MgO that possesses the larger average particle size has higher crystal ordering.

For the pore structures (Figures 2.21) MgO calcined from the carbonates display the lowest cumulative pore volume within pore sizes 36-2000 Å where a high number of pores were found in the pore size range of mesopores 200-300 Å (Figure 2.22). Within the same pore size range MgO obtained from the oxalate has slightly higher cumulative pore volume (Figures 2.21) than that obtained from the carbonates, and a high number of pores were found in pore size range of mesopores 250-450 Å (Figure 2.22). MgO calcined from the hydroxide has the highest pore volume with a large number of pores in the range 36-1000 Å. These results indicate that the hydroxide precursor gives MgO with a higher number of pores than the other precursors. The higher number of pores are supposed to result in a higher surface area of MgO. From Table 2.6 it was noted that the values of surface area are in accordance with the cumulative pore volume of these pores (36-1000 Å). This supports the conclusion that the high surface area of MgO is a result of the large number of these pores.

It was also observed that MgO calcined from the oxalate and basic carbonate exhibited an additional increase in pore volume consistent with a pore size in the range 8000-12000 Å. This increase in pore volume, however, was not found to be associated with an increase in the surface area of MgO and was most likely due to the intrusion of mercury into small cracks or macropores contained within the mesopores (200-500 Å). It was also noted for these two MgO samples that there are two types of molecules evolved during the decomposition of precursors (H_2O and CO_2 from basic carbonate, and CO and CO_2 from the oxalate). The cracks or very large pores may arise from the evolution of different gases at different temperatures during the decomposition of precursors.

It is concluded that there is a relationship between the crystal ordering and the morphology of MgO obtained from different Mg salts. The morphology of MgO calcined from the hydroxide is the model having less defects in the microstructure. With respect to this and the pore structure data it may be concluded that the high surface area, high pore volume within pore size range 36-1000 Å are the characteristics of MgO with high crystal ordering or with less defects.

2.6 Conclusion

A number of MgO samples were prepared via different methods of preparation and precursors. These are summarised in Tables 2.7.

Table 2.7 MgO prepared from different methods and precursors.

MgO	Precursors	Calcination T (°C)
ex OH9.5, TP	$Mg(OH)_2$ precipitated at pH 9.5	temperature programmed; 15°C/min to 350°C, 350° 45 min, 5°C/min to 850°C, 850°C 10 min
ex OH10.0, TP	$Mg(OH)_2$ precipitated at pH 10.0	the same as above
ex OH11.0, TP	$Mg(OH)_2$ precipitated at pH 11.0	the same as above
ex OH, TP	$Mg(OH)_2$ precipitated at pH 10.0	temperature programmed; 15°C/min to 350°C, 350° 45 min, 5°C/min to 800°C, 800°C 4 h
ex OH, 400	$Mg(OH)_2$ precipitated at pH 10.0	400°C in Ar for 4 h
ex OH, 600	the same as above	600°C in Ar for 4 h
ex OH, 800	the same as above	800°C in Ar for 4 h
ex OH, hyd	$Mg(OH)_2$ from the hydrolysis of $Mg(CH_3COO)_2$	the same as above
ex CO_3	$MgCO_3.H_2O$	800°C in Ar for 4 h
ex ba. CO_3	$4MgCO_3.Mg(OH)_2.5H_2O$	800°C in Ar for 4 h
ex Ox	$MgC_2O_4.2H_2O$	800°C in Ar for 4 h

These MgO were characterized for the surface areas, particle size distributions and pore structures. The results are summarised in Table 2.8.

Table 2.8 Surface areas, particle size distributions and pore volumes of MgO obtained from different preparation methods and precursors.

MgO	Surface area, BET (m^2/g)	Particle size distributions			Pore volume (36-3000 Å) (mL/g)
		< 1 μm (%)	1-10 μm (%)	> 10 μm (%)	
ex OH9.5, TP	80	4.8	56.2	39.0	1.05
ex OH10.0, TP	82	1.3	71.3	28.7	1.35
ex OH11.0, TP	80	5.8	60.7	33.5	1.25
ex OH, TP	89	0.6	49.0	50.4	1.70
ex OH, 400	210	10.2	81.3	8.5	1.40
ex OH, 600	95	9.6	83.5	6.9	1.23
ex OH, 800	49	5.6	68.4	26.0	1.23
ex OH, hyd	38	6.1	82.8	11.1	0.90
ex CO_3	24	23.4	68.4	8.2	0.71
ex ba. CO_3	23	11.9	48.8	39.3	0.67
ex Ox	30	5.7	93.7	0.6	0.70

From Table 2.8 it can be seen that the pH during the precipitation of $Mg(OH)_2$ does not have a significant effect on the MgO surface area provided that the residual NO_3^- ions have been removed. However, the effect of pH during the precipitation of

$Mg(OH)_2$ on MgO surface structure was observed from the porosimetry characteristics of mercury porosity and particle size distribution profiles. The particle size distribution of MgO ex OH9.5, TP showed the broadest shape and largest average particle size, whereas MgO ex OH10.0, TP displayed the narrowest shape and smallest average particle size. From mercury porosimetry it was found that the MgO ex OH10.0, TP has the highest cumulative pore volume and also the largest pore size, while MgO ex OH9.5, TP has the lowest cumulative pore volume and the smallest pore size.

The presence of residual NO_3^- left in the $Mg(OH)_2$ precursor seems to have a significant effect on MgO surface area. Without thorough washing to remove residual NO_3^-, a large variation in MgO surface areas was obtained. Data from UV spectroscopy in conjunction with the BET surface areas have indicated that the presence of residual NO_3^- in $Mg(OH)_2$ probrably activates the sintering process and cause the reduction in MgO surface area. The particle size of MgO was also found to be influenced by the presence of residual NO_3^-; the higher the concentration of NO_3^- left in the precursor, the smaller the average particle size. The presence of residual NO_3^- left in the $Mg(OH)_2$ precipitate was observed to have only a slight effect on the cumulative pore volume and average pore size.

For MgO obtained from $Mg(OH)_2$ calcined at different calcining temperatures (400, 600 and 800°C for 4 h), it was observed that lower surface area, larger particle size and larger average pore size were obtained using a higher calcination temperature, while the cumulative pore volume is unchanged with temperature. The calcining procedure was also found to have a significant effect on MgO morphology. It can be seen from the comparison between MgO ex OH, 800 and ex OH TP that temperature programmed (TP) calcining gives the higher surface area, larger particle size, larger pore size and higher cumulative pore volume than MgO obtained by heating to 800°C

directly. This may be due to the slow heating rate of the temperature programmed procedure allowing the primary particles to assemble more fully. Considering MgO calcined using the temperature programmed procedure (ex OH10.0, TP and ex OH, TP), it is likely that holding the temperature after the final ramp (800°C 4 h) seems to increase the particle size, pore size and (only slightly) the surface area, but the cumulative pore volume is slightly decreased. Sintering of the MgO particles is the possible cause of these effects.

MgO calcined from different precursors shows a variety of surface properties. MgO calcined from the oxalate exhibits a narrower particle size distribution and smaller average particle size than that of prepared from the hydroxide, while MgO calcined from the carbonates have irregular particle distribution profiles. For the pore structures, MgO calcined from the hydroxide displays the highest cumulative pore volume in the pore sizes range 36-3000 Å with large number of pores sizes about 200-1000 Å. MgO prepared from the carbonates and the oxalate have a low cumulative pore volume in the pore size range 36-3000 Å. Since MgO obtained from the hydroxide has the highly orientated microstructure (Green, 1983), it is assumed that this MgO has a higher degree of crystal ordering than that obtained by the other precursors. The morphology of MgO calcined from the hydroxide is associated with low defects in microstructures. The defect concentration in MgO crystals is supposed to be in the order ex CO_3 and ba. CO_3 > ex Ox > ex OH.

References

Adamson, A. W. (1976a), Physical Chemistry of Surfaces, 3rd, Los Angeles, John Wiley & Son, p 523.

Adamson, A. W. (1976b), Physical Chemistry of Surfaces, 3rd, Los Angeles, John Wiley & Son, p 278.

American Public Health Association, Standard Methods for the Examination of Water and Waste Water (1992), 18th Edition, edited by Greenberg, A. E., Clescerl, L. S., and Eaton, A. D., Washington, pp 4-87 - 4-88.

Anderson, W. C., J. Chem Soc. 87, 257 (1905).

Anderson, P. J. and Horlock, R. F. (1962), Trans. Faraday Soc. **58**, 1993.

Boudart, M., Delbouille, A. Dumesic, J. A., Khammouma, S., and Topse, H. (1975), J. Catal. **37**, 486.

Choudhary, V. R. and Pandit, M. Y. (1991), Appl. Catal. **71**, 265.

Choudhary, V. R., Rane, V. H. and Gadre, R. V. (1994), J. Catal. **145**, 300.

Coluccia, S., Marchese, L., Lavagnino, S., and Anpo, M. (1987), Spectrochim. Acta **43A** (12), 1573.

Copperthwaite, M. and Brett, N. H. (1976), Sci. Ceram. **8**, 85.

Delannay, F. (1984), Characterization of Heterogeneous Catalysts, New york, Marcel Dekker, pp 54-57.

Dell, R. M. and Weller, S. W. (1959), Trans. Faraday Soc. **55**, 2203.

Dubinin, M. M. (1960), Chem. Rev. **60**, 235.

Dunski, H., Jozwiak, W. K., and Sugier, H. (1994), J. Catal. **146**, 166.

Green, J. (1983), Mater. Sci. **18**, 637.

Gregg, S. J. and Razouk, R. I. (1949), J. Chem. Soc. s36.

Gregg, S. J. (1982), Adsorption, Surface area and Porosity, London, Academic Press, pp 173-190.

Hargreaves, J. S. J., Hutchings, G. J., and Joyner, R. W. (1990), Catal. Today **6**, 481.

Hattori, H., Shimazu, K., Yoshii, N., and Tanabe, K. (1976), Bull. Chem. Soc. Japan **49**, 969.

Hattori, H. (1985) in " Adsorption and Catalysis on Oxide Surfaces" ed. Che, M. and Bond, G. C., Elsevier, Amsterdam, pp 319-330.

Holt, T. E., Logan, A. D., Chakraborti, S., and Datye, A. K.(1987), Appl. Catal. **34**, 199.

IUPAC Manual of Symbols and Terminology, Appendix 2, Pt. 1, Colloid and Surface Chemistry. Pure Appl. Chem. (1972) **31**, 578.

Jenkins, H. D. B. and Thakur, K. P. (1979), J. Chem. Educ., **56**, 576.

Logan, A. D. and Datye, A. K. (1988), J. Catal. **112**, 595.

Lopez, T., Gracia-Cruz, I., and Gomez, R. (1991), J. Catal. **127**, 75.

Moodie, A. F. and Warble, C. E. (1971), J. Cryst. Growth **10**, 26.

Razouk, R. I. and Mikhail, R. S. (1957), J. Phys. Chem. **61**, 886.

Razouk, R. I. and Mikhail, R. S. (1959), J. Phys. Chem. **63**, 1050.

Rhodes, W. H. and Wuensch, B. J. (1973), J. Amer. Ceram. Soc. **56**, 495.

Shastri, A. G., Chae, H. B., Bretz, M., and Schwank, J. (1985), J. Phys. Chem. **89**, 3761.

Sidjabat, O., Trimm, D. L., and Wainwright, M. S. (1993), J. Chem. Tech. Biotechol. **56**, 241.

Stone, J. M. (1963), Radiation and optiocs, San Francisco, New York, pp 175-176.

Svehla, G. (1979), Qualitative Inorganic Analysis, 6th Edition, Longman Scientific & Technical, p139.

Tanabe, K., Misono, M., Ono, Y., and Hattori, H. (1989), New Solid Acids and Bases, Tokyo, Kodansha, p 14.

Tauster, S. J., Murrell, L. L., and deLuca, J. P. (1977), J. Catal. **48**, 258.

Thomas, J. M. and Thomas, W. J. (1981a), Introduction to the Principles of Heterogeneous Catalysis, 5th Printing, London, Academic Press, p 181.

Thomas, J. M. and Thomas, W. J. (1981b), Introduction to the Principles of Heterogeneous Catalysis, 5th Printing, London, Academic Press, pp 45-48.

Vinek, H., Latzel, J., Noller, H., and Ebel, M. (1978), J. Chem. Soc. Faraday Trans. **174**, 2092.

Waida, T. (1941a), J Chem. Soc. Japan **62**, 955.

Waida, T. (1941b), J Chem. Soc. Japan **62**, 964.

CHAPTER 3

ACTIVE SITES AND BASICITY OF MgO

3.1 Introduction

It has long been recognised that some knowledge of the acid-base properties of the active sites on a catalyst surface helps in the understanding of observed catalytic activities (Tanabe et al., 1988). The measurement of surface acidity is a well established technique for the characterization of solid acid catalysts such as SiO_2-Al_2O_3, Al_2O_3 and zeolites. On the other hand little work has been carried out on the basicity of solid basic catalysts such as MgO and CaO. Heterogeneous solid base catalysts currently have replaced homogeneous liquid-based catalysts in the chemical industry because they tend not to corrode the reactor, do not cause major environmental problems in disposal, may be used repeatedly with or without regeneration, are easily separated after reaction, and require low energy synthesis (Tanabe, 1985). An investigation of the basicity of active sites of solid base catalysts is crucial to the interpretation and optimisation of industrial processes.

The basic strength of a solid surface is defined as the ability of the surface to donate an electron pair to an adsorbed acidic gas. Basicity is expressed as the number (or mmol) of basic sites on the solid surface per unit weight or per unit surface area of the solid (Tanabe et al., 1989). There are two main methods used to explore basic strength and basicity; benzoic acid titration using indicators, and the adsorption of gaseous acids. The benzoic titration method is generally not suitable for measuring the basicity of a catalyst because it is carried out at room temperature which is significantly different from the usual operating conditions of catalytic reactions (Choudhary and Rane, 1990). Adsorption of acidic gases is therefore preferred and the most widely used for the measurement of basicity. Probe molecules which have been used include carbon monoxide (Wang et al.,1983), carbon dioxide (Zhang et al.,

1988; Choudhary and Rane, 1990), sulphur dioxide, hydrogen (Ito et al., 1981), phenol (Xu et al., 1988) and water (Dunski et al., 1994).

The aim of the work described in this Chapter was to investigate the chemical behaviour of the surface of MgO and to identify an effective method to determine its surface sites and their relative basicity.

3.2 Literature Review

Prior to the commencement of this work, three main groups have studied the characteristics of the active centres on the surface of MgO. Coluccia et al. (1982, 1983, 1987) mainly used infrared and photoluminescence spectroscopies to obtain information of the MgO surface structure while both Ito et al. (1981, 1983a, 1983b) and Tanabe's group (Wang et al., 1983, Xu et al., 1988, and Zhang et al., 1988) relied on the temperature programmed desorption technique.

Infrared spectroscopic studies of the adsorption of three adsorbate gases, CO, H_2 and NH_3, on MgO have been reported (Guglielminotti et al., 1979, and Coluccia et al., 1982, 1983). Using carbon monoxide four structural forms were observed adsorbed on the MgO surface at room temperature. There were monomeric, dimeric and polymeric carbon monoxide as well as a carbonate structure (Guglielminotti et al., 1979). Hydrogen is adsorbed by heterolytic dissociation on MgO at 298 K, but an undissociated hydrogen appears at lower temperatures (Coluccia et al., 1982). Several adsorbed molecular species of ammonia are found on both cation and anion sites of the MgO surface (Coluccia et al., 1983). A small fraction (< 10 %) of ammonia is adsorbed in a heterolytic dissociation process on adjacent cation and anion sites and forms NH_2^- and OH^- species. The low coordination number surface species $Mg_{lc}^{2+}O_{lc}^{2-}$ (lc denotes a coordination number of less than 6, the number found in the cubic structure of bulk MgO) are assumed to be the active sites and to be responsible for all adsorptions.

The technique of photoluminescence has been introduced to study the surface structure of MgO since it was found that high surface area MgO absorbs UV light at 274 and 230 nm. These values are much lower in energy than the absorption of intrinsic bulk MgO at 160 nm. The absorption of energy leads to the formation of an excited state, Mg^+O^-, due to the electron transfer process on surface ion pairs (Coluccia et al., 1978).

$$Mg^{2+}O^{2-} + h\nu \leftrightarrow Mg^+O^-$$

The emission bands at about 400 nm were obtained as a result of the relaxation of the excited Mg^+O^- back to $Mg^{2+}O^{2-}$. As two excitation bands at 230 nm and 274 nm were employed to excite the MgO surface, it was supposed that two differently coordinated sites on the surface were activated. The band obtained by the lower excitation energies (274 nm) corresponded to the lower coordination number, 3-coordinated O^{2-} ions (O_{3C}^{2-}), while the band obtained by the excitation at 230 nm was associated with 4-coordinated O^{2-}ions (O_{4C}^{2-}) (Coluccia and Tench, 1979). The oxygen ions of coordination number 5 (O_{5C}^{2-}) were not considered to be involved in the photoluminescence process because the energies for the (100) surfaces are only slightly shifted from the bulk.

A comparison of the optical spectra of MgO smoke prepared from burning Mg ribbon in air, and MgO prepared from decomposition of hydroxide or carbonate compounds has shown different intensities of their two emission bands (Coluccia et al., 1979). The ratio of the intensities measured at the maximum of the emission spectra excited at 274 and 230 nm, I_{274}/I_{230} for MgO smoke samples was found to be approximately 0.3, whereas for MgO prepared by thermal decomposition a value of at least 1.6 was found. This was explained in terms of the variation of the proportions of surface ions in coordination states of 3 and 4. MgO specimens prepared by thermal decomposition gave a high value of I_{274}/I_{230} because of their extreme roughness and the subsequent large number of 3-coordinated ions. On the other hand, the regular

smoke particles gave spectra which were dominated by the high energy emission due to the large number of 4-cordinated ions.

Further study was carried out on MgO smoke (Coluccia et al., 1979). By adsorption of water vapour on the surface of MgO smoke and outgassing at 1200 K, the number of surface sites of low coordination was increased without the change in surface area (Figure 3.1).

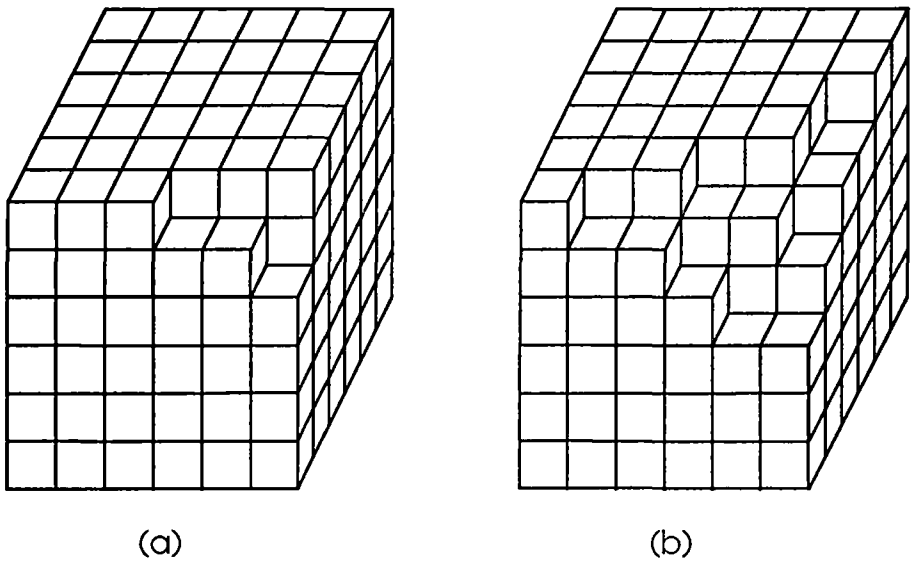

Figure 3.1 The model of etched MgO surfaces (Coluccia et al., 1979).

From this model (Figure 3.1) water vapour eroded the surface of MgO smoke (a) and resulted in MgO (b) with high number of surface site of low coordination. It was found (Coluccia et al., 1981) that photoluminescence spectra of MgO smoke after prolonged water contact (MgO (b)) showed a higher ratio of I_{274}/I_{230} than that of MgO smoke (MgO (a).

Based on this findings the authors (Coluccia et al., 1979) concluded that the differences in optical spectra of MgO prepared via different routes were due to the variation of proportions of surface ions in coordination states of three and four. In

addition, the proportions of 3- and 4-coordinated ions could be changed by erosion of the surface of MgO by water vapour.

An extensive study on MgO smoke by photoluminescence and electron spin resonance (ESR) was carried out by Coluccia et al. (1981). Adsorptions of oxygen and nitrobenzene on MgO smoke and etched MgO smoke (by the adsorption of water vapour for 20 h then out gassing at 1200 K) were studied by ESR.. It was found that etched MgO smoke showed a higher number of adsorbed O^{2-} and nitrobenzene negative ions than MgO smoke. From the emission spectra (exited at 274 nm), it was found that the etched MgO smoke showed a higher intensity of peak at 400 nm. These results indicated a higher number of surface sites of low coordination number on etched MgO smoke than on the MgO smoke.

The Temperature Programmed Desorption (TPD) technique was applied by Ito et al.(1981) to study the adsorption of hydrogen on MgO at 308 K. It was shown that MgO outgassed at 773 K displays only one TPD peak at 385 K, whilst MgO outgassed at 1123 K shows three new TPD peaks at 480, 550 and 680 K as well as the peak at 385 K. It was proposed that the adsorbed species are the result of the dissociative adsorption of H_2 on a low coordinated $Mg_{lc}^{2+}O_{lc}^{2-}$ species in various coordination environments, mainly 3 or 4. Another study of the MgO-H_2 adsorption system was carried out by gradually lowering the temperature to 77 K after exposing the sample to H_2 or D_2 at room temperature (Ito et al., 1983a). MgO powders outgassed at 1123 K showed eight different states of adsorbed species at 77 K (reversibly adsorbed), 190, 229, 283, 327, 460, 500 and 608 K respectively. The dominant site (327 K) was explored in detail and was found that the formation of these species is consistent with a heterolytic dissociation of hydrogen on a surface ion pair $Mg^{2+}O^{2-}$ with low coordination numbers.

Theoretical calculations were carried out on the active sites for hydrogen adsorption on MgO (Ito et al., 1983b). Based on the TPD results and the

spectroscopic data available from the work of Coluccia et al. (1978, 1979, 1980, 1981, 1982) and Zecchina et al. (1975) coordination numbers of the active sites were assigned as follows :

active sites/TPD peak (K)	coordination number O_{lc}^{2-}	Mg_{lc}^{2+}
190, 229	4	3
283, 327	3	4
460, 500, 608	3	3

To obtain more information, UV-irradiation-induced adsorption of hydrogen at 77 K on MgO (outgassed at 723 K) was investigated by Ito et al. (1988). Three types of adsorptions: in the dark only, pre-irradiated under vacuum, and irradiated were compared. Three desorption peaks at 190, 229 and 283 K were found for adsorption in the dark only. These were attributed to hydrogen desorptions a pair of 3- and 4- coordinated ions, O_{lc}^{2-}-Mg_{lc}^{2+}, at the nearest lattice position adsorbed hydrogen with heterolytic dissociation. TPD spectra of the pre-irradiated (obtained by the difference between adsorption at 77 K in the dark without any irradiation and that after the completion of the preirradiation in vacuo at 77 K for 1 h) displayed desorption peak at 530 K. This was assigned to the homolytic dissociation of hydrogen adsorbed on two aggregations of four O_{4c}^{2-}ions and four Mg_{4c}^{2+} ions located apart from each other. The adsorption under the influence of UV-irradiation (obtained by the difference between adsorption at 77 K for 1 h without irradiation and that under the influence of irradiation) also proceeded and gave a broad TPD peak at 320 K as well as 530 K. The adsorption sites for TPD peak at 320 K was proposed to arise from homolytic dissociation of hydrogen adsorbed on O_{3c}^{2-} and Mg_{3c}^{2+} (or Mg_{4c}^{2+}) located separately from each other.

Chemisorption of CH_4 on MgO using TPD techniques and a theoretical study using the ab initio molecular orbital method have also been carried out by Ito et al.

(1990, 1991). They identified three types of adsorption sites. Based on EPR spectroscopic evidence (Ito et al., 1987), the authors identified that all arise from the heterolytic dissociative adsorption of CH_4 (CH_3^- and H^+ species adsorbed on Mg_{lc}^{2+} and O_{lc}^{2-} respectively). The first sites corresponding to TPD peaks at 300, 360 and 440 K, were assumed to belong to the low coordination Mg_{lc}^{2+} and O_{lc}^{2-} that constitute the nearest lattice pair. The second sites were associated with TPD peak at ~ 973 K obtained when CH_4 was adsorbed at 773 K and cooled down to 223 K under a CH_4 atmosphere. These sites were assigned to be the separately located Mg_{lc}^{2+} and O_{lc}^{2-} which required thermal activation for the adsorption of CH_4. The final species associated with TPD peak at 350-800 K obtained from an irradiation, were also proposed to be the separately located Mg_{lc}^{2+} and O_{lc}^{2-}. This site could adsorb CH_4 only under more severe adsorption conditions; UV-irradiation caused activation of the site to produce O_{lc}^- from O_{lc}^{2-} prior to the adsorption process.

The Tanabe group (Tanabe, 1985, 1988; Hattori, 1985, and Wang et al., 1983) has intensively studied acid-base catalysis and has pointed out that the basic properties and the catalytic activities of solid bases are dependent on the preparation method. According to Coluccia and Tench (Coluccia and Tench, 1980) there are three types of active site, S_I, S_{II} and S_{III}, depending on the pretreatment temperature of alkaline earth metal oxides. It was supposed that the higher calcination temperature would result in the lower coordinated ions on MgO surface (Hattori, 1985). Site S_I, which appears on treatment at low temperatures, was proposed to be $Mg_{4c}^{2+}O_{4c}^{2-}$ ion pairs (Figures 3.2 and 3.3). With the higher pretreatment temperatures, S_{II} and S_{III} are obtained. Site S_{III} was assigned to be $Mg_{3c}^{2+}O_{3c}^{2-}$ since it was obtained at the highest calcination temperatures. Site S_{II} was poisoned by O_2 (Hattori and Satoh , 1976), and $3Mg_{3c}^{2+}O_{4c}^{2-}$ was considered to be most accessible to O_2 (Hattori, 1984), therefore site S_{II} was assigned to $3Mg_{3c}^{2+}O_{4c}^{2-}$.

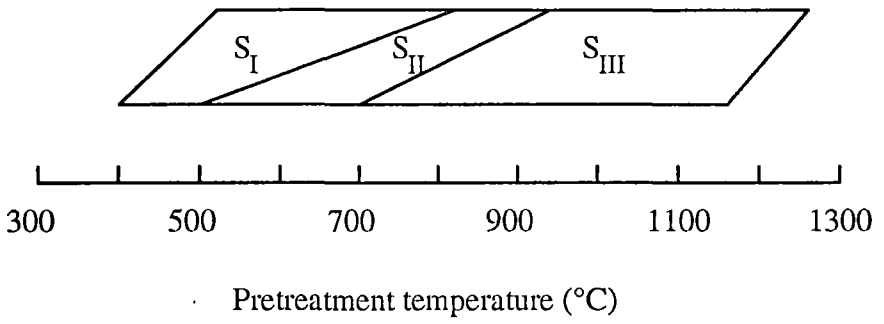

Figure 3.2 Types of sites on MgO surface calcined at different temperatures (Coluccia and Tench, 1980).

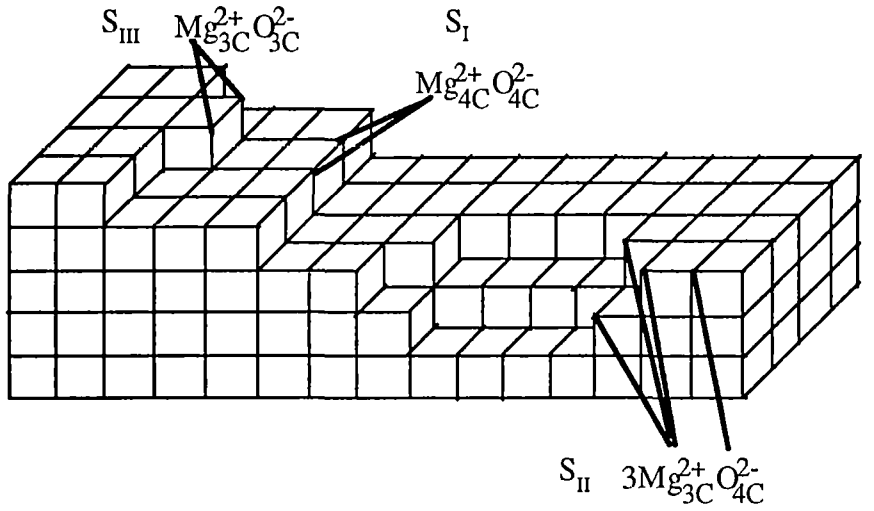

Figure 3.3 Proposed surface sites of MgO (Hattori, 1985).

The efficiency of acid and base catalysts has been discussed in terms of acid-base bifunctional catalysis (Tanabe, 1988). It was assumed that the distance between an acidic sites (metal) and basic sites (O), for particular molecules, is important for catalytic efficiency. However, most of the acid-base catalysts are more or less amorphous and it is difficult to accurately determine the distance between the metal and oxygen atoms. One promising technique for the characterization of the bifunctional nature of solid catalysts is the use of probe molecules such as phenol, which have both acidic and basic groups.

The temperature programmed desorption of phenol and infrared spectroscopic techniques were employed to study the acid-base properties of SiO_2-Al_2O_3 (SA), MgO and ZnO_2 by Xu et al. (1988). It was found that the desorption of phenol gave a single peak in the TPD profiles of SA and ZrO_2 at 363 and 780 K respectively, but complicated profiles, ranging between 373 K and 723 K, were obtained for MgO. All these profiles were consistent with heterolytic dissociation of phenol into the phenolate ion and a proton. However, the orientation of phenolate ions on the MgO and SA surfaces are different. According to the difference in ortho-selectivity of alkylation of phenol over MgO and SA catalysts, the authors suggested that the plane of benzene ring of the phenolate ion is parallel to the surface on SA, but almost perpendicular to the surface on MgO. The perpendicular orientation of benzene ring on the surface of MgO results in the higher ortho-selective products (Tanabe and Nishizaki, 1977). It was pointed out that the acid strength of SA is very high, and can interact with the π-electrons of the benzene ring, but this interaction does not appear on weakly acidic MgO.

The temperature programmed desorption of CO_2 on alkaline earth oxides, MgO, CaO, SrO and BaO, has been used by the Tanabe group (Zhang et al., 1988). It was estimated that the base strength of these catalysts was in the order BaO>SrO>CaO>MgO. However, the TPD profile of CO_2 varies depending on the adsorption conditions, with only a broad desorption peak occurring if too much CO_2 is adsorbed. IR spectroscopic evidence reported by Evans and Whately (1967) showed that there are different forms of CO_2 adsorbed on MgO: unidentates, bidentates, carbonates and bicarbonate species depending on the adsorption conditions.

Stepwise thermal desorption (STD) of CO_2 on MgO and CaO was studied by Choudhary and Rane (1990). CO_2 was desorbed in a number of successive temperature steps, 50-150°C, 150-300°C, 300-450°C, 450-600°C, 600-900°C. The temperature was increased at a rate of 30°C/min and the maximum temperature of

each step was maintained for 30 min to desorb the volatile CO_2. It was found that the increase in calcination temperature from 600 to 950°C resulted in a large decrease in both the total number of basic sites and the base strength per unit weight on both MgO and CaO. A decrease in base strength per unit surface area on both catalysts was also observed.

Three desorption peaks for CO on MgO were observed at 430K, 470K and 560 K by means of temperature programmed desorption (Wang et al., 1983). The relative amounts of the three types of adsorbed CO varied with the pretreatment temperature of MgO and with the adsorption conditions. It was revealed by IR measurement that the adsorbed species at 430 K and 560 K were $(CO)_6^{2-}$ and $(CO)_2^{2-}$ (Wang and Hattori, 1984).

Dunski et al. (1994) have carried out temperature programmed desorption of water on the surface of MgO to look at the influence of the dehydroxylation process on the generation of the low coordinated sites, $Mg_{3c}^{2+}O_{4c}^{2-}$ and $Mg_{4c}^{2+}O_{3c}^{2-}$, which occur at the corners of the MgO crystal (100) face. It was found that there were at least four energetically different forms of adsorbed water, which gave TPD peaks at about 370, 570, 700 and 1150 K respectively. The first peak at about 370 K was proposed to be the desorption of water molecules weakly bounded (via hydrogen bonding) with the hydroxylated MgO surface. The second peak at about 570 K was assigned to the desorption of water molecules with a hydroxyl group pair condensed on the flat surface of MgO. The third TPD peak at 700 K was attributed to the desorption of more strongly bound water from the vicinity of the low coordinated MgO sites and the removal of the more isolated remaining hydroxyl groups on the flat surface. The last peak at about 1150 K was assigned to the desorption of water from the low coordinated MgO sites.

3.3 Experimental and Results

Several different approaches based on temperature programmed desorption of an adsorbed gas were attempted. These included the use of fourier transform infra-red spectroscopy to study the species adsorbed on the surface as a function of increasing temperature, differential thermal analysis to observe any thermal changes which occurred during the desorption process and the use of a thermal conductivity detector to detect desorbed material and a microbalance to determine the mass loss of sample during desorption.

3.3.1 Infrared spectroscopic study of adsorbed species on the surface of MgO

Infrared spectroscopy, which is a well established technique (Fierro, 1990) for the study of adsorbed species, was used to investigate the surface of MgO prior to and after the adsorption of phenol. The infrared cell (Figure 3.4) used by Larkins and Nordin (1989) for in situ catalytic analysis was employed. Vycor tubing of 18.5 mm outside diameter (o.d.), 15.5 mm inside diameter (i.d.). was used as the cell body. At each end calcium fluoride windows were attached by means of Cajon Ultra Torr fittings on brass flanges. The gas inlet was connected to one flange and the gas outlet to the other. The sample was mounted between quartz tubes of 14.5 mm o.d., 11.5 mm i.d.. The cell body was heated by a removable microfurnace which was controlled by an electronic temperature controller via a small thermocouple situated on the sample surface. The maximum temperature attainable by the furnace was 750°C which is slightly less than the maximum value of 800°C used in other experiments.

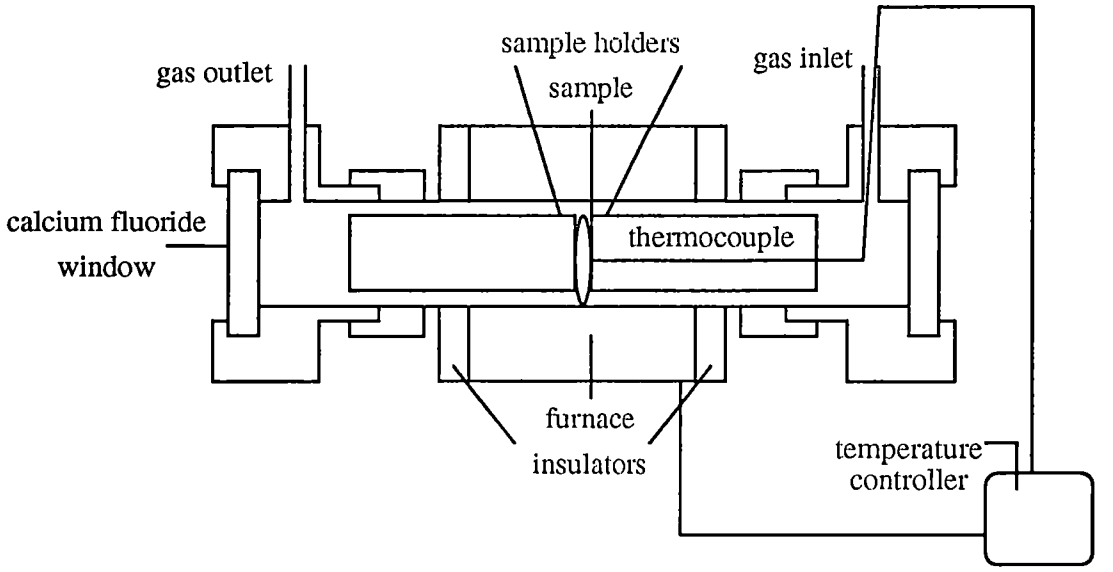

Figure 3.4 The profile of an infrared cells.

Approximately 15-20 mg of $Mg(OH)_2$ was compressed into a self-supporting disc of 11 mm in diameter and mounted in the cell. It was then calcined under argon (CIG, high purity) at a flow rate of 10 mL/min at desired temperatures (400, 600 and 750°C for 4 h) and cooled to room temperature. A background infrared spectrum of MgO was recorded by a Digilab FTS-20E FTIR Spectrophotometer over the frequency range 4000 cm^{-1} to 1000 cm^{-1}. The sample was then exposed to the phenol (Aldrich 99 % +) for 30 min (at a carrier gas (argon) flow rate of 10 mL/min) and then purged with carrier gas for 1 h at a high flow rate of 50 mL/min. The MgO was then heated at a rate of 5°C/min and the spectra were recorded at a range of temperatures. The background MgO spectrum was subtracted from each of the obtained spectra.

3.3.1.1 MgO spectra

Coluccia et al. (1987) and Dunski et al. (1994) investigated water adsorbed on the surface of MgO and found that at temperatures over 673 K (400°C) but lower than 1073 K (800°C) residual OH species were observed on the MgO surface. These

OH species were predominantly free of any hydrogen bonding to other neighbours. In addition, Kuroda et al. (1988) reported that during the preparation of MgO bulk OH can be dehydrated at temperatures lower than those of surface free OH. As a result it is likely that MgO samples obtained by calcining at temperatures of 400°C and 600°C for 4 h may have residual OH species remaining on the surface. To clarify this infrared spectroscopy was employed. The IR spectra, in the 4000-2000 cm^{-1} region, of MgO samples calcined at different temperatures are shown in Figure 3.5.

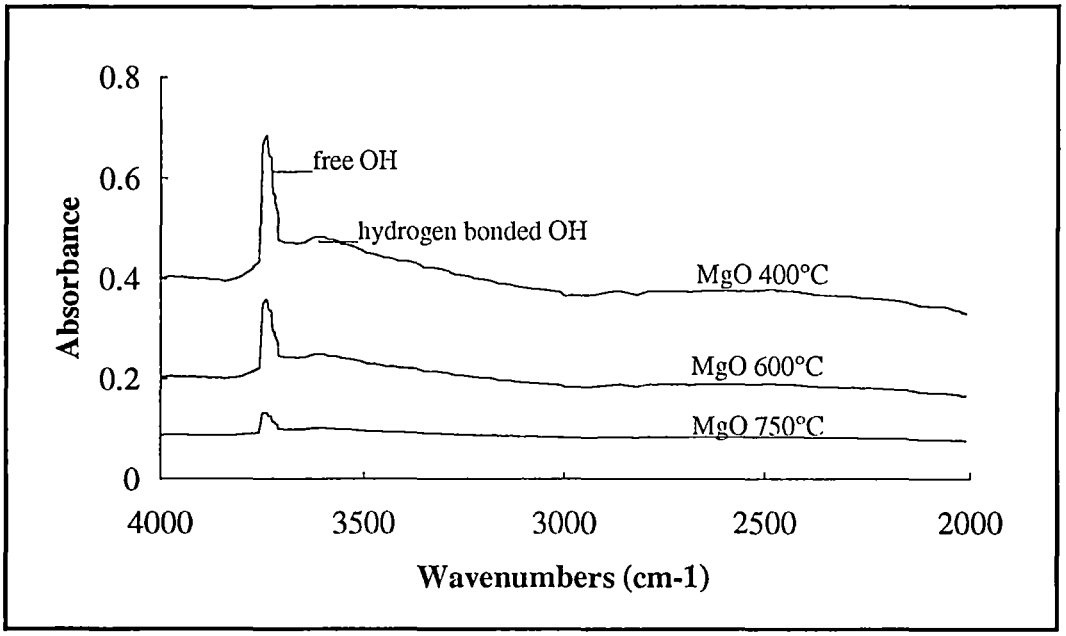

Figure 3.5 The infrared spectra (at 35°C) of MgO (~ 30 mg) calcined from $Mg(OH)_2$ at 400, 600 and 750°C for 4 h.

It can be seen that the sharp peak at 3740 cm^{-1} decreases with increasing calcination temperature and almost disappears at the calcining temperature of 750°C. This peak was identified by Echterhoff and Knozinger (1988) as being characteristic of free OH without hydrogen bonding, while the broad band centred at 3550 cm^{-1} was assigned to OH stretching vibration associated with hydrogen bonding as follows:

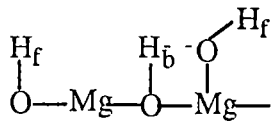

OH_b = hydrogen bonded OH, OH_f = free OH.

Coluccia et al.(1987) have also proposed that the sharp peak observed at 3740 cm^{-1} is the OH stretching vibration on corners and edges, and the peak at 3450-3650 cm^{-1} is the OH stretching vibration on the extended planes. The hydroxyls on extended faces are expected to absorb at lower frequencies (3450-3650 cm^{-1}) due to more extensive hydrogen bonding, while the OH groups on corners and edges are perturbed by a lower number of next-neighbours and absorb at 3740 cm^{-1}. Accordingly, it can be concluded that the residual OH species were retained on the surface of MgO calcined at temperature of lower than 800°C.

The amount of residual OH remaining on the MgO surface after calcining at 400°C, 600°C and 800°C for 4 h was determined by means of thermo-gravimetric analysis. The in situ MgO samples were heated at a ramp rate of 5°C/min from 30 to 900°C and held at this final temperature for 10 min. The residual OH groups were determined from the total weight loss as the amount of water desorbed from the MgO (see Figure 3.6). No significant amount of weight loss was observed from the TG experiment for MgO calcined at 800°C.

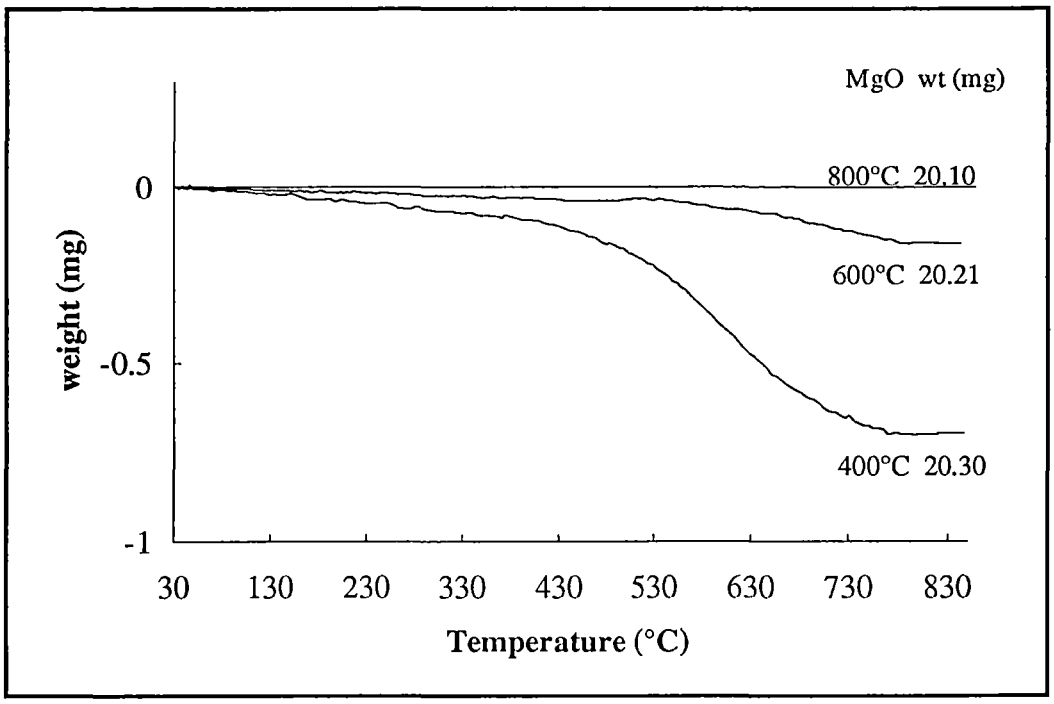

Figure 3.6 Weight loss profiles of MgO calcined at 400°C, 600°C and 800°C; the ramp rate was 5°C/min.

From Figure 3.6 the weight loss for MgO calcined at 400 and 600 were 0.7 and 0.15 mg respectively. It was estimated that about 1.91 and 0.41 mmol of water was retained on 1 g of MgO calcined at 400°C and 600°C respectively. The surface area occupied by these residual OH groups was determined using the assumption that an area of 100 $Å^2$ contains a monolayer of adsorbed water corresponding to 12 H_2O molecules or 24 OH groups (Coluccia et al., 1987). It was found that about 96 m^2/g or 46 % of the total surface area (210 m^2/g; determined by BET method) for MgO calcined at 400°C, and about 21 m^2/g or 22 % of the total surface area (95 m^2/g) for MgO calcined at 600°C was occupied by residual OH groups.

Using infrared spectroscopy, Coluccia et al. (1987) have carried out the dehydroxylation of water from the surface of MgO (obtained from slow decomposition of $Mg(OH)_2$ in vacuo at 493 K and finally outgassed at 1123 K). Water was adsorbed on MgO at room temperature and heated to 373, 473, 573, 673,

773, 873, 973 1073 K for 30 min. The residual OH coverages at these temperatures were found as follows:

Temperature (K)	373	473	573	673	773	873	973	1073
Residual OH coverage	1.00	0.55	0.36	0.25	0.15	0.09	0.03	0.00

The coverages on the surface of MgO at 400 and 600°C (673 and 873 K) were 25 and 9 % of surface area respectively. These values are less than the values obtained in the present work by a factor of 2. This is likely to be due to different conditions used. Coluccia et al. (1987) carried out their experiment under vacuum condition, while this work was carried out under an argon atmosphere. These results indicate the influence of condition used on the surface of MgO.

3.3.1.2 Infrared spectra of phenol adsorbed on MgO

The IR spectra of phenol adsorbed on the surface of MgO were recorded at a number of temperatures. The spectrum at each temperature was obtained via the difference between the absorption of adsorbed phenol on MgO and a reference spectrum of the clean MgO surface (which were recorded at the same temperatures). Results are displayed in Figure 3.7 and Figure 3.8 respectively.

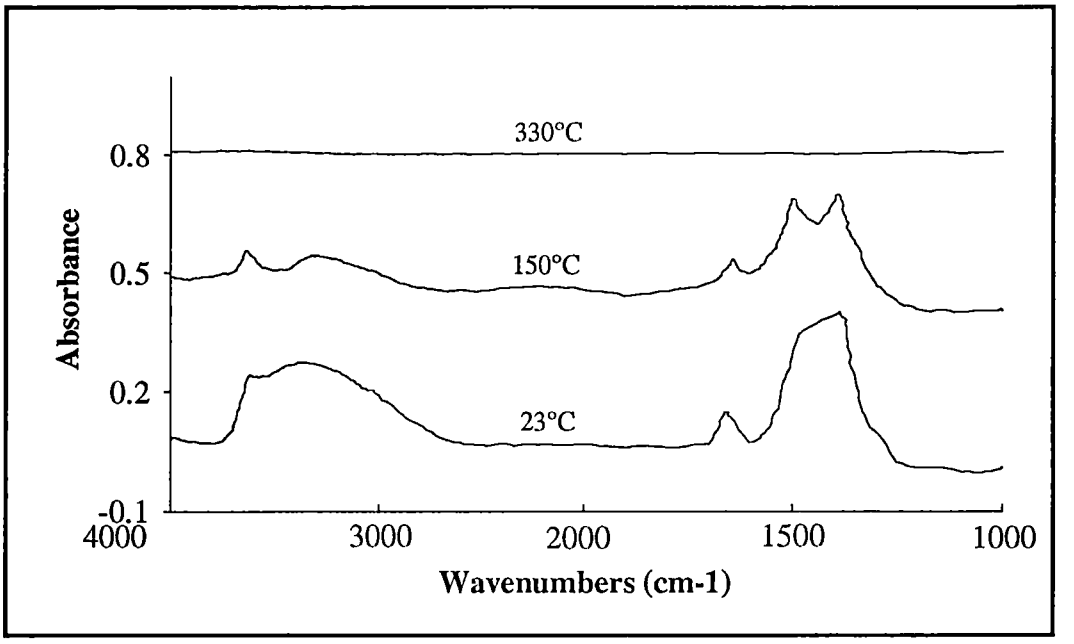

Figure 3.7 IR spectra of phenol adsorbed on MgO (calcined at 600°C for 4 h) recorded at room temperature, 150°C and 330°C.

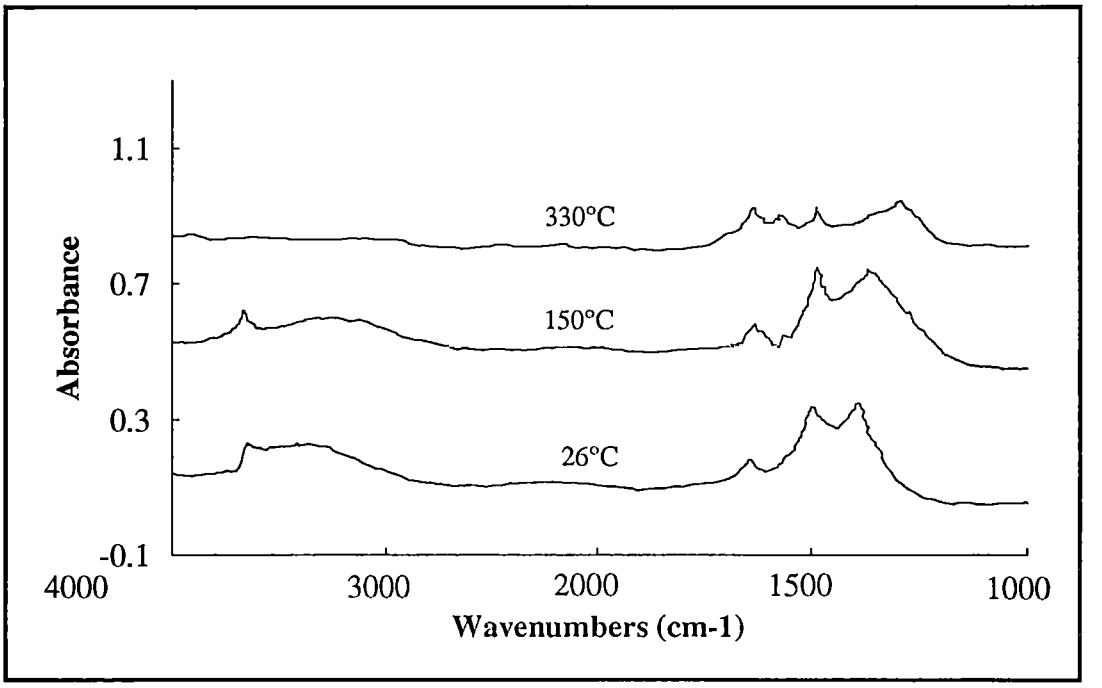

Figure 3.8 IR spectra of phenol adsorbed on MgO (calcined at 750°C for 4 h) recorded at room temperature, 150°C and 330°C.

From Figures 3.7 and 3.8 it can be observed that phenol adsorbed on MgO displays two strong absorption regions, namely at 2800-3650 cm^{-1} and 1300-1600 cm^{-1}. The broad band at 2800-3650 cm^{-1} significantly decreased with increasing temperature and disappeared at temperatures above 150°C. This band is assigned to the absorption of OH species arising from the dissociative adsorption of proton from phenol adsorbed on the O^{2-} of the MgO surface (and a phenolate ion adsorbed on Mg^{2+}). At low temperatures these OH species may from a hydrogen bond with their near neighbours or physisorbed phenol that is loosely bound to this chemisorbed species as follows:

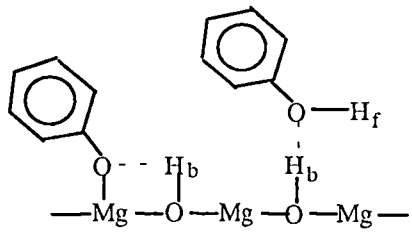

OH_b = hydrogen bonded OH, OH_f = free OH.

As the temperature was increased to 150°C this band became less prominent due to the elimination of the physisorbed species. It was noted that the intensity of this band was observed to be higher for MgO calcined at 600°C. This is likely to be due to the residual OH groups that were initially present on the MgO surface prior to the adsorption of phenol; the more OH species on the MgO surface, the stronger the absorption in the 2800-3650 cm^{-1} region.

The absorption in the 1300-1600 cm^{-1} region was attributed to phenolate species, from the C=C stretching of the benzene ring of phenol and the C–O stretching vibration (Xu et al., 1988; Silverstein et al., 1981). The skeletal vibrations, involving C=C stretching within the ring, absorb in the 1600-1585 cm^{-1} and in the 1500-1400 cm^{-1} regions. The C–O stretching vibrations of phenols produce a strong band in the 1300-1000 cm^{-1} region. The IR spectra of phenol and phenolate ion (Na^+OPh^-) were recorded as the references to help identify the adsorbed species on the MgO surface. These are displayed in Figures 3.9 and 3.10.

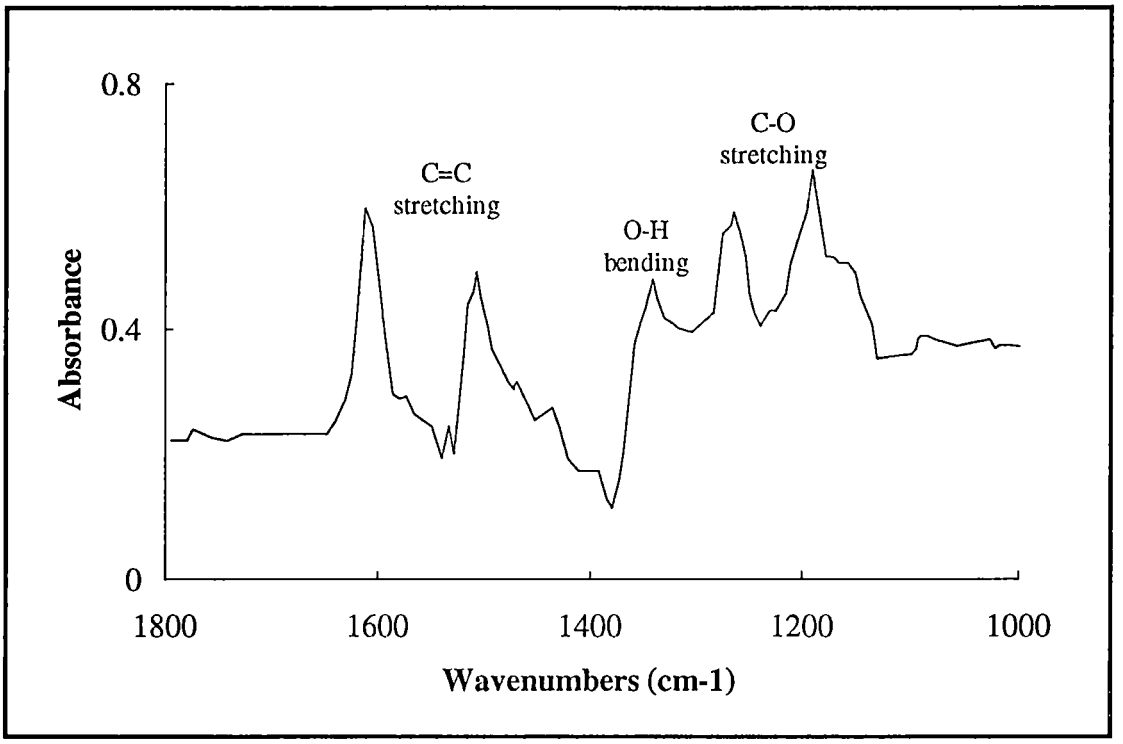

Figure 3.9 The absorption spectrum of phenol gas (at 70°C).

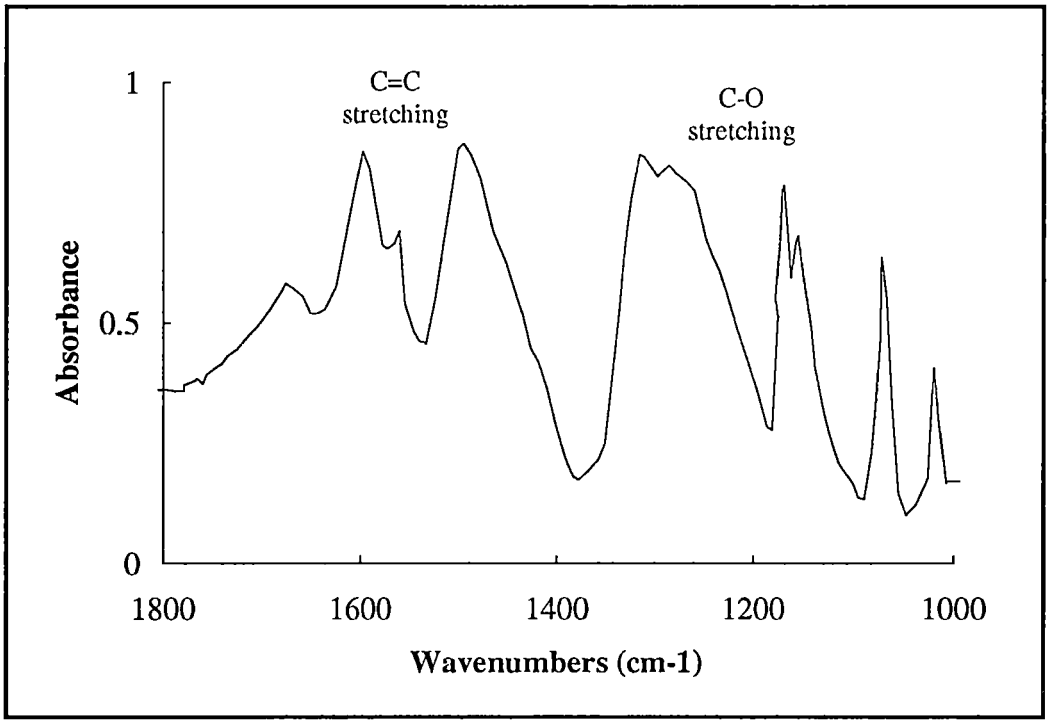

Figure 3.10 The absorption spectrum of phenolate ion (Na^+OPh^-) in KBr disc (at room temperature).

In the 1000-1800 cm^{-1} region, it was observed that phenol displays five absorption bands at 1617 cm^{-1}, 1510 cm^{-1}, 1340 cm^{-1}, 1260 cm^{-1} and 1180 cm^{-1} (Figure 3.9). The absorptions at 1617 cm^{-1} and 1510 cm^{-1} have been attributed to the stretching vibration of C=C of the aromatic ring (Xu et al., 1988; Silverstien et al., 1981). According to Silverstein et al. (1981) the absorption band at 1340 cm^{-1} is due to O–H in plane bending, and the absorption bands at 1260 cm^{-1} and 1180 cm^{-1} are the characteristic C–O vibrational mode. The absorption spectrum of phenolate ion (Figure 3.10) shows four major bands at 1600 cm^{-1} , 1500 cm^{-1} , 1300 cm^{-1} , and 1180 cm^{-1}. The absorption at 1600 cm^{-1} with a side band at 1650 cm^{-1}, and the absorption at 1500 cm^{-1} are assigned to the C=C stretching of the benzene ring, while the bands between 1000 and 1300 cm^{-1} are characteristic of the C–O stretching vibration.

For phenol adsorbed on MgO at room temperature and at 150°C (Figures 3.7 and 3.8), the absorption bands at 1650 cm^{-1}, 1600 cm^{-1} and 1300 cm^{-1} were observed only in low intensities, while two broad bands centred around 1500 cm^{-1} and 1380 cm^{-1} were clearly displayed. At 330°C for MgO calcined at 750°C, the intensity of absorption bands at 1650 cm^{-1}, 1600 cm^{-1} and 1300 cm^{-1} increased, while the broad band at 1500 cm^{-1} was found to decrease and the band centred at 1380 cm^{-1} almost disappeared. There was no sign of the adsorbed gas remaining on the MgO surface at 330°C for the MgO sample calcined at 600°C.

It is likely that the broad bands centred at 1500 cm^{-1} and 1380 cm^{-1} were predominantly due to the adsorption of phenolate species and undissociated phenol molecules that physisorbed on the chemisorbed species. The interaction amongst these species results in the broad absorption bands as observed at room temperature. As the temperature was increased, the physisorbed molecules were eliminated, and accordingly the physical interaction was reduced. The characteristic of these broad bands were still observed at 150°C, but with less intensity than that observed at the ambient temperature. This was postulated to be due to the interaction between the

chemisorbed species and their neighbours which disappeared at higher temperatures (330°C). At such a temperature all phenolate species were removed from the surface of MgO calcined at 600°C. However, some evidence for free phenolate was observed for MgO calcined at 750°C. The bands at 1650 cm^{-1}, 1600 cm^{-1} and 1300 cm^{-1} indicate that the interaction among adsorbed molecules was eliminated due to the distance between these species.

To obtain more details about the desorption of phenol from MgO the IR spectrum from 1700-1150 cm^{-1} of phenol adsorbed onto two samples of MgO prepared from $Mg(OH)_2$ calcined at 600 and 750°C was studied at several temperatures in the range 100 to 350°C (Figures 3.11 and 3.12).

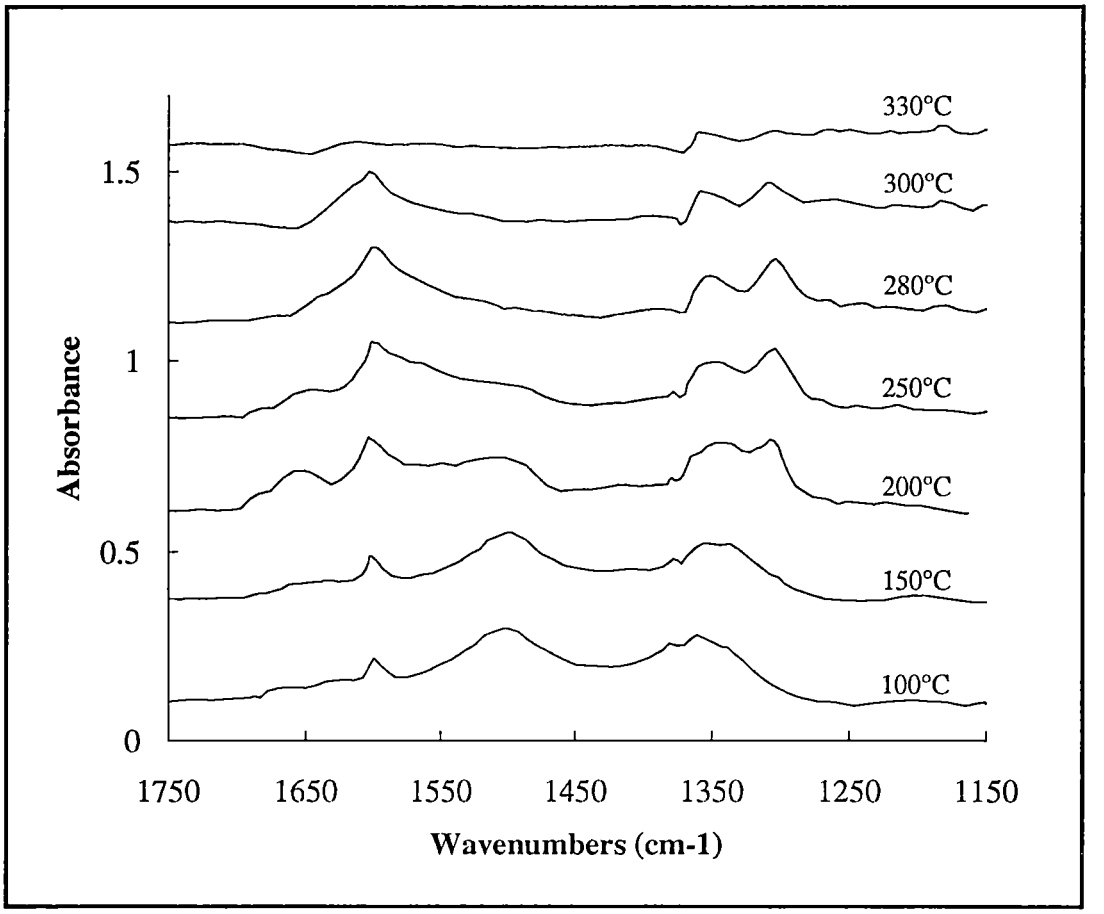

Figure 3.11 IR spectra of phenol adsorbed on MgO (calcined at 600° for 4 h) at different temperatures during a temperature programmed desorption.

Table 3.1 Intensity of each band for IR spectra (in 1150-1750 cm^{-1} region) of phenol adsorbed on MgO (calcined at 600° for 4 h) at different temperatures during a temperature programmed desorption.

band (cm^{-1})	≤ 1300	1340-1360	1380	1500	1600	1650
characteristics	C-O	O-H		C=C	C=C	C=C
species	phenol, phenolate	phenol	phenol, phenolate	phenol, phenolate	phenol, phenolate	phenolate
100°C	1	5	4	5	2	1
150°C	2	4	2	5	2	1
200°C	5	5	1	4	4	3
250°C	5	4	1	2	5	2
280°C	4	4	-	1	5	2
300°C	3	3	-	-	4	1
330°C	-	1	-	-	-	-

Numbers 1-5 denote the intensity from low to high respectively.

From Figure 3.11 and Table 3.1 it was noted that at temperatures in excess of 200°C the broad bands centred at 1500 cm^{-1} and 1380 cm^{-1} became less intense, while the bands at 1650 cm^{-1} , 1600 cm^{-1} and 1300 cm^{-1} became more dominant. Another band at 1357 cm^{-1} was also observed at temperatures greater than 200°C. This band may correspond to the O–H in plane bending of phenol as observed in Figure 3.9. It was presumed that this band represents the phenol desorbing from the surface.

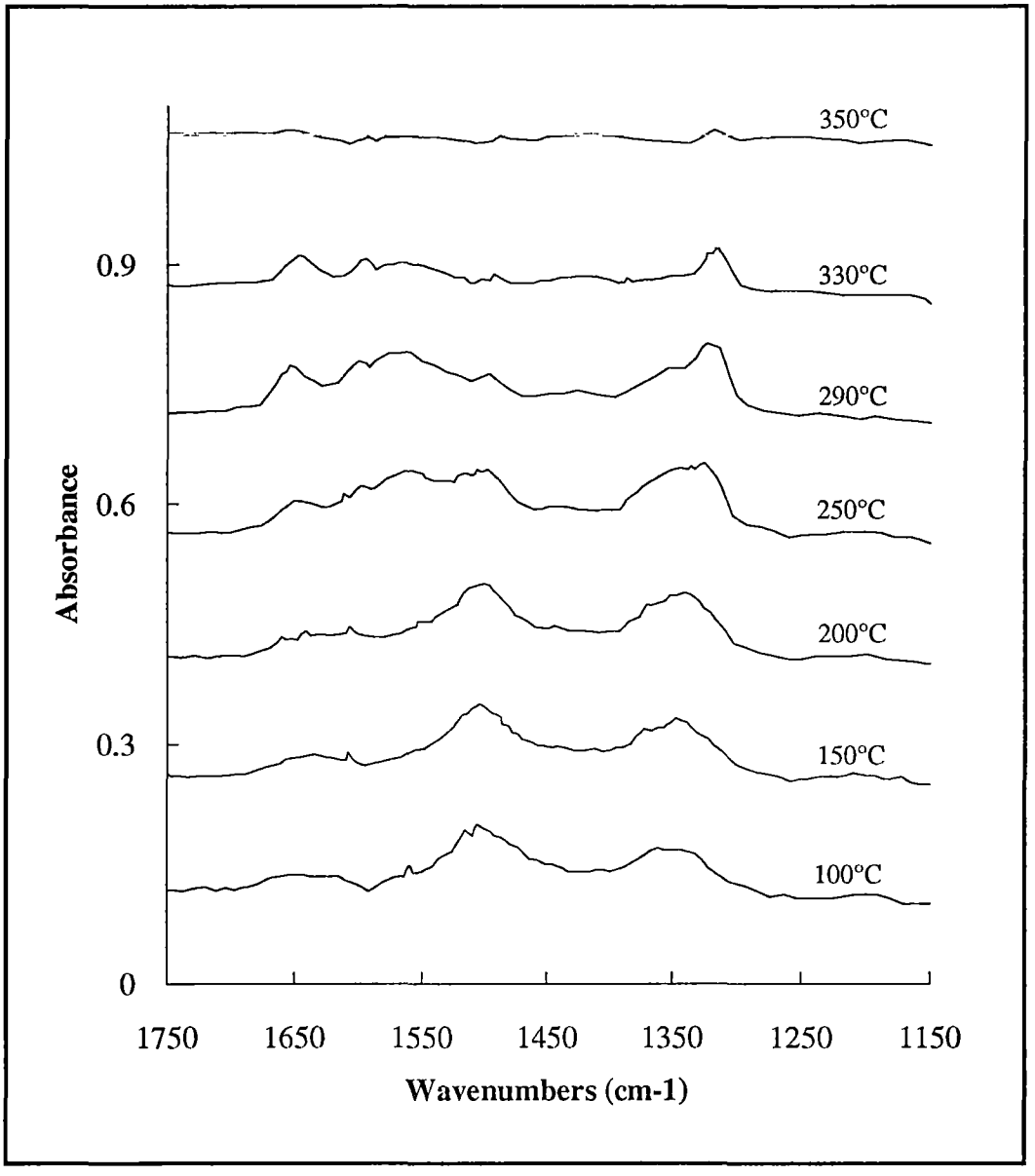

Figure 3.12 IR spectra of phenol adsorbed on MgO (calcined at 750°C for 4 h) at different temperatures during the temperature programmed desorption.

Table 3.2 Intensity of each band (in 1150-1750 cm^{-1} region) for IR spectra of phenol adsorbed on MgO (calcined at 750°C for 4 h) at different temperatures during the temperature programmed desorption.

band (cm^{-1})	1300	1340-1360	1380	1500	1600	1650
characteristics	C-O	O-H		C=C	C=C	C=C
species	phenol, phenolate	phenol	phenol, phenolate	phenol, phenolate	phenol, phenolate	phenolate
100°C	1	4	3	5	1	1
150°C	2	4	3	5	1	1
200°C	3	4	3	5	1	2
250°C	4	5	3	4	2	3
290°C	5	4	1	2	3	4
330°C	3	-	-	1	2	3
350°C	1	-	-	1	1	1

Numbers 1-5 denote the intensity from low to high respectively.

Similar spectra profiles were observed for phenol adsorbed on MgO calcined at 750°C (Figure 3.12 and Table 3.2) except that the appearance and disappearance of the various bands occurred at higher temperatures than that observed for MgO calcined at 600°C. It was likely that the bond strength of phenol adsorbed on MgO calcined at 750°C is higher than that of phenol adsorbed on MgO calcined at 600°C. In other words MgO calcined at 750°C may have the stronger basic sites available for the adsorption of phenol. More information about the basic sites on MgO surfaces calcined at different temperatures will be presented in section 3.3.3.

3.3.1.3 Conclusion and discussion

The appearance of the spectra for phenol adsorbed onto MgO calcined at 600 and 750°C is similar except MgO calcined at 600°C has a prominent peak at 1600 cm^{-1} which is not lost until 300°C. This peak is presumably associated with either water strongly adsorbed onto the surface or free water being desorbed from the

surface. This would be in accord with the observations made earlier where it has been shown that the last traces of hydroxyl groups are not removed unless the MgO has been calcined at 800°C.

The remaining peaks undergo changes in intensity as the temperature is increased. These peaks may broadly be grouped as follows:

Intensity approximately constant:	1350 cm^{-1}
Intensity decreases and peak disappears at 250-290°C	1500 cm^{-1}
Peak appears at 200 and disappears at 300-330°C	1300, 1570 and 1650 cm^{-1}

These results indicate the desorption of phenol from different surface sites of different basic strengths of MgO. Further details of different surface sites will be investigated using the TPD technique described in the next section.

It should be noted that the appearance of these spectra are very much different from those observed by Xu et al. (1988). In their study Merck and Co. MgO was calcined under vacuum at 800°C for two hours before being cooled and exposed to phenol at room temperature. Their spectra essentially consisted of four major bands at 1600, 1500, 1300 and 1160 cm^{-1} respectively. As the temperature was increased all bands decreased in intensity with the 1300 cm^{-1} band resolving into two components of variable intensity at 1300 and 1250 cm^{-1}. The band at 1600 cm^{-1} and 1500 cm^{-1} were assigned to stretching vibrations of the phenyl ring and the 1300 cm^{-1} was assigned to a substituent sensitive mode. Spectra were observed up to temperatures of 600°C and a small amount of benzene was formed at these temperatures.

The differences between the two sets of results can only be attributable to the very different conditions under which the experiments were conducted. The exposure of the evacuated MgO to phenol may allow for the phenol to be adsorbed not only on the surface but into the bulk of material. When adsorption takes place in the presence of argon, the argon atoms may prevent the entry of phenol into the very small pores

and channels in the MgO and cause most of the adsorption to take place on the surface.

It is difficult to determine what species are responsible for the different bands observed in the spectrum. Phenol may be adsorbed onto the surface either through the phenolic hydrogen or via a phenoxide species with the oxygen linked to the magnesium and the hydrogen to an adjoining oxygen in a four centre arrangement. Phenol when observed in the solid state have bands between 1330 and 1390 cm^{-1} and the C-O stretching vibration is also in this region.

3.3.2 TPD of phenol from MgO with thermal conductivity detector (TCD)

To investigate and identify the active sites on the surface of MgO catalyst the TPD of phenol using thermal conductivity detector was carried out. The flow-chart of the TPD apparatus is displayed in Figure 3.13

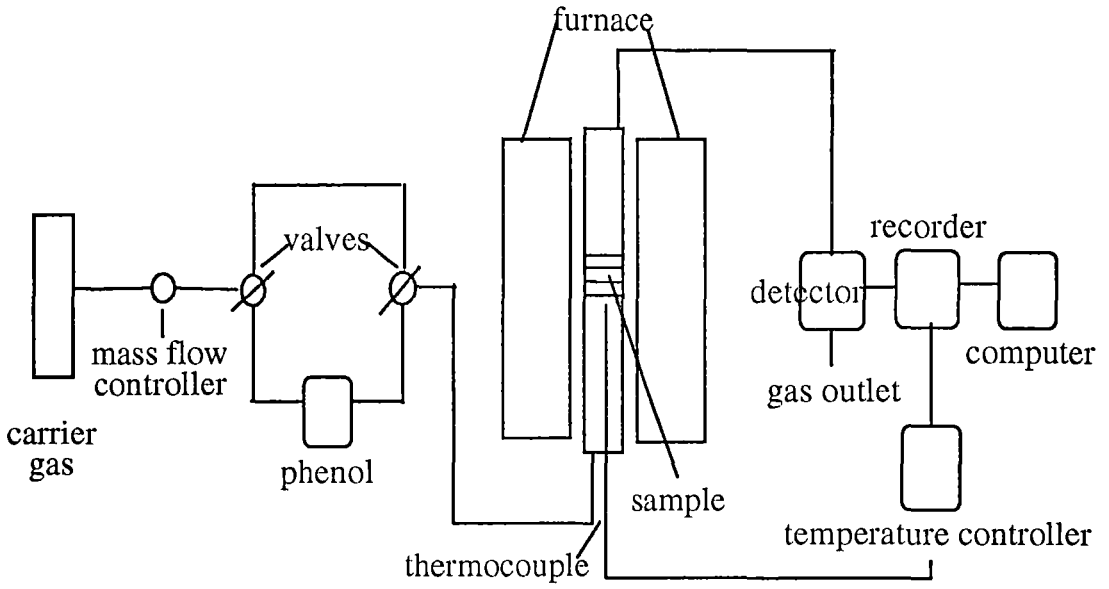

Figure 3.13 TPD apparatus flow chart.

Initially, experiments were carried out using 100 mg of MgO sample, the same amount used by Xu et al.(1988). Approximately 150 mg of $Mg(OH)_2$ was packed between quartz wool in a quartz tube 27 cm long and 0.7 cm in diameter. The sample was then calcined under helium (high purity, CIG) atmosphere at a flow rate of 10 mL/min. The calcined MgO sample was cooled to room temperature under helium and then exposed to phenol by switching the carrier gas to pass, in series, though the phenol (dried with $CaSO_4$) and the sample. The sample was exposed to phenol for half an hour. Excess phenol was removed by flowing helium until a constant base line on the recorder was obtained. Temperature programmed desorption was then carried out with a heating rate of 10°C/min to 800°C and a carrier gas flow rate of 10 mL/min. The TPD profile was acquired by means of a thermal conductivity detector (TCD) which was interfaced to both a chart recorder and computer.

With the above conditions several difficulties were encountered. Firstly, to obtain a constant baseline during the removal of excess phenol prior to the TPD process a significant time was needed. Secondly, complex and irreproducible TPD profiles were obtained. As suggested by Falconer and Schwartz (1983) this may be due to the catalyst bed being too long causing an increased pressure drop and possible gas readsorption. Consequently, the experiment was performed with a reduced amount of sample. It was observed that the smaller the amount of sample used, the simpler and more reproducible were the TPD profiles obtained. However, this approach was limited by the sensitivity of the detector.

Finally TPD peak as shown in Figure 3.14 was obtained when phenol was desorbed using a heating rate of 10°C/min and a carrier gas flow rate of 10 mL/min.

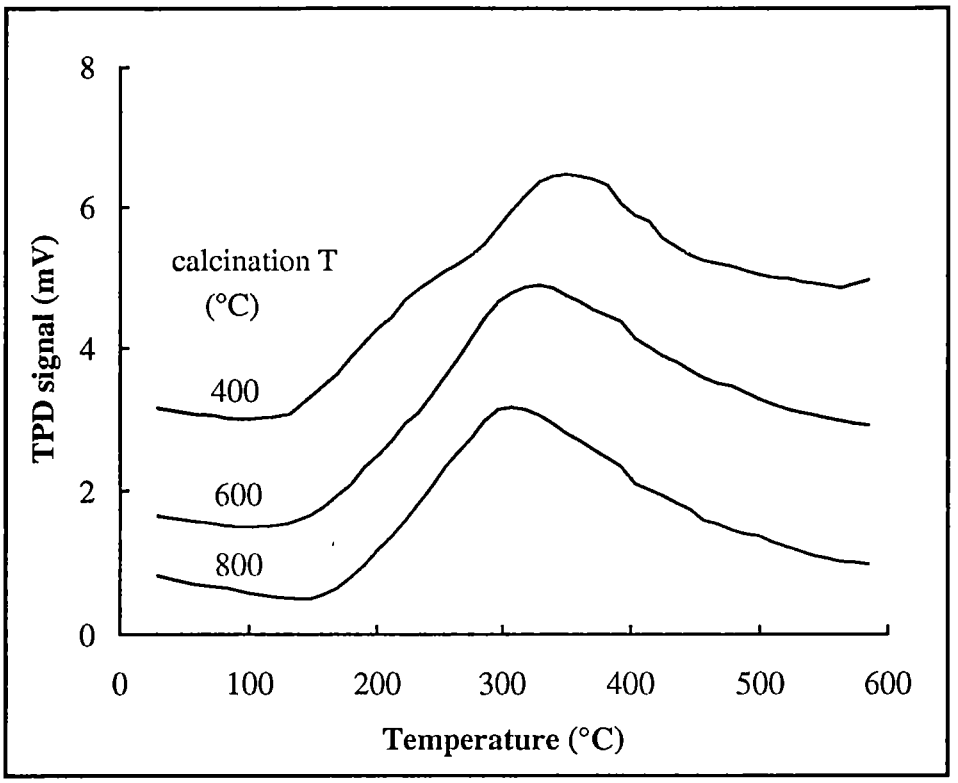

Figure 3.14 TPD profiles of phenol from MgO surfaces using a heating rate of 10°C/min, carrier gas flow rate of 10 mL/min with a comparatively long distance from reactor to detector. The sample weight was about 9-10 mg.

The lack of resolution of TPD profiles in Figure 3.14 was attributed to the phenol adsorbing on the copper gas line between the quartz reactor and the detector. The distance between the reactor and the detector was therefore reduced and the metal gas line was warmed to 120°C. In addition the flow rate of carrier gas was increased, and as a result the signal was reduced due to the lower concentration of phenol. A carrier gas flow rate of 30 mL/min was found to be optimal. The heating rate of 5°C/min was found to result in better resolution than that of 10°C/min. The TPD profiles of phenol desorbed from MgO calcined from $Mg(OH)_2$ at different calcination temperatures are displayed in Figure 3.15.

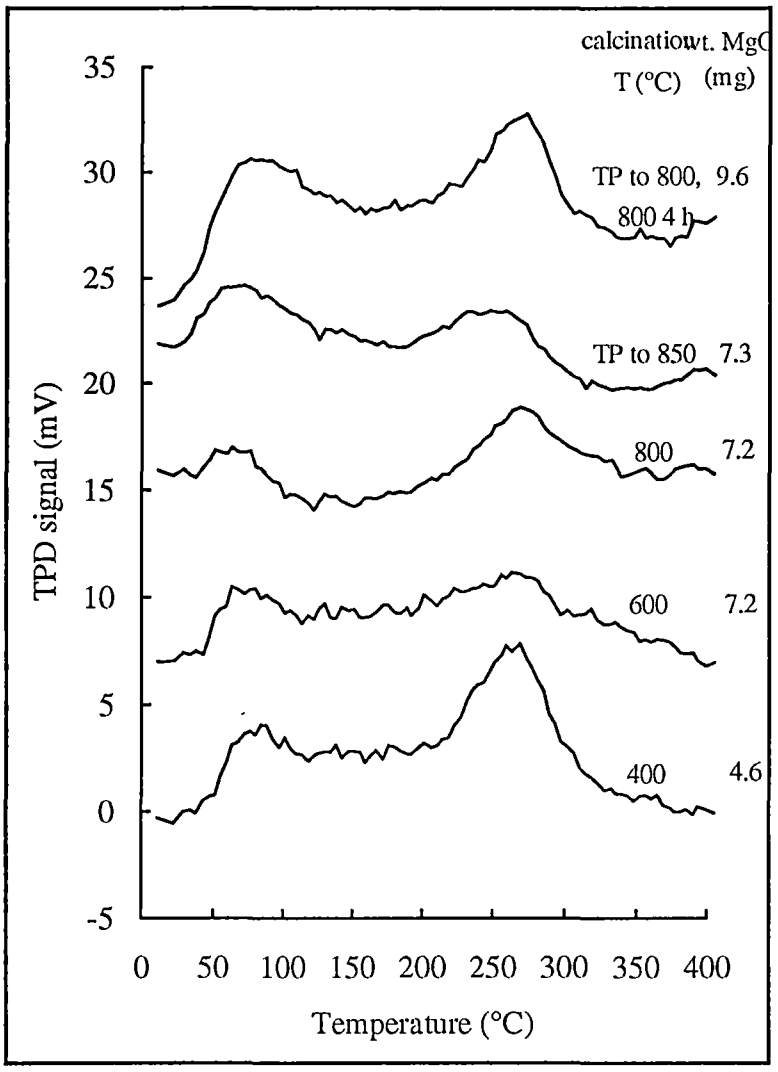

Figure 3.15 TPD profiles of phenol from MgO samples calcined from $Mg(OH)_2$ at different temperatures.

Two distinct peaks at 75°C (348 K) and 275°C (548 K) were observed for the temperature programmed desorption (linear ramp rate 5°C/min) of phenol from MgO. These two peaks may be attributed to the physisorption and chemisorption of phenol on MgO; the TPD peak at being 75°C attributed to physisorption and the peak at 275°C representing chemisorption. It is likely that there may be an additional chemisorption peak at ca. 160-180°C. To clarify this a new approach was employed as described in the next section.

3.3.3 TPD of phenol from MgO with thermo-gravimetric (TG) detector

In the TPD experiments using the thermal conductivity detector problems were encountered (as stated earlier) with desorption of the phenol onto metal gas lines before the detector. It was also found that the time required to obtain a stable baseline was excessively long. To overcome these problems an alternative approach, using a thermobalance as a detector was investigated and found to be satisfactory.

A Setaram TGA 92 thermoanalyser which consists of a vertical furnace (capable of being heated to 1800°C), a thermobalance (± 0.01 mg) and a CS 92 controller for controlling programmable heating rates from 0.1 to 99.9 °C/min, was used to investigate the weight loss from samples of MgO which have been exposed to phenol.

Approximately 40 mg of MgO precursor was calcined and exposed to phenol as described earlier. The sample was then rapidly transferred to a pretared alumina crucible and placed in the TGA 92. An argon flow of 20 mL/min was passed over the sample and its mass was determined.

3.3.3.1 TPD profiles obtained from the TG method

Different sites on MgO surface were determined from the rate of mass loss (DTG) profiles which indicate the rate at which phenol is desorbed from MgO at different temperatures. The basicity of each type of site was determined from the weight loss corresponding to the temperature range of desorption from that such type of sites. A typical TPD profile of phenol desorbed from MgO by thermo-gravimetric method is displayed in Figure 3.16.

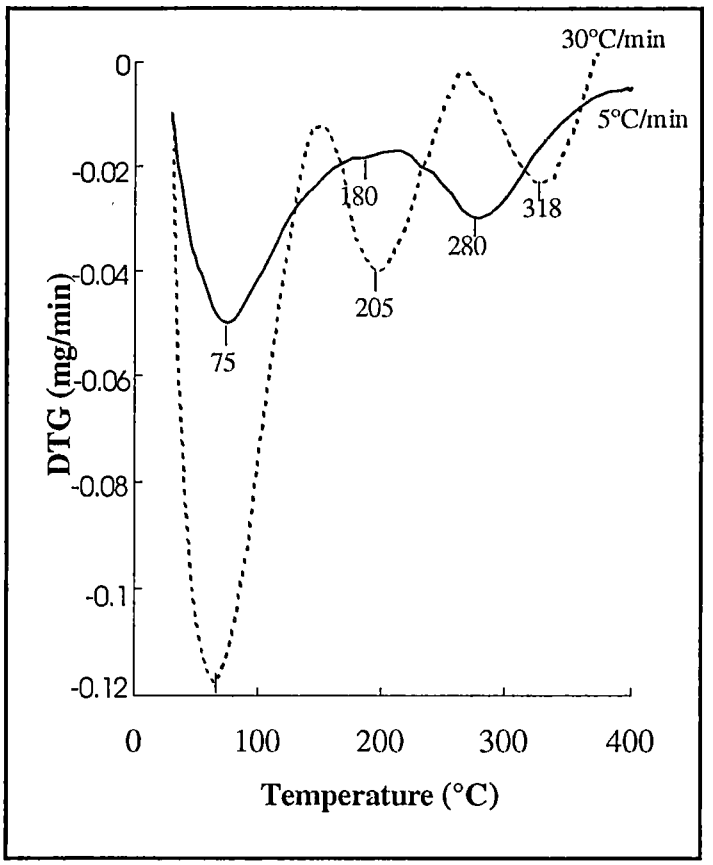

Figure 3.16 TPD profiles of phenol adsorbed on MgO (calcined from $Mg(OH)_2$ at 600°C) obtained by the TG method with a ramp rate of 5°C/min and 30°C/min.

From Figure 3.16 the differential weight loss (DTG) was plotted against the progressive temperature. The temperatures at which the maximum desorption (T_M) of phenol occurred were evaluated from the minimum positions of the DTG curve. From the DTG curves at the highest ramp rate three peaks are discernible at 75, 205 and 308°C. At the lower ramp rate two peaks at 75 and 280°C are clearly seen but the intermediate peak is not resolvable, but is clearly observed from the DSC experiment (page 98). To determine the basicity of each site it was decided to use the results at the lower ramp rate and to arbitrarily choose a temperature range from which desorption occurs. The main reason for adopting this approach was that the mass loss measurement over a particular temperature range was much more precise at the lower ramp rate. The desorption ranges chosen were 30-120°C, 120-230°C and

230-380°C, based on DSC data, and the mass loss was determined directly from the TG vs temperature curve.

3.3.3.2 Identification of sites on the surface of MgO

MgO samples obtained via the thermal decomposition of $Mg(OH)_2$ at different temperatures for 4 h were exposed to phenol at room temperature. The TPD was then carried out at a ramp rate of 5°C/min to 800°C under an atmosphere of argon at a flow rate of 20 mL/min. The weight losses due to the desorption of the adsorbate are displayed as a function of temperature in Figure 3.17.

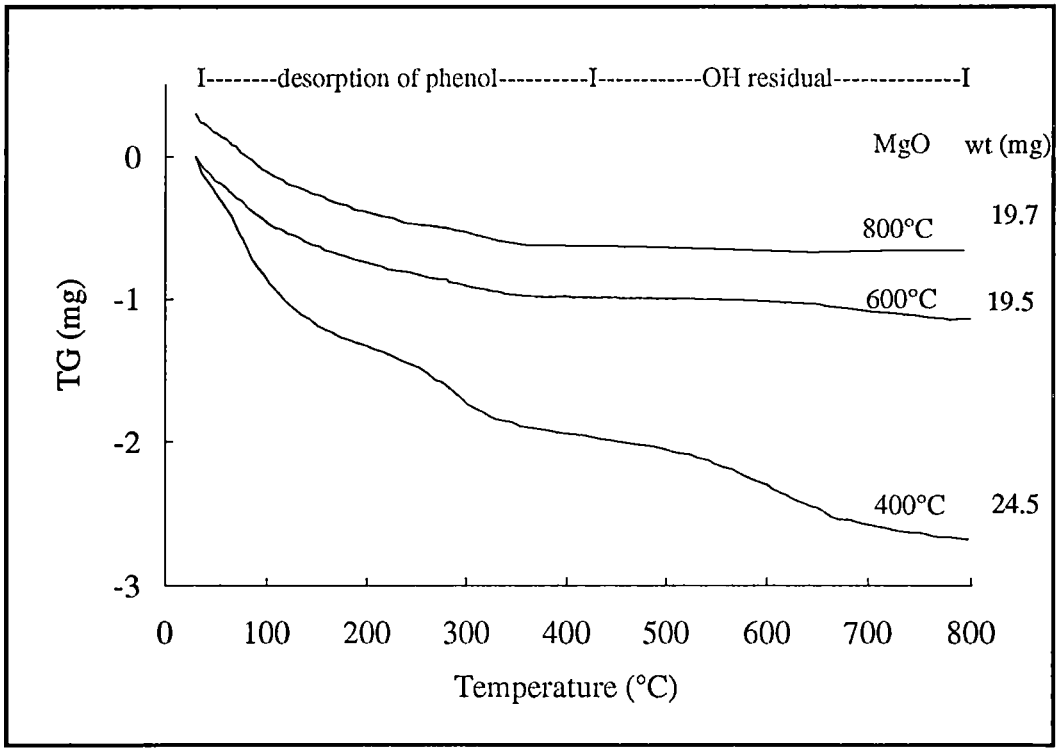

Figure 3.17 Weight loss profiles during the TPD of phenol from MgO calcined at different temperatures for 4 h.

It was noted that for MgO calcined at 800°C the weight loss occurred over the temperature range 30-400°C, while the MgO calcined at 400°C and at 600°C displayed weight loss over the temperature range of 30-800°C. According to the infrared spectroscopy coupled with TGA of pure MgO (Figures 3.5 and 3.6) it was likely that the weight loss occurring between room temperature and 400°C was due to

the desorption of phenol. The weight losses observed beyond 400°C for MgO calcined at 400°C and 600°C are attributed to the dehydroxylation of residual OH species remaining on the surface of these MgO samples, as demonstrated before in section 3.3.1. The weight losses observed beyond 400°C here were comparable to those previously observed in Figure 3.6. In subsequent discussion, the TPD profiles of phenol from MgO were examined over the temperature range 30-400°C.

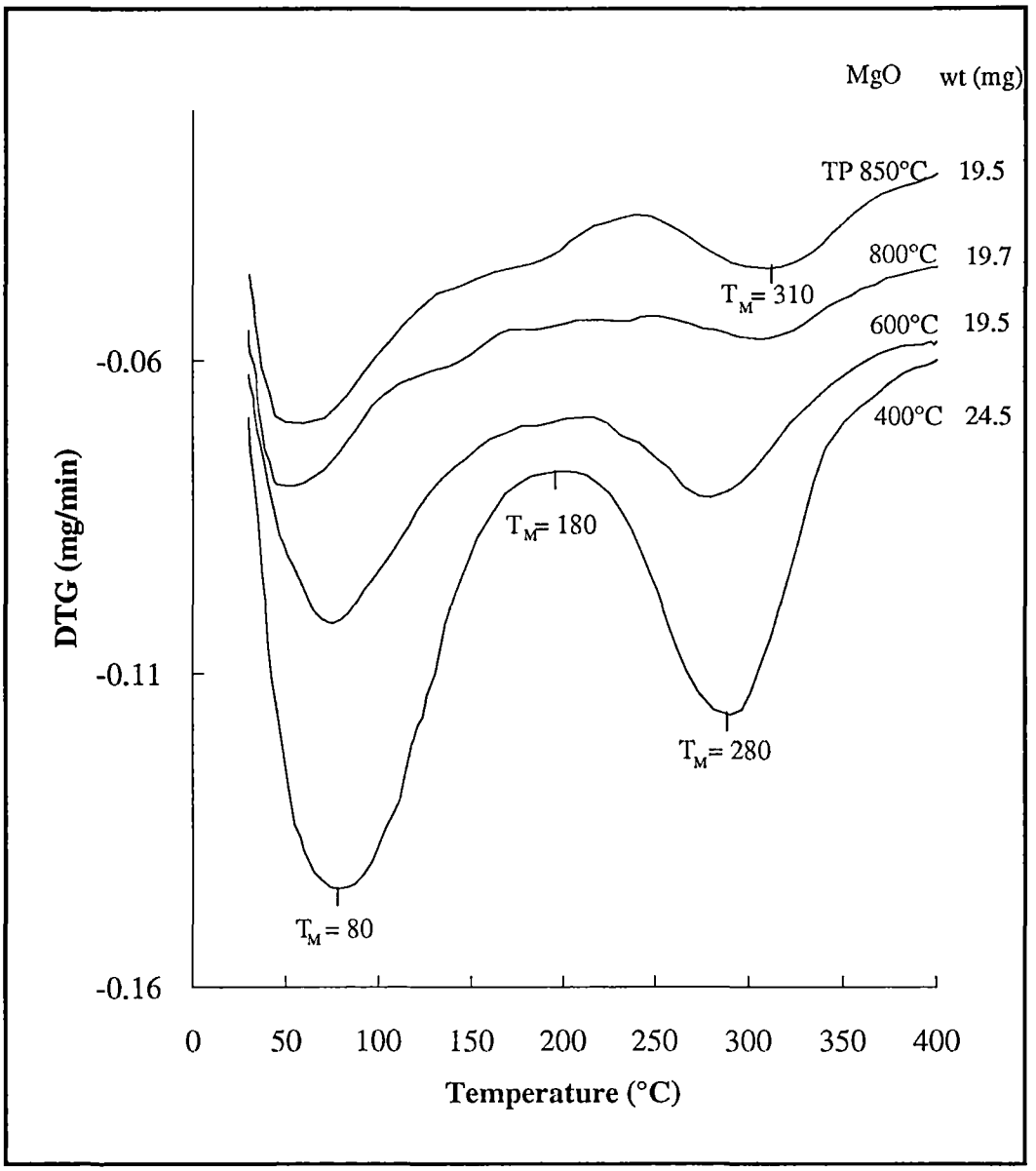

Figure 3.18 TPD profiles of phenol on MgO calcined at different temperatures. The ramp rate is 5°C/min.

Phenol desorbs from MgO (calcined from $Mg(OH)_2$ at different temperatures for 4 h) in four main temperature regions over the range 30-400°C (Figure 3.18). The temperature of maximum desorption (T_M) of each desorption range is obtained from the minimum point of the DTG finger-print profile. The first desorption is assigned to the physisorption of phenol since its T_M is lower than 100°C (according to infrared spectra in Figures 3.7 and 3.8 the physical interaction was intensively observed at the temperature lower than 150°C). The second desorption (T_M ~ 180°C) occurred over the temperature range 130-240°C is less prominent than the other desorptions, being particularly difficult to observe at low ramp rates. The third desorption with T_M ~ 280 °C was observed, in the range of 240-325°C, for MgO calcined at temperature lower than 800°C such as 400°C and 600°C. The fourth desorption with T_M ~ 310°C was observed for MgO calcined at 800°C for 4 h, and MgO calcined by the temperature programmed to 850°C.

In conclusion four T_M' s can be observed for phenol adsorbed on MgO obtained from the thermal decomposition of $Mg(OH)_2$ at different temperatures. The first T_M arises from physisorbed phenol while the other three T_M' s are from chemisorbed of phenol, which may imply that there are three different sites on the surface of MgO. The second T_M at 180°C which was weak at low ramp rate, indicates a site with a lower basic strength than the others observed at higher T_M. This site was clearly observed at high ramp rate such as 30°C/min as shown in Figure 3.16. However, the ramp rate of 5°C/min was mostly used in this work because this ramp rate gave a better accuracy in determination the T_M and basicity of sites.

The second site is associated with the desorption with T_M at 280°C which was found at high intensity for the desorption of phenol on MgO calcined at 400°C and 600°C for 4 h (Figure 3.18). However, this peak was very weak or disappeared for the TPD of phenol on MgO calcined at 800°C for 4 h, or 850°C. The third site on the surface of MgO is indicated by the desorption with T_M at 308°C (Figure 3.18)

which was dominant for the desorption of phenol from MgO obtained at a high calcination temperatures.

Coluccia and Tench (1980) have proposed a surface model of MgO calcined at different temperatures as shown in Figure 3.19.

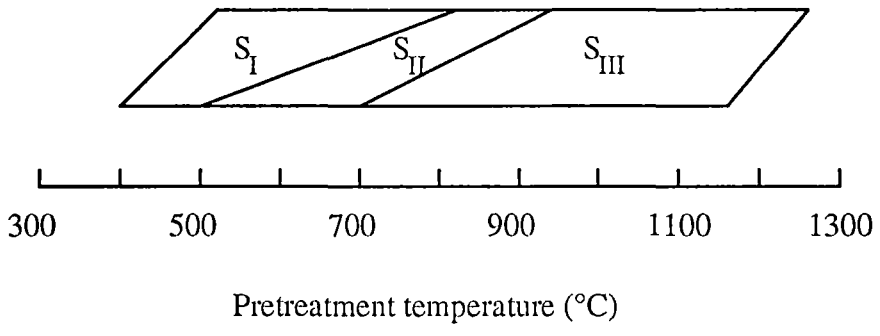

Figure 3.19 Three types of sites on MgO with increasing pretreatment temperature (Coluccia and Tench, 1980).

It is likely that site S_I corresponds to the T_M at 280°C. It is observed predominantly for MgO calcined at 400°C and 600°C for 4 h respectively. As the calcination temperature was increased to 800°C, this TPD peak disappeared (Figure 3.19). On the other hand site S_{III} becomes dominant at high pretreatment temperature of 800°C and above. This site is therefore attributed to the desorption with T_M at 308°C which was observed only for MgO calcined at temperatures ≥ 800°C. Site S_{II} is therefore assumed to be represented by the desorption with T_M at 180°C which could be observed from MgO that had been calcined at 600°C for 4 h (see Table 3.3). All these sites, S_I, S_{II} and S_{III}, have been assigned to the low coordinated (lc) ions, O_{lc}^{2-} and Mg_{lc}^{2+}, on MgO surfaces (Hattori, 1985).

From the T_M's which indicate the basic strength of each site and from the work of Hattori (1985) and Dunski et al. (1994), the desorption with T_M at 308°C, site S_{III}, which displays the highest basic strength should consist of the high ratio of the lower coordination site, the corners, i.e. $Mg_{3c}^{2+}O_{3c}^{2-}$, $Mg_{4c}^{2+}O_{3c}^{2-}$, $Mg_{3c}^{2+}O_{4c}^{2-}$.

According to Hattori (1985) and Dunski et al. (1994) these unsaturated sites were mostly generated when high pretreatment temperatures (>800°C) were used. At such temperatures the residual OH species were completely removed from the MgO surface, producing lower coordinated ions. The dehydration model of the residual hydroxyl groups which produces the corners and edges of MgO crystal (100) face was proposed by Dunski et al. (1994), as shown in Figure 3.20.

The TPD of phenol for MgO with T_M at 280°C, site S_I, shows a lower basic strength than that of the desorption with T_M at 308°C but higher than that of the desorption with T_M 180°C, site S_{II}. From earlier work (Dunski et al., 1994) it should therefore be composed of higher coordination number of O_{lc}^{2-} and Mg_{lc}^{2+} ions than those of the corners, but lower than those of the site represented by the desorption with T_M at 180°C. Extended edges are possibly the major contributor for site S_I. Such sites dominate at low calcination temperatures when the lower coordinated sites were still occupied by residual OH species. At higher calcination temperatures the lower coordinated ions, the corners, are generated. The combination of the edges and the corners creates a new site represented by the desorption with T_M at 308°C, site S_{III}. Due to its lowest basic strength, the desorption with T_M at 180°C, site S_{II}, should represent the $Mg_{5c}^{2+}O_{5c}^{2-}$ on the flat surface of MgO.

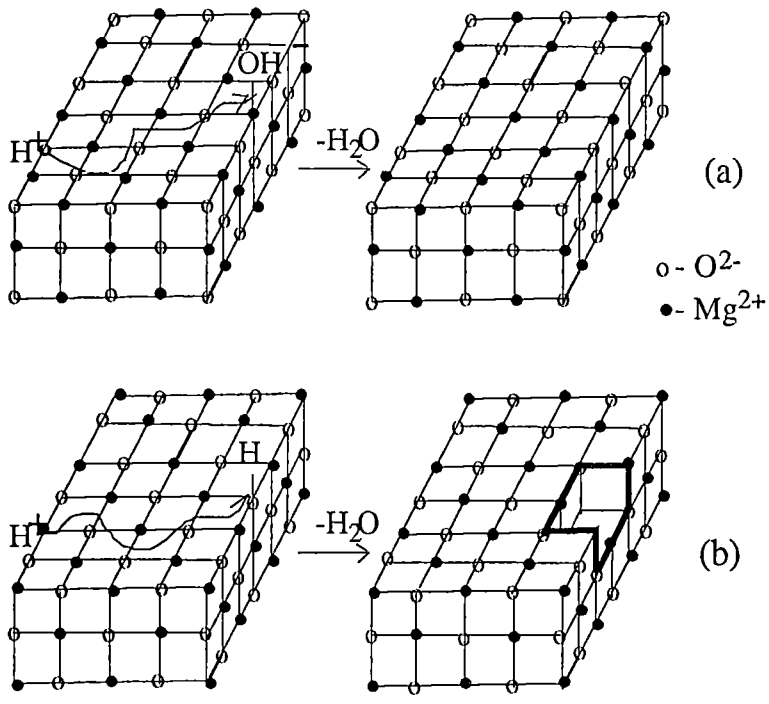

Figure 3.20 The dehydration model of residual hydroxyl groups on MgO crystal; (a) involving the mobile surface proton and the isolated OH group at the edge still maintains the edge structure and (b) involving the lattice O^{2-} constitutes the hydroxyl group may result in additional corner site formation (Dunski et al., 1994).

From Figure 3.20 at low calcination temperatures dehydroxylation involving the mobile surface proton and the isolated OH group at the edge still maintains the edge structure (a), whereas at high calcination temperatures the process involving the lattice O^{2-} forming the hydroxyl group may result in additional corner site formation (b). The TPD results obtained in the present work for MgO calcined at different temperatures seem to agree with the dehydroxylation model proposed by Dunski et al. (1994). As discussed above, site S_I (assigned to the edges and represented by the TPD of phenol T_M at 280°C) was mainly observed on the surface of MgO calcined at low temperatures as only isolated OH groups were removed. On the other hand, the generation of corners, found in site S_{III} needs a high temperature such as 800°C

because it involves the removal of the lattice O^{2-} on the edge. The model for corners, edges and the flat surface sites on the surface of MgO is displayed in Figure 3.21.

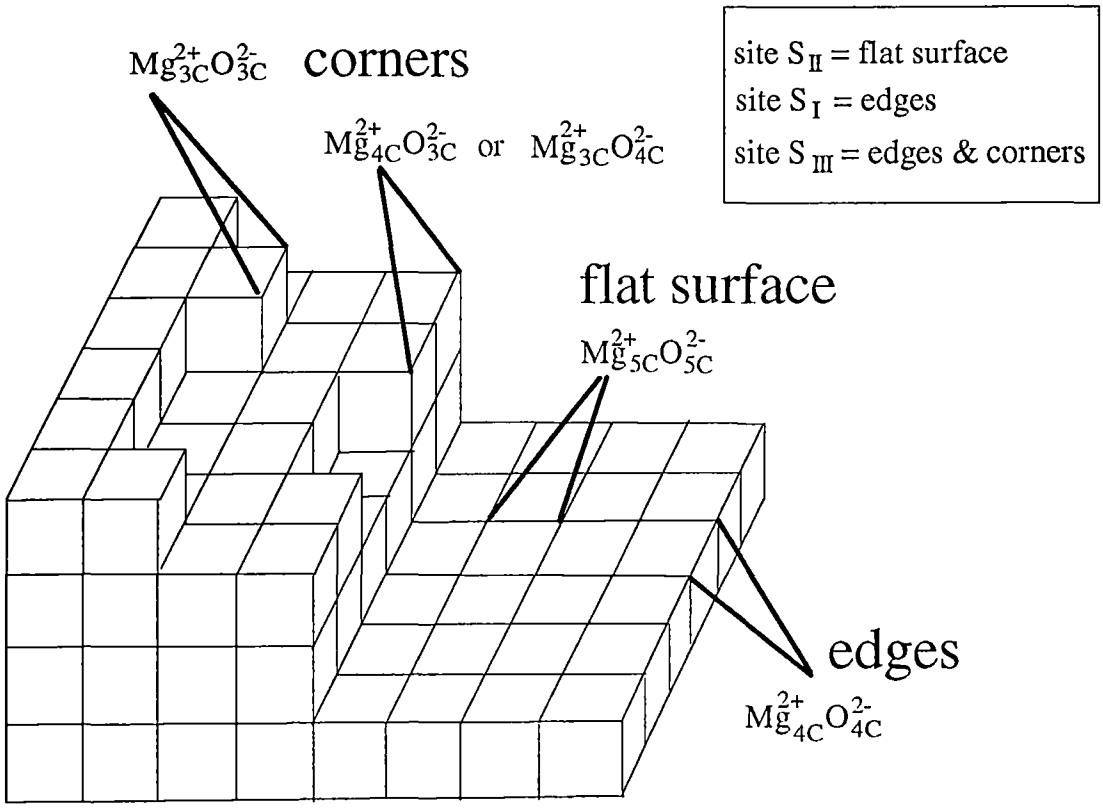

Figure 3.21 Model for the low coordination sites on MgO surface.

It is noted that the identification of MgO surface sites carried out in the present work slightly differs from that proposed by Hattori (1985). Hattori proposed that site S_I is $Mg_{4c}^{2+}O_{4c}^{2-}$ which is also proposed by the present work. However, the former identified site S_{III} as $Mg_{3c}^{2+}O_{3c}^{2-}$. This is not likely to be correct as Dunski et al. (1994) showed that this ion pair was found in a very small numbers in comparison with $Mg_{4c}^{2+}O_{3c}^{2-}$ and $Mg_{3c}^{2+}O_{4c}^{2-}$. From the TPD evidence presented in this work site S_{III} is assigned to be the combination of edges and corners ($Mg_{4c}^{2+}O_{4c}^{2-}$, $Mg_{4c}^{2+}O_{3c}^{2-}$, $Mg_{3c}^{2+}O_{4c}^{2-}$ and $Mg_{3c}^{2+}O_{3c}^{2-}$) which are in accord with the surface sites proposed by Dunski et al. (1994). Hattori proposed that site S_{II}

is $3Mg_{3c}^{2+}O_{4c}^{2-}$. This proposal is not likely to be true as the possibility to obtain this group of ions is very low and Hattori did not consider the flat surface sites, $Mg_{5c}^{2+}O_{5c}^{2-}$ which are found in significant numbers on the MgO surface.

3.3.3.3 Basicity of the surface sites of MgO

The amount of phenol adsorbed on the chemisorption sites S_I, S_{II} and S_{III} was determined from the weight loss of the adsorbed sample under the progressive temperature change. It was found that different calcination temperatures result in different basicities for each site as shown in Table 3.3. The ratio of sites on each MgO sample were also estimated.

Table 3.3 The basicities (mmol of phenol/weight of MgO) of MgO obtained from $Mg(OH)_2$ precipitated at pH 10.0 and calcined at different temperatures.

calcination T (°C)	site S_I (mmol/g)	site S_{II} (mmol/g)	site S_{III} (mmol/g)	ratio of sites		
				site S_I	site S_{II}	site S_{III}
400	0.34	0.15	-	7	3	-
600	0.30	0.17	-	5	3	-
800	-	0.11	0.15	-	2	3
TP to 850°C	-	0.14	0.15	-	1	1

The area occupied by each site can be evaluated from the basicities if the cross sectional area of the adsorbed gas is known. In the present work it is assumed that the cross sectional area of phenol is the same as that of benzene, which has been used as an adsorbate for surface area determination over a number of years. The cross sectional area of benzene (and therefore phenol) which corresponds to random orientation is 30.7 $Å^2$ (Gregg and Sing, 1982). The cross sectional area for the

molecule in a flat position is 40 $Å^2$, while that for end-on orientation is 25 $Å^2$. The random orientation figure was used in this work and the area occupied by each site on the MgO surface is displayed in Table 3.4. The total surface area obtained by the BET method using N_2 is also presented to allow comparison with the values obtained from the adsorption of phenol. For MgO calcined at 400°C and 600°C, the surface occupied by residual OH groups is also considered.

Table 3.4 The surface areas occupied by different sites on MgO calcined at different temperatures.

Calcination T (°C)	Total surface area, BET (m^2/g)	Area occupied by residual OH (m^2/g)	site S_I (m^2/g)	site S_{II} (m^2/g)	site S_{III} (m^2/g)	Total OH + S_I + S_{II} + S_{III} (m^2/g)
400	210	96	63	28	-	187
600	95	21	55	31	-	107
800	49	0	-	20	30	50
TP to 850	80	0	-	26	28	54

In general the surface area values obtained via the adsorption of phenol are in agreement with the values obtained by BET method. The differences between these values may be due to the effect of the orientation of phenol. The density of sites, the number of adsorbed phenol molecules per unit surface area (BET), may cause differences in the orientation of adsorbed phenol. For MgO samples calcined at 400°C and temperature programmed to 850°C, the densities of sites were relatively low so that the flat orientation on the surface was most likely to appear. The surface area estimation using the cross sectional area of random orientation in these cases would result in a lower surface area. Pore size distribution is also important, as

nitrogen is smaller than phenol, so it will enter smaller pores and give higher surface area reading.

3.3.4 TPD of phenol using Differential Scanning Calorimetry (DSC)

TPD of phenol using DSC technique was an alternative approach used to explore the surface of MgO catalysts. It was anticipated that desorption of phenol from different types of surface sites would result in different heats of desorption.

A Setaram DSC 92 differential scanning calorimeter (comprising a CS 92 controller, DSC 92 calorimeter, PC 92 computer and a printer) was employed to analyse the enthalpy change of the desorption of phenol from the surface of MgO. Approximately 100 mg of MgO precursor was calcined at desired temperatures under argon, cooled to room temperature and exposed to phenol as described in section 3.3.2. The MgO was divided into two portions. One was transferred to a DSC aluminium crucible (6 mm inner diameter and 5 mm long). A temperature programmed desorption was carried out at a heating rate of 5°C/min under an atmosphere of argon. DSC results were obtained by the difference between TPD-DSC of the adsorbed MgO and TPD-DSC of clean MgO surface carried out at the same ramp rate.

The other portion of MgO was transferred to the TG furnace and the TPD of phenol was also carried out to determine the number of phenol molecules desorbed from each type of site. From the DSC and TG results the enthalpy changes for phenol desorbed from each type of sites on the surface of MgO can be estimated in terms of per mol of phenol.

The TPD-DSC profiles of phenol desorbed from MgO were obtained from the plot of heat flow against temperature as shown in Figure 3.22.

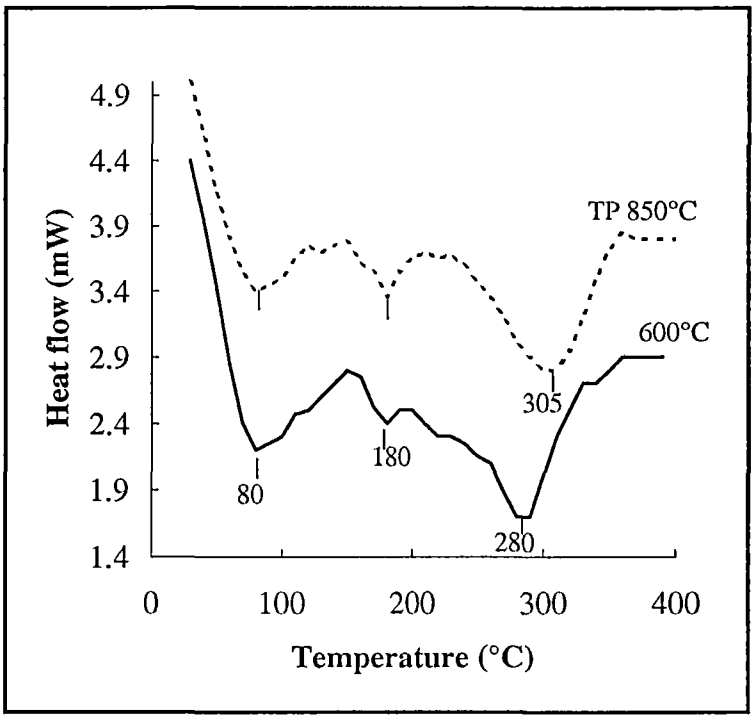

Figure 3.22 TPD profiles of phenol desorbed from MgO calcined at 600 and 850°C.

In Figure 3.22 it is noted that the TPD profiles obtained from DSC experiment are similar to that obtained from the TG experiment. Three desorption peaks were observed at 80, 180 and 280°C for MgO calcined at 600°C, and at 80, 180 and 305°C for MgO calcined at 850°C. These results strongly support the data obtained from the TG experiment that there are three types of site depending on the calcination temperatures could be found on the surface of MgO. It is also noted that the heat of desorption peak at 80°C is relatively small (30 kJ/mol of phenol) which indicates that desorption peak at 80°C is a physisorption. The heat of desorption peak at 305°C (120 kJ/mol of phenol) is higher than that of the peak at 280°C (80 kJ/mol of phenol) which means that the higher activation energy of desorption requires the higher energy to break the chemisorbed bond on MgO surface.

3.3.5 TPD of water, methanol and methane using TG technique

Water, methanol and methane all of which are less acidic than phenol (Streitwieser and Heathcock, 1981a) were also used as probe molecules to explore the surface of MgO.

The MgO sample was exposed to water vapour at room temperature in a calcining unit prior to transferring to the TG unit as carrying out for adsorption of phenol. In situ calcined MgO was exposed to water vapour by passing the carrier gas through a packed bed of $FeSO_4.7H_2O$ (Aldrich 99 % +) and then through the sample at a flow rate of 80 mL/min for 40 min (Parkinson and Day, 1981). The adsorbed MgO was transferred to the TG crucible and the TPD-TG was then carried out at a ramp rate of 5°C/min.

A similar procedure was used to adsorb methanol onto MgO. Adsorption was achieved by bubbling the carrier gas at a rate of 60 mL/min through dry methanol (BDH 99 % +) and then over the MgO sample for 40 min. It was assumed that moisture in air has no or slight effect on the methanol chemisorbed species because the period of transferring is only 2-3 min. In addition, methanol has the same acidity as water (pKa of methanol and water are 15.5 and 15.7 respectively (Streitwieser and Heathcock, 1981b)).

For methane adsorption the MgO sample was calcined and cooled down under argon condition (20 mL/min) in the TG unit and directly exposed to methane at a flow rate of 10 mL/min for 40 min by switching the valve from carrier gas to methane. The weight of MgO was estimated from the weight of precursor and mass loss after calcination.

The TPD profiles of water, methanol, methane and phenol are displayed in Figure3.23.

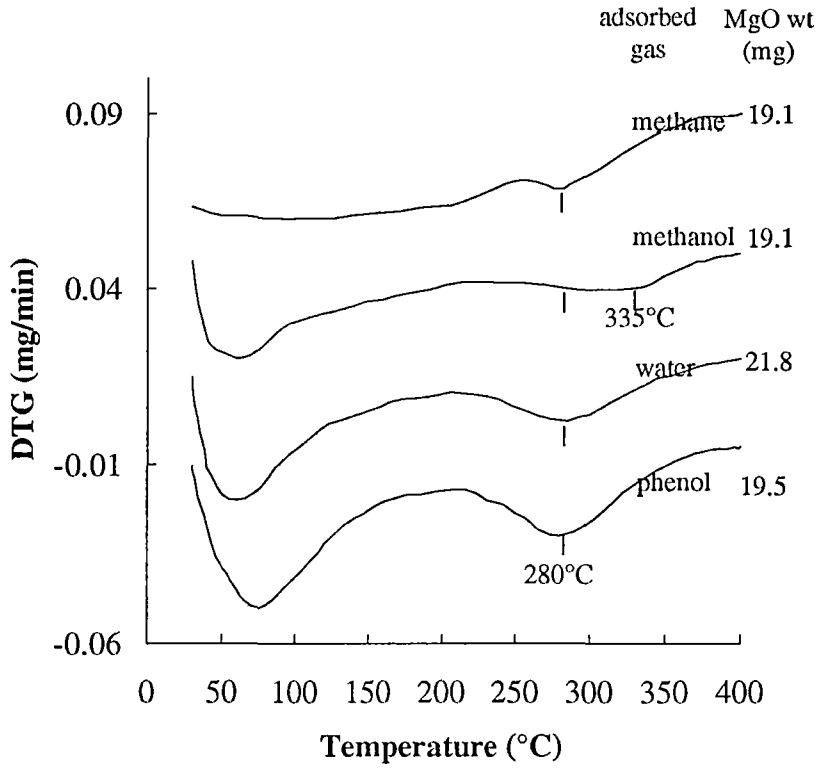

Figure 3.23 TPD-DTG profiles of phenol, water, methane and methanol on MgO.

The TPD-TG analysis of water and methane from MgO show the same T_M (280°C) as that obtained using phenol (Figure 3.23). These results indicate that the desorption peak at 280°C of phenol, water and methane from MgO have the same activation energy. More details of the activation energies of phenol, water, methanol and methane desorbed from MgO are presented in Chapter 6.

Water differs from phenol in that with increasing exposure time it seems to interact more with the bulk MgO sample (Figure 3.24 a). The longer the period of exposure, the larger the amount of water that desorbed from the MgO sample. Moreover, the T_M appears to shift to higher temperature (> 280°C) as shown in Figure 3.24 a. It may mean that water can diffuse into the bulk MgO to form $Mg(OH)_2$ (Figure 3.24 b) which is usually found when MgO is exposed to air that contains moisture. This phenomenon was not observed for phenol adsorbed on MgO; after 30 min the amount of phenol adsorbed on MgO was constant.

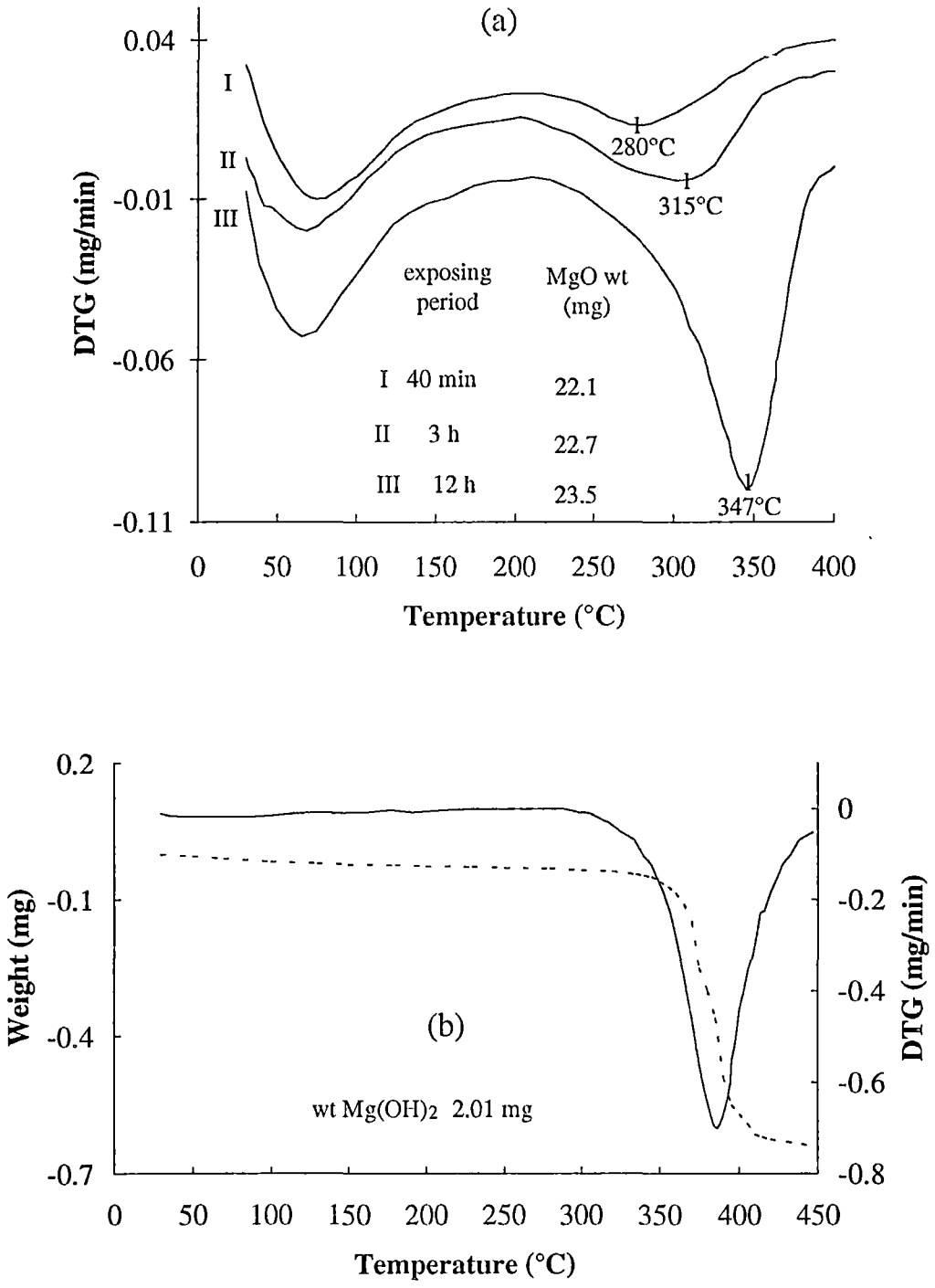

Figure 3.24 TPD profiles of (a) of water from MgO (with different exposure periods), (b) of $Mg(OH)_2$ at a heating rate of 5°C/min.

From Figure 3.23, the TPD of methane shows its own characteristic profile as there is virtually no desorption trace at T_M 180°C and T_M ~ 80°C. These imply that methane does not dissociative adsorbed on the flat surface, $Mg_{5c}^{2+}O_{5c}^{2-}$, of MgO. In addition, there is no methane species loosely physisorbed either. Methanol showed a broad T_M which cover temperature between 280°C and 335°C for the third peak.

Virtually all TPD experimental systems are contaminated by moisture to some extent, even those using ultra high vacuum condition (Peng and Barteau, 1990). As a result, the probe molecule used as an adsorbate for the TPD process must be more competitive than water. For a basic catalyst such as MgO, phenol, which is more acidic than water, is therefore suitable since it should be preferentially adsorbed on the catalyst surface before moisture. Hence minor contamination with moisture will not interfere with the adsorption of phenol on the clean MgO surface. Methanol has an acidity equal to or only slightly higher than water but its third desorption peak has a broad T_M which seems to compose of two desorption peaks. This indicates the complicated desorption mechanism (see Figure 6.5, page 223) which may interfere the determination of T_M and therefore the type of sites. Methane is less acidic than water, and it is therefore less likely that no moisture interference will result when used as TPD probe.

Water itself can be used as a probe molecule to examine the active sites on the surface of MgO (Coluccia et al., 1987; Kuroda et al., 1988; Peng and Barteua, 1990, 1991; Russo and Noguera, 1991; Dunski et al., 1994). However, careful adsorption must be carried out since water can further diffuse into the bulk material to form hydroxide compound as demonstrated in Figure 3.24. Phenol was therefore used as a probe molecule in the present work.

3.3.6 TPD of carbon monoxide and sulphur dioxide from MgO

CO and SO_2 were also used as probe molecules to explore the surface of MgO. Approximately 4-8 mg of MgO precursor was packed between quartz wool in a quartz tube. The sample was then calcined under helium (high purity, CIG) atmosphere at a flow rate of 10 mL/min. The calcined MgO sample was cooled to room temperature under helium and then exposed to CO or SO_2 at a flow rate of 10 mL/min for 30 min. Excess adsorbed gas was removed by flowing helium until a constant base line on the recorder was obtained. The temperature programmed desorption was then carried out at a heating rate of 5°C/min to 800°C and a carrier gas flow rate was 30 mL/min. The TPD profile was acquired by means of a thermal conductivity detector (TCD).

It was found for the desorption of CO from MgO that a big broad peak over wide range of temperature and a side band were observed (Figure 3.25), while the desorption of SO_2 showed a physisorption peak at 50°C and a chemisorption peak, at 380°C for MgO calcined at 400°C and at 450°C for MgO calcined at 600 and 800°C (Figure 3.26). Determination of sites of MgO using these gases seems to be complicated since there are a number of species generated.

According to Guglielminotti et al. (1979) IR spectra of CO adsorbed at room temperature indicate the presence of a large number of adsorbed species which show absorption bands in the 2200-1000 cm^{-1} range. These bands were assigned to various species, including diatomic CO, cyclics of several resonance rings, polymers, carbonate structure, and so on. For the adsorption of SO_2 Waqif et al. (1992) also reported that there were several types of adsorption species, such as sulfites, hydrogen sulfide on the surface OH groups, and sulfate species. All can be formed on the catalyst surface. These complicated adsorptions cause possible interference in identification of active sites and subsequent calculations of activation energy. Finally,

phenol was chosen to determine the active sites and the basicities of the MgO surface sites due to its simple adsorption species.

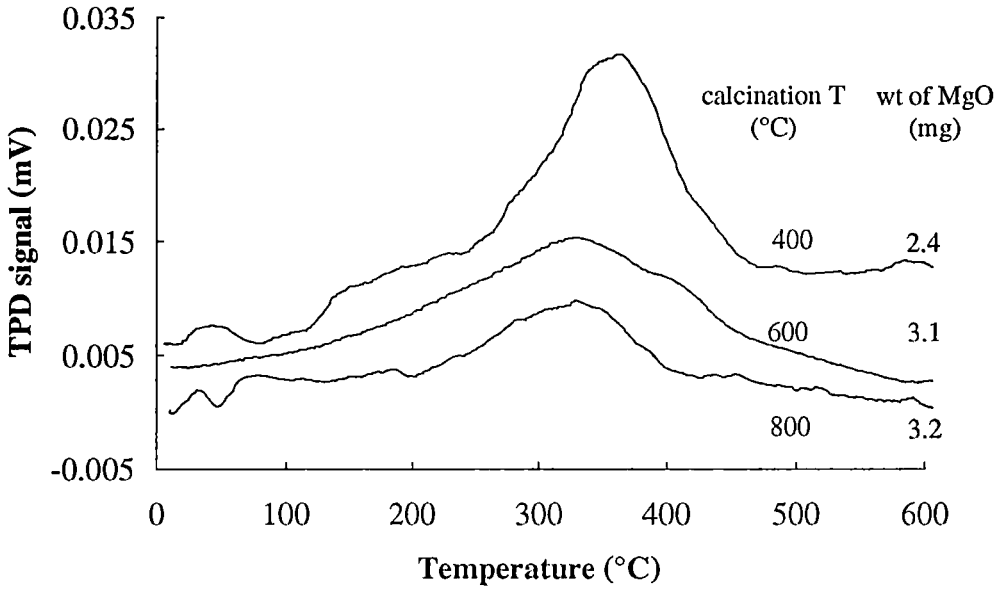

Figure 3.25 TPD of CO from MgO calcined at different temperatures (using a thermal conductivity detector).

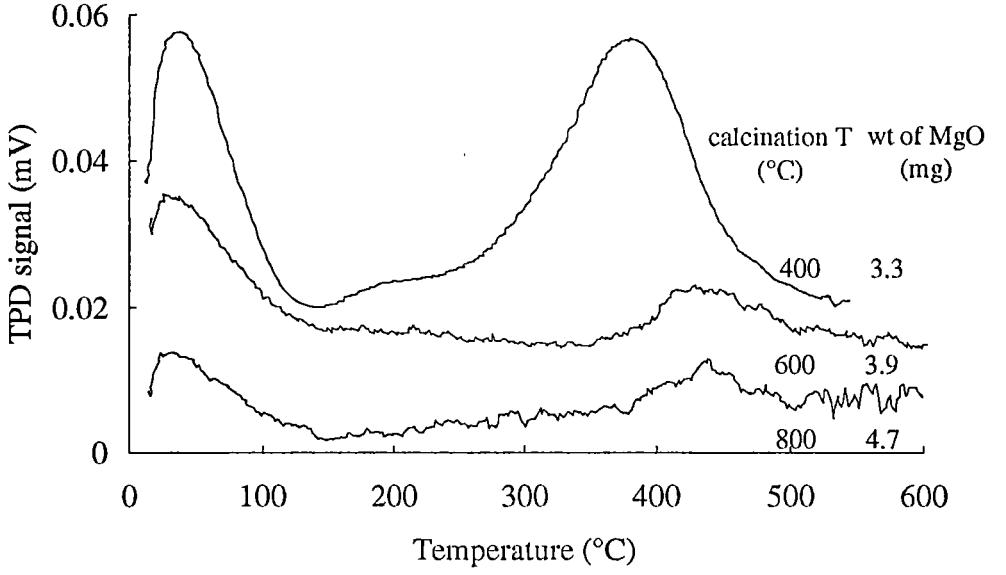

Figure 3.26 TPD of SO_2 from MgO calcined at different temperatures (using a thermal conductivity detector) .

3.4 Conclusion

Temperature programmed desorption of acidic gas was employed to explore the active sites and basicity of MgO. It was noted that the TPD using thermal gravimetric analysis (TGA) method provides more advantages than using a thermal conductivity detector (TCD), since not only the amount of desorbed molecules could be determined by the weight loss, but a more precise determination of the T_M from the DTG curve could also be observed using the TGA. This may be because the TG technique is an in situ analysis in which the weight change due to the desorption of the adsorbate can be promptly detected, whereas some relaxation due to the distance between the sample and the detector is inevitable using the TCD method. There are several factors to be considered (mainly, the carrier gas flow rate, the distance between sample and detector, and the adsorption of acidic gas on the metal gas line between sample and detector) if the TCD technique is employed. The TPD using the TGA method was therefore employed to distinguish and determine the number of different sites on the surface of MgO catalysts in the following Chapter.

A number of acidic gases were considered, mainly sulphur di oxide, carbon monoxide, phenol, water, methanol, and methane. However, there were many reasons for selecting phenol as the probe molecule to determine the sites and basicity on MgO catalysts. Firstly, strong acidic gases such as SO_2 and CO can be adsorbed on the catalyst surface in several forms of adsorptive species (Waqif et al., 1992; Gugliminotti et al., 1979) which may cause difficulty in the determination of the T_M and therefore the surface sites. Secondly, very weak acidic gas such as methane is very sensitive to contamination by water which is always found in the system even under ultra high vacuum condition (Peng and Barteau, 1990). Hence, some interference from the adsorption of water is likely to occur. Thirdly, methanol which has the same acidity as water displayed a very broad T_M. This indicates that desorption of methanol on MgO surface has more than one desorption mechanism. Finally, water which was used by several researchers to determine active sites on the

MgO surface can further react and diffuse into the bulk. The use of water as a probe molecule hence requires careful adsorption processes. As a result, phenol was selected as the probe molecule.

References

Choudhary, V. R. and Rane, V. H. (1990), Catal. Letters, **4**, 101.

Coluccia, S., Deane, A.M., and Tench, A. J. (1978), J. Chem. Soc., Faraday Tran I, **74**, 2913.

Coluccia, S., Tench, A. J., and Segall, R. L. (1979), **75**, 1769.

Coluccia, S. and Tench, A. J.(1980), Proc. 7th Intrrn. Congr. Catal., p 1160.

Coluccia, S., Boccuzzi, F., Ghiotti, G., and Mirra, C. (1980), Z. Phys. Chem. (Frankfurt am Main), **121**, 141.

Coluccia, S., Barton, A., and Tench, A. J., J. Chem. Soc. (1981), Faraday Tran I, **77**, 2203.

Coluccia, S., Boccuzzi, F., Ghiotti, G., and Morterra, C. (1982), J. Chem. Soc., Faraday Tran I, **78**, 211.

Coluccia, S., Garrone, E., and Borello, E. (1983), J. Chem. Soc., Faraday Tran I, **79**, 607.

Coluccia, S., Marchese, L., Lavagnino, S., and Anpo, M. (1987), Spetrochim. Acta, **43A** (12), 1573.

Delanney, F. and Delmon, B. (1984), Characterization of Heterogeneous Catalysts, New York, Marcel Dekker, p 18.

Dunski, H., Jozwiak, W. K., and Sugier, H. (1994), J. Catal., **146**, 166.

Echterhoff, R. and Knozinger, E. (1988), J. Mol. Structure, **174**, 343.

Evans, J. V. and Whateley, T. L. (1967), Trans. Faraday Soc., **63**, 2769.

Falconer, J. L. and Schwarz, J. A. (1983), Catal. Rev.-Sci. Eng., **25** (2), 141.

Fierro, J. L. G. (1990), Spectroscopic Characterization of Heterogeneous Catalysts Part B; Chemisorption of Probe Molecules, ed Fierro, Amsterdam, Elsevier Science Publishers B. V., pp B67-B143.

Gregg, S. J. and Sing, K. S. W. (1982), Adsorption, Surface Area and Porosity, 2nd ed, Academic Press Inc., London, p 81.

Guglielminotti, E., Coluccia, S., Garrone, E., Cerruti, L., and Zecchina, A. (1979), J. Chem. Soc., Faraday Trans. I, **75**, 96.

Hattori, H. (1985) in " Adsorption and Catalysis on Oxide Surfaces" ed. Che, M. and Bond, G. C., Elsevier, Amsterdam, pp 319-330.

Hattori, H. and Satoh, A. (1976), J. Catal., **45**, 32.

Ito, T., Sekino, T., Moriai, N., and Tokuda, T. (1981), J. Chem. Soc., Faraday Tran I, **77**, 2181.

Ito, T., Murakami, T., and Tokuda, T. (1983a), J. Chem. Soc., Faraday Tran I, **79**, 913.

Ito, T., Kuramoto, M., Yoshika, M., and Tokuda, T. (1983b), J. Phys. Chem., **87**, 4411.

Ito, T., Kawanami, A., Toi, K., Shirakawa, T., and Tokuda, T. (1988), J. Phys. Chem., **92**, 3910.

Ito, T., Tashiro, T., Watanabe, T., Kawasaki, M., and Toi, K. (1990), J. Chem. Soc., Faraday Tran I, **86**, 4071.

Ito, T., Tashiro, T., Kawasaki, M., Watanabe, T., Toi, K., and Kobayashi, H. (1991), J. Phys. Chem. , **95**, 4476.

Kuroda, Y., Ysugi, E., Aoi, H., Miura, K., and Morimoto, T. (1988), J. Chem. Soc., Faraday Tran I, **84** (7), 2421.

Lemaitre, J. L. (1984), Characterization of Heterogeneous Catalysts, ed Delannay, F., New York, Marcel Dekker, pp 32-40.

Parkinson, K. J. and Day, W. (1981), J. Experimental Botany, **33** (127), 411.

Peng, X. D. and Barteau, M. A. (1990), Surf. Sci., **233**, 283.

Peng, X. D. and Barteau, M. A. (1991), Langmuir, **7**, 1426.

Russo, R. and Noguera, C. (1991), Surf. Sci., **251/252**, 1081.

Silverstein, R. M., Bassler, G. C., Morrill, T. C. (1981), Spectrometric Identification of Organic Compounds, 4th Ed, John wiley & Sons Inc., pp 111-115.

Streitwieser, A. and Heathcock, C. H. (1981a), Introduction to Organic Chemistry, 2nd, Macmillan Publishing Co., Inc., p 998.

Streitwieser, A. and Heathcock, C. H. (1981b), Introduction to Organic Chemistry, 2nd, Macmillan Publishing Co., Inc., p 238.

Tanabe, K. (1985), in "Catalysis by Acids and Bases", ed. Imelik, B., Naccache, C., Coudurier, G., Taarit, Y. B., and Vedrine, J.C., Elsevier, Amsterdam, pp 1-14.

Tanabe, K. (1989), in " Acid-Base Catalysis", ed Tanabe, K., Hattori, H., Yamaguchi, T., and Tanaka, T., Sapporo, pp 513-527.

Tanabe, K. and Nishizaki, T. (1977), Proc. 6th Intern. Congr. Catalysis, 2, 863.

Tanabe, K., Misono, M., Ono, Y., and Hattori, H. (1989), New Solid Acids and Bases, Tokyo, Kodansha, p 14.

Wang, G. W., Ito, H., Hattori, H., and Tanabe, K. (1983), J. Chem. Soc., Faraday Tran I, **79**, 1373.

Wang, G. W. and Hattori, H. (1984), J. Chem. Soc., Faraday Tran I, **80**, 1039.

Waqif, M., Saad, A. M., Bensitel, M., Bachelier, J., Saur, O., and Lavalley, J-C. (1992), J. Chem. Soc. Faraday Trans., **88** (19), 2931.

Xu, B., Yamaguchi, T., and Tanabe, K. (1988), Mater. Chem. and Phys., **19**, 291.

Zechhina, A., Lofthouse, M. G., and Stone, F. S. (1975), J. Chem. Soc., Faraday Tran I, **71**, 1476.

Zhang, G., Hattori, H., and Tanabe, K. (1988), Appl. Catal., **36**, 189.

CHAPTER 4

ACTIVE SITES & CATALYTIC PERFORMANCE OF MgO CATALYSTS FOR OXIDATIVE COUPLING OF METHANE

4.1 Introduction

A number of promising catalysts, such as Li/MgO (Ito et al., 1985), Mn/MgO (Labinger et al., 1987), PbO-MgO (Bartek et al., 1988), Cl/Li/MgO (Khan and Ruckenstein, 1992) used in the oxidative coupling of methane are based on MgO. Since MgO is a main component of these catalysts, it is likely that their catalytic performance is influenced by the properties of MgO. As a result, some investigations (Anpo et al., 1988; Hargreaves, et al., 1992; Wu et al., 1993; Choudhary et al., 1994) have been undertaken to identify the active sites of MgO. It is anticipated that a thorough knowledge of MgO active sites will enable more active catalysts to be developed and the catalyst activity may be enhanced by simply increasing the concentration of active sites on catalyst surface.

Keller and Bhasin (1982) screened a great number of metal oxides, supported on an alpha-alumina for their catalytic performance in the oxidative coupling of methane. MgO was reported (Keller and Bhasin) to be an active catalyst for C_2-formation, however, less active than the oxides of Mn, Sn, Sb, Pb, Bi, Tl and Cd. Driscoll et al. (1985), observed that when methane was passed over MgO at 500°C, methyl radicals were produced on the surface and released to the gas phase. These methyl radicals were trapped in a solid argon matrix and analysed by EPR spectroscopy. The activity of MgO was observed to depend on whether the MgO was pretreated under vacuum or a flow of oxygen. Vacuum conditioning led to essentially no activity while oxygen conditioning resulted in substantial radical production. Over MgO it was believed that intrinsic cation vacancies react with molecular oxygen to

give O^- centre which can abstract a hydrogen atom from methane to produce a methyl radical.

The role of surface O^-, however, was studied by Hutchings et al. (1987). These workers found that O^- is not only the selective species for activation of CH_4 as in previous studies (Driscoll et al., 1985), but also has a second role which becomes more dominant at higher temperatures. As a consequence, the production of the undesired total oxidation products was enhanced. Mehandru et al. (1988) showed in a theoretical study that an O^- ion in a $Mg_{21}O_{20}^{3+}$ cluster model is capable of abstracting an $H\cdot$ atom from CH_4 and, that the reaction of the resulting $CH_3\cdot$ radical with the surface to form $CH_3O_s^-$ is favoured when corner Mg^{2+} sites are available. These results led to the proposition (Lunsford et al., 1989) that roughened surfaces or small crystallites would promote the non-selective oxidation of methane. By contrast, extended {100} surfaces would favour the oxidative coupling reaction.

To confirm the above proposition the relationship between the surface morphology and the reactivity of MgO was then determined (Lunsford et al., 1989) using electron microscopy to monitor catalyst morphology and e.s.r. in combination with a matrix-isolation technique to examine the catalyst ability to generate and react with gas phase methyl radicals. It was found that MgO samples with many more corner sites did not manifest a significantly greater specific activity for reaction with methyl radicals than the MgO which has larger crystal or less corner sites. Lunsford et al. therefore concluded that morphology including corner sites, defect sites, kinks etc.- which would enhance the concentration of Mg^{2+} in low coordination was not the important factor for the reaction.

Hargreaves, Hutchings and Joyner (1990) investigated the structure and catalytic performance of two MgO catalysts used for methane coupling . MgO

prepared by burning Mg metal ribbon in air consisted mainly of single MgO crystallites with regular cubic structure while MgO obtained from the thermal decomposition of basic carbonate comprised of agglomerates of smaller MgO crystallites. It was found that the MgO obtained from the carbonate was more selective for the formation of C_2-hydrocarbon products and also gave higher methane conversions under comparable reaction conditions. Based on electron micrograph evidence and the catalytic data, the authors concluded that the morphology of MgO was a significant factor in the oxidative coupling reaction of methane.

To confirm their argument on the importance of catalyst morphology, Hargreaves and co-workers (Hargreaves et al., 1992) tested MgO samples obtained from thermal decomposition of hydroxide, burning Mg ribbon in air, and thermal decomposition of basic carbonate. The catalysts were examined for their morphologies by transmission electron microscopy. The correlation between catalyst morphology and catalytic performance for the oxidative coupling of methane was then discussed. It was demonstrated that MgO prepared from the hydroxide and from burning Mg ribbon in air showed similar morphologies, exposing largely {100} planes; they also exhibited very similar catalytic selectivities and specific activities. The ribbon residue, however, had a cube length which was greater than that of the material obtained from the hydroxide by a factor of 5-10. These results lead to the conclusion that steps and corner sites play no significant role in the catalytic activity since MgO prepared from hydroxide has much greater density of these sites than the ribbon residue, but the catalytic performance was unchanged. It was proposed that the active sites should be located on the {100} flat surfaces for these two MgO catalysts.

The MgO sample obtained by thermal decomposition of basic carbonate was found to be the most selective catalyst and possessed a greater proportion of higher index mean crystal planes (e.g., {111}) than the less selective forms of MgO. As a

result, the ratio of steps, edges and corners to flat surfaces were much higher for this catalyst. This result suggested that these low-coordination sites are now present in sufficient numbers to contribute to catalyst performance; the greater proximity of these low-coordinate sites may also enhance C_2-selectivity. However, an alternative possibility, that the formed " bottom step " sites, shown in Figure 4.1 are catalytically active was suggested by the authors (Hargreaves et al., 1992).

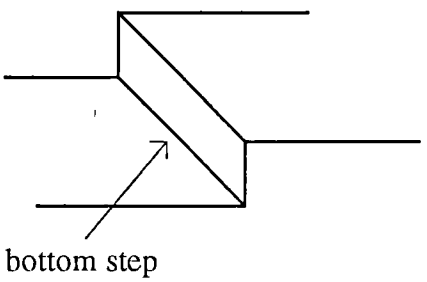

Figure 4.1 The bottom step site on MgO surface.

Wu et al.(1993) investigated the partial oxidation of methane to ethane over pure and Li-promoted MgO catalysts prepared under well-controlled, ultra high vacuum (UHV) conditions using a combination of surface science techniques and elevated-pressure kinetic measurements. By means of electron energy loss spectroscopy in conjunction with elevated-pressure kinetic measurements, a variety of surface defects and possible active sites which might be responsible for the methane coupling reaction were identified. For pure MgO films it was demonstrated that the generation of F-type defects, which are active sites for the methane coupling, occurs in the 1200-1400K temperature range. More information of F-type centres on Li-promoted MgO catalysts will be presented in the next Chapter.

Since the nature of active sites on MgO for the oxidative coupling of methane is still a topic of controversy in the literature, the present work was undertaken to provide further details and subsequently identify the active sites on the MgO surface. In this chapter the relationship between the surface morphology, surface sites and catalytic performance of MgO catalysts is described. MgO samples of different morphology were characterized to allow the surface sites to be determined prior to catalytic testing. The temperature programmed desorption (TPD) technique was employed to characterise the catalysts, as it has been suggested by Falconer and Schwarz (1983) that this technique is sensitive to catalyst properties, such as changes due to weight loading, preparation procedure, alloying, support and so forth. Moreover, it is a quick method. Phenol was used as a probe molecule, and the number of sites (including their basic strength/basicity) was determined from the finger print-type desorption spectra of this probe molecule.

The catalytic performance of MgO catalysts was determined using a conventional flow reactor operating under an atmospheric pressure. The correlation between surface sites and their catalytic performance was investigated, and the active sites for methane coupling were consequently identified. MgO catalysts were also examined for surface sites after catalytic testing in order to explore any changes in the nature of the active sites on the catalyst surface. Finally, the relationship between morphologies, active sites and catalytic activity of MgO will be discussed at the end of this Chapter.

4.2 Experimental

4.2.1 Determination of surface sites and the basicity of MgO catalysts prior to and after catalytic testing

MgO catalyst with different morphologies arising from the different precursors and preparation methods were characterised. The number of sites was determined using the temperature programmed desorption of phenol (coupling with thermal gravimetric analysis technique) using a ramp rate of 5 °C/min. An amount of 18-25 mg of sample was used. The sample was exposed to phenol for 30 min, purged with carrier gas (Ar, CIG, high purity) and then submitted to a linear temperature ramp as described in section 3.3.4. From the DTG fingerprint spectra, the different sites and the number of each site on MgO catalysts were determined and expressed in term of the amount of phenol (mmol) adsorbed (desorbed) per unit weight of catalyst (g). The deviation for the determination of surface sites on MgO was found to be ± 20 % which was estimated from repeating determinations on several samples.

The used MgO catalysts were pretreated under an atmosphere of Ar at a flow rate of 10 mL/min at 800°C for 1 h to remove all the adsorbed species that had formed on the catalyst surfaces during the catalytic reaction. They were then exposed to phenol for 30 min, purged with Ar and submitted to the temperature programmed desorption as conducted for the fresh MgO catalysts.

4.2.2 Catalytic activity determination

4.2.2.1 Reactor design

According to Kalenik and Wolf (1990) the residence time (which is defined as the heated volume per unit flow rate) of the reactants is one of the key factors that can cause an effect of the gas-phase reaction in the absence of the catalyst. The reactor

used for screening the catalysts in the oxidative coupling methane in the present work was consequently designed to minimise this effect by reducing the void volume in the reactor as much as possible. The reactor design is shown in Figure 4.2.

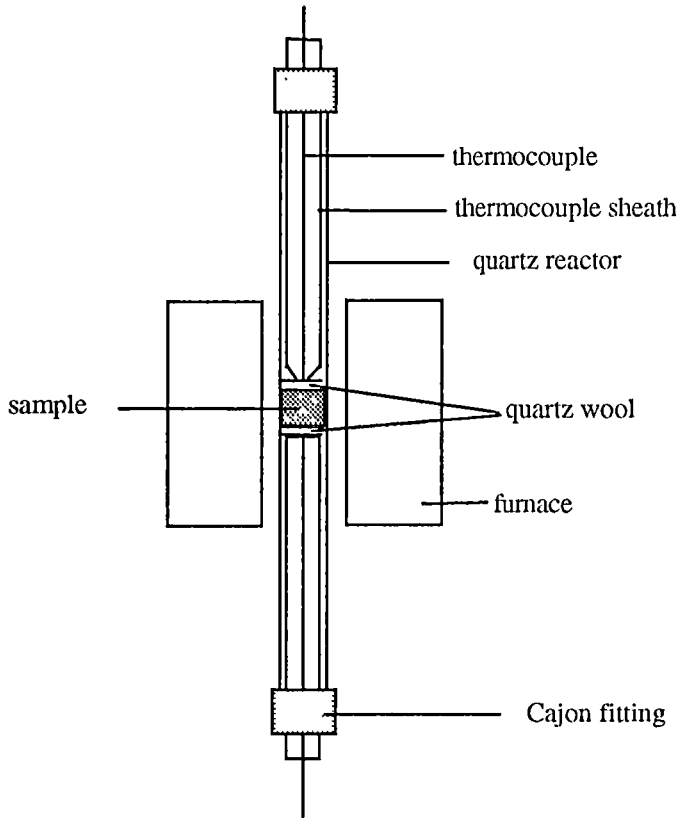

Figure 4.2 The reactor used for the catalytic test.

A quartz tube with an internal diameter of 0.8 cm and 27 cm long was used as a reactor. Approximately 0.1 g of MgO catalyst was placed between quartz wool in the middle of the reactor and pretreated in Ar at 750°C for 2 h prior to cofeeding the reactants. For the in situ prepared catalysts the calcination was carried out in this reactor at 800°C for 4 h in Ar and the catalytic testing was then performed without further pretreatment. To reduce the free heated volume, two quartz tubes with an outside diameter 0.7 cm and one end sealed were used as the thermocouple sheathes

placed on top and bottom of the catalyst bed. These two quartz tubes were filled with quartz chips to make a reliable thermal contact with the thermocouples (K type, range 0-1100°C). The reaction volume hence depends largely on the volume of catalyst packed in the quart reactor. This volume was varied between 1-2 mL depending on the density of samples.

The reactor was heated by a small tubular furnace with an inside diameter of 1.8 cm and a short heating zone of 6 cm. An electronic temperature controller (± 0.3 % of reading temperature i.e.± 2°C at 750°C) was used to control the furnace via the upper thermocouple inside the reactor. The temperature gradient of the furnace was examined prior to use by placing one thermocouple at the hottest spot (0.5 cm above the middle) of furnace, and the temperatures at several spots along the furnace were measured by another thermocouple. It was observed that when the temperature at the hottest zone was 800°C, the temperature at ± 1.5 cm from this position was found to be 790°C.

4.2.2.2 The feeding operation

Continuous cofeeding of the gas reactants, methane and oxygen, and a diluent, argon, was employed. Mass flow controllers were used to control the flow rate of each gas; 3.6 mL/min (110 torr) for O_2 (CIG, 99.6 %), 7.2 mL/min (220 torr) for CH_4 (CIG, instrument grade, 99.7 %), and Ar (CIG, high purity grade, 99.995 %) was added to make up to the total flow rate of 25 mL/min (the total pressure was 760 torr at room temperature). The composition ratio of the gas stream was 1:2:4 for O_2:CH_4:Ar on a pressure basis. These gases were thoroughly mixed by passing though a mixing coil prior to the reactor as displayed in Figure 4.3. The reactor was connected between the mixing coil and the product analysis unit via two Ultra-torr

Cajon fittings. The product analysis was conducted after at least 2 h to allow the reaction to reach steady state.

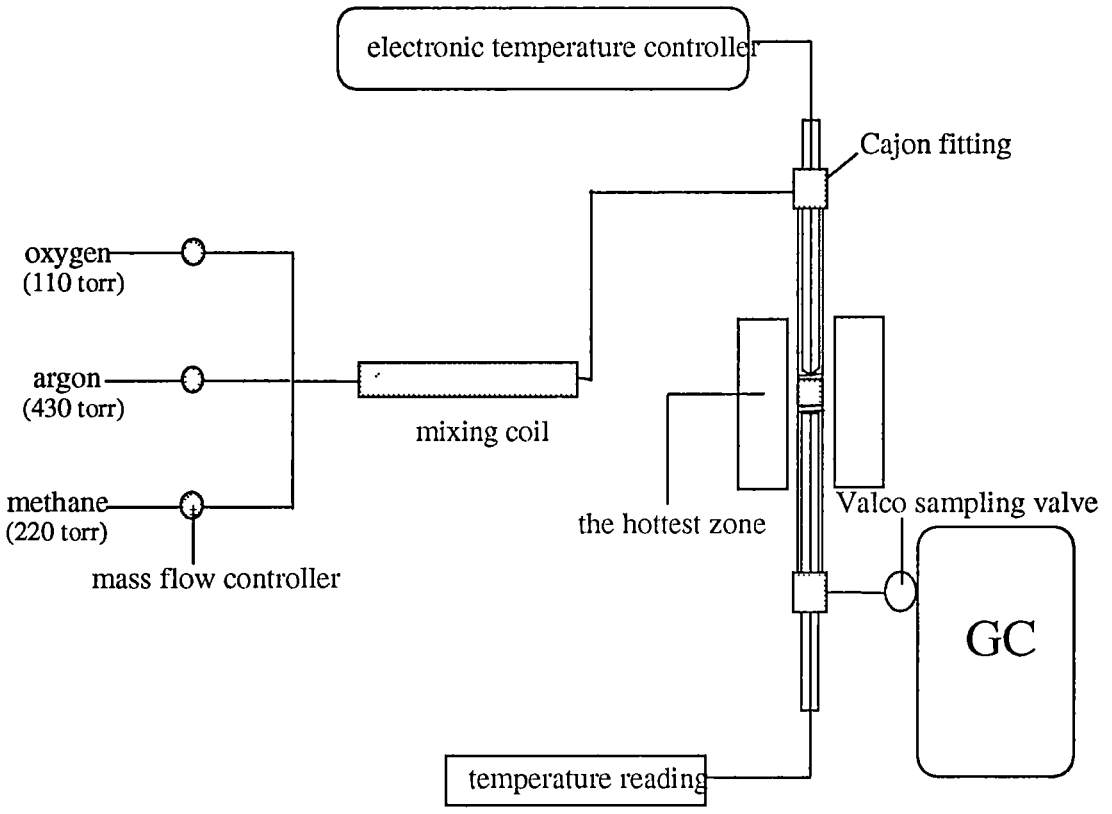

Figure 4.3 The flow chart of catalytic reactor system.

4.2.2.3 Product analysis

The gas stream from the reactor was continuously flown though the injection unit. A Valco sampling valve with a sample loop of 0.25 mL was installed as an injector to deliver the gas sample to the column. A HP 5890 series II gas chromatograph with a Carbosive S-II column and a thermal conductivity detector was employed to analyse the composition of the gas stream from the reactor. Argon (CIG,

high purity) at 180 kPa column head pressure was used as a carrier gas at a total flow rate of 45 mL/min and a reference flow rate of 15 mL/min. To achieve a good separation between the gas products, the column was heated at a temperature of 30°C for 1 min, then it was increased at a ramp rate of 15°C/min to 180°C and held at 180°C for 10 min.

The products were identified and calibrated by comparison with three standard mixtures. The first one was CH_4 (5.98 ± 0.12 %), CO (37.3 ± 0.2 %), CO_2 (31.3 ± 0.2 %) and H_2 (25.4 ± 0.2 %) by volume from CIG. The second mixture wais CH_4 (0.971 %), C_2H_6 (1.040 %), N-C_3H_8 (0.994 %), N-C_4H_{10} (1.000 %) and N-C_5H_{12} (1.000 %) by volume in He, obtained from Scott Specialty Gases. The last mixture was C_2H_4 (0.998 %), C_3H_6 (1.000 %), 1-C_4H_8 (1.000 %) and 1-C_5H_{10} (1.000 %) by volume in He, obtained from Scott Specialty Gases. The amount of each product was estimated from the area under peak which was assumed to be linearly realated to the area under the peak of the standard.

The amount of methane and oxygen reacted were estimated from the difference of peak areas between the catalytic and blank reactions.

4.2.3 Terms and definitions for activity comparison

The following definitions of terms and units were used thoughout this work. The term *methane conversion* is used to indicate the fraction of methane reacted, relative to the methane fed, expressed as a percentage. Likewise the *oxygen conversion* is defined as the fraction of oxygen reacted, relative to the oxygen fed, and also expressed as a percentage. The term *C_2-selectivity* represents the amount of methane converted to ethane and ethylene relative to the total amount of methane reacted, express as a percentage. Similarly the term *nonselective oxidation* or CO_x

indicates the amount of CO_2 and CO products as a percentage relative to the total amount of methane reacted.

There have been a variety of reaction conditions employed by various investigators in numerous studies, so it is sometimes difficult to compare the activity of catalysts if a quantitative comparison between these reports is not possible. It is therefore essential to report the common terms and units used to correlate the present work with the others. Such quantities are related to the reaction rate. The first one is the space velocity (SV) defined in terms of the volumetric flow rate (F) of the reactants and the catalyst volume (V):

space velocity (SV) = F/V s^{-1} (Boudart and Djéga-Mariadassou, 1984) [4.1]

Frequently this quantity is expressed in h^{-1}, and in gaseous system is called the *gaseous hourly space velocity* (GHSV). The inverse of the space velocity is the space time (τ).

$$\tau = V/F \quad s \text{ (Boudart and Djéga-Mariadassou)} \qquad [4.2]$$

The term *space time yield* (STY) is the quantity of a product formed per quantity of catalyst per time unit, and expressed in $\mu mol.s^{-1}.g^{-1}$(Boudart and Djéga-Mariadassou).

The second quantity related to the reaction rate is the *contact time* (CT) defined as the weight of catalyst (W) divided by the flow rate of reactant (Amenomiya et al., 1990).

$$CT = W/F \quad g.s.mL^{-1} \qquad [4.3]$$

The third term used by some investigators, in particular for the blank reaction, is the *residence time* (RT), defined as the heated volume divided by the reactant flow rate, and expressed in time unit (Hatano et al., 1990).

Among the reaction conditions, the contact time seems to have greatest effect on the C_2 yield (Otsuka and Komatsu, 1987 ; Lane and Wolf, 1988), and it is believed (Amenomiya et al., 1990) to be a better measure for the comparison of catalytic performance than the space velocity when very small amounts of catalysts are used. However, the gaseous hourly space velocity and the space time yield are also used by some investigators (Hargreaves et al., 1992; Amenomiya et al., 1990). The calculation of these quantities for the conditions employed in this work is demonstrated as follows.

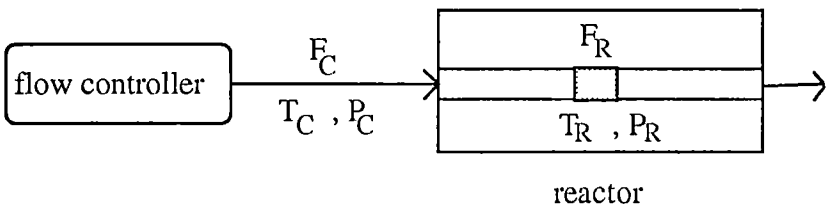

T_C, P_C and F_C are the temperature (K), pressure (atm) and the flow rate (mL/min) from the flow controller, while the T_R, F_R and F_R are the values under the reaction conditions. The flow rate under the reaction conditionis estimated using the gas law, and hence;

$$F_R = F_C.(T_R/T_C)(P_C/P_R) \qquad [4.4]$$

For a flow rate of 25 mL/min at 298 K and 1 atm at the flow controller, the flow rate under the reaction conditions of 1023 K and 1 atm is therefore 86 mL/min.

The amount of MgO used in the present work was 0.100 ± 0.005 g, the contact time was hence 0.07 g.s.mL^{-1}. The heated volume in the reactor was less than 3 mL, the residence time was consequently less than 0.03 min or 2.1 s. The gaseous hourly space velocity was varied between 2575-5150 h^{-1} due to the variation of catalyst volumes (due to their different density) between 1-2 mL.

4.2.4 Gas-phase reaction in the blank reactor

Blank reactor corrections was critically discussed between the Lunsford group (Hatano et al., 1990) and Yates and Zlotin (1990) because of the difference in reaction conditions used by these authors. It was pointed out (Hatano et al., 1990) that the key factor for the gas-phase or blank reaction was the residence time (RT). Kalenik and Wolf (1990) have reported that the gas-phase reactions became important when the reaction temperature is greater than 650°C, reactant partial pressures exceed 0.4 atm, and the residence times of reaction gases were longer than 0.1 min. To compare results from different studies, the residence time of reactants and reactant partial pressure should be clearly defined. In the present work the partial pressure of reactants was 0.43 atm (O_2:CH_4:Ar = 1:2:4 at total pressure 1 atm), and the reaction temperature was 750°C which results in a residence time was less than 0.03 min or 2.1 second.

The noncatalyzed thermal reaction was investigated for the reactor used in this work by filling the reactor with quartz wool (occupied volume 2 mL) instead of the catalyst. Under the conditions described above, it was observed that the methane conversion was 2 % with C_2-selectivity of 70 %, and the oxygen consumption was less than 5 % for the gas-phase reaction detected after the reaction had proceeded for 2 h. It was therefore assumed that the reaction conditions used here were suitable for screening the activity of catalysts.

4.3 Results

4.3.1 The surface sites and basicity of each site on MgO catalysts prior to the catalytic test

A number MgO catalysts with different surface areas and physical profiles (particle size/particle distribution profiles and pore structures) were examined to determine their surface sites and basicity. These catalysts were prepared from different precursors and calcining conditions as described in Chapter 2. Details of the precursors and calcining conditions for the MgO samples are displayed in Table 4.1. The abbreviations for each MgO (displayed in the first column) will be used to identify the catalysts thoughout this Chapter.

Table 4.1 MgO catalysts prepared from various precursors and calcination conditions.

MgO	precursor	calcination condition
ex CO_3	$MgCO_3.H_2O$	800°C in Ar for 4 h
ex ba. CO_3	$4MgCO_3.Mg(OH)_2.5H_2O$	800°C in Ar for 4 h
ex Ox	$MgC_2O_4.2H_2O$	800°C in Ar for 4 h
ex OH	$Mg(OH)_2$ precipitated at pH 10.0	800°C in Ar for 4 h
ex OH, hyd	$Mg(OH)_2$ from the hydrolysis of $Mg(CH_3COO)_2$	800°C in Ar for 4 h
ex OH, TP	$Mg(OH)_2$ precipitated at pH 10.0	temperature programmed; 15°C/min to 350°C, 350° 45 min, 5°C/min to 800°C, 800°C 4 h
ex OH9.5, TP	$Mg(OH)_2$ precipitated at pH 9.5	temperature programmed; 15°C/min to 350°C, 350° 45 min, 5°C/min to 850°C, 850°C 10 min
ex OH10.0, TP	$Mg(OH)_2$ precipitated at pH 10.0	temperature programmed; 15°C/min to 350°C, 350° 45 min, 5°C/min to 850°C, 850°C 10 min
ex OH11.0, TP	$Mg(OH)_2$ precipitated at pH 11.0	temperature programmed; 15°C/min to 350°C, 350° 45 min, 5°C/min to 850°C, 850°C 10 min

Since all MgO catalysts screened for catalytic activity in the oxidative coupling of methane were calcined at 800°C and over, sites S_{II} and S_{III} were therefore expected to appear on the catalyst surface. The amount of site S_{II} assigned to be on the planar

{100} surface was estimated from the weight loss on TG curve due to the desorption of phenol over the temperature range of 120-210°C. The amount of site S_{III} (the combination of the edges, $Mg_{4c}^{2+}O_{4c}^{2-}$ and the corners, $Mg_{4c}^{2+}O_{3c}^{2-}$, $Mg_{3c}^{2+}O_{4c}^{2-}$ and $Mg_{3c}^{2+}O_{3c}^{2-}$), namely the surface sites of low coordination was estimated from the weight loss on TG curve due to the desorption of phenol over the temperature of 210-390°C.

Table 4.2 The basicity of each type of sites of MgO catalysts prior to catalytic testing.

MgO catalyst	surface area, BET (m^2/g)	surface sites on the planar {100} surface, site S_{II} (mmol/g) ± 10-20 %	surface sites of low coordination, site S_{III} (mmol/g) ± 10-20 %	Total no. of sites (mmol/g) ± 20 %
ex CO_3	24	0.08	0.12	0.20
ex ba. CO_3	25	0.09	0.13	0.22
ex Ox	30	0.11	0.13	0.24
ex OH	49	0.12	0.16	0.28
ex OH, hyd	38	0.05	0.06	0.11
ex OH, TP	89	0.22	0.17	0.39
ex OH9.5, TP	79	0.15	0.16	0.31
ex OH10.0, TP	82	0.15	0.17	0.32
ex OH11.0, TP	79	0.14	0.17	0.31

In Table 4.2 the total number of the surface sites observed for MgO catalysts seems to correlate with the surface areas (BET) except MgO ex OH prepared by the hydrolysis method. For MgO calcined from different precursors at 800°C for 4 h it was found that the number of sites as well as the surface areas of MgO calcined from the carbonate and basic carbonate precursors are similar. The number of sites on the surface of MgO calcined from the oxalate salt is slightly higher than that of MgO obtained from the carbonate precursors, but lower than that of MgO prepared from $Mg(OH)_2$.

Considering MgO obtained from the same precursor, $Mg(OH)_2$, but using different preparation methods and calcining conditions, the total number of surface sites also correlates with the surface areas except for the MgO prepared by the hydrolysis method. The number of sites on MgO obtained by the hydrolysis method was found to be very low relative to its surface area. However, it was observed that the colour of MgO ex OH, hyd is slightly grey which may indicate the possible deposition of carbon in the sample. The carbon impurity may occur from decomposition of the residual acetate of the precursor, magnesium acetate, remaining in the $Mg(OH)_2$ precipitate. The carbon contamination is likely to cause the lower number of MgO active surface sites. It may replace the basic sites that are responsible for the adsorption of phenol.

The basicity of the MgO samples displayed in Table 4.2 shows only the number of (each) sites on 1 g of the catalysts. There is, however, another aspect to keep in mind when considering the basicity of catalysts, namely the density of the surface sites per unit surface area of the catalyst. The latter is derived from the former by dividing the number of sites by the surface area. The basicity of each type of surface site in term of the density of sites per unit surface area is displayed in Table 4.3.

Table 4.3 The basicity of sites in term of the density of sites per unit surface area.

MgO catalyst	total surface area, BET (m^2/g) ± 10 %	surface sites on the planar {100} surface ($\mu mol/m^2$) ± 20-30 %	surface sites of low coordination ($\mu mol/m^2$) ± 20-30 %
ex CO_3	24	3.3	5.0
ex ba. CO_3	25	3.6	5.2
ex Ox	30	3.7	4.3
ex OH	49	2.4	3.3
ex OH, hyd	38	1.3	1.6
ex OH, TP	89	2.4	2.0
ex OH9.5, TP	79	1.9	2.1
ex OH10.0, TP	82	1.8	2.0
ex OH11.0, TP	79	1.8	2.0

From Table 4.3 considering the density of the surface sites on MgO prepared from different precursors, it is apparent that the samples obtained from the carbonate and hydroxy carbonate possess the highest density of sites per unit surface area, in

particular the density of the surface sites of low coordination. The high density of the low coordinated ions, the edges ($Mg_{4c}^{2+}O_{4c}^{2-}$) and the corners ($Mg_{4c}^{2+}O_{3c}^{2-}$, $Mg_{3c}^{2+}O_{4c}^{2-}$ and $Mg_{3c}^{2+}O_{3c}^{2-}$), indicates the degree of roughness on the catalyst surface. The results obtained here agree with the TEM data obtained by Moodie and Warble (1971), and Hargreaves et al. (1992). These micrographs showed that MgO calcined from the basic carbonate exhibited a great preponderance of microfacetted, high index planes e.g. {111} and {110}, than were observed with the MgO calcined from the hydroxide precursor. This means that MgO prepared from the basic carbonate possesses a much higher number of corner and step sites than MgO ex OH. These results indicate that the TPD of phenol using TG in conjuction with DSC techniques is a sensitive and reproducible medthod for exploring the surface structure of MgO catalysts.

The density of the surface sites of low coordination on MgO calcined from the oxalate was observed to be higher than that prepared from the hydroxide, but lower than that prepared from the carbonates. This may mean that the degree of roughness on the MgO surfaces is in the order ex CO_3 and ex ba CO_3 > ex Ox > ex OH. The degree of roughness on the catalyst surfaces is in turn an indicator of the defects in MgO crystallites. Consequently, it can be concluded that the ordering in MgO microstructure is ex OH > ex Ox > ex CO_3 and ex ba CO_3 which is the inversion of the degree of roughness.

The higher ordering of the MgO crystals prepared from the hydroxide is supposed to arise from the topotactical decomposition mechanism-the highly orientated layers of $Mg(OH)_2$ crystals that occur during thinckening/washing etc. result in a large multiple layer of MgO crystals during calcination. Such microstructures are not noted in MgO obtained from other precursors such as $MgCO_3$ and MgC_2O_4 (Green 1983). In the latter materials, crystal growth will be more

influenced by bulk impurity and defect concentrations in MgO crystals than in MgO derived from $Mg(OH)_2$ where an additional contribution owing to the highly preferred orientation of multiple layers will be present.

For MgO calcined from $Mg(OH)_2$ samples that were precipitated at different pH, the densities of the surface sites as well as the surface areas were similar. These results indicate that the pH during the precipitation of $Mg(OH)_2$ has no significant effect on the MgO surface sites under the same calcining condition.

The effect of calcining conditions on the surface sites can be seen by comparing MgO ex OH, ex OH, TP and ex OH10, TP. The MgO ex OH was found to have the highest density of the surface sites of low coordination, whereas the MgO ex OH TP and the MgO ex OH10.0, TP displayed similar densities of these sites. These results indicate that the rate of heating to final temperature has an effect on the density of surface sites on MgO, while the period of holding the final temperature has no significant effect on MgO calcined by the temperature programmed method. Based on the assumption that the high density of the surface sites of low coordination is an indicator of the less ordering in MgO microstructure, it can be concluded that the procedure allowing $Mg(OH)_2$ to decompose at low temperature, 350°C, and then slowly increasing the temperature to 800°C results in MgO (ex OH,TP) with higher crystal ordering than the normal (ex OH) procedure of increasing the temperature to 800°C directly.

4.3.2 Catalytic activity comparison of the in situ MgO and the aged MgO catalysts

To investigate the effect of aging on the catalytic activity of MgO, two sets of the catalysts were studied. One set consisted of MgO prepared in situ by calcining the

approximate precursors at 800°C for 4 h under argon at a flow rate of 14 mL/min. The amount of precursor and the estimated amount of MgO are displayed in Table 4.4.

Table 4.4 The amount of precursors and estimated amount of MgO catalysts.

precursor wt (g)	0.260 (CO_3)	0.243 (ba CO_3)	0.369 (Ox)	0.144 (OH)
MgO catalyst (g)	0.102	0.101	0.100	0.099

The catalytic testing was carried out at 750°C straight away after the calcination.

The second set is the aged MgO catalysts that had been prepared and stored for 6 months before use. Aproximately 0.100 ± 0.004 g of the aged catalyst was pretreated in Ar at 800°C for 2 h prior to cofeeding the gaseous reactants. The products were analysed after the reaction had proceeded for 2 h. Results are displayed in Table 4.5.

Table 4.5 Oxidative coupling of methane over in situ and aged MgO catalysts at 750°C.

catalyst	GHSV (h^{-1})	%CH_4 con.	%O_2 con.	%C_2 selectivity			%CO_x		
				C_2H_6	C_2H_4	total	CO	CO_2	total
F ex CO_3	2574	33	94	*18*	*27*	45	*11*	*44*	55
ex CO_3	3275	33	77	*22*	*25*	47	*16*	*37*	53
F ex ba. CO_3	2860	29	90	*18*	*26*	44	*13*	*43*	56
ex ba. CO_3	5000	29	75	*23*	*25*	48	*15*	*37*	52
F ex Ox	3400	34	71	*15*	*16*	31	*17*	*52*	69
ex Ox	5200	29	65	*16*	*14*	30	*21*	*49*	70

F ex OH	4290	30	60	*11*	*9*	20	*22*	*58*	80
ex OH	5148	29	62	*12*	*10*	22	*25*	*53*	78

F denotes the in situ calcined catalysts.

It was found that most of the hydrocarbon products were ethane and ethylene. Acetylene and other higher hydrocarbons were also detected but they were not significant in comparison with ethane, ethylene and CO_x products.

From Table 4.5 it can be seen that there was no difference for the methane conversion over the in situ prepared catalysts and the catalysts that had been stored in a desiccator prior to use. For the oxygen conversion, however, the fresh calcined catalysts except the ex OH seemed to be slightly more active than the aged catalysts. The ratio of C_2H_4 to C_2H_6 and the ratio of CO_2 to CO were observed to be in agreement with the oxygen consumption. According to Hargreaves et al. (1990, 1991), both C_2H_4 and CO_2 are secondary products which increased with greater residence time. The slightly higher yield of these secondary products for the in situ prepared catalysts is probably due to their higher of the heated volume and consequently residence time. From Table 4.5 it can be seen that the values of GHSV of the in situ catalysts are lower than the aged catalysts because the heated volume for the former was equal to the packing volume of precursors which was higher than that latter.

In general the total C_2-selectivity and the total nonselective CO_x of the fresh catalysts and the aged catalysts were found not to be significantly different relative to the experimental error which was estimated to be about 3-5 %.

The catalytic performance with times on stream of these catalysts are displayed in Figure 4.4.

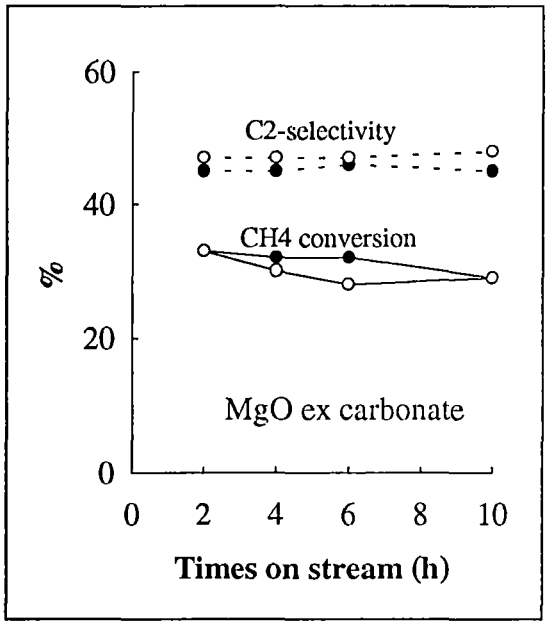
60
40
20
0
%
C2-selectivity
CH4 conversion
MgO ex carbonate
0 2 4 6 8 10
Times on stream (h)

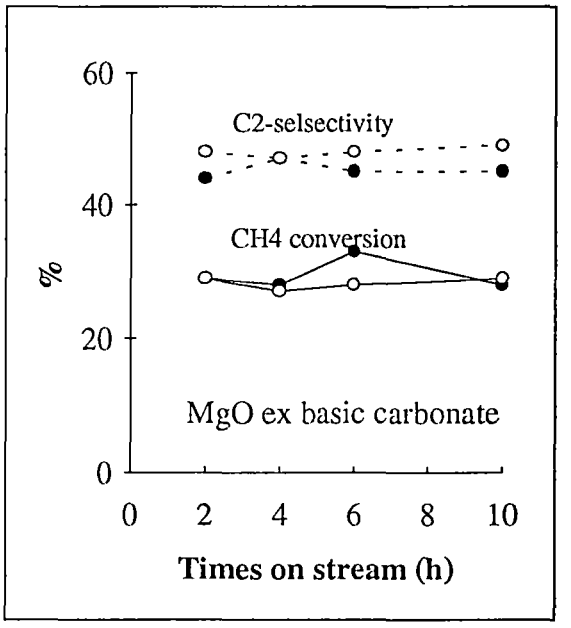
60
40
20
0
%
C2-selsectivity
CH4 conversion
MgO ex basic carbonate
0 2 4 6 8 10
Times on stream (h)

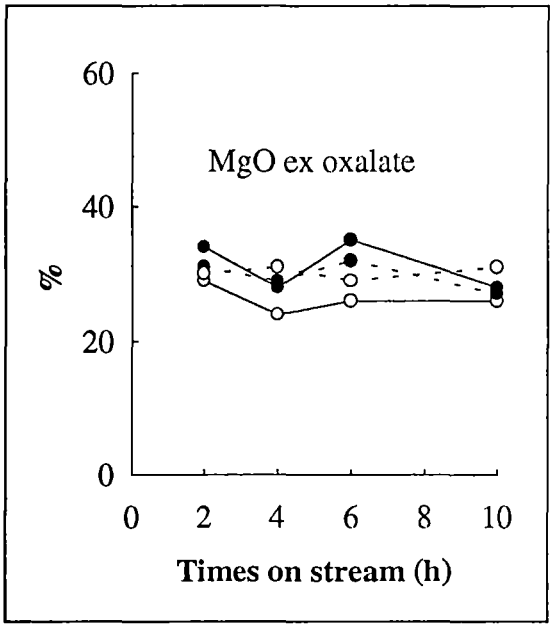
60
40
20
0
%
MgO ex oxalate
0 2 4 6 8 10
Times on stream (h)

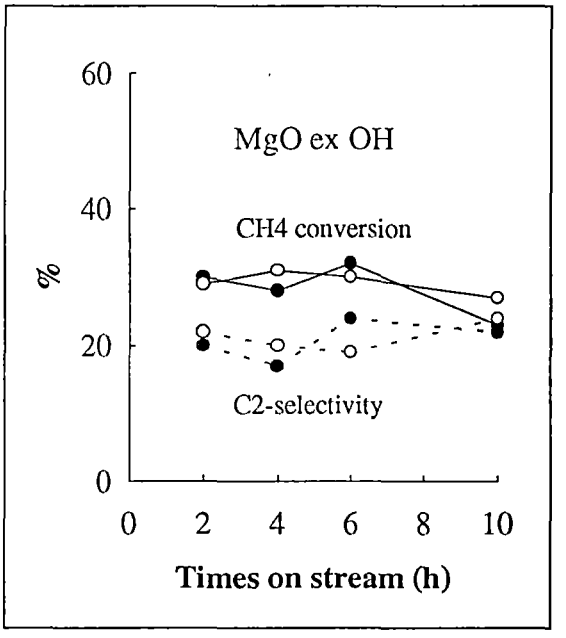
60
40
20
0
%
MgO ex OH
CH4 conversion
C2-selectivity
0 2 4 6 8 10
Times on stream (h)

Figure 4.4 The catalytic performance with times on stream of the in situ calcined MgO (•) and the MgO that had been prepared and stored (o) for six months before used.

It was noted that in a period of 10 h the amount of methane converted over the catalysts remained constant at about 30 %. The selectivity to ethane and ethylene was also observed to be steady, being approximately 50 % for MgO prepared from the carbonates, 30 % for MgO calcined from the oxalate and 20 % for MgO obtained from the hydroxide. From these results it can be seen that the catalytic ability for methane conversion and selectivity to C_2-products of the in situ prepared and the aged catalysts are not significantly different in comparison with the differences observed for MgO prepared from different precursors. It can be concluded that the fresh calcined and the aged catalysts had a similar number of active sites for methane activation. In other words careful storage and pretreatment prior to use is not likely to have any effect on the catalytic activity of MgO catalysts.

4.3.3 Catalytic activity of various MgO catalysts

MgO catalysts of different morphologies and basicities were investigated for their catalytic activity towards the oxidative coupling of methane. The catalysts were pretreated in Ar at 800°C for 2 h prior to cofeeding the gaseous reactants. Product analysis was carried out after the reaction had proceeded at 750°C for 2 h. The results are displayed in Table 4.6.

From Table 4.6 it is noted that all the MgO catalysts except the MgO prepared by the hydrolysis method exhibit similar activities for methane conversion of 30 ± 3 %, but differ in their oxygen consumption, which was observed to vary in the range of 60-80 %. MgO calcined from $Mg(OH)_2$ prepared by the hydrolysis method possessed the lowest activity having a low methane conversion and low selectivity to ethane and

ethylene. The most promising catalysts are MgO obtained from thermal decomposition of the carbonate compounds that give C_2-selectivity of nearly 50 %.

These findings agree with the results obtained by Hargreaves et al. (1992) that MgO preparared from the basic carbonate displays a higher C_2-selectivity (50-60 %) than MgO preared from the hydroxide (ca. 30 %) (at reaction temperature 750°C, CH_4:O_2 = 5, CH_4: diluent = 1 and total flow rate 50 mL/min).

Table 4.6 Oxidative coupling of methane at 750°C over different MgO catalysts.

catalyst	GHSV (h^{-1})	%CH_4 con.	%O_2 con.	%C_2-selectivity			%CO_x		
				C_2H_6	*C_2H_4*	total	*CO*	*CO_2*	total
ex CO_3	3275	33	77	*22*	*25*	47	*16*	*37*	53
ex ba. CO_3	5000	29	75	*23*	*25*	48	*15*	*37*	52
ex Ox	5200	29	65	*16*	*14*	30	*21*	*49*	70
ex OH	5148	29	62	*12*	*10*	22	*25*	*53*	78
ex OH, hyd	5250	10	37	*6*	*6*	12	*41*	*47*	88
ex OH, TP	5100	28	61	*12*	*7*	19	*25*	*56*	81
ex OH9.5, TP	5130	30	82	*11*	*8*	19	*18*	*63*	81
ex OH10.0, TP	4945	32	81	*14*	*12*	26	*17*	*57*	74
ex OH11.0, TP	5058	30	77	*13*	*9*	22	*24*	*54*	78

For MgO catalysts prepared from different precursors, the selectivity to the hydrocarbon products in the oxidative coupling of methane was found to be in the order of ex carbonates > ex oxalate > ex hydroxide. The amount of oxygen consumption over these catalysts was in accordance with the selectivity to C_2-products. It was also observed that the amount of ethylene (C_2H_4) obtained over MgO ex carbonates was slightly higher than the amount of ethane (C_2H_6) whereas the amount of C_2H_6 was found to be higher over MgO prepared from the other precursors. The catalytic performance of MgO samples calcined from $Mg(OH)_2$ at different temperatures was found to vary only slightly. The selectivity to C_2-hydrocarbons over these catalysts was 19-26 %.

It can be seen from these results that the precursors of the MgO catalysts had the most significant effect on the observed catalytic performance. The calcining procedure and the pH during the precipitation of $Mg(OH)_2$ had only a slight effect on the catalytic activity of the MgO catalysts.

4.3.4 The correlation between the catalytic performance and the surface sites of catalysts

To identify the active sites for methane activation on MgO catalysts, the relationship between catalytic activity (Table 4.6) and the basicity of each site (Table 4.2 and Table 4.3) was considered. From Table 4.2 the number of sites on MgO increased with surface area, but the catalytic activity (in particular the selectivity to C_2-hydrocarbons) decreased. As a consequence, the number of sites is not the only factor determining the catalytic activity of MgO catalysts. According to many authors (Iwamatsu et al., 1987, 1988; Lin et al., 1988) high C_2 selectivities were observed

over catalysts with low surface areas and this indicates that both factors should be considered in trying to explain the high selectivity to C_2-products.

From Table 4.3, the density of the surface sites of low coordination, i.e. the edges and the corners, on the MgO catalysts was observed to correlate with the selectivity to C_2-products. The basicity of the surface sites of low coordination in term of the density of sites per unit surface area (Table 4.3) is in the order : MgO ex carbonates > ex oxalate > ex hydroxide (via precipitation) > ex hydroxide (via hydrolysis). Such an order corresponds to the selectivity to C_2-products for these catalysts as shown in previous discussion. In addition, the MgO ex CO_3 and ex ba CO_3 which possess the highest density of surface sites of low coordination exhibit a greater tendency to produce the secondary C_2-product, C_2H_4, which is assumed to occur via hydrogen abstraction from C_2H_6 by the catalyst. As a result the density of surface sites of low coordination is suggested to be critical for methane activation.

The density of the surface sites located on the flat surface {100} is not likely to be responsible for the high C_2-selectivity of the MgO catalysts. MgO ex Ox containing a slightly higher density of these sites possessed a significantly lower selectivity to the C_2-products than the MgO ex CO_3 and ba CO_3. The surface sites located on the planar surface are therefore suspected to promote complete oxidation.

The correlation between the density of the surface sites of low coordination and the catalytic selectivity to ethane and ethylene is displayed in Figure 4. 5.

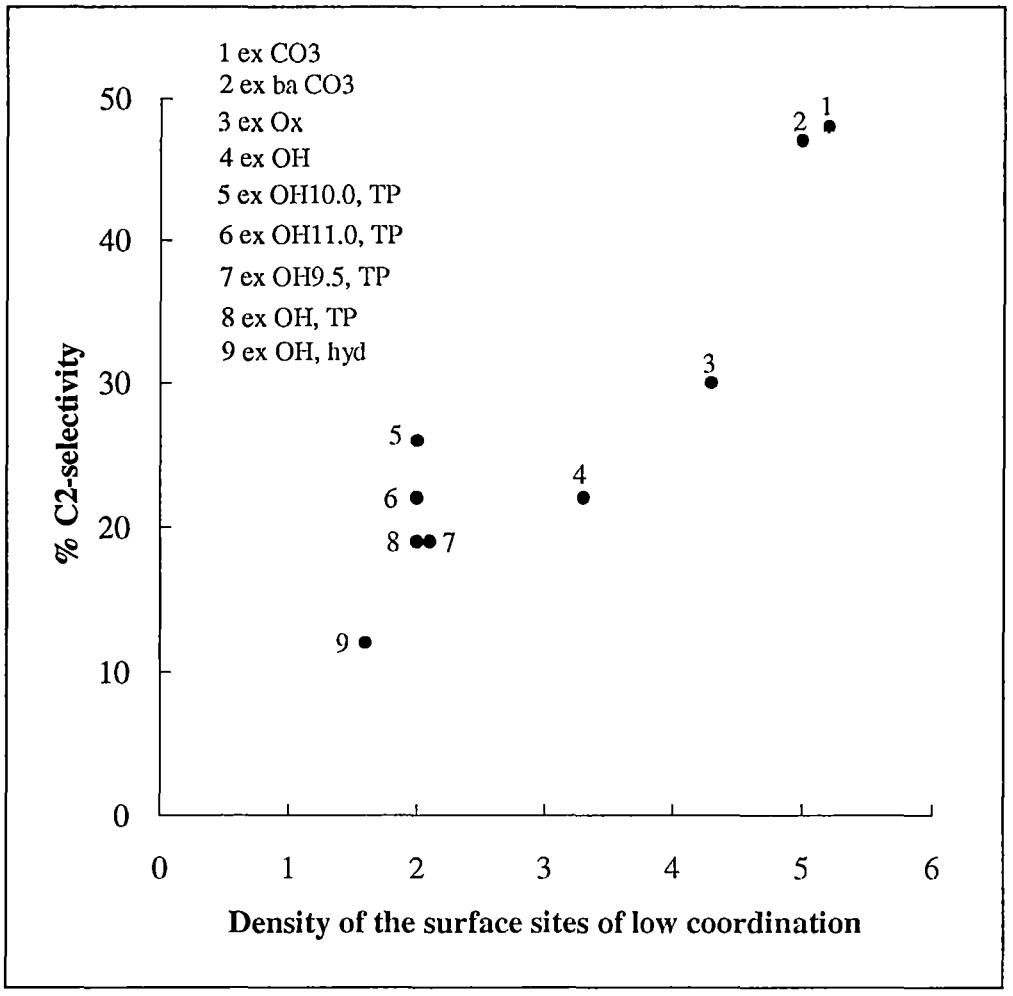

Figure 4.5 The relation between C_2-products and the density of the surface sites of low coordination (μmol phenol/m^2).

Figure 4.5 displays the increasing selectivity to C_2-hydrocarbons for methane coupling with the density of the surface sites of low coordination. It can be seen that a good trend was obtained from this relation. Hence, the density of the surface sites of low coordination is believed to be a key factor determining the selectivity to C_2-hydrocarbon on the MgO catalyst surfaces. There is, however, slight deviations from the trend that may indicate that other factors are involved in selectivity of the catalysts. For example, MgO ex oxalate, its ability to convert methane to ethane and ethylene was relatively low compare with the density of active sites. This may be due to this

catalyst possessing a high density of sites located on the plana surface {100}. If this assumption is true, it means that the surface sites on the planar surface {100} of MgO catalysts are responsible for the complete oxidation.

For the amount of methane reacted over the catalysts, it is likely that both the number of active sites (the surface of low coordination) and the density of active sites (number of sites per unit surface area) are responsible. The high number of active sites absolutely increases the amount of methane activated, while the high density of active sites may promote the rate of methane conversion. From Table 4.2 and 4.3 it was found that MgO containing a high number of the active sites exhibits the low density of active sites, while MgO containing a lower number of active sites has a higher density of active sites. As a result the conversion of methane was steady at about 30 % for most catalysts except the MgO ex OH, hyd which showed the lowest methane conversion due to its low number and density of active sites.

In conclusion the surface sites of low coordination, the edge and corner sites, on the MgO catalysts are proposed to be the active centres for methane activation. The catalytic performance of the catalysts is dependent on the number and the density of these sites. The sites located on the flat surface exposure {100} are likely to promote the nonselective products.

4.3.5 Catalytic performance with time on stream and the number of active sites after the catalytic reaction for 20 h.

The catalytic performance of MgO catalysts used in the oxidative coupling of methane at varying times on stream was studied. Results are displayed in Figure 4.6. It was noted that the activity of the catalysts was steady for up to 10 h. The ability of the catalysts for methane conversion was, however, found to decrease after prolonged times on stream. At the reaction time of 20 h the efficiency for methane conversion

for most catalysts decreased by more than 10 % from the original value of about 30 % (time on stream-2 h).

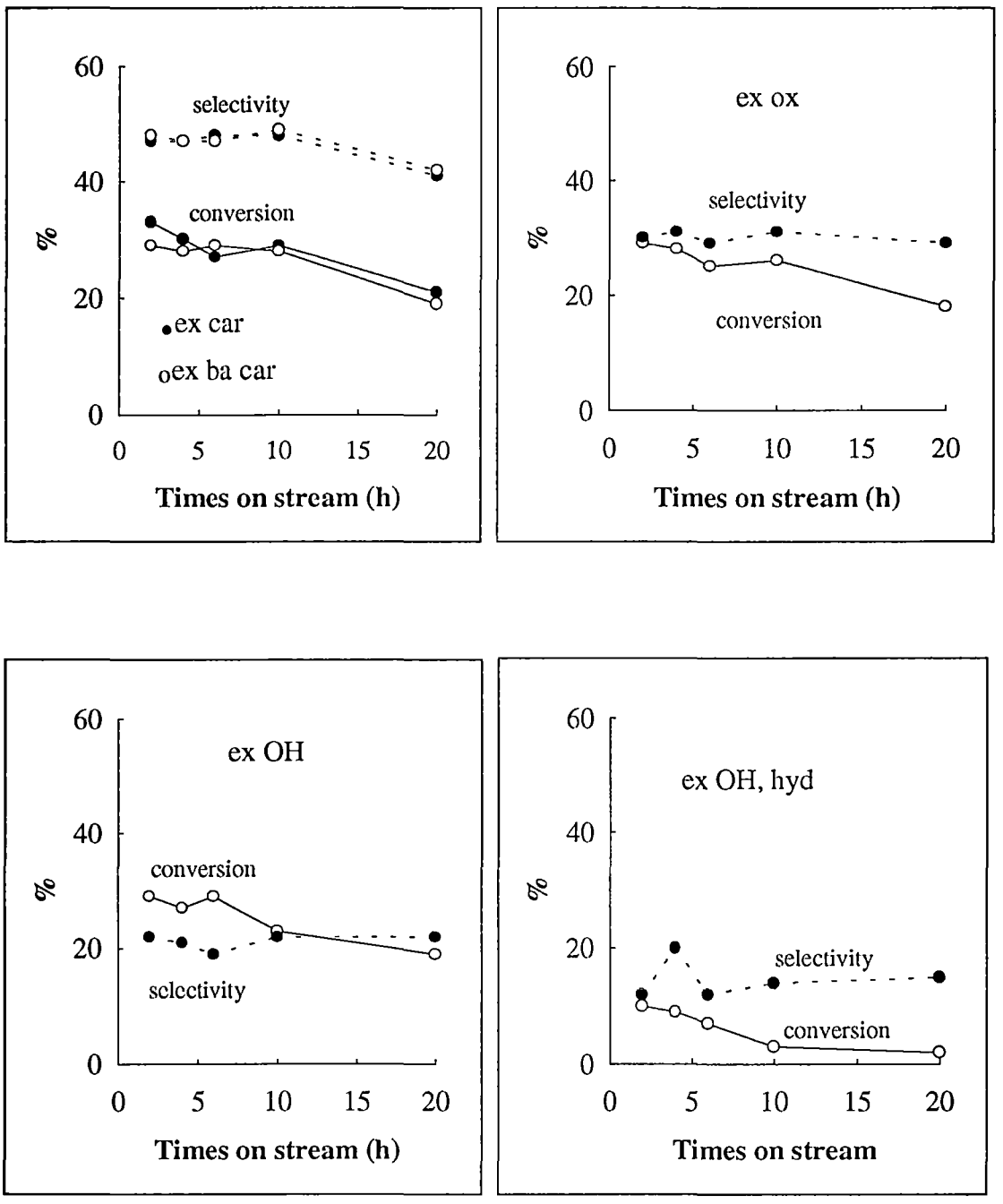

Figure 4.6 Catalytic performance with time on stream of MgO obtained from different precursors.

The selectivity to C_2-hydrocarbons from MgO obtained from the carbonates was observed to significantly decrease, while the selectivities to C_2-hydrocarbons for other catalysts were found to only slightly decrease or remain steady for period of up to 20 h. These results seem to indicate that there was some change in the nature of the the active sites after longer times on stream during the catalytic reaction. To clarify this, the catalysts were analysed for their surface areas and the amount of sites after the catalytic reaction for 20 h and the results are displayed in Table 4.7.

Table 4.7 Catalytic activity of MgO catalysts at 20 h time on stream.

catalyst	%CH_4 con.	%O_2 con.	%C_2-selectivity			%CO_x		
			C_2H_6	*C_2H_4*	total	*CO*	*CO_2*	total
ex CO_3	21	83	*17*	*24*	41	*17*	*42*	59
ex ba. CO_3	19	74	*23*	*19*	42	*26*	*32*	58
ex Ox	18	60	*15*	*14*	29	*4*	*67*	71
ex OH	19	55	*11*	*11*	22	*22*	*56*	78
ex OH, hyd	2	18	*8*	*6*	14	*47*	*39*	86

Table 4.8 The amount of sites and surface area of MgO catalysts after 20 h of catalytic reaction for oxidative coupling of methane.

MgO catalysts	surface area (m^2/g)	basicity of flat surface sites		basicity of surface sites of low coordination	
		mmol/g	$\mu mol/m^2$	mmol/g	$\mu mol/m^2$
ex CO_3	13	0.06	4.2	0.05	3.8
ex ba. CO_3	14	0.05	3.6	0.05	3.6
ex Ox	14	0.06	4.2	0.04	2.9
ex OH	25	0.15	6.0	0.06	2.4
ex OH, hyd	20	0.05	2.5	0.01	0.5

From Table 4.7 and 4.8 it was again observed that MgO containing a high density of surface sites of low coordination displayed the highest selectivity to C_2-hydrocarbons. These results confirm the assumption made in the previous discussion that the density of the surface sites of low coordination is the key factor for the methane coupling in the oxidative coupling of methane over MgO catalysts.

To look for any changes in the nature and number of surface sites on MgO after catalytic reaction for 20 h, Tables 4.2 (page 126) and 4.8 need to be compared. It can be seen that the number of surface sites of low coordination and the surface areas of the catalysts decreased significantly after being exposed to experimental conditions for 20 h. The catalyst ability for methane conversion also decreased significantly at 20 h time on stream as shown in Figure 4.6 and Table 4.7. Methane

conversions 20 h on stream was generally about 20 % or less, while the methane conversion at 2 h on stream was approximately 30 % (Table 4.6). These results indicate that the reduction in methane conversion results from the decrease in the number of active sites on the catalyst surfaces. The TPD-DTG profiles of phenol desorbed from MgO (ex Ox) before and after catalytic reaction are presented in Figure 4.7.

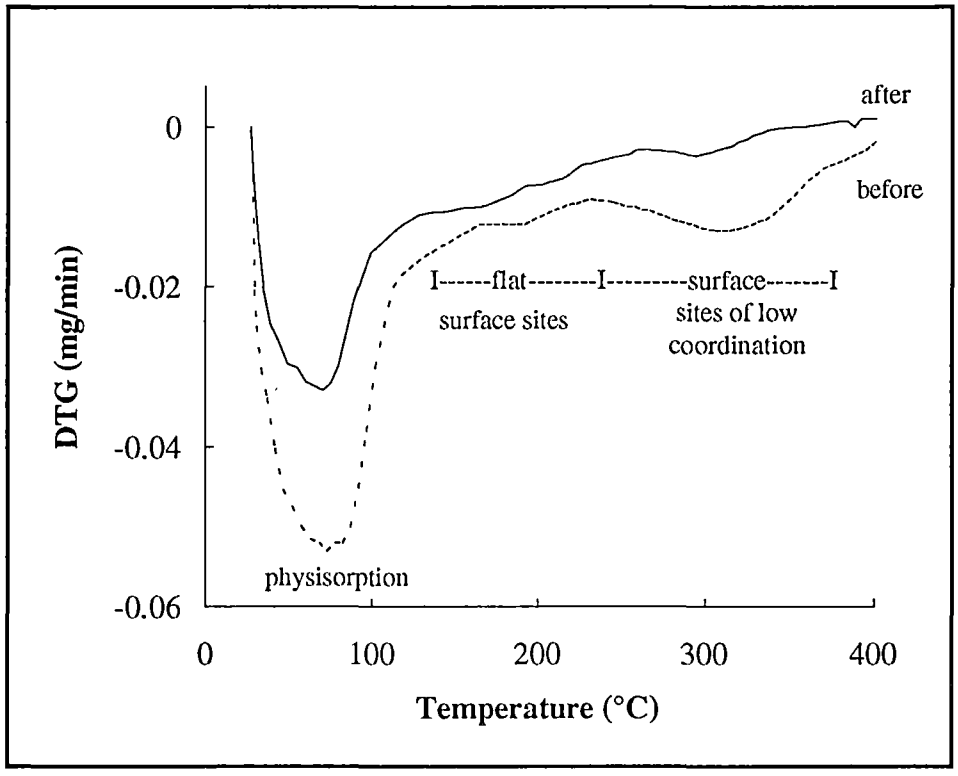

Figur 4.7 TPD-DTG profiles of phenol desorbed from MgO (ex Ox) before (19.8 mg) and after (22.2 mg) catalytic reaction.

It was noted that the intensity of phenol desorbed from the used MgO (ex Ox) is lower than that observed for the fresh catalyst. These results indicate a decrease in the number of surface sites (especially, the surface sites of low coordination) during the catalytic reaction due to sintering of MgO at high reaction temperature.

Moreover, the presence of water vapour from the reaction can enhance the sintering process (Green, 1983).

The C_2-selectivity of the catalysts was observed to be steady or to slightly decrease with time on stream. The C_2-selectivities over MgO calcined from the carbonate precursors decreased from 47-48 % at time on stream 2 h to 41-42 % at time on stream 20 h. The C_2-selectivities over MgO ex oxalate, ex hydroxide and ex hydroxide prepared from the hydrolysis method were steady at about 30 % , 22 % and 14 % respectively. The relatively constant C_2-selectivity may be attributed to the change in density of the surface sites of low coordination being small. However, the error in determining the density of sites on MgO after reaction for 20 h was relatively high due to the low surface area of the catalysts and weak signal from the small weight loss of the probe molecule used on the catalysts.

In general it is believed that the deactivation of the MgO catalysts with time on stream results from a reduction in the number of active sites (the low coordinated ions on the catalyst surface). This would suggest that pure MgO is not likely to be a suitable catalyst for the catalytic oxidative coupling of methane which takes place at high temperatures because at such temperatures sintering decreases the surface sites as well as the surface area of MgO.

4.3.6 The relationship between catalyst morphology, active sites and catalytic performance in the oxidative coupling of methane

It has been shown that the number and the density of the low coordinated ions on MgO surfaces are indicators of the yield of C_2-hydrocarbons in the oxidative coupling of methane. The high number of surface sites of low coordination is an indicator of the roughness on the catalyst surface, which arises from the many defects in the MgO microstructure. The defects in the crystalline structure must have an

influence the MgO catalyst physical profile, e.g. particle size and pore structure. As a consequence catalyst morphology, active sites and catalytic performance in the oxidative coupling of methane may be interrelated.

4.3.6.1 The particle size

The particle size distribution profiles (Figure 2.14) showed the presence of a large number of very fine particles as well as some larger particles. Moreover, the particle size distribution was dependent upon the MgO precursor. It might be expected that a regular particle size distribution would be associated with a more ordered MgO structure, i.e. a MgO with less defects and a lower density of surface sites of low coordination. It might also be expected that the density of surface sites of low coordination would increase with a decrease in particle size.

In the present work, the lower activity catalysts, MgO ex Ox and MgO ex OH do show a more regular distribution of particle size than the higher activity catalysts, MgO ex CO_3 and MgO ex ba CO_3 (Figure 4.8).

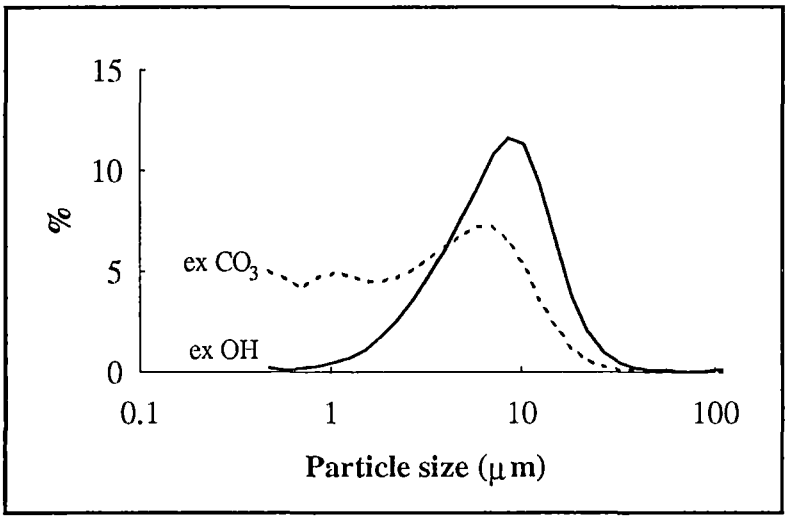

Figure 4.8 Particle size distribution profiles of MgO ex CO_3 and MgO ex OH.

Furthermore, the catalysts with a larger number of smaller particles display higher activity and selectivity. For example, MgO ex Ox and MgO ex OH both have a regular distribution of particles, however, MgO ex Ox has on average a smaller particle size distribution (Figure 4.9) and this correlates well with its higher activity.

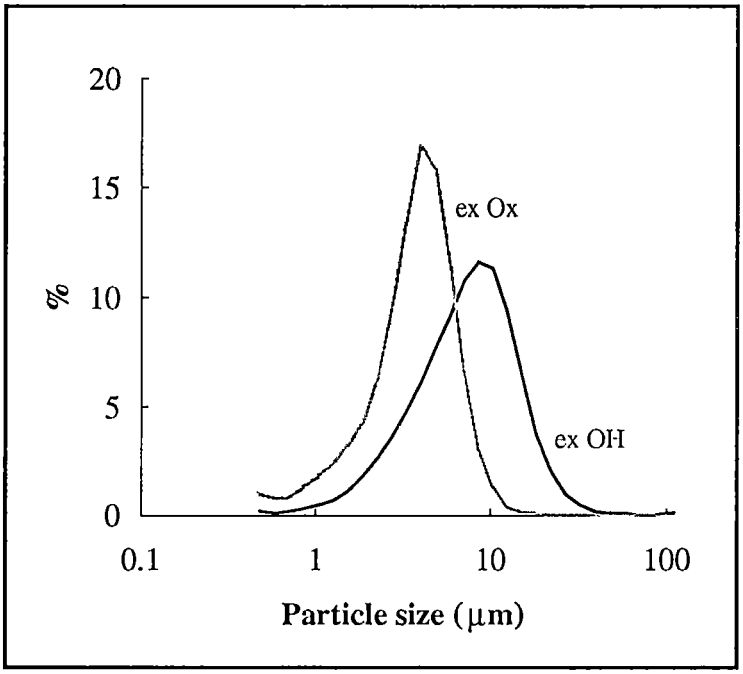

Figure 4.9 Particle size distribution profiles of MgO ex Ox and MgO ex OH.

The above assumption can be applied to other MgO catalysts. Considering MgO calcined from $Mg(OH)_2$ precipitated at different pH, it was observed that the MgO obtained from the precursor precipitated at pH 10.0 shows slightly smaller average particle size than the MgO calcined from the precursors precipitated at pH 9.5 and 11.0 (Figure 2.7). It was found from their catalytic activities that the MgO precipitated at pH 10.0 displayed slightly higher C_2-selectivity than the others. The MgO calcined from $Mg(OH)_2$ which was prepared by the hydrolysis method is not included for comparison since it was contaminated by carbon impurity which lowers the active sites on the surface.

4.3.6.2 Pore size and pore volume

In order to examine the influence of pore structure on catalytic activity in the oxidative coupling of methane over MgO catalysts, the relationship between pore size/pore distribution and catalytic performance was investigated. The MgO samples calcined from various precursors seem to be the best model for studying since they exhibited obvious distinctions in both their morphology and their catalytic activity. As the molecular size (the cross sectional area) of the reactants and the products are approximately 10-30 Å, the mesopores with pore access of approximately 36-500 Å (the smallest pore size that can be determined by mercury porosimetry is 36 Å) and macropores with pore access of 500-1000 Å will be considered. Those macropores greater than 1000 Å are not likely to have a large effect on the diffusion of the reactants into and the products out of the pores.

Since the pore features determined in Chapter 2 were presented over the wide range of pore size, 36-10,000 Å, they are not suitable for examination here. For comparison purposes the pore size/pore distribution of MgO catalysts prepared from different precursors are displayed again within the pore size range 36-1000 Å.

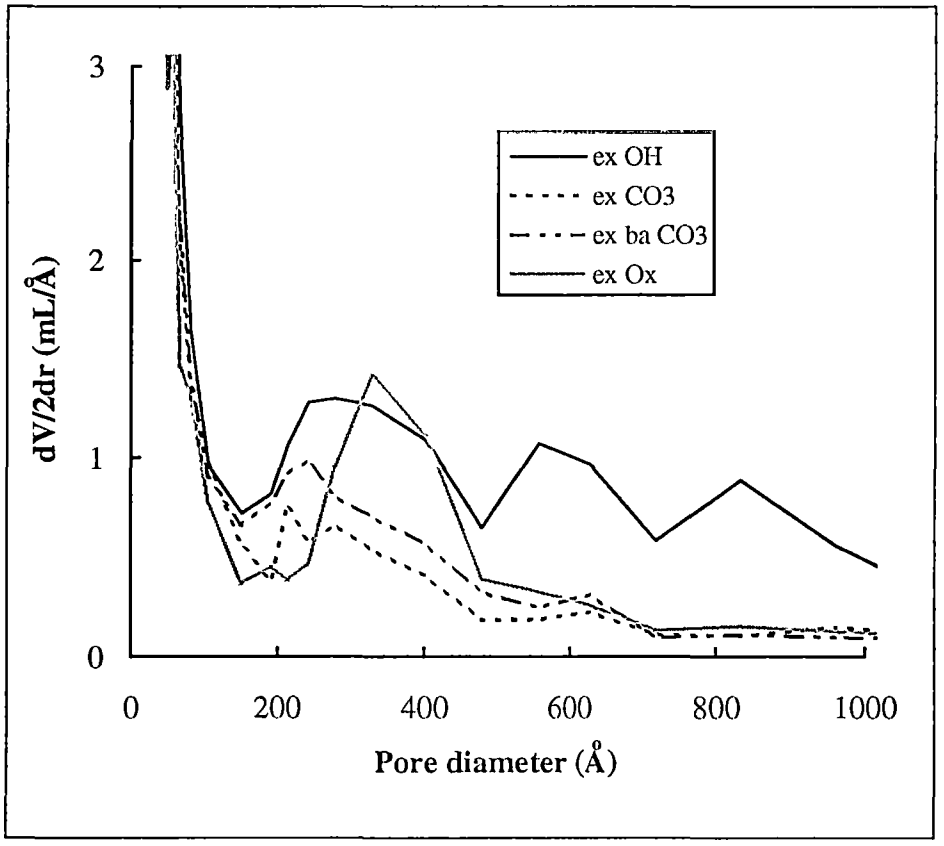

Figure 4.10 Pore size distribution of MgO prepared from thermal decomposition of different Mg salts.

Figure 4.10 shows a comparison of pore size distribution for MgO catalysts calcined from different precursors. It was observed that there are two major common pore size ranges, 36-180 and 180-480 Å, which were found for all the catalysts. It was not possible to distinguish the differences between MgO obtained from different precursors in the pore size range 36-180 Å due to the limitation of the mercury porosimetry technique. For the pore size range 180-480 Å, MgO ex CO_3 displayed the smallest average pore size, while the MgO ex OH and ex Ox displayed the biggest average pore sizes. The MgO ex OH displayed a distinct profile showing a high number of pores size larger than 500 Å.

According to the pore size distribution data in Figure 4.10, the majority of pores are in the range of 36-480 Å. As a consequence the cumulative pore volume will be considered within this pore size range.

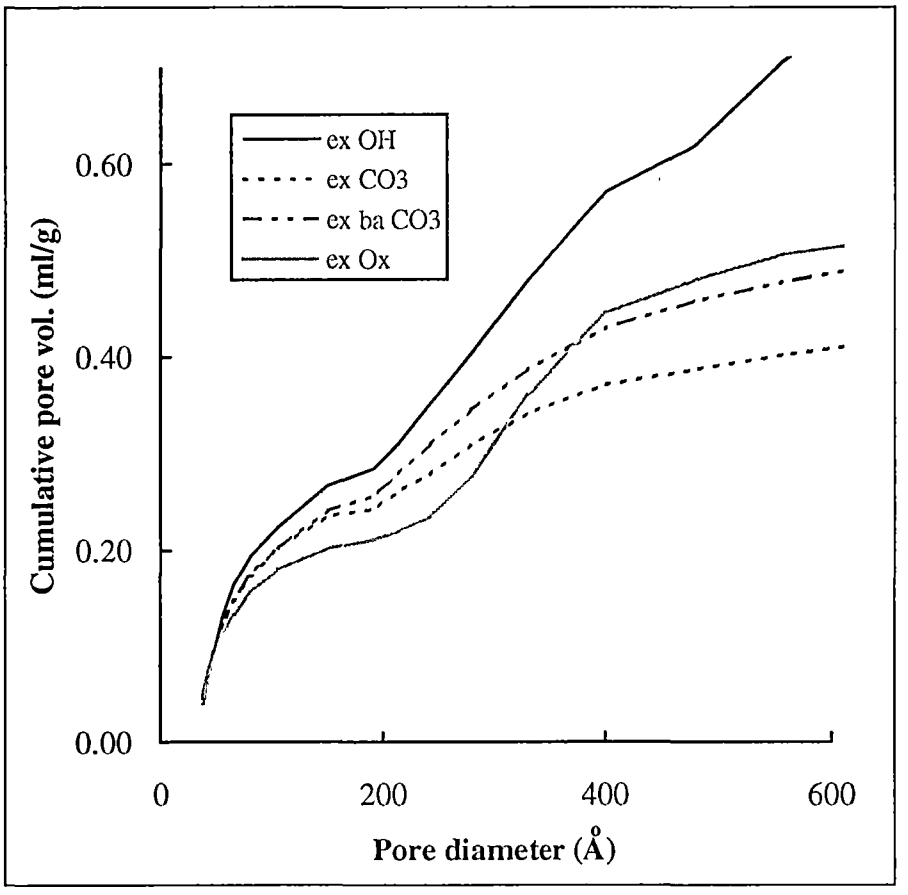

Figure 4.11 Cumulative pore volume of MgO prepared from thermal decomposition of different Mg salts.

It is noted from Figure 4.11 that the cumulative pore volume profiles of MgO have a characteristic bimodal distribution with pores in the pore sizes range 36-500 Å. These are in accord with the pore size distribution results that there are two major common pore size ranges, 36-180 and 180-500Å. The MgO ex OH has the highest cumulative pore volume. The MgO ex Ox has cumulative pore volume lower than MgO ex CO_3 and ex ba CO_3 in the pore sizes range 36-180 Å. However, the pore

volume of MgO ex Ox increases at a higher rate with the increase of pore size and results in a higher cumulative pore volume than MgO ex CO_3 and ex ba CO_3. The cumulative pore volume of MgO catalysts was therefore in the order of ex OH > ex Ox > ex CO_3 and ex ba CO_3. Such an order is the inverse of the C_2-selectivity order of the catalysts for the oxidative coupling of methane. This would indicate that highly porous structure is not a suitable characteristic for C_2-selectivity. Deep pore may retain the hydrocarbon products within MgO particle at longer time leading to complete oxidation.

Considering MgO calcined from $Mg(OH)_2$ that had been precipitated at different pH' s (Figure 4.9), it is noted that there are three common pore size ranges, 36-200, 200-480 and 480-700 Å (Figure 4.12). The cumulative pore volume of these MgO catalysts are slightly different (Figure 4.13). These results correlate with their slightly different catalytic performance.

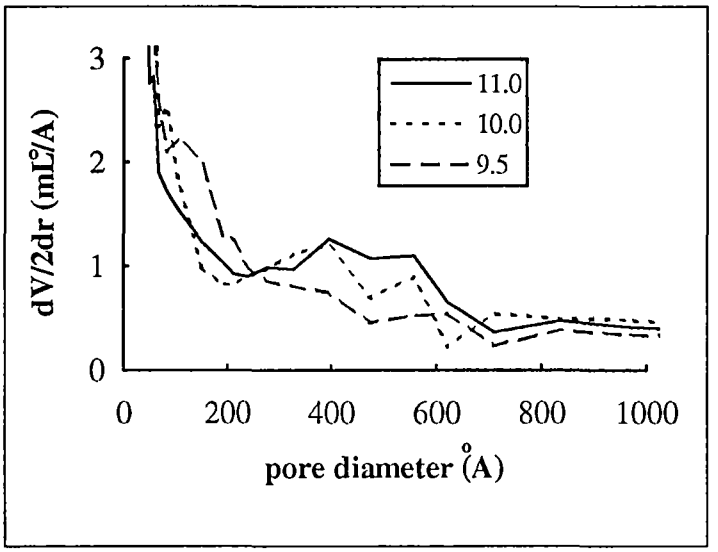

Figure 4.12 Pore size distribution of MgO calcined from $Mg(OH)_2$ precipitated at different pH.

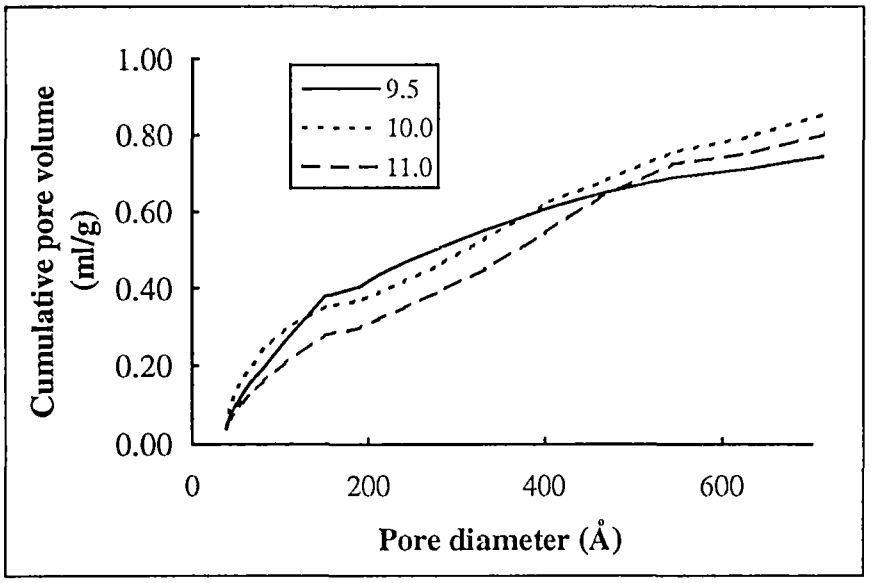

Figure 4.13 Cumulative pore volume of MgO calcined from $Mg(OH)_2$ precipitated at different pH.

With respect to the results obtained from MgO prepared from different precursors, it is expected that a higher cumulative pore volume will result in a lower C_2-selectivity. It is also necessary to consider other factors such as particle size/particle size distribution for catalysts of similar values of pore volume. From Figure 4.13 MgO ex OH9.5 showed the highest pore volume in the pore sizes range 36-480 Å and gave the lowest C_2-selectivity as expected. However, its cumulative pore volume was the lowest when the pore sizes increase to 700 Å. MgO ex OH10.0, TP displayed a higher pore volume than MgO ex OH11.0, TP, however, it exhibited a higher C_2-selectivity. It was noted from the particle size distribution data that all these catalysts have regular particle size distribution profiles with the average particle size in the order of 9.5> 11.0> 10.0. Such an order is expected for the C_2-selectivity of 9.5< 11.0 < 10.0.

4.4 Discussion and Conclusion

It has been demonstrated in this work that morphology, active sites and catalytic performance in oxidative coupling of methane on MgO catalysts are closely interrelated. High C_2-selectivity was found to be associated with small particle size, low cumulative pore volume (36-500 Å) and high density of surface sites of low coordination or the roughness of surface. These surface properties are believed to be governed by the defects in MgO microstructures, i.e. high defects in MgO crystals result in the small particle size, low cumulative pore volume and high degree of surface roughness. The findings obtained in the present work therefore support the comment made by Hargreaves et al. (1992) that the catalytic performance for oxidative coupling of methane over MgO catalysts is influenced by the morphology of catalysts.

Lunsford et al. (1989) have pointed out from radical scavenging experiments that the morphology of MgO did not manifest significant differences in methyl radical generation and reaction. Two MgO samples used in their study were MgO (JM) (John Matthey Puratonic Grade, 99.998 %) and MgO (A) (Aldrich Gold Label, 99.99 %). The MgO (JM) was found to exist in the form of small cubes similar to those which have been observed when Mg ribbon is burned in air. The MgO (A) was converted to hydroxide by boiling in water and evaporating the slurry to dryness. The material was converted back to oxide by heating for 2 h at 500°C under flowing O_2. The crucial point is that at calcination temperature of 500°C residual OH species will remain in high numbers on the MgO surface, especially on the surface sites of low coordination as demonstrated in Chapter 3. This is the most likely reason why the MgO (A) sample, with many more corner sites, did not manifest a significantly greater specific activity for methyl radical generation than did the MgO (JM) sample.

Hargreaves et al. (1992), who strongly believe that catalytic performance of MgO is governed by morphology, suggested from TEM results that the high selectivity to C_2-hydrocarbons over MgO calcined from the basic carbonate is due to the high density of surface sites of low coordination. Similar results were also observed in the present work. However, Hargreaves suggested that the site involved in the rate-determining step on MgO prepared by burning Mg ribbon (MgO RR) and thermal decomposition of the hydroxide (MgO ex OH) may not involve the surface sites of low coordination. They observed that these two catalysts exhibited similar catalytic performances, although they have different density of surface sites of low coordination. These two MgO samples have similar morphology, exposing mainly the {100} plane, however, the cube size of MgO RR is 1000-2000 Å, 5 to 10 times that of the MgO ex OH (200-400 Å). As a result, the latter should have a significantly larger number of edges and corners than the former, if both samples were composed of perfect cubes.

It is noted that Hargreaves et al (1992) determined the number of surface sites of low coordination without considering the defects on the {100} plane. These defects (e.g. oxygen vacancy or cation vacancy) may exist in significant numbers on MgO RR. Hargreaves also found from the phase contrast and other diffraction contrast micrographs of this MgO catalyst that the cubes which comprise it were not perfect. In the present work, the number of surface sites of low coordination was determined by the TPD of phenol which could thoroughly probe the surface sites of the catalysts.

Wu et al. (1993) studied the partial oxidation of methane to ethane over model MgO catalysts prepared under well-controlled, ultra high vacuum conditions using a combination of surface science techniques and elevated-pressure kinetic measurements. The authors concluded that the F-type centres (oxygen vacancies

containing two electrons) in the near-surface region were responsible for methane activation since the number of these F-type defects was found to be closely related to the amount of ethane produced. These intrinsic defects can be thermally generated in the temperature range 1200-1400K. This finding closely corresponds to the results obtained in the present work showing that the surface sites of low coordination are the active sites for methane activation. These sites are mostly generated at high calcination temperatures of 800°C and over as shown in Chapter 3. It is consequently believed that the generation of methyl radicals occurs via the surface sites of low coordination caused by the F-type defects.

Recently Choudhary and coworkers (Choudhary et al., 1994) investigated the influence of precursors used in the preparation of MgO on its surface properties and catalytic activity in the oxidative coupling of methane. The MgO catalysts were prepared from thermal decomposition of different precursors (i.e. hydrated MgO, magnesium acetate, magnesium nitrate, magnesium hydroxide, and magnesium carbonate). These catalysts were characterised for their surface properties (viz., acidity/acid strength distribution, basicity/basic strength distribution, surface area, morphology and surface composition) while their catalytic activity/selectivity in the oxidative coupling of methane was established. The acid strength distribution on the catalysts was determined by the TPD of ammonia (chemisorbed at 100°C) from 50-900°C using a linear heating rate of 20°C/min with helium as the carrier gas. The basicity and base strength distribution of the catalysts was determined by the stepwise thermal desorption (STD) of CO_2 (chemisorbed at 50°C and desorbed in a number of successive temperature steps, 50-250°C, 250-500°C, 500-700°C and 700-980°C).

Based on their findings Choudhary et al (1994) concluded that there was no direct correlation between the catalytic activity/selectivity and acidity/basicity of the catalysts. For the basicity, it is likely that the technique used by these investigators is

not effective enough to distinguish each type of site and its basicity. Firstly, Choudhary used CO_2 as a probe molecule. CO_2 is a strong acidic gas which could be adsorbed on MgO in several forms including unidentate carbonate, bidentate carbonate, carbonate ions, bicarbonate and bridging carbonate (Philipp et al., 1992). Such adsorption creates difficulty in the determination of the number of sites which is not directly related to the number of adsorbed (desorbed) CO_2 molecules. Moreover, it is also difficult to assign the type of site corresponding to the desorptions.

Secondly, the STD method used by Choudhary could determine only the number of CO_2 molecules desorbed at each successive temperature. This would provide only rough estimation of basicity of surface sites and be unable to distinguish between the different types of site. Finally, Choudhary stated that the exact amount of CO_2 chemisorption on the catalysts could not be obtained. It was noted that there was residual CO_2 content in MgO catalysts prepared from the carbonates and especially the acetate. The amount of CO_2 chemisorbed was estimated by subtracting the amount of CO_2 in STD experiment by the amount of CO_2 content which was determined by measuring the quantity of CO_2 evolved when catalysts were heated from room temperature to 1000°C in flowing N_2. It was very difficult to determine whether the CO_2 content exists as chemisorbed CO_2 or bulk carbonate phase. As a result Choudhary et al. (1994) could not correlate the basic properties of MgO to their catalytic performance as obtained in the present work.

In conclusion, the active sites and catalytic performance in oxidative coupling of methane on MgO catalysts are dependent on the morphology. The basic property is also a key factor in determining the catalytic reaction of the MgO catalysts.

References

Amenomiya, Y., Briss, V. I., Goledzinowski, M., Galuszka (1990), J., and Sanger, A. R., Catal. Rev.-Sci. Eng., **32**(3), 163.

Bartek, J. P., Hupp, J. M., Brazdil, J. F., and Grasselli, R. K.(1988), Catal. Today, **3**, 117.

Boudart, M. and Djéga-Mariadassou, G. (1984), Kinetics of Heterogeneous Catalytic Reactions, Princeton University Press, Princeton, New Jersey, pp 8-9.

Choudhary, V. R., Rane, V. H., and Gadre, R. V. (1994), J. Catal., **145**, 300.

Driscoll, D. J., Martir, W., Wang, J-X., and Lunsford, J. H. (1985), J. Am. Chem. Soc., **107**, 58.

Falconer, J. L. and Schwarz, J. A. (1983), Catal. Rev., Sci. Eng., **25**, 2 , 141.

Green, J. (1983), Mater. Sci. **18**, 637.

Hargreaves, J. S. J., Hutchings, G. J., and Joyner, R. W. (1990), Catal. Today, **6**, 481.

Hargreaves, J. S. J., Hutchings, G. J., and Joyner, R. W. (1990), Nature (London) **348**, 428.

Hargreaves, J. S. J., Hutchings, G. J., and Joyner, R. W. (1991), Stud. Surf. Sci. Catal., **61**, 155.

Hargreaves, J. S. J., Hutchings, G. J., Joyner, and Kiely, C. J. (1992), J. Catal., **135**, 576.

Hatano, M., Hinson, P. G., Vines, K. S., and Lunsford, J. H. (1990), J. Catal., **124**, 557.

Hutching, G. J., Scurrel, M. S., and Woodhouse, J. R. (1987), J. Chem. Soc., Chem. Commu., 1388.

Ito, T., Wang, J., Lin, C., and Lunsford, J.H. (1985), Am. Chem. Soc., **107**, 5062.

Iwamatsu, E., Moriyama, T., Takasaki, N., and Aika, K. (1987), J. Chem. Soc. Chem. Comm., 19.

Iwamatsu, E., Moriyama, T., Takasaki, N., and Aika, K. (1988), J. Catal., **113**, 25.

Kalenik, Z. and Wolf, E. E. (1990), J. Catal., **124**, 566.

Keller, G. E. and Bhasin, M. M. (1982), J. Catal., **73**, 9.

Khan, A. Z. and Ruckenstein, E. (1992), J. Catal., **138**, 322.

Labinger, J. A., Ott, K. C., Mehta, S., Rockstand, H. K., and Zoulmalan, S. (1987), J. Chem. Soc. Chem. Commun., 543.

Lane, G. S. and Wolf, E. E. (1988), J. Catal., **113**, 144.

Lin, C-H., Wang, J-X., and Lunsford, J.H. (1988), J. Catal, **111**, 302.

Liu, H.-F., Liu, R.-S., Liew, K. Y., Johnson, R. E., and Lunsford, J. H. (1984), J. Am. Chem. Soc., **106**, 4117.

Lunsford, J. H., Cisneros, M. D., Hinson, P. G., Tong, Y., and Zhang, H. (1989), Faraday Discuss. Chem. Soc., **87**, 13.

Mehandru, S. P., Anderson, A. B., and Brazdil, J. F. (1988), J. Am. Chem. Soc., **110**, 1715.

Moodie, A. F. and Warble, C. E. (1971), J. Cryst. Growth, **10**, 26.

Otsuka, K. and Komatsu, T. (1987), J. Chem. Soc. Chem. Commun., 388.

Philipp, R., Omata, K., Aoki, A., and Fujimoto, K. (1992), J. Catal., **134**, 422.

Wu, M-C., Truong, C. M., and Coulter, K. (1993), J. Catal., **140**, 344.

Yates, D. J. C. and Zlotin, N. E. (1988), J. Catal., **111**, 317.

Yates, D. J. C. and Zlotin, N. E. (1990), J. Catal., **124**, 562.

CHAPTER 5

ACTIVE SITES & CATALYTIC PERFORMANCE OF Li/MgO CATALYSTS FOR OXIDATIVE COUPLING OF METHANE

5.1 Introduction

Several studies using a variety of techniques have been carried out to identify the active centres of Li/MgO catalysts (Driscoll et al., 1985; Anpo et al., 1988; Hargreaves et al., 1992; Wu et al., 1993). These catalysts have been found to offer high selectivity to C_2-hydrocarbons (ethane and ethylene) in the oxidative coupling of methane. The nature of active centres of Li/MgO catalysts for the activation of methane was the subject of further detailed studies (Driscoll et al., 1985; Anpo et al., 1988; Hargreaves et al., 1992; Wu et al., 1993). Controversy exists in the literature about whether the active sites of Li/MgO catalysts are located on the $[Li^+O^-]$ centres or the surface sites of the MgO matrix generated from the modification of the MgO surface structure (morphology) by the addition of Li.

Pioneering work by Lunsford and co-workers (Driscoll et al., 1985) used EPR spectroscopy to analyse and identify the catalytic active centres which were responsible for the activation of methane coupling over pure and Li-doped MgO catalysts. For Li/MgO samples, $[Li^+O^-]$ was proposed to be the active centres for abstracting hydrogen atoms from methane (Ito et al., 1985). These centres are formed by oxygen vacant holes ([ ]) trapped at O^{2-} ions adjacent to Li^+ ions as follows:

$$2Li^+O^{2-} + [\ ] + 1/2O_2 \leftrightarrow 2Li^+O^- + O^{2-} \qquad [5.1]$$

$$Li^+O^- + CH_4 \rightarrow Li^+OH^- + CH_3\cdot \qquad [5.2]$$

The $[Li^+O^-]$ centres are regenerated by

$$2Li^+OH^- \rightarrow Li^+O^{2-} + Li^+[\ ] + H_2O \qquad [5.3]$$

$$Li^+O^{2-} + Li[\ ] + 1/2O_2 \leftrightarrow 2Li^+O^- \qquad [5.4]$$

or

$$2Li^+OH^- \rightarrow Li^+O^- + Li^+[e^-] + H_2O \qquad [5.5]$$

$$Li^+[e^-] + 1/2O_2\ Li^+[e^-] + \rightarrow Li^+O^- \qquad [5.6]$$

The authors (Driscoll et al., 1985) also claimed that a good correlation between the amount of $CH_3\cdot$ radicals produced and the number of $[Li^+O^-]$ centres was obtained.

Subsequent work (Wang and Lunsford, 1986) on Li/MgO catalysts found, from the dipolar broadening of EPR signals (due to the adsorption of oxygen), that most of these centres were in the bulk of the catalyst. However, the relationship between the number of these centres on the catalyst surface and the activity of the catalyst was not clarified. Lunsford et al. (1989) employed electron microscopy to examine the morphology of pure MgO and Li-doped MgO derived from these materials and ESR was used to investigate their ability to generate and react with gas-phase methyl radicals. It was found that the surface area and related morphological factors did not have any effect on the oxidative coupling of methane.

An alternative approach to the question of active sites on Li/MgO catalysts was proposed by Mirodatos et al. (1987) from a study of catalyst deactivation. Under the reaction conditions (about 1000K) employed for oxidative coupling, Li will exist in the catalyst during the reaction as molten Li_2CO_3 in equilibrium with Li_2O and CO_2 (McCarty et al., 1988). The catalyst will deactivate due to the loss of Li and MgO sintering. MgO obtained from calcination of $Mg(OH)_2$ reversibly dissolved in the

molten Li_2CO_3 will lead to the growth of larger crystal with the melting Li_2CO_3 blocking smaller pores on the surface (Mirodatos et al, 1987). For a catalyst in such a state of flux the assumption of isolated, rigid [Li^+O^-] centres are difficult to recocile. The precise role of each catalyst component and how they interact has been the subject of much interest for some time (Amenomiya et al, 1990).

Another proposal concerning the nature of active sites for Li/MgO catalysts was suggested by Anpo et al. (1988). By means of photoluminescent spectroscopy the authors observed that undoped MgO, degassed at 953K, showed only emissions due to four-coordinate sites, while the Li-doped catalysts exhibited a second band at lower energy which was assigned to lower coordination sites. The intensity of the second band was observed to increase with the amount of Li added, passing through a maximum at a concentration level of 3 mol%. A good correlation between the intensity of this photoluminescent band and the activity of Li-doped MgO catalysts for methane coupling reaction was also obtained. It was therefore suggested that the unsaturated surface sites with coordination number lower than four play a significant role in the oxidative coupling reaction of methane.

Hargreaves et al. (1991) investigated lithium doped MgO catalysts obtained by the thermal decomposition of the basic carbonate. From electron micrographs it was demonstrated that addition of Li^+ induces anion vacancies in the MgO structure which subsequently facilitate sintering and crystal grain growth rates. Grain boundary dislocations were also observed with increased Li^+ concentrations. These dislocations were immobile and were suggested (Hargreaves et al., 1991) to be the type a/2(110) and were probably pinned by Li^+ segregating to the line of the defect. The authors also noted that MgO was the major phase observed on the surface of the Li/MgO catalysts and no trace of Li_2O particles was found. The emergence of these defects on the surface form a charged region, and as a result either a cation or anion vacancy.

These defects were assumed to be important with respect to the selective activation of methane.

Subsequent work was carried out to determine the relationship between morphology and the catalytic performance of Li/MgO and Au/MgO catalysts (Hargreaves et al., 1992). Similar results to those found in previous work (Hargreaves et al., 1991) were obtained for Li-doped MgO catalysts. The addition of Li caused a loss in surface area of the precursor MgO. Two main structural features were found; the formation of grain boundary dislocations (formed to relieve strain when misorientated MgO crystallites impinge on each other), and dislocations in the bulk of MgO grain. The bulk dislocations were mainly burgers vectors type a/2<110>. The emergence of these defects on the surface formed a charge region as a result of either a cation or anion vacancy. It was suggested (Hargreaves et al., 1991) that these defects were important with respect to the formation of active sites for methane activation.

Using high-resolution electron energy loss spectroscopy (HREELS) and elevated-pressure kinetic measurements, Wu et al. (1993) found that $[Li^+O^-]$ centres do not play a direct role in the methane activation step since it was observed that at a Li^+ concentration of 10 %, the $[Li^+O^-]$ HREELS intensity remains essentially constant in the 1000-1300K temperature region, whereas a 10-fold increase was observed in ethane yield. F centres (F aggregates), the surface sites of low coordination on the surface, were suggested to be responsible directly for the methane activation step because their concentration changed in accordance with the ethane production. In addition, Abraham and co-workers (Chen et al., 1977; Lacy et al., 1978; Boldu et al., 1979) showed that the production of F-type centres was found to increase with increasing Li content.

For pure MgO Wu et al. (1993) demonstrated that the generation of F-type defects occurs in the 1200-1400K range, while Li-doped MgO F-defects may be produced via an additional route, i.e., the thermal desorption of Li_2O precipitating at high temperatures, which results in the formation of vacancies in the bulk MgO. It was also found from thermal desorption studies that pure Li_2O films desorb between ~1000-1250 K, which leads to a decrease in the number of stable centres. On the other hand, the remaining Li_2O precipitates produced more $[Li^+O^-]$ centres due to enhanced thermal diffusion of Li^+ at high temperatures. These competitive processes may explain why the $[Li^+O^-]$ HREELS intensity remains essentially constant over the 1000-1300K temperature range.

In summary the nature of active sites on Li/MgO catalysts is still obscure. To clarify this problem further information about the surface sites and the catalytic activity of Li/MgO catalysts used in the oxidative coupling of methane is required. As a result an attempt has been made in the present study to investigate the active sites on Li/MgO catalysts that are responsible for methane coupling.

The physical morphology of a number of catalysts, prepared using various methods with different amount of Li loading, were thoroughly characterised (e.g surface area, particle size distribution and pore size/pore distribution). The temperature programmed desorption technique, using phenol as a probe molecule, was employed to examine the surface sites and basicity on the catalyst surfaces. The surface sites of these catalysts were analysed both prior and after catalytic testing to enable any change in the nature and number of surface sites to be examined. The correlation between these physicochemical properties and the observed catalytic performance in methane coupling of Li promoted MgO catalysts was then established, and the active sites for methane coupling were assigned.

5.2 Catalyst Preparation

Li-doped MgO catalysts were prepared from the thermal decomposition of several precursors prepared from different methods. It is noted that a high concentration of Li was used in the starting solutions for the coprecipitation of Li and Mg salts. This is beccause Li salts have much higher solubility constants than Mg of the similar salts. In addition, Li concentration also decreases during the calcination which was carried out at 800°C for 4 h under an inert argon atmosphere due to the sublimation followed by reaction of Li species and the container. The calcined catalysts were then ground and sieved (180 μm sieve) prior to use. The catalysts precursors were prepared as follows.

5.2.1 $LiOH/Mg(OH)_2$ (i)

$LiOH/Mg(OH)_2$ was precipitated by the slow addition of 70 mL solution of 3.5 M $LiNO_3$ ($LiNO_3.3H_2O$, AR grade, BDH) and 3.5 M $Mg(NO_3)_2$ ($Mg(NO_3)_2 .6H_2O$, AR grade, BDH) to 80 mL of 25 % NH_3 solution (AR grade, BDH). The mixture was stirred and left overnight. The precipitate was separated by suction filtration and washed with saturated LiOH solution for 3 times (by stirring the precipitate in 300 mL of the washing solution and filter). It was then dried under vacuum at 115-120°C for 3 h, ground and sieved (180 μm sieve) before final calcination.

5.2.2 $Li_2CO_3/MgCO_3$

70 mL of 3.5 M $LiNO_3$ and 3.5 M $Mg(NO_3)_2$ solution was slowly added to 70 mL of 3 M $(NH_4)_2CO_3$ (AR grade, Ajax Chemicals). The mixture was stirred and left overnight. The $LiCO_3/MgCO_3$ (the basic carbonate form of Mg may also exist) formed was filtered and washed with several portions of deionized water. It was then

dried under vacuum at 115-120°C for 3 h, ground and sieved (180 μm sieve) prior to calcination.

5.2.3 $Li_2C_2O_4/MgC_2O_4$

To 100 mL of 0.7 M $(NH_4)_2C_2O_4$ (20 g $(NH_4)_2C_2O_4$ (AR grade, BDH), 10 mL concentrated HCl, 250 mL deionized water) solution, 70 mL of 0.8 M $LiNO_3$ and 2 M $Mg(NO_3)_2$ solution, 5-10 drops methyl red indicator, and 25 g of solid urea were added. The container was then covered and gently boiled for 30-40 min until the indicator turned yellow. After cooling, the $Li_2C_2O_4/MgC_2O_4$ precipitate was separated by suction filtration and washed with deionized water several times. The precipitate was then dried in a vacuum oven at 115-120°C for 3 h, ground and sieved (180 μm sieve) before calcination.

5.2.4 $LiOH/Mg(OH)_2$ (ii)

A 200 mL saturated solution of CH_3COOLi and $Mg(CH_3COO)_2$ (40 g of $CH_3COOLi.2H_2O$ (98 %, Aldrich) and 50 g $Mg(CH_3COO)_2.4H_2O$ (AR grade, Ajax Chemicals) was stirred and heated for 1 week. A small amount of deionized water was continuously pumped to the mixture to sustain the reaction, and the acetic acid was removed from the mixture as a vapour. This hydrolysis reaction was very slow so that at least one week was required to precipitate about 2-3 g of $LiOH/Mg(OH)_2$. The precipitate was washed with saturated LiOH solution, then filtered. It was dried at 115-120°C under vacuum for 3 h, ground and sieved (180 μm sieve) before calcination.

5.2.5 $Li_2CO_3/Mg(OH)_2$

Most Li promoted MgO catalysts studied by other groups were prepared using the impregnation method. In the present work this method was employed to prepare four catalysts containing, 0.5, 1.0, 5.0 and 10.0 wt % Li. The weight percentage was defined as the ratio of Li to the sum of Li plus MgO. MgO (99.9 %, Aldrich) was added to boiling water and stirred for 1 h. The required amount of Li_2CO_3 (99.1 %, J. T. Baker Chemicals) was then added. This liquid/solid suspension was continuously stirred and evaporated until only a thick paste remained. The paste was left overnight and dried in a vacuum oven at 115-120°C for 10 h. It was then ground and sieved (180 μm sieve) before calcination.

5.2.6 $Li_2C_2O_4/Mg(OH)_2$

$Li_2C_2O_4$ was precipitated from $LiNO_3$ and $(NH_4)_2C_2O_4$ using the procedure as described in section 5.3.3. $Mg(OH)_2$ was obtained by the precipitation of $Mg(NO_3)_2$ with NH_3 solution at pH 10.0 as described in section 2.3.1. These two compounds were physically mixed together (0.55 g $Li_2C_2O_4$ and 1.80 g $Mg(OH)_2$) and calcined.

5.3 The Physicochemical and Catalytic Characterizations

5.3.1 Surface area determination

The BET adsorption method using nitrogen at -196°C as described in section 2.4.2 was used to determine the surface area of the Li/MgO catalysts. This method is generally applicable to any catalysts whose surface area is at least 1 m^2/g (Young and

Crowell, 1962) Hence it is important to note that the error in surface area determination is very high for Li/MgO catalysts with surface areas lower than 1 m^2/g.

5.3.2 Pore size/pore distribution

A Micromeritics Auto pore 9200 instrument was used to analyse the pore structure, pore size and pore distribution of the catalysts. Details were described in section 2.4.5.

5.3.3 Particle size distribution

The particle size distribution profile of catalysts was determined using Mastersizer/E Malvern instrument. Details are in section 2.4.6.

5.3.4 Amount of Li on Li/MgO catalysts

The amount of Li on Li/MgO catalysts was analysed prior to and after catalytic testing. A Varian AA-1475 series Atomic Absorption Spectrometer was used. Approximate 30-50 mg samples were dissolved in hot concentrated nitric acid and then diluted to a working concentration. Potassium nitrate containing 2000 μm/mL K^+ was added to the solution in order to suppress any ionization that may have occurred in the air-acetylene flame. Standard solutions were prepared by dissolving 5.324 g of Li_2CO_3 (99.997 %, Aldrich) in a minimum volume of 1:5 nitric acid and diluted to 1 L to give 1000 μmol/mL Li. From this stock solution, 0.5, 1.0, 2.0 and 5.0 μmol/mL Li solutions were prepared by accurate dilution, and potassium nitrate was added to make these standard solution to contain 2000 μmol/mL K^+.

5.3.5 Surface sites and basicity

The temperature programmed desorption of phenol using thermo-gravimetric analysis (TGA) was employed to characterise the surface sites of Li/MgO catalysts. Approximately 90-120 mg of catalyst was first heated at 800°C under argon atmosphere (10 mL/min) for 1 h. The catalyst was then exposed to an Ar/phenol stream saturated with phenol at 35-40°C for 3 h. The sample was then transferred to the TG furnance and heated at 5°C/min to 800°C. More details about the technique are described in section 3.3.4. From the TG curve the amount of each site on the Li/MgO catalysts was determined and expressed in terms of the amount of phenol adsorbed (μmol) per weight of catalyst (g). The reproducibility of the determination of Li/MgO surface sites was ± 30-50 %. The cause of the variation mainly arises from the estimation of desorption range of each type of sites. In addition, Li doped MgO are very basic. Desorption of CO_2 from their surface does not occur completely until temperatures above 900°C. This may be a reason for inaccuracy of surface area determination and uncertainties in observed desorption of phenol.

5.3.6 Catalytic activity determination

Approximately 0.2 g of Li/MgO catalyst was packed between quartz wool in a vertical quartz reactor, and heated under argon at a flow rate of 15 mL/min at 750°C for 2 h before cofeeding of reactants. The details of the reactor, feeding operation and product analysis are described in section 4.2.2. As the Li species reacted with the reactor wall, a new quartz reactor was used for each catalytic test.

5.3.7 Catalytic quantities related to the reaction rate

For a flow rate of 25 mL/min (at 298 K and 1 atm at the flow controller), and catalyst volume of 0.5-1.0 mL, the GHSV was about 5150-10300 h^{-1}. The heated volume was 1-2 mL, hence the residence time for Li/MgO catalysts was 1.4 s or 0.02 min. The contact time was evaluated to be about 0.14 $g.s.mL^{-1}$. Details of calculation for these quantities was described in section 4.2.3.

5.4 Results and Discussion

5.4.1 Surface areas and Li content of Li/MgO catalysts

The surface areas and Li content of all Li/MgO catalysts calcined from different precursors, using a variety of preparation methods, are displayed in Table 5.1. The Li content of the Li/MgO catalysts is presented as weight percentage of Li.

Table 5.1 Surface areas and Li content of various Li/MgO catalysts.

Li/MgO catalysts	precursor preparation	Li wt %	surface area (m^2/g)
copre Ox	coprecipitation of $Li_2C_2O_4$ and MgC_2O_4	0.1	9.0
copre OH	coprecipitation of LiOH and $Mg(OH)_2$	0.5	3.0
hyd OH	hydrolysis of $Li_2C_2O_4$ and MgC_2O_4	0.5	9.0
phy mixed	physically mix of $Li_2C_2O_4$ and $Mg(OH)_2$	3.9	0.8
copre CO_3	coprecipitation of Li_2CO_3 and $MgCO_3$	6.0	0.5
impreg (a)	0.5 wt % Li, Li_2CO_3 impregnated MgO	0.2	10.0
impreg (b)	1.0 wt % Li, Li_2CO_3 impregnated MgO	0.6	4.0

impreg (c)	5.0 wt % Li, Li_2CO_3 impregnated MgO	3.5	1.0
impreg (d)	10.0 wt % Li, Li_2CO_3 impregnated MgO	7.2	0.6

From Table 5.1 it can be seen that in general the higher the Li concentration of the Li/MgO catalysts, the lower the surface area obtained. This is in accord with what was found by others (Lunsford et al., 1989; Korf et al., 1990; Hargreaves et al., 1991) namely that doping MgO with Li causes a decrease in catalyst surface area to a great extent. It is thought that the reduction in MgO surface area arises from sintering processes which are promoted by the addition of Li (Green, 1983).

However, although Li/MgO samples prepared from $LiOH/Mg(OH)_2$ were prepared via different routes (namely coprecipitation and hydrolysis), both possessed similar Li contents after calcination, Li/MgO prepared from the hydrolysis method showed a significantly higher surface area than the Li/MgO prepared via the coprecipitation method. This clearly shows the influence of preparation method on final catalyst morphology. In the hydrolysis method, $Mg(OH)_2$ was slowly precipitated, leading to more ordered crystal growth and better particle formation. The highly ordered $Mg(OH)_2$ subsequently formed highly ordered MgO, which maintains porous characteristic resulting in a higher surface area. Further details about pore structures are presented in section 5.4.2.

5.4.2 Particle size distribution and pore structure of Li/MgO catalysts

Five Li/MgO catalysts, copre CO_3, copre Ox, copre OH, hyd OH and mix Ox/OH were analysed for their particle size distribution profiles and pore structures. Results are displayed in Table 5.2, Figures 5.1, 5.2 and 5.3 respectively.

Table 5.2 Particle size distribution of Li/MgO catalysts.

Li/MgO catalysts	Particle sizes < 1 μm (%)	Particle sizes 1-10 μm (%)	Particle sizes > 10 μm (%)	Average particle size (μm)
copre Ox	16.8	82.0	1.2	2.9
copre OH	36.4	34.8	28.8	3.8
hyd OH	12.5	80.6	6.9	3.16
phy mixed	55.2	25.8	19.0	0.9
copre CO_3	20.0	38.3	41.7	7.7

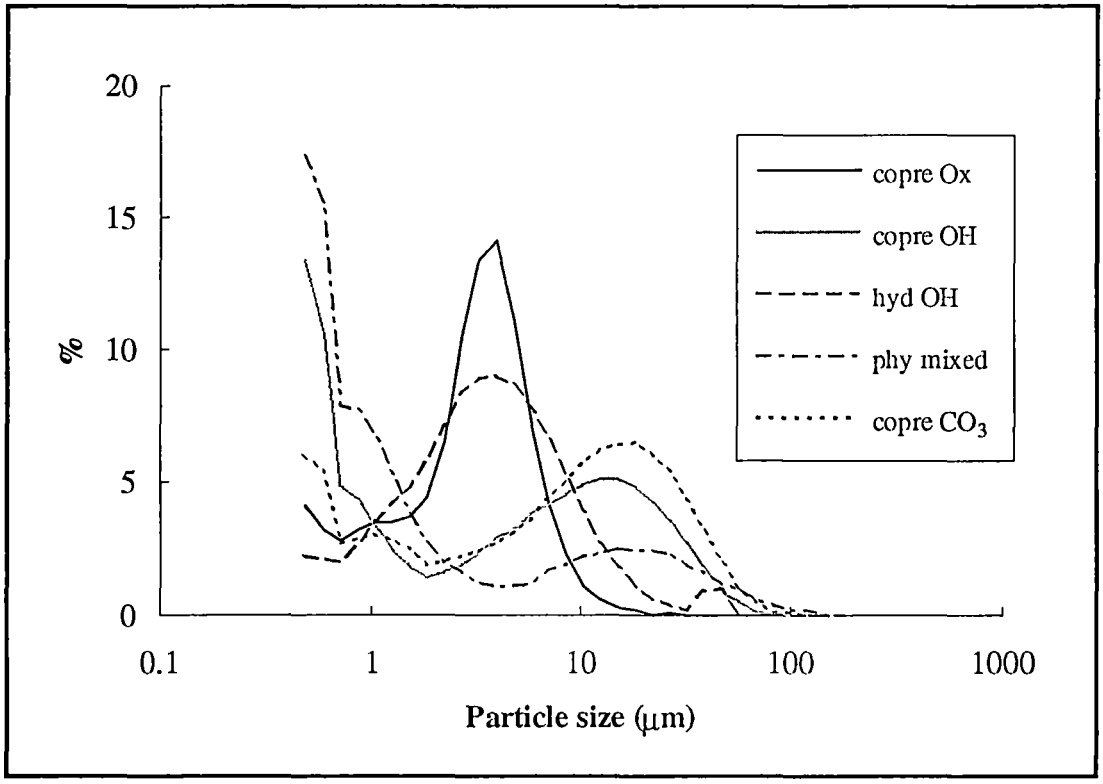

Figure 5.1 Particle size distribution of Li/MgO catalysts prepared using different preparation methods.

From Figure 5.1 it can be seen that Li/MgO catalysts (copre OH, phy mixed and copre CO_3) show irregular particle size distribution profiles containing both very fine and large particles. Li/MgO prepared via the hydrolysis method and from the coprecipitation of oxalates (which have higher surface areas than other Li/MgO catalysts) show more regular particle size distribution profiles, with the most common particle sizes being about 3-5 μm. Li/MgO prepared from the coprecipitation of the hydroxides, and physically mixed $Li_2C_2O_4$ and $Mg(OH)_2$ (which displayed the lowest surface areas) exhibited a high number of small particles with particle sizes less than 1 μm. It can be concluded from these results that low surface area Li/MgO catalysts are likely to be associated with irregular particle profiles of the large number of very fine particles, while higher surface areas are characterized by more regular particle profiles.

When the particle size distribution profiles of these Li/MgO catalysts are compared with pure MgO (Figure 5.2) that calcined from similar Mg salts obtained via similar preparation method, it was found that doping MgO with Li reduces the particle sizes of the catalysts. It was found that the higher the Li concentration, the smaller was the particle size.

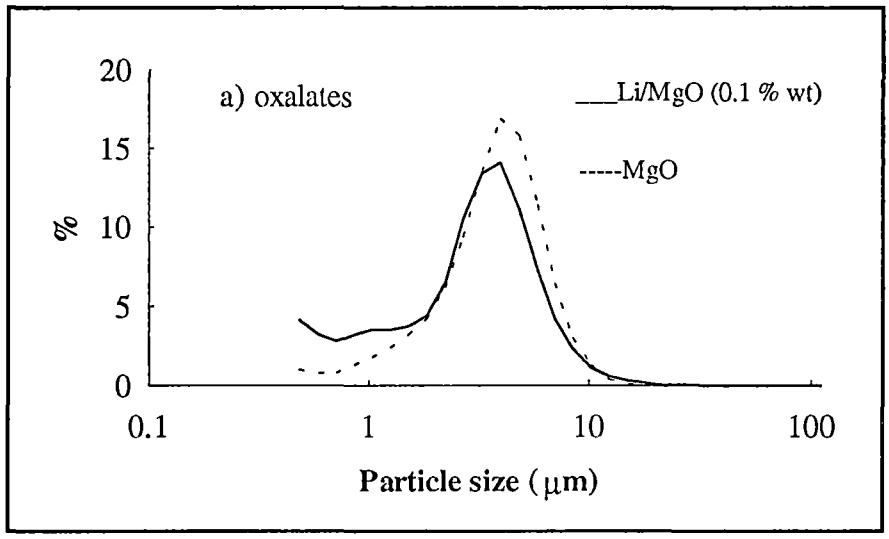

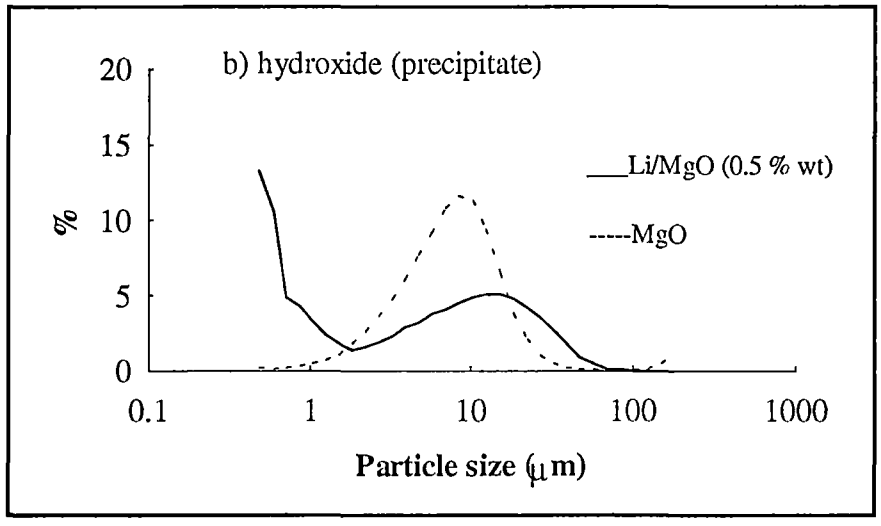

Figure 5.2 The comparison of particle size distribution profiles of pure and Li-doped MgO catalysts.

It is likely that Li interferes with the ordering of crystal growth and particle formation of the MgO matrix giving rise to smaller particle sizes and less regular particle profiles. The very large particles, > 10 μm, found for some Li/MgO catalysts (copre OH, copre CO_3 and phy mixed) possibly resulted from the sintering of smaller particles.

When MgO is doped with Li there is a marked decrease in the cumulative pore volume (Figure 5.4). The pore size distribution (dV/dr) of Li/MgO catalysts displayed in Figure 5.3 indicates that the most common pore sizes are 50-70 Å.

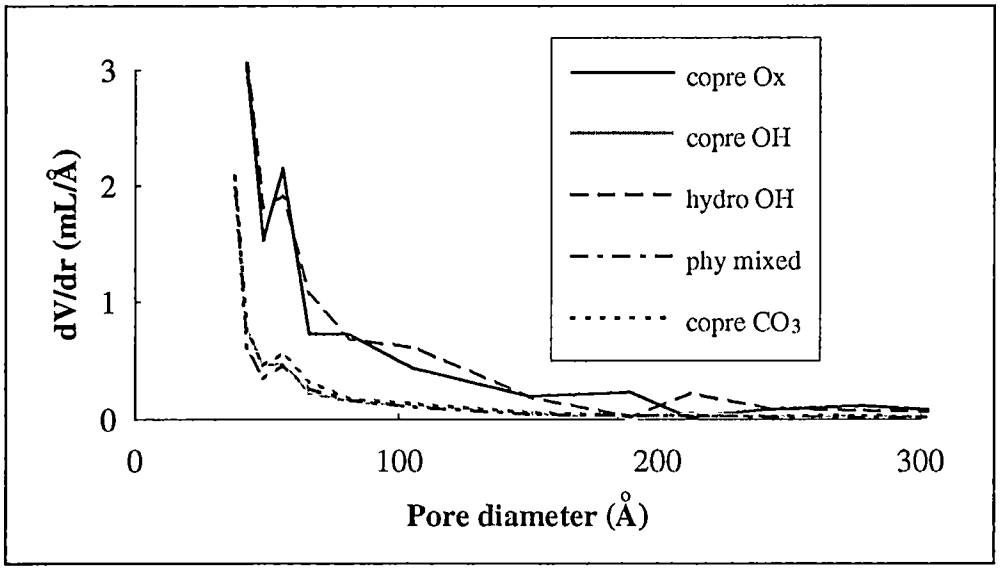

Figure 5.3 Pore size distribution of different Li/MgO catalysts.

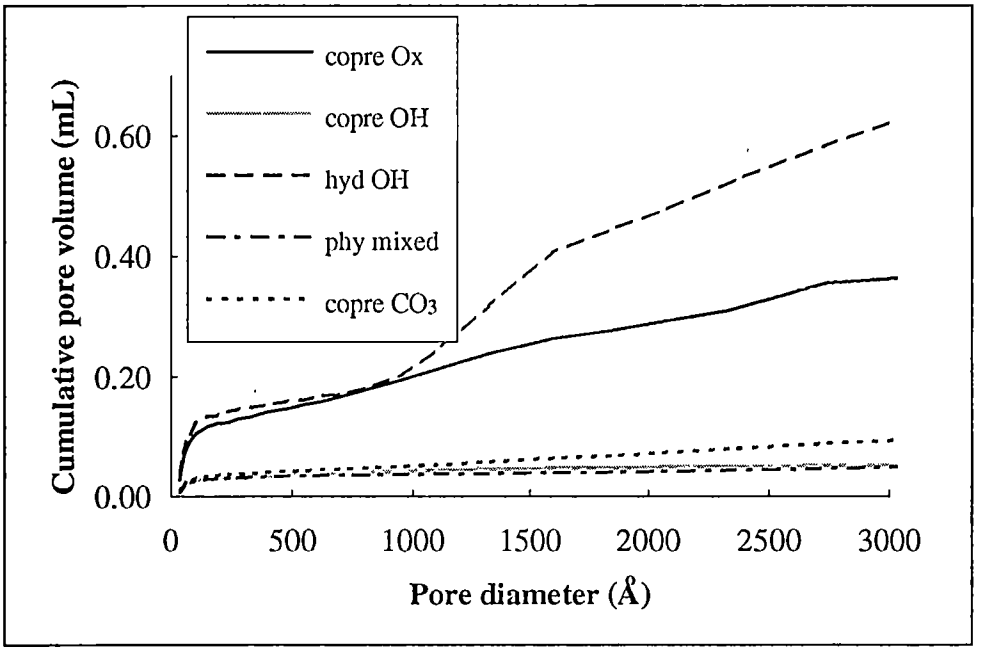

Figure 5.4 Cumulative pore volume of various Li/MgO catalysts.

The cumulative pore volume of Li/MgO catalysts displayed in Figure 5.4 were found to be in agreement with their surface areas; those catalysts with high surface areas had high cumulative pore volumes.

5.4.3 Sites and basicities on Li/MgO catalysts

It has been previously shown that phenol desorbs from MgO (calcined at 800°C for 4 h) over three temperatures ranges. These regions have been assigned as physisorbed phenol (T_M < 100), phenol desorbed from flat surface exposure {100} (T_M ~ 190°C), and phenol desorbed from the surface sites of low coordination (T_M ~ 310°C). For Li/MgO catalysts the desorption of phenol was observed to occur over four temperature ranges (Figure 5.5).

In Figure 5.5 it can be seen that the desorption of phenol over Li/MgO catalyst exhibits four T_M' s where three of them, (I), (II) and (III), were similar to that observed over pure MgO surface. These desorptions are therefore attributed to be due to desorptions from the surface sites of the MgO matrix. As discussed before, the desorption (I) with T_M at about 80-100°C arises from loosely adsorbed species over the catalyst surface. The desorption (II) with T_M at about 190-200°C was previously assigned as phenol desorption from the planar MgO surface exposures {100}, while the desorption (III) with T_M at about 300°C was assigned to phenol desorption from MgO surface sites of low coordination of the MgO matrix.

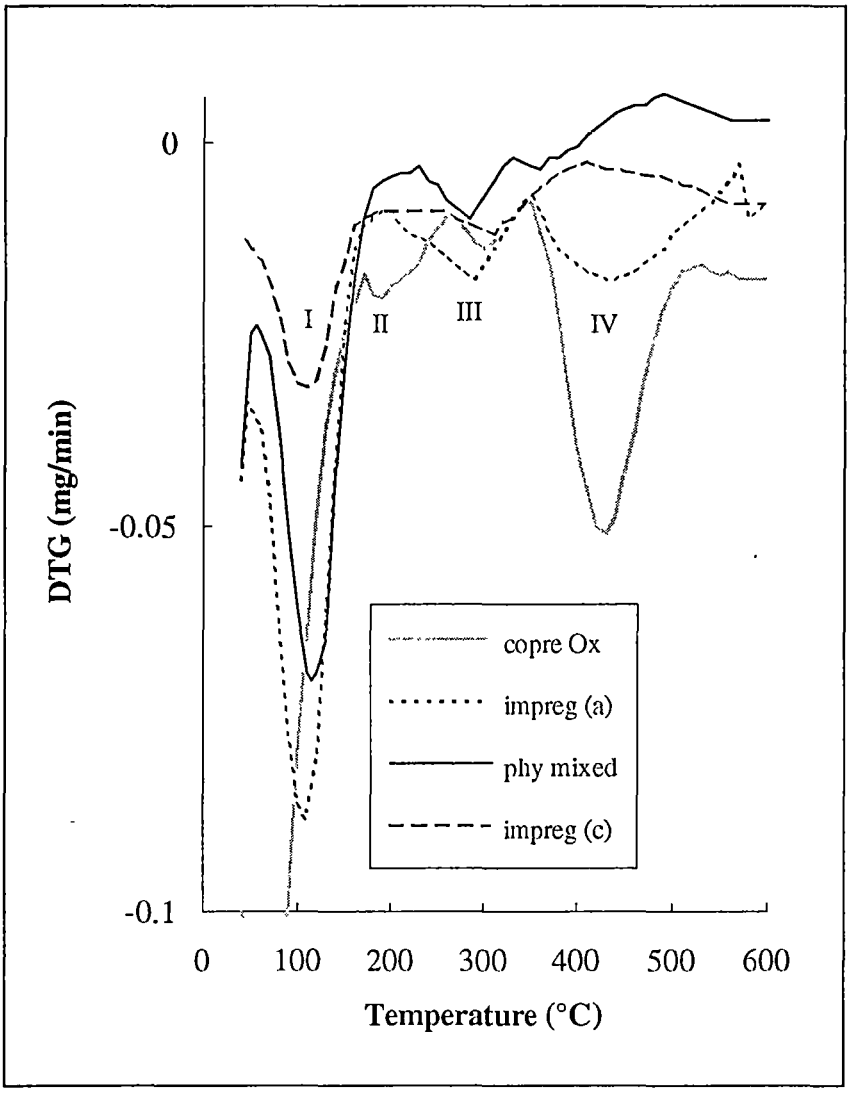

Figure 5.5 TPD profiles of phenol desorbed from Li/MgO catalysts.

The desorption (IV) with T_M at about 430°C was observed only on Li/MgO catalyst surfaces not pure MgO surfaces. It was therefore assumed to be due to the desorption of phenol from surface sites that were generated from the addition of Li to MgO. Since this desorption occurred at a higher T_M, this would imply that these sites have a higher basic strength than the MgO surface sites of low coordination. According to Driscoll et al. (1985), Li-doped MgO is in fact not Li deposited on MgO, but involves the replacement of Mg^{2+} by Li^{+}. The substitution leads to the formation of $[Li^{+}O^{2-}]$ centres. As a result the desorption of phenol from Li/MgO

catalysts at T_M of about 430°C is attributed to $[Li^+O^{2-}]$ centres. These sites were suggested (Ito et al., 1986) to react with oxygen vacant holes and O_2 to give $[Li^+O^-]$ centres (equation [5.1]-[5.6] in section 5.1), the active centres for methane activation. The number of $[Li^+O^-]$ centres on the catalyst surface should closely depend on the number of $[Li^+O^{2-}]$ species.

The number of surface sites on the Li/MgO catalysts was determined by the amount of phenol (μmol) adsorbed (desorbed) from these sites from 1 g of each catalyst. The results are displayed in Table 5.3.

Table 5.3 Basicity of Li/MgO catalysts.

Li/MgO catalysts	Li wt %	surface area (m^2/g)	surface sites of flat surface (μmol/g)(1)	surface sites of low coordination (μmol/g)(1)	surface sites generated by addition of Li (μmol/g)(1)	total of sites (μmol/g)
copre Ox	0.1	9.0	15.0	18.0	24.0	57.0
copre OH	0.5	3.0	5.8	10.0	10.5	26.3
hyd OH	0.5	9.0	32.0	26.0	27.0	85.0
phy mixed	3.9	0.8	2.4	15.2	*(2)	17.6
copre CO_3	6.0	0.5	5.0	5.0	6.0	16.0
impreg (a)	0.2	10.0	11.0	21.0	28.2	60.2
impreg (b)	0.6	4.0	8.3	12.2	16.0	36.5
impreg (c)	3.5	1.0	4.7	21.0	*(2)	25.7
impreg (d)	7.2	0.6	5.2	5.3	7.4	17.9

(1) The deviation in the number of surface sites is ± 30-50 %.

(2) * denotes an uncertain value due to a low signal response (lower than 1.0 μmol/g).

Table 5.3 shows that Li/MgO obtained from various precursors displays a different number of surface sites as well as various Li loadings and surface areas. The variation in the nature and number of surface sites of Li/MgO catalysts arises from the preparation method and the differences in Li loading. For Li/MgO catalysts prepared from the coprecipitation of the hydroxides and the hydrolysis techniques, the two catalysts contain the same amount of Li, however, they possess different surface areas and surface sites. These results show the influence of precursor preparation on the surface sites of catalysts. As previously discussed in section 5.4.1 the MgO matrix that possesses a highly ordered crystal structure was likely to have a high surface area and a highly porous structure. The higher surface area results in a higher number of surface sites.

In considering the effect of Li loading, it is simpler to examine the Li/MgO catalysts prepared by impregnation methods. These catalysts were prepared from the same precursors and preparation techniques, the only difference being the Li loading. At low Li loadings (0.1-0.2 wt %) sites arising from the addition of Li were readily observed. With increasing the Li loading to 0.6 wt %, the total number of surface sites due to the reduction in the surface area. However, the $[Li^+O^{2-}]$ sites decreased at a greater rate than the other surface sites. At a Li loading of 3.5 % the surface sites of low coordination of the MgO matrix dominated. It was surprising that the surface sites arising from $[Li^+O^{2-}]$ were observed at very low level of Li concentration. A similar surface site distribution, with a high number of surface sites of low coordination and a very low number of $[Li^+O^{2-}]$ species, was also found for Li/MgO prepared from physically mixing $Li_2C_2O_4$ and $Mg(OH)_2$, which had a Li content of 3.9 wt %. With an increase of Li loading to 7.2 wt %, the number of surface sites of low coordination on the MgO matrix decreased, while the number of $[Li^+O^{2-}]$ species increased slightly.

The variation in the relative amount of these surface sites with Li loading indicates the change in the catalyst surface structure. This change is attributed to the defects in the crystal structure of the MgO matrix caused by the Li impurity. At low loadings the MgO matrix maintains its crystal ordering, hence the highest surface area was observed for Li/MgO with the lowest Li loading. The surface sites of low coordination, which were thought to arise from defects in MgO crystal structure, were therefore observed only in small numbers, while the formation of $[Li^+O^{2-}]$ species that were previously reported by Driscoll et al. (1985) to occur from the substitution of Li^+ ions, were observed at a higher level on the surface.

It would be expected that increasing the Li loading to 3.5 wt % would result in a greater number of defects in the MgO crystal structure and these defects would cause roughness on the catalyst surface on an atomic scale (Boudart and Djéga-Mariadassou, 1984). As a consequence, the surface sites of low coordination increased, while most of the $[Li^+O^{2-}]$ species remained in the bulk rather than on the surface. Lunsford and coworkers (Driscoll et al.,1985)) used EPR spectroscopy to detect and identify the $[Li^+O^-]$ centres which originated from $[Li^+O^{2-}]$ species in Li/MgO catalysts. While they presented a good correlation between $[Li^+O^-]$ and the amount of $CH_3\cdot$ radicals produced, Wang and Lunsford (1986) found from the dipolar broadening (due to the adsorption of oxygen) of EPR signals that most of the $[Li^+O^-]$ species were in the bulk of the Li/MgO catalyst (7 wt % before calcination which should be about 5 wt % after calcination). These results indicate that at high Li loading (ca 3.5-5 wt %) most of $[Li^+O^{2-}]$ species are mainly in the bulk.

The surface sites of the Li/MgO catalyst changed again at a Li concentration of 7.2 %. At this Li concentration the catalyst surface may be covered with Li_2CO_3, which was not totally decomposed, leading to a smoother surface that may result in a lower number of surface sites of low coordination.

Another aspect of the catalyst surface is the density of sites per unit surface area. In Chapter 4 it was found that this feature is likely to be a key factor for high selectivities to C_2-hydrocarbons in the oxidative coupling of methane over MgO catalysts. This parameter is worth considering here since it may also influence the catalytic activity of Li/MgO catalysts. The density of each surface site is displayed in Table 5.4.

Table 5.4 The basicity of sites in terms of density of sites on Li/MgO catalysts.

Li/MgO catalysts	Li wt %	surface sites of flat surface ($\mu mol/m^2$)(1)	surface sites of low coordination ($\mu mol/m^2$)(1)	surface sites generated by addition of Li ($\mu mol/m^2$)(1)
copre Ox	0.1	1.7	2.0	2.7
impreg (a)	0.2	1.1	2.1	2.8
copre OH	0.5	1.9	3.3	3.5
impreg (b)	0.6	2.1	3.1	4.0
hyd OH	0.5	3.6	2.9	3.0
phy mixed	3.9	2.5	18.8	*(2)
impreg (c)	3.5	4.7	21.0	*(2)
copre CO_3	6.0	10.0	10.0	12.0
impreg (d)	7.2	8.4	8.4	12.3

(1) The deviation for all surface sites is ± 30-50 %.

(2) * denotes an uncertain value due to a low number of sites (< 1 $\mu mol/m^2$).

From Table 5.4 the density of each surface site seems to closely relate to the Li loading. At low Li loadings of 0.1-0.2 %, the density of the flat surface sites exposure {100} of the MgO matrix was low, while the sites assigned to $[Li^+O^{2-}]$ centers were found in higher numbers. With increasing the Li loading to 0.5-0.6 %, the densities of all the surface sites increased. This is attributed to the reduction in catalyst surface areas due to the increasing amount of Li impurity in the MgO matrix.

It was found that at higher Li loadings (3.5-4.0 %), the density of surface sites of low coordination was significantly increased, while the density of $[Li^+O^{2-}]$ centres was impossible quantify. These results indicate that the roughness of catalyst surfaces arises from the defects in the MgO crystal structures. Increasing the Li loading to 6.0-7.2 % decreased the density of the surface sites of low coordination by a factor of 2. This implies that the catalyst surfaces were smoother than in those Li/MgO catalysts with a Li loading between 3.5-4.0 %. At this high Li loading the Li_2O component may diffuse through the MgO matrix and equilibrate between the surface and the bulk leading to catalysts with smoother surfaces.

5.4.4 Catalytic performance of Li/MgO catalysts in the oxidative coupling of methane

The activity of Li/MgO catalysts prepared via different methods for the oxidative coupling of methane was investigated and the results are displayed in Table 5.5.

Table 5.5 Oxidative coupling of methane at 750°C over different MgO catalysts at times-on-stream 2 h.

Li/MgO catalysts	GHSV (h^{-1})	Li wt %	$\%CH_4$ con.[1]	$\%O_2$ con.[1]	$\%C_2$-selectivity			$\%CO_x$		
					C_2H_6	C_2H_4	total[2]	CO	CO_2	total[2]
copre Ox	5340	0.1	37	99	15	19	34	6	60	66
impreg (a)	6100	0.2	37	89	25	30	55	5	40	45
copre OH	9200	0.5	26	39	32	30	62	8	30	38
impreg (b)	7130	0.6	34	60	29	33	62	4	34	38
hyd OH	5300	0.5	32	57	27	29	56	7	37	44
phy mixed	8150	3.9	23	30	41	29	70	2	28	30
impreg (c)	9950	3.5	27	34	37	33	70	3	27	30
copre CO_3	10250	6.0	13	14	50	29	79	0	21	21
impreg (d)	10058	7.2	13	16	48	26	74	4	22	26

[1] The deviation is ± 3 %.

[2] The deviation is ± 4 %.

From Table 5.5 it was observed that at low Li loadings (0.1-0.2 %) the methane conversion was 37 %, while the selectivity to C_2-hydrocarbon products was about 34-55 %. An increase in the Li loading decreased the amount of methane converted, whereas the C_2 selectivity increased. At high Li loadings (6.0-7.2 %) the methane conversion decreased to 13 %, while the C_2 selectivity increased to 74-79 %. The O_2 consumption closely corresponded to the amount of methane converted. The higher the methane conversion, the higher the amount of O_2 consumed. It was also noted that at methane conversions over 30 % the ethane concentration was found to be lower than ethylene. On the other hand at methane conversions lower than 30 %, the amount of ethane was found to be higher than ethylene. For the nonselective products, the amount of CO_2 produced was found to be significantly higher number than the amount of CO, at any methane conversion level.

5.4.5 The relationship between the surface sites and the catalytic performance of Li/MgO catalysts

To clarify which surface sites are active for the oxidative coupling of methane on Li/MgO catalysts, the relationship between the various surface sites of these catalysts and their catalytic performance was considered. From Tables 5.3 and 5.5, it is likely that the number of sites is an indicator of the high activity for methane conversion. However, the number of sites seems not to be the only factor determining the high selectivity to C_2-hydrocarbons. High methane conversion but low C_2-selectivity were found over Li/MgO catalysts (copre Ox and impreg (a)) that possessed the high number of surface sites. In contrast, low methane conversion and high selectivity to C_2-hydrocarbons were found over Li/MgO catalysts (copre CO_3 and impreg (d)) that had the low number of surface sites. These data imply that the

high number of surface sites results in high methane conversion. However, the total number of sites cannot explain the high C_2-selectivity.

In Chapter 4 it was found that the density of surface sites of low coordination, which takes into accout in the surface area of the catalysts along with the number of surface sites, is an indicator of high C_2-selectivity. Several authors (Iwamatsu et al., 1987; 1988; Lin et al., 1988) have reported that high C_2-selectivities were observed for catalysts with low surface areas and from the results presented here a similar relationship appears to hold. Previously it was shown that the density of flat surface exposure {100} is likely to promote the complete oxiation products. For the Li/MgO catalysts it is necessary to consider the relative importance of the surface sites of low coordination and the $[Li^+O^{2-}]$ centers.

There has been some argument between investigators (Anpo et al., 1988; Lunsford, 1990; Wu et al., 1993) whether the $[Li^+O^-]$ centres generated from $[Li^+O^{2-}]$, or the sites generated or located on the surface sites of low coordination are the active centres for methane activation and methane coupling. To clarify this the correlation between the percentage of C_2-products and the density of $[Li^+O^{2-}]$ centres, the density of the surface sites of low coordination and the total density of these two sites was carried out. Results are displayed in Figures 5.6, 5.7 and 5.8 respectively.

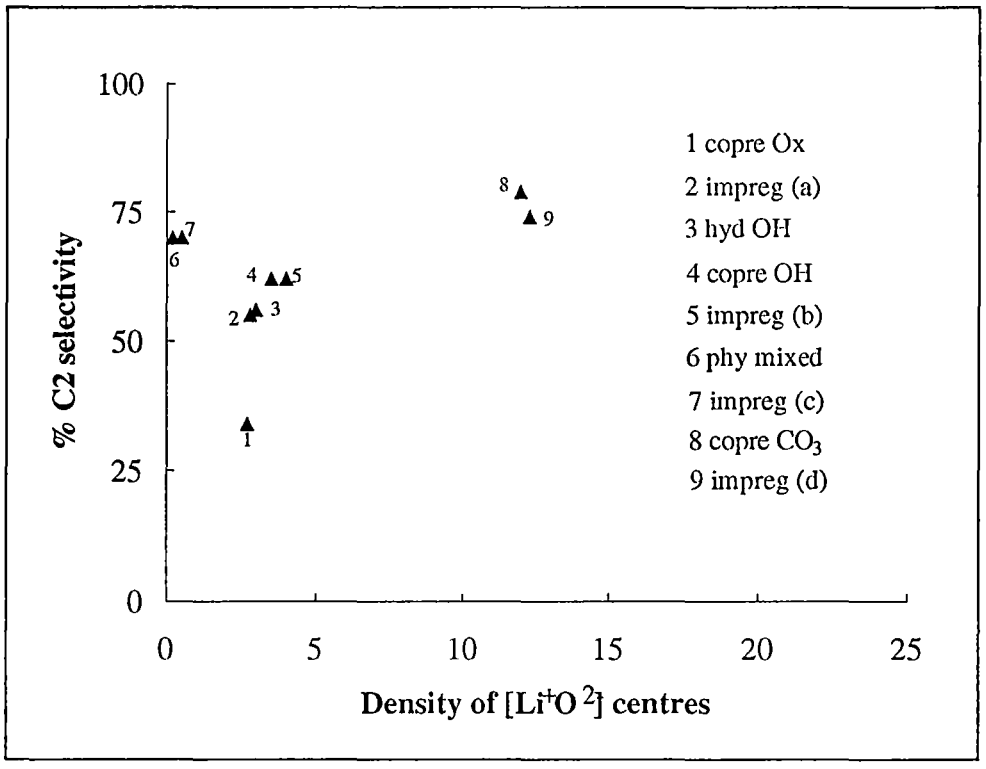

Figure 5.6 The correlation between the $[Li^+O^{2-}]$ centres and the catalytic selectivity to C_2-hydrocarbons on Li/MgO catalysts.

From Figure 5.6 the correlation between C_2-selectivity and the density of $[Li^+O^{2-}]$ sites is shown. The percentage C_2-products increased with increasing density of $[Li^+O^{2-}]$ centres on the Li/MgO catalysts, except for the phy mixed and the impreg (c) catalysts which exhibited optimum performance at nearly 30 % methane conversion and 70 % C_2 products. It was surprising that the amount of $[Li^+O^{2-}]$ centres was found to be very low, while the number of the surface sites of low coordination was observed to be extremely high. This would indicate that the majority of active centres are not likely to be located on $[Li^+O^{2-}]$ centres on the surface.

Considering Figure 5.7 shows the correlation between C_2-selectivity and the density of surface sites of low coordination on the MgO matrix. The evidence seems to imply that these sites were responsible for methane coupling. It can be seen that increasing C_2-selectivity results from greater density of surface sites of low coordination, reaching a maximum of 75 %. This would suggest that the selectivity to C_2 products cannot be enhanced over this maximum limit by increasing the density of these active sites.

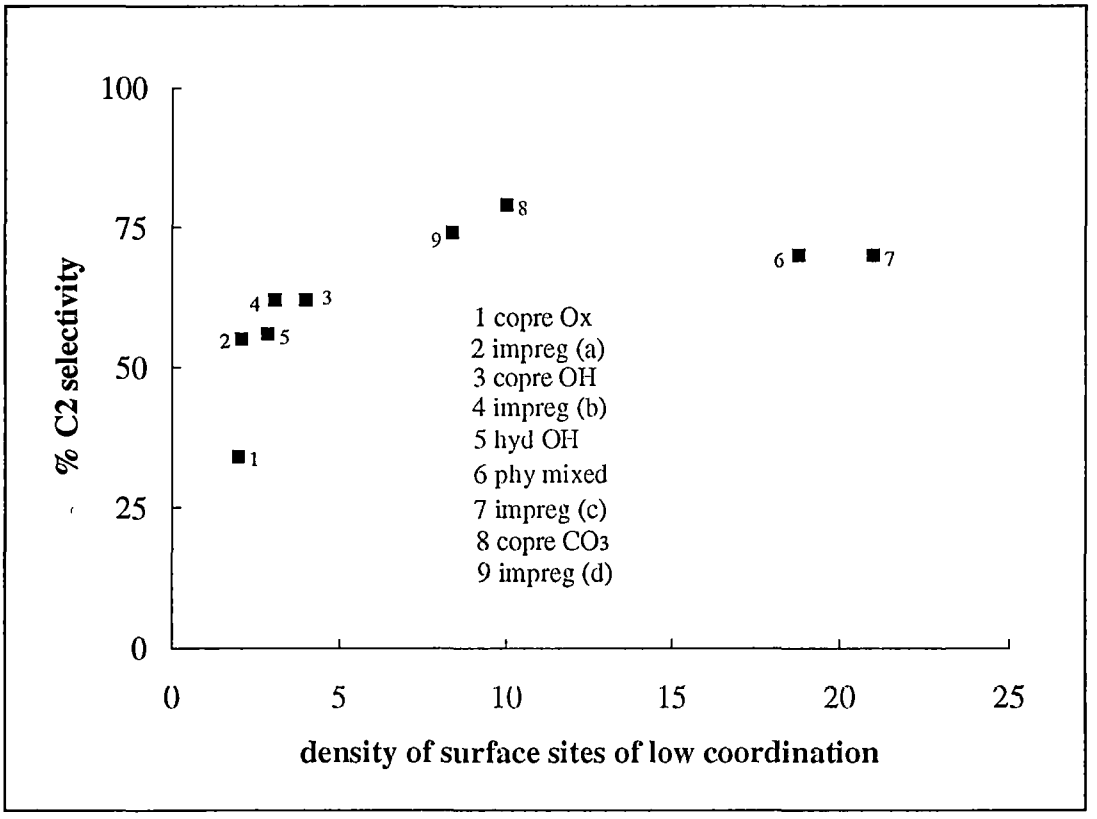

Figure 5.7 The correlation between the surface sites of low coordination and the selectivity to C_2-hydrocarbons on Li/MgO catalysts.

Another correlation between C_2-selectivity and the sum of the density of surface sites of low coordination and $[Li^+O^{2-}]$ centres is displayed in Figure 5.8.

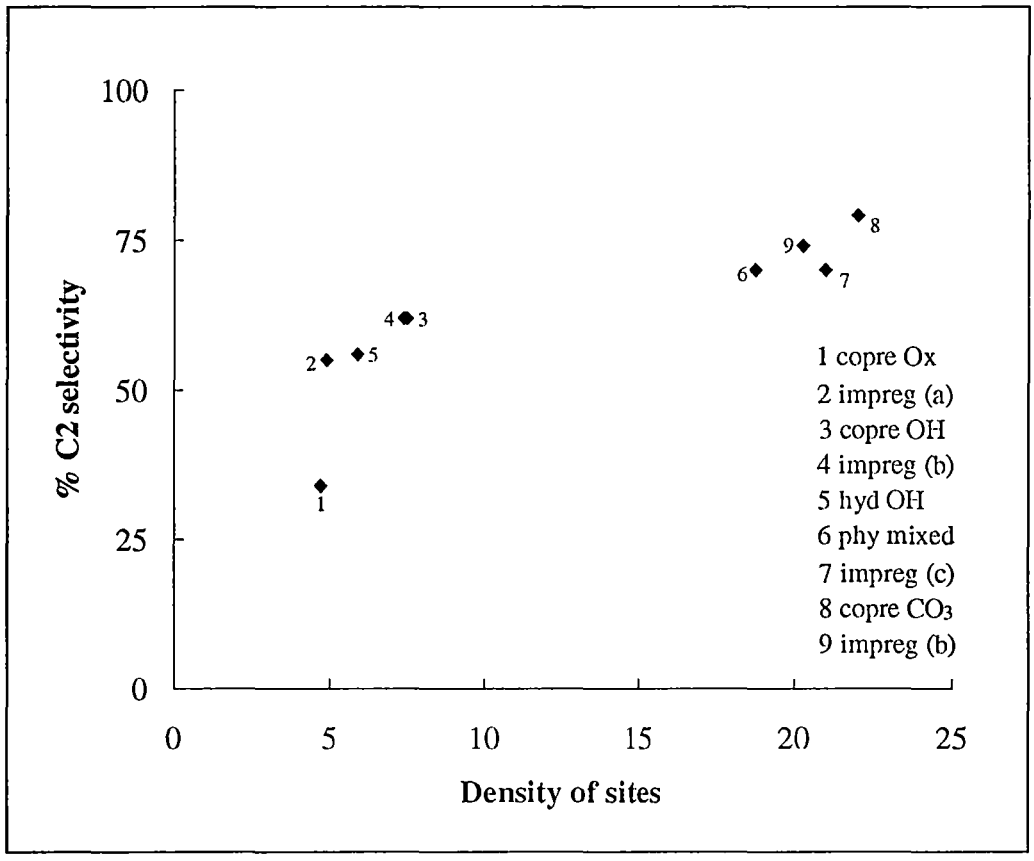

Figure 5.8 The correlation between the selectivity to C_2-hydrocarbons and the sum of the density of surface sites of low coordination and $[Li^+O^{2-}]$ centres on Li/MgO catalysts.

The correlation between the selectivity to C_2-hydrocarbons and the total density of surface sites of low coordination and $[Li^+O^{2-}]$ centres predicts that the C_2-selectivity will be significantly increased with greater density of these two sites. This trend indicates that the selectivity to C_2-products could be increased, but at a very low rate after the selectivity has initially reached 70 %. Recall the trend predicted from the

correlation between the density of surface sites of low coordination and the C_2-selectivity, where a selectivity limit was found at about 70-75 %.

Based on these findings it was obvious that the surface sites of low coordination on the MgO matrix, which were observed in a significant number on Li/MgO catalyst surfaces, are involved in methane activation and methane coupling reactions. The $[Li^+O^{2-}]$ centres are also suggested to be involved in the oxidative coupling of methane as it was found that the presence of these species significantly increased the rate of methane conversion (Table 5.6).

Table 5.6 The comparison of the number of active sites for methane activation and methane conversion between MgO and Li/MgO catalysts.

Catalyst	surface sites of lc (μmol/g)	Li^+O^{2-} (μmol/g)	Total (μmol/g)	wt of catalyst (g)	No. of sites for methane activation (μmol)	% CH_4 con.
MgO ex CO_3	120	-	120	0.102	12.2	33
MgO ex Ox	130	-	130	0.104	13.5	29
Li/MgO copre Ox	18.0	24.0	42.0	0.206	8.7	37
Li/MgO impreg (a)	21.0	28.0	49.0	0.200	9.8	37

From Table 5.6 it is clear that the presence of Li^+O^{2-} species has increased the rate of methane conversion. This indicates that these species are more active in methane activation. However, these $[Li^+O^{2-}]$ centres were observed in low number on the surface of Li/MgO catalysts with Li contents of 3.5-4.0 wt % that displayed the

best performance (high C_2-selectivity with moderate methane conversion). A large number of [Li^+O^{2-}] centres were observed on Li/MgO catalysts with low Li loadings that exhibited the high methane conversions but low selectivities to C_2-hydrocarbons. These centres were also observed in significant number for Li/MgO catalysts with high Li loadings, 6.0-7.0 wt % which showed high C_2-selectivities but low methane conversions. As a result it can be concluded that the active sites for Li/MgO catalysts are mainly generated or located on the surface sites of low coordination.

The results observed here seemed agree with the data obtained by Wu et al. (1993) showing that the [Li^+O^-] centres on 6 wt % Li/MgO were only observed in a low number on the surface in comparison with F-type defects (surface oxygen vacancies containing two electrons), namely, the surface sites of low coordination. Furthermore, Wang and Lunsford (1986) also found from the dipolar broadening of EPR signals due to the adsorption of oxygen that most of the [Li^+O^-] centres on 7 wt % Li/MgO were in the bulk. This evidence supports the findings found in this work showing that the number of [Li^+O^{2-}] species (which are the precursors of the [Li^+O^-] centres) present on the surface of Li/MgO are smaller than the number of surface sites of low coordination found in the MgO matrix. The concentrations of Li presented by Wu et al. (1993) and Wang and Lunsford (1986) were the initial loading. These catalysts seem to be comparable to the Li/MgO with Li concentration 3.5-4 % after calcination used in the present work.

These results also confirm the findings obtained by Anpo et al. (1988) that the surface sites of low coordination are the active sites for methane coupling of Li/MgO catalysts. These authors found from photoluminescence spectra that pure MgO exhibited an emission spectrum at 360 nm (exited at 220-270 nm). Doping MgO with Li resulted in a new emission band at around 450 nm (exited at 269-290 nm) which was attributed to the surface sites of low coordination (less than four). The intensity

of this emission was found to correlate with the C_2 yield in methane coupling of Li/MgO catalysts that increased with Li concentration giving a maximum value at 3 mol % Li and then decreasing. However, the MgO catalyst used by Anpo was calcined at 680°C, while Li/MgO was calcined at 800°C. Different calcination temperatures may confuse the results presented by these authors since the higher calcination temperature will result in more unsaturated surface sites on MgO as shown in Chapter 3 and less Li concentration.

5.4.6 The catalytic performance of Li/MgO catalysts with time on stream

5.4.6.1 Li/MgO catalysts of low Li loading

The percentage methane conversion and selectivity to C_2-hydrocarbons with time on stream over Li/MgO catalysts with Li loadings less than 1 wt % are shown in Figure 5.9.

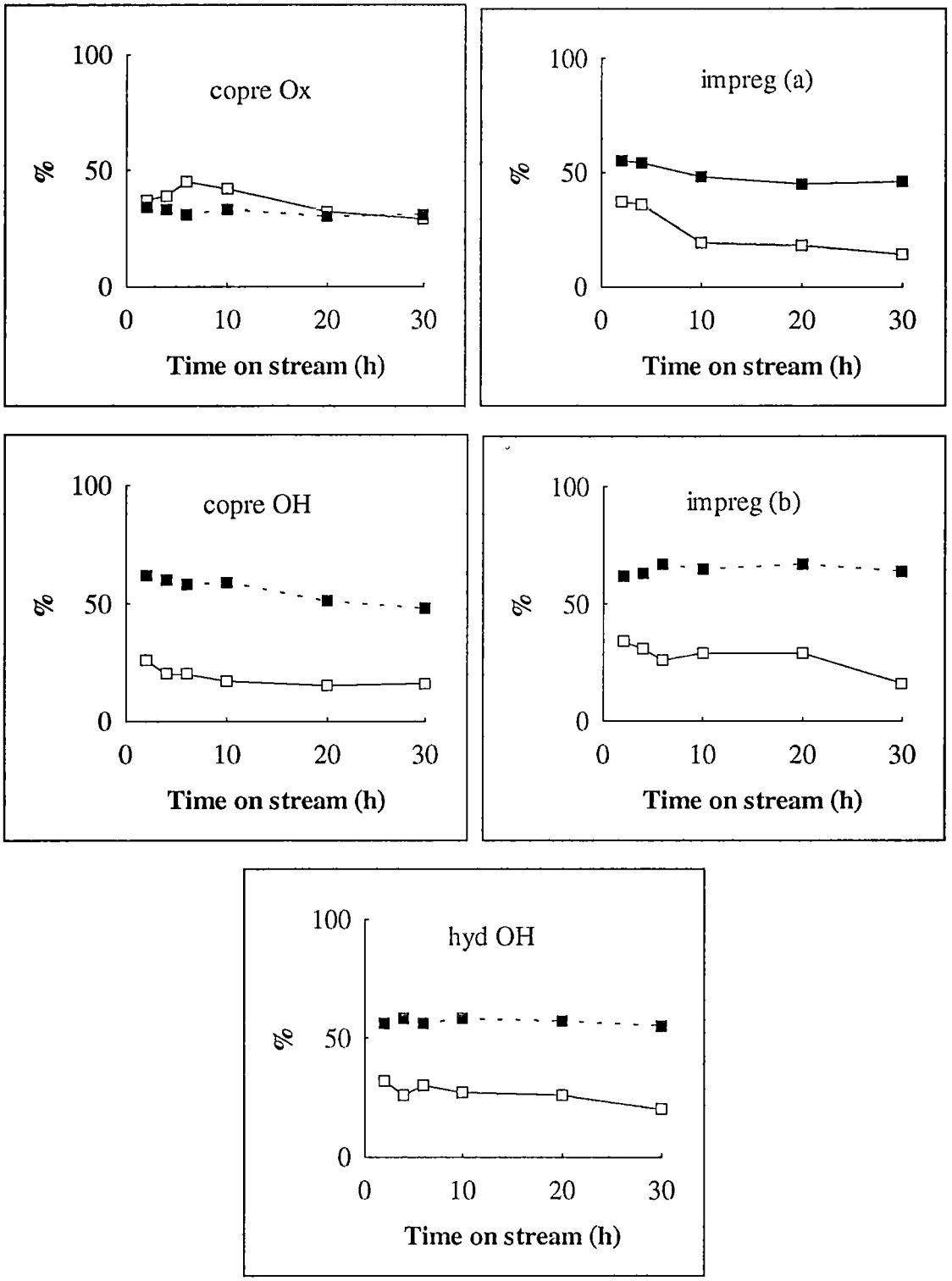

Figure 5.9 The activity (□) and selectivity (■) of Li/MgO catalysts with Li loadings 0.1-0.6 wt % against time on stream.

From Figure 5.9 it can be seen that the percentage methane conversion decreases with time on stream. The methane conversion decreased at a relatively high rate over the Li/MgO catalysts prepared by the impregnation methods. However, the selectivity to C_2-products of most of the Li/MgO catalysts only slightly decreased with time on stream. The decrease in the capacity of the catalysts to convert methane of the catalysts may be due to a reduction in the number of surface sites involved in methane activation, while the steady selectivity may be due to a constant density of active sites. The catalyst surface areas decreased with time on stream as well as the total number of active sites, so that the density of the surface sites involved in methane activation remained constant. To confirm these assumptions three Li/MgO catalysts, copre Ox, impreg (a) and impreg (b), were analysed to determine their surface sites, surface areas and Li contents after catalytic testing and the results are displayed in Table 5.7.

Table 5.7 Surface characteristics of Li/MgO catalysts before and after catalytic testing for Li loadings between 0.1-0.6 wt %.

Li/MgO catalysts	Li wt %	surface area (m^2/g)	flat surface sites number density ($\mu mol/g$) ($\mu mol/m^2$)		surface sites of lc number density ($\mu mol/g$) ($\mu mol/m^2$)		Li^+O^{2-} number density ($\mu mol/g$) ($\mu mol/m^2$)	
copre Ox (1)	0.10	9.0	15.0	1.7	18.0	2.0	24.0	2.7
copre Ox (2)	0.03	5.0	20.0	4.0	13.7	2.7	18.0	3.6
impreg (a) (1)	0.20	10.0	11.0	1.1	21.0	2.1	28.2	2.8
impreg (a) (2)	0.08	4.0	8.0	2.0	8.9	2.2	8.0	2.0
impreg (b) (1)	0.60	4.0	8.3	2.7	12.2	3.1	16.0	4.0
impreg (b) (2)	0.20	2.5	9.6	3.8	6.9	2.8	8.9	3.5

(1) and (2) denote the catalysts before and after catalytic testing.

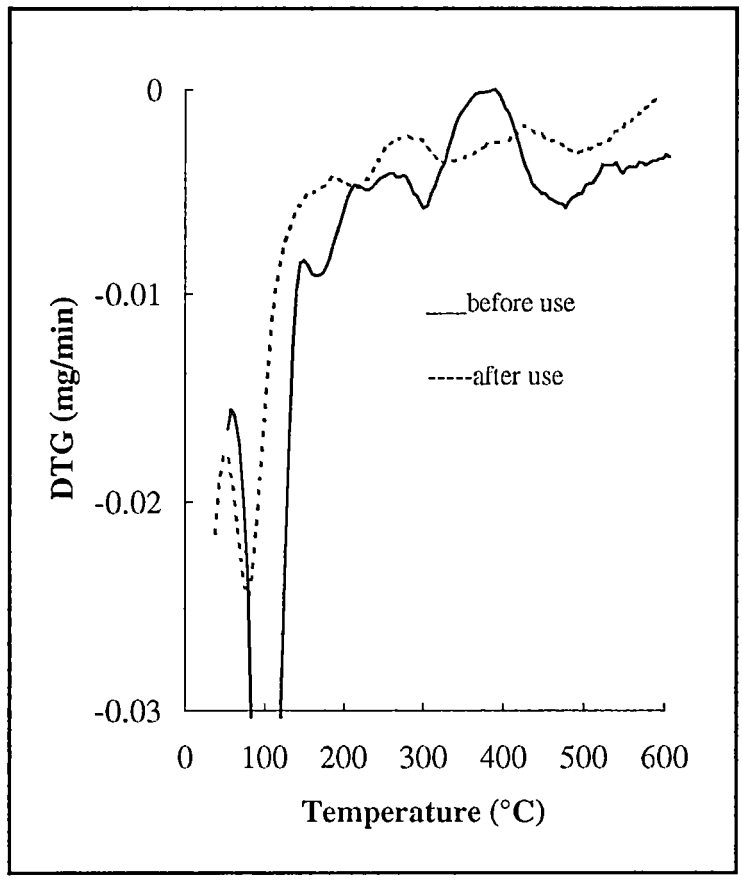

Figure 5. 10 TPD profiles of Li/MgO (impreg (b)) before and after catalytic reaction.

From Table 5.7 and Figure 5.10 it can be seen that the number of surface sites of low coordination and $[Li^{+}O^{2-}]$ centres decreased after catalytic runs of 30 h for all Li/MgO catalysts considered. A significant reduction in the number of these sites was observed for Li/MgO catalysts prepared by impregnation methods, impreg (a) and impreg (b). These results agree with their observed catalytic performance which showed a significant decrease after times on stream of 30 h. The decrease in the number of surface sites involved in the methane activation reaction was mainly attributed to the loss of Li during the catalytic reaction. As can be seen from Table 5.7 the Li concentration of the catalysts after catalytic testing was at least 60 % lower than that of the original catalyst.

It has already been mentioned that Li impurities is supposed cause defects in the MgO matrix leading to increased roughness and a high number of surface sites of low coordination on the catalyst surface. The loss of Li, along with catalyst sintering, will therefore result in a smoother catalyst surface and consequently a lower number of surface sites of low coordination. In addition, $[Li^{+}O^{2-}]$ centres which have been shown to be involved in methane activation were found to decrease with decreasing Li content.

The loss of Li content after the catalytic testing has been reported by several authors (Kimble and Kolts, 1986; 1987; Korf et al., 1990). It was believed (Korf et al., 1990) that at high reaction temperature the Li species would melt and react with the reactor quartz wall to form Li_2SiO_3. In addition, it was proposed (Korf et al., 1990) that in the presence of water (from the reaction) volatile LiOH was formed and evaporated from the catalyst resulting a white deposit on the reactor wall. The white deposit on the reactor wall after catalytic reaction was also observed in the present work.

The density of active sites after catalytic testing was found to have slightly increased. It was expected that this would have resulted in a slightly higher selectivity to C_2-products. However, it was observed that the selectivity to C_2-products of these catalysts remained steady or was slightly decreased. This may be due to the increasing number of flat surface sites exposured {100} on the MgO matrix which did not activate methane, but rather promoted the formation of nonselective products by providing access for O_2 to attack the hydrocarbon products and cause complete oxidation. These discrepancies could also have been the result of changes in Li loading (through loss) during the reaction. This would in turn lead to changes in overall surface basicity and variations in carbon dioxide and water coverage on that

surface. Under such conditions stronger activation of oxygen can be anticipated, giving rise to deep oxidation products.

The results obtained here are consistent with the work carried out by Korf et al. (1990). They reported that all Li/MgO catalysts were deactivated with time on stream. The C_2 yield decreased, however, the C_2-selectivity was constant.

5.4.6.2 Li/MgO catalysts with Li loadings between 3.5-7.0 wt %

The catalytic performance of these catalysts with time on stream is shown in Figure 5.11.

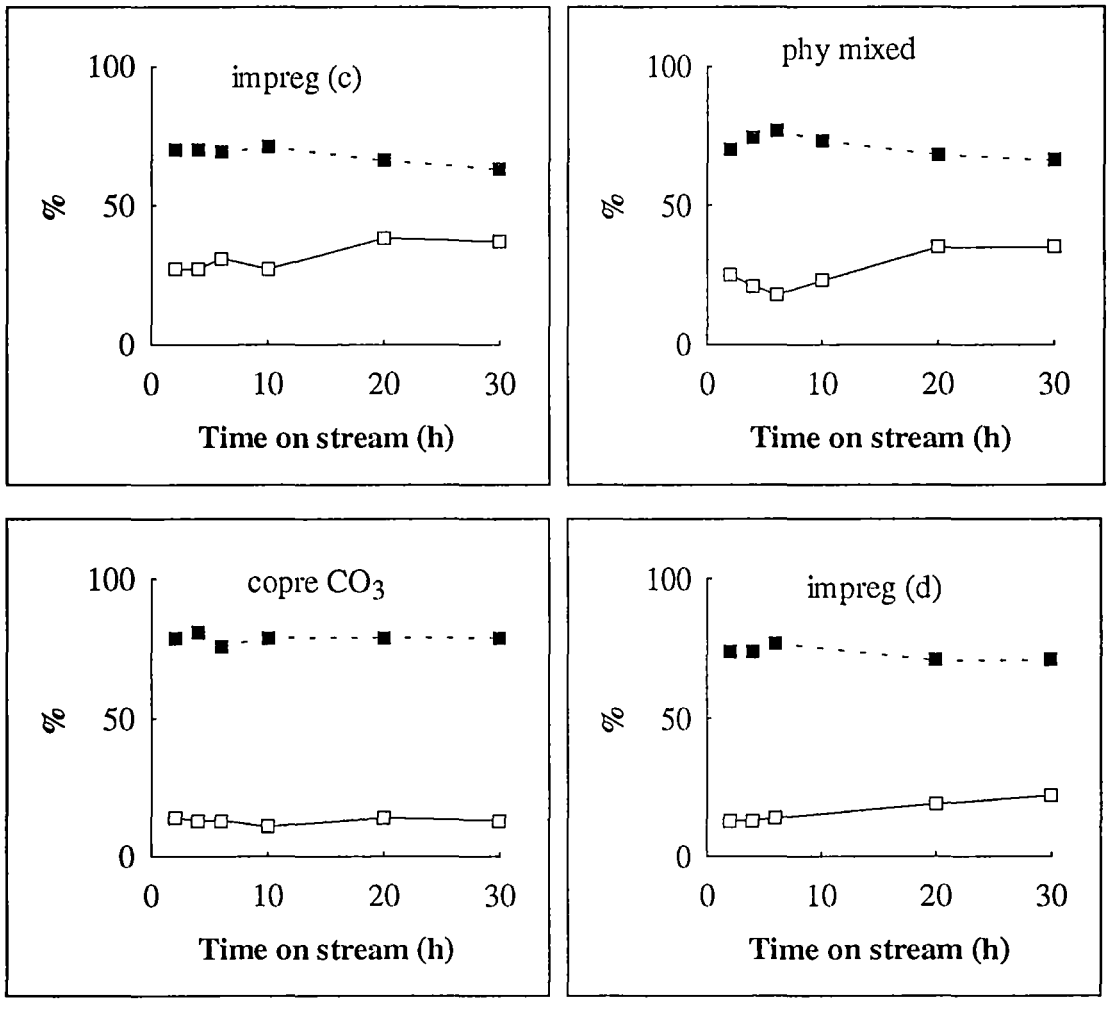

Figure 5.11 The catalytic performance ((□) methane conversion and (■) C_2-selectivity) of Li/MgO catalysts with Li loadings between 3.5-7.0 wt % against time on stream.

From Figure 5.11 it was surprising to find that the percentages methane conversion over Li/MgO catalysts with original Li contents of ~ 3.5-4.0 wt % (phy mixed and impreg (c)) were significantly increased with time on stream, while the selectivity to C_2-products was slightly decreased. An increase in methane conversion, and a slight decrease in selectivity to C_2-hydrocarbons was observed for Li/MgO catalysts with original Li loading between 6.0-7.0 wt % (copre CO_3 and impreg (d)). These results also show the change in the number of surface sites on the catalyst surfaces during the catalytic runs. It was therefore interesting to examine these catalysts after catalytic testing for their Li content, surface areas and surface sites, and to compare these results with those of the catalysts before catalytic testing. Results are displayed in Table 5.8.

Table 5.8 Surface characteristics of Li/MgO catalysts before and after catalytic testing for Li loading between 3.5 and 7.2 wt %.

Li/MgO catalysts	Li wt %	surface area (m^2/g)	flat surface sites number density ($\mu mol/g$) ($\mu mol/m^2$)		surface sites of lc number density ($\mu mol/g$) ($\mu mol/m^2$)		Li^+O^- number density ($\mu mol/g$) ($\mu mol/m^2$)	
phy mixed (1)	3.9	0.8	2.4	2.5	15.2	18.8	-	
phy mixed (2)	1.1	0.6	9.3	12.2	15.9	26.5	1.9	3.2
impreg (c) (1)	3.5	1.0	4.7	4.7	21.0	21.0	-	
impreg (c) (2)	1.0	0.7	11.6	16.4	15.6	22.3	7.4	10.6
impreg (d) (1)	7.2	0.6	5.2	8.4	5.3	8.4	7.4	12.3
impreg (d) (2)	2.3	0.5	24.3	48.6	14.4	28.8	0.9	1.8

copre CO_3 (1)	6.0	0.5	5.0	10.0	5.0	10.0	6.0	12.0
copre CO_3 (2)	2.5	0.5	6.0	12.0	13.0	26.0	1.0	2.0

(1) and (2) denote the catalysts before and after catalytic testing.

From Table 5.8 it was found that the Li content of the Li/MgO catalysts was significantly decreased after undergoing the oxidative coupling of methane reaction for 30 h. The surface areas of the catalysts were also found to have decreased slightly, and the surface sites on the Li/MgO catalysts, phy mixed and impreg (a), the number of surface sites of low coordination were observed to be slightly decreased (Figure 5.12). The surface sites on the flat surface exposure {100} were found to have significantly increased, and the $[Li^+O^{2-}]$ centres also increased after catalytic reaction. In general, the total number of sites that are supposed to be involved in the methane activation reaction (the surface sites of low coordination, the $[Li^+O^{2-}]$ centres, as well as the sites belonging to the flat surface of the MgO matrix) increased after the catalytic run for 30 h. However, it should be noted that the TPD traces were not as easy to interpret because of the small mass of phenol adsorbed and the small surface areas giving a high level of uncertainty to the conclusion.

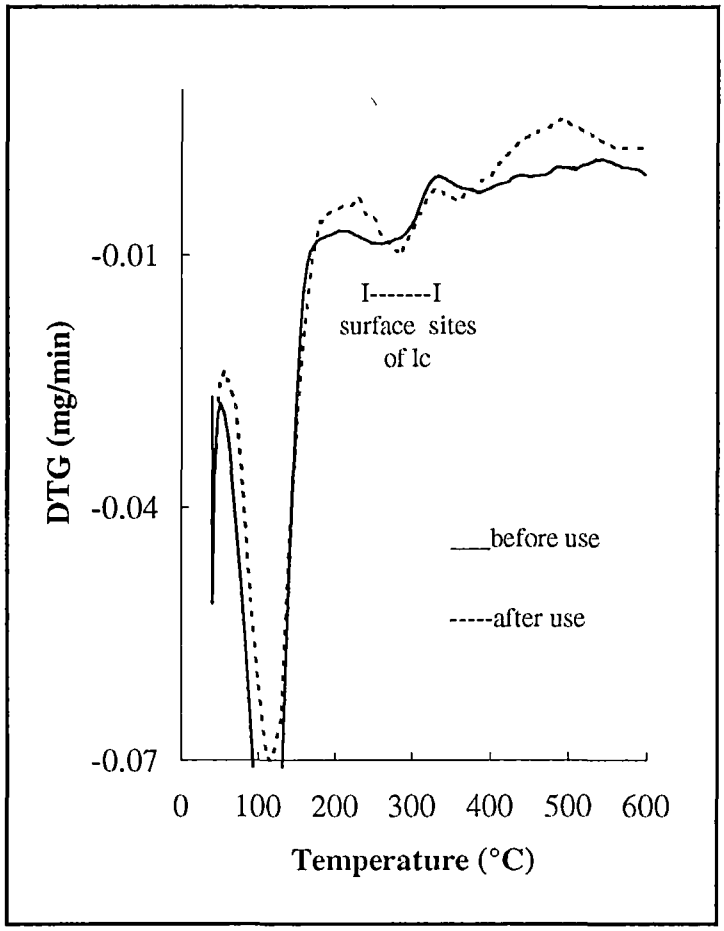

Figure 5.12 TPD profiles of Li/MgO (phy mix) before and after catalytic reaction for 30 h.

The increase in methane conversion after times on stream of 30 h for Li/MgO catalysts phy mixed and impreg (c) (shown in Figure 5.11) can be explained in terms of the number of surface sites involved in methane activation, along with higher density of these sites. However, the selectivity to C_2-hydrocarbons of these catalysts was found to decline even though the density of active sites increased on the catalyst surface. This was thought to be due to the significant increase in the number of surface sites of flat surface exposure {100}. As mentioned previously, the presence of these sites may promote nonselective reactions by giving access to O_2 to attack and oxidise the hydrocarbon product species.

Similar trends were observed for the impreg (d) Li/MgO catalyst, as all the surface sites were found to have increased after the catalytic reaction. The increase in the number of these surface sites was found to agree with the relative methane conversion. These results confirmed the relationship between the number of surface sites and the rate of methane conversion. The decrease in the selectivity to C_2-hydrocarbons on the catalyst surface after a reaction time of 30 h was presumed to be due to an increase in the number of surface sites on the flat surface exposure {100}. For copre CO_3 Li/MgO, the number of surface sites of low coordination was also found to have significantly increased, while the number of $[Li^+O^{2-}]$ centres was observed to have decreased after 30 h time on stream. However, the total number of these two sites remained steady which corresponds to the percentage methane conversion. The surface sites on the flat surface exposure {100} were found to be only slightly changed. As a result the selectivity to C_2-hydrocarbons was found to be steady with time on stream.

The change in the number of surface sites on the Li/MgO catalysts was presumed to be due to the loss of Li, as well as sintering that would have occurred during the high temperature catalytic reaction. Li/MgO catalysts of less than 1 wt % Li were found to rapidly deactivate, while higher methane conversions were maintained on catalysts with high Li loadings. These results indicate the effect of Li on the number of surface sites involved in methane activation on the catalyst surface. The number of these sites significantly decreased after 30 h time on stream due to Li loss for Li/MgO catalysts with low Li contents, while the number of these sites remained high for those catalysts with high Li loadings after catalytic reaction for 30 h. It is possible that at low Li loading only the Li^+O^{2-} species exist, while at the high Li loading the original Li salt may remain and slowly decompose to Li^+O^{2-} species during the catalytic reaction. This keeps the Li^+O^{2-} concentration constant and maintains the

constant high level of defects in MgO, leading to a constant high number of active sites for methane activation.

It is noted that the deviation in surface site determination of Li/MgO catalysts is very high due to the low surface area and small amount of phenol adsorbed. However, the trend of the relationship between catalytic performance and the relative number of surface sites with different Li loadings was found to be consistent.

5.4.7 The methane activation reaction and the nature of the catalytic active sites

The initial step involved in methane activation is still a topic of much controversy in the literature. Both homolytic (Ito et al., 1985; Nelson et al., 1989) or heterolytic (Choudhary and Rane, 1991; Maitra et al., 1992; Lapszewicz and Jiang, 1992) C-H bond cleavage to give $CH_3\cdot$ radicals have been proposed. Homolytic C-H bond cleavage (Ito et al., 1985; Nelson et al., 1989) is thought to occur from interaction between methane and active form of oxygen species (O^-, O_2^{2-}, O_2^- etc.) on the catalyst surface. This process results in the formation of the $CH_3\cdot$ radical directly. Lunsford and co-workers (Driscoll et al., 1985; Ito et al., 1985) first proposed that the O^- species of $[Li^+O^-]$ centres were the active sites for methane activation. These $[Li^+O^-]$ centres are generated from oxygen vacant holes trapped at O^{2-} ions adjacent to Li^+ ions.

The mechanism of methane coupling proposed for Li/MgO catalysts by Lunsford and co-workers (Ito et al., 1985) is displayed as follows.

$$2CH_3\cdot \rightarrow C_2H_6 \qquad [5.7]$$

The methyl radicals also produce COx through a series of chain reactions in the gas phase:

$$CH_3^{\bullet} + O_2 \leftrightarrow CH_3O_2^{\bullet} \quad [5.8]$$

$$CH_3O_2^{\bullet} + C_2H_6 \rightarrow CH_3O_2H + C_2H_5^{\bullet} \quad [5.9]$$

$$2CH_3O_2^{\bullet} \rightarrow CH_2O + CH_3OH + O_2 + CO, CO_2 \quad [5.10]$$

$$CH_3O_2H \rightarrow CH_3O^{\bullet} + OH^{\bullet} \quad [5.11]$$

$$CH_3O^{\bullet} + CH_4 \rightarrow CH_3OH + CH_3^{\bullet} \quad [5.12]$$

$$OH^{\bullet} + CH_4 \rightarrow CH_3^{\bullet} + H_2O \quad [5.13]$$

or on the surface:

$$CH_3^{\bullet} + O^{2-}(\text{surface}) \rightarrow CH_3O^{-} + e^{-} \quad [5.14]$$

$$CH_3O^{-} \rightarrow CH_3OH, CH_2O + CO, CO_2 \quad [5.15]$$

Ethane produced by the coupling reaction further reacts to form ethylene either on the surface:

$$C_2H_6 + [M^+O^-] \rightarrow C_2H_5^{\bullet} + [M^+OH^-]s \quad [5.16]$$

$$C_2H_5^{\bullet} + O^{2-} \rightarrow C_2H_5O^{-} + e^{-} \quad [5.17]$$

$$C_2H_5O^{-} \rightarrow C_2H_4 + OH^{-} \quad [5.18]$$

or in the gas phase through equations [5.9], [5.19], [5.20] and [5.21]:

$$CH_3^{\bullet} + C_2H_6 \rightarrow CH_4 + C_2H_5^{\bullet} \quad [5.19]$$

$$C_2H_5^{\bullet} \rightarrow C_2H_4 + H^{\bullet} \quad [5.20]$$

$$C_2H_5^{\bullet} + O_2 \rightarrow C_2H_4 + HO_2^{\bullet} \quad [5.21]$$

According to several workers (Sinev et al., 1986; Otsuka et al., 1991; Yamashita et al., 1991; Dissanayake et al., 1993), Lunsford (Lunsford 1993) the peroxide ion (O_2^{2-}) is a more likely candidate for the active centre than either [Li^+O^-] or F-centres. The peroxide ions arise from the adsorption of O_2 on Li/MgO catalysts. Sinev et al. (1986)and Otsuka et al. (1991) have demonstrated that Na_2O_2 and BaO_2 are able to convert methane to ethane at low temperatures (< 500°C). However, the process was found not to be catalytic because the carbonates formed during the reaction reaction did not decompose. Yamashita et al. (1991) investigated Ba/La_2O_3 catalysts by X-ray photoelectron spectroscopy (XPS) and concluded that BaO_2 or O^- ions derived from peroxide are the active centres.

Lunsford and co-workers (Dissanayate et al., 1993) investigated a series of Ba/MgO catalysts with different Ba loadings (0.2-4.0 mol %) by XPS to determine the amount of stable carbonates (at T > 800°C) and peroxide ions on their respective surfaces. A good correlation between the peroxide concentration on the surface and the coupling activity was obtained. The authors concluded that O_2^{2-} ions, or perhaps O^- ions derived from the reaction $O_2^{2-} \leftrightarrow 2O^-$, are responsible for the activation of CH_4 via homolytic C-H bond cleavage.

The O_2^- or superoxide species was reported (Osada et al., 1990; Yang et al.,1993) to be the active species for methane activation at temperatures typically used in the oxidative coupling of methane. Liu et al. (1993) examined the activity of various oxygen species, O^-, O_2^{2-}, O_2^-, towards the oxidative coupling of methane. These authors believed that O_2^- species are the most C_2 selective oxygen species due to their low reactivity toward C_2-hydrocarbon products, while O^- and O_2^{2-} may be too active to be selective. These adsorbed oxygen species are supposed to transform on the surface of the catalyst as follows:

$$O_2 \leftrightarrow O_2(s) \rightarrow^{e} O_2^-(s) \rightarrow^{e} O_2^{2-}(s) \rightarrow 2O^-(s) \rightarrow^{2e} 2O^{2-}(s)$$

(s) denotes the adsorbed species on the catalyst surface.

In addition, Yang et al.(1993) found from EPR spectra that only O_2^- species are present on La_2O_3/MgO catalysts which display rather high activity and selectivity for the oxidative coupling of methane.

Heterolytic C-H bond cleavage has also been suggested by a number of authors (Choudhary and Rane, 1991; Maitra et al., 1992; Lapszewicz and Jiang, 1992). This process considers the interaction of CH_4 with the catalyst surface as an acid-base reaction. When methane interacts with an acid-base pair ($M_{lc}^{n+}O_{lc}^{2-}$) on the metal oxide surface(see [5.22]), it undergoes heterolytic C-H bond rupture, resulting in CH_3^- and H^+ ions which can interact with catalyst acidic sites (M_{lc}^{n+}) and basic sites (O_{lc}^{2-}), respectively (Choudhary and Rane, 1991).

$$\begin{array}{l} H_3C\text{—}H \quad H_3C^{-\delta}\cdots H^{+\delta} \quad H_3C^- \quad H^+ \qquad\qquad O_2^- \quad H^+ \\ M_{lc}^{n+}O_{lc}^{2-} \leftrightarrow M_{lc}^{n+}O_{lc}^{2-} \rightarrow M_{lc}^{n+}O_{lc}^{2-} \rightarrow O_2 \rightarrow M_{lc}^{n+}O_{lc}^{2-} + CH_3\cdot \end{array} \quad [5.22]$$

In the presence of O_2, electron transfer occurs from carbanions (CH_3^-) to O_2, resulting in O_2^-. The methyl radical is released to the gas phase or oxidised on the catalyst surface. The anion (basic) site is generated by the dehydroxylation of the catalyst surface at the high reaction temperature leading to the formation of water (see [5.23]).

$$2M_{lc}^{n+}(OH)_{lc}^- \rightarrow M_{lc}^{n+}O_{lc}^{2-} + M_{lc}^{n+}\square_{lc}^{2-} + H_2O \quad [5.23]$$

($\square_{lc}^{2-}$ is vacant anion site)

$$O_2^- + \square_{lc}^{2-} \rightarrow O_{lc}^{2-} + O^- \quad [5.24]$$

The O^- species formed from O_2^- (equation [5.24]) may further give rise to methyl radicals from methane by the mechanism similar to that described by Lunsford and co-workers (Ito et al., 1985), equations [5.7] to [5.21].

Qualitatively, the heterolytic mechanism is supported by the fact that most oxidative coupling catalysts are strongly basic oxides (Lunsford, 1993). Sokolovski and co-workers (Sokolovskii et al., 1989; Buevskaya et al., 1987) have shown that CH_4 conversion and C_2-formation activity correlate nicely with the basicity of catalysts, as determined by benzoic acid adsorption. There have been other attempts to correlate oxidative coupling activity with basicity of catalysts, however, they have not been as successful (Lapszewicz and Jiang, 1992; Choudhary et al., 1994). Lapszewicz and Jiang conducted the CH_4/D_4 exchange reaction which was thought to occur via the heterolytic dissociation of C-H bonds. It was found that there was no simple correlation between the CH_4/D_4 exchange and the oxidative coupling reaction. Choudhary and co-workers investigated the acidity/acid strength and basicity/basic strength of MgO catalysts prepared by thermal decomposition of several precursors. The correlation between the acid-base properties and the oxidative coupling reaction was found to be complicated.

Using the temperature programmed desorption of phenol coupled with a TG technique developed in the present work, a correlation between basicity and catalytic performance in the oxidative coupling of methane over MgO and Li/MgO catalysts was observed. The technique used was able to distinguish the different surface sites with different basic strengths, hence the relative basicity of each type of surface site was obtained. The catalytic performance of both MgO and Li/MgO catalysts was demonstrated to be closely related to the surface sites of low coordination on MgO. The methane conversion was observed to depend on the number of the surface sites of

low coordination, while the C_2-selectivity was found to correlate with the density of these sites.

In addition, for Li/MgO catalysts of low Li loading (0.1-0.2 wt %) it was observed from the TPD of phenol that the sites proposed to be $[Li^+O^{2-}]$ centres have a significantly higher basic strength than the surface sites of low coordination. It was also observed from catalytic testing that methane conversion over these Li/MgO catalysts was significantly higher than that obtained over pure MgO catalysts which possessed a higher number of active sites. These results show that catalytic activity closely depends on the basic strength of the catalysts. The stronger basic sites in Li/MgO increased the rate of methane activation in Li/MgO

In summary the results obtained in this work indicate the effect of basic strength and basicity of active sites for methane activation in the catalytic performance of MgO and Li/MgO catalysts. This evidence seems to support the heterolytic C-H bond rupture via the acid-base reaction.

5.4.8 The relationship between morphology and catalytic performance in the oxidative coupling of methane

Hargreaves et al., (1991; 1992) found from TEM micrographs that addition of Li caused a loss in surface area of the MgO precursor. Two main structural features were found; the formation of grain boundary dislocations (formed to relieve strain when misorientated MgO crystallites impinge on each other), and dislocations in the bulk of the MgO grain. The bulk dislocations were mainly burgers vectors type a/2<110>. The emergence of these defects were thought to create a charge region as a result of either a cation or anion vacancy. It was suggested (Hargreaves et al., 1991) that these defects were important with respect to the formation of active sites for methane activation. Based on these findings the authors concluded that catalyst

morphology was an important factor for the catalytic activity of Li/MgO catalysts in the oxidative coupling of methane.

Using an alternative appoach a similar conclusion was also obtained in the present work. It has been demonstrated in sections 5.4.1, 5.4.2 and 5.4.3 that doping MgO with Li changes the MgO morphology and the nature and number of surface sites. The variation in surface structure and surface sites depends on the concentration of Li in the MgO matrix. Pure MgO typically has a structure with high porosity and high surface area (as shown in Chapter 4). Doping with Li resulted in the destruction of the pore system of the MgO matrix leading to a lower surface area, and the higher the Li loading the more destruction there is to the pore system of the MgO matrix. The collapse of the MgO porous structure was thought to arise from defects caused by the Li impurity. These defects also had a large effect on the surface sites of the MgO matrix. The surface sites of low coordination, found to be present on Li/MgO catalysts, have a significant role in the oxidative coupling of methane. As a result the morphology, surface sites and catalytic performance of Li/MgO catalysts are closely interrelated.

5.4.8.1 The particle size

From Figure 5.1 it was found that most Li/MgO catalysts displayed irregular particle size distribution profiles. As discussed before, irregular particle size distribution profiles result from a high number of defects in the MgO microstructure. These defects were found to interfere with the crystal growth and the particle formation of MgO. Considering Figure 5.1 in combination with Table 5.5, showing the catalytic performance of various Li/MgO catalysts, it was found that Li/MgO with a Li loading of 3.9 % (phy mixed) displayed optimum performance for methane conversion (23 %) and C_2-selectivity (70 %). This catalyst had the most irregular

particle size distribution profile with a high number of very fine particles and the surface sites of low coordination were found in much higher numbers than the other surface sites.

Li/MgO prepared from coprecipitation of the hydroxide was also observed to exhibit a relatively high activity, having a methane conversion of 26 % and C_2-selectivity of 62 %. This catalyst also had a more irregular particle size distribution profile with a high number of very fine particles. More regular particle size distribution profiles were found for Li/MgO catalysts prepared from the hydrolysis method and coprecipitation of oxalate salts. These catalysts displayed high methane conversion, over 30 %, due to their high number of surface sites, but low selectivity to C_2-hydrocarbons (less than 60 %) due to their low density of surface sites of low coordination. From these observations it is likely that good catalytic performance with high C_2-selectivity and moderate methane conversion is associated with irregular particle size distribution profiles including a high number of very fine particles.

5.4.8.2 Pore size and pore volume

In section 4.3.6.2 it was observed for pure MgO catalysts that there was some association between the low cumulative pore volume and high number of small pores and high C_2-selectivities. A similar trend was also found for Li/MgO catalysts. From Figure 5.4 it was observed that Li/MgO catalysts prepared from the phy mixed, copre OH, copre CO_3 percursors have very low cumulative pore volumes, less than 0.05 mL/g in the pore range 36-1000 Å. These catalysts displayed high selectivity to C_2-hydrocarbons when compared with Li/MgO prepared from the hydro OH and copre Ox precursors which had higher cumulative pore volumes, ca. 0.2 mL/g in the pore range 36-1000 Å. However, all Li/MgO catalysts had similar common pore sizes (Figure 5.3) of about 50-70 Å.

If the pore structures of Li/MgO (Figures 5.3 and 5.5) and pure MgO (Figures 4.10 and 4.11) are compared, it can be seen that doping MgO with Li reduces the cumulative pore volume of the MgO matrix. It was noted that the most common pores of the MgO catalysts were in the range 200-400 Å, while the most common pores of the Li/MgO catalysts were in the range 50-70 Å. As a higher C_2-selectivity was observed over Li/MgO catalysts, it is likely that small pores are more suitable for high C_2-selectivity. It is reasonable that the high porosity increases the diffusion paths leading to increased residence time of primary product, which in turn increases their chance of being oxidised to CO_x. The low cumulative pore volume and small pore sizes that are associated with high C_2-selectivity indicate to some extent of the roughness of the catalyst surface on a microscale. Observations seem to agree with the assumption that a high density of surface sites of low coordination or high degree of roughness on the catalyst surface is a critical factor for high C_2-selectivity.

5.5 Conclusion

From the results obtained in the present work it is proposed that on pure MgO catalysts there are two major active sites of different basic strengths. Both sites are responsible for the oxidative coupling of methane; however, the more basic site is more effective for producing C_2 products. The other site appears to be responsible for a pathway favouring oxidation to carbon monoxide and carbon dioxide.

By using different precursors the relative numbers of the two sites as well as their density could be altered. On the basis of the relative number of sites with increasing calcination temperature, the more basic site is considered to be the one of lowest coordination and the less basic site is assigned to those located on the flat surface exposing {100} plane. Variation of these sites is dependent on the defects in MgO microstructures, i. e. high density of surface sites of low coordination arise from

the high defects which also influence the morphology of catalysts. High density of surface sites of low coordination was found to be associated with small particle size and low cumulative pore volume.

Doping MgO with Li has increased the defects in MgO crystals leading to destruction of the pore system and consequently to the lower surface area. Such defects have increased the degree of roughness on the catalyst surface resulting in a higher density of surface sites of low coordination and hence a higher C_2-selectivity in the oxidative coupling of methane reaction. Addition of Li to MgO has also generated another basic site with higher basic strength, assigned to Li^+O^{2-} species, on the surface of catalysts. The variation of surface sites on Li/MgO is strongly dependent upon the concentration of Li. The model of MgO before and after doping with Li is displayed in Figure 5.13.

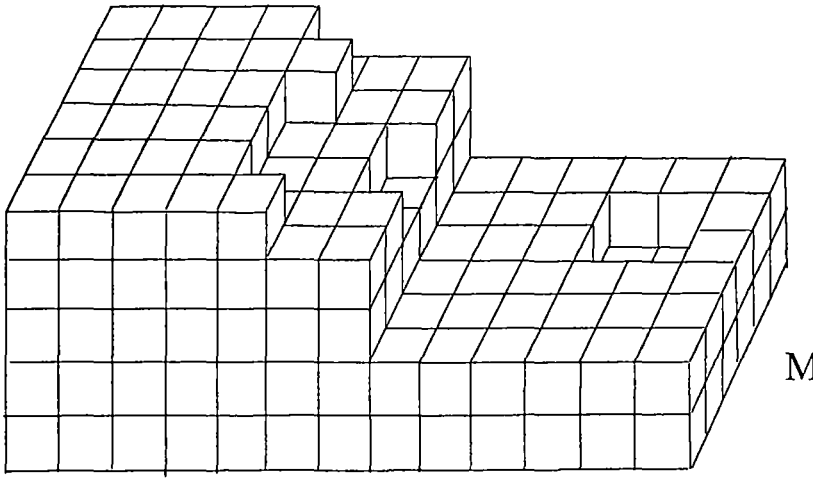

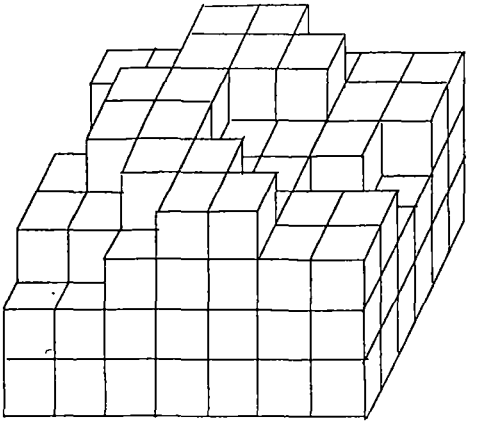

Figure 5.13 Model for the surface sites on MgO and Li-doped MgO.

Based on the results obtained in this work, the catalytic performance in the oxidative coupling of methane is strongly depending on the basic strength and basicity of MgO and Li/MgO catalysts. High basic strength and high basicity can enhance the rate of methane activation resulting in high methane conversion, while the density of the strong basic sites promotes the rate of methane coupling leading to the high C_2-selectivity (Figure 5.14). This finding supports the assumption that the methane activation occurs as a heterolytic dissociation via an acid-base reaction.

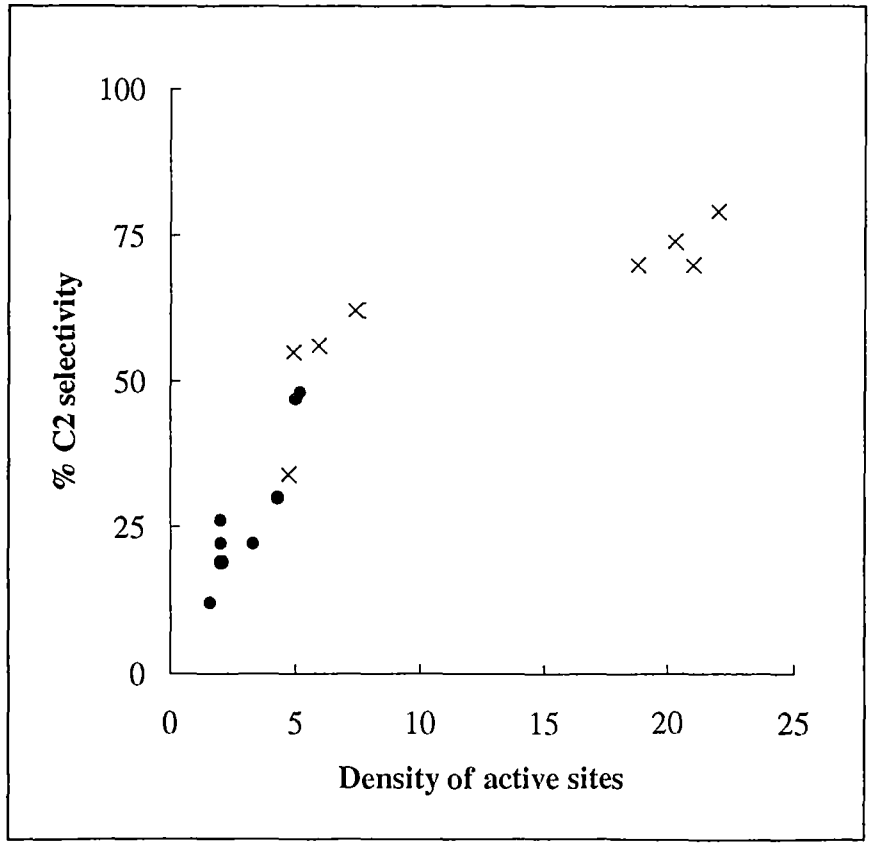

Figure 5.14 The relationship between density of the active sites (surface sites of low coordination on MgO matrix and Li^+O^{2-} centres) and C_2-selectivity in the oxidative coupling of methane over (•) pure MgO and (×) Li/MgO catalysts.

References

Anpo, M., Sunamoto, M., Doi, T., and Matsuura, I. (1988), Chem. Lett., 701.

Boldu, J. L., Abraham, M.M., and Chen, Y. (1979), Phys. Rev. B, **19**, 4421.

Boudart, M. and Djéga-Mariadassou, G. (1984), Kinetics of Heterogeneous Catalytic Reactions, Princeton University Press, Princeton, New Jersey, pp 38-39.

Buyevskaya, O. V., Suleimanov, A. I., Aliev, S. M., and Sokolovskii, V. D. (1987), React. Kinet. Catal. Lett., **33**, 223.

Chen, Y., Tohver, H.T., Narayan, J., and Abraham, M.M. (1977), Phys. Rev. B, **16**, 5535.

Choudhary, V. R. and Rane, V. H. (1991), J. Catal., **130**, 411.

Choudhary, V. R., Rane, V. H., and Gadre, R. V. (1994), J. Catal., **145**, 300.

Dissanayake, D., Kharas, K. C. C., Lunsford, J. H., and Rosynek, M. P. (1993), J. Catal., **139**, 652.

Driscoll, D.J., Martir, W., Wang, J-X, and Lunsford, J.H. (1985), J. Am. Chem. Soc., **107**, 58.

Hargreaves, J.S.J., Hutchings, G.J., and Joyner, R.W. (1990), Catal. Today, **6**, 481.

Hargreaves, J.S.J., Hutchings, G.J., Joyner, R.W., and Kiely, C.S. (1991), Catal. Today, **10**, 259.

Hargreaves, J.S.J., Hutchings, G.J., Joyner, R.W., and Kiely, C.S. (1992), J. Catal., **135**, 576.

Ito, T., Wang, J., Lin, C., and Lunsford, J.H. (1985), Am. Chem. Soc., **107**, 5062.

Iwamatsu, E., Moriyama, T., Takasaki, N., and Aika, K. (1987), J. Chem. Soc. Chem. Comm., 19.

Iwamatsu, E., Moriyama, T., Takasaki, N., and Aika, K. (1988), J. Catal., **113**, 25.

Kimble, J. B. and Kolts, J. H. (1987), Chemtech., 501.

Kimble, J. B. and Kolts, J. H. (1986), Energy Progress, **6**, 226.

Korf, S. J., Ross, J. A., Debruijn, N. A., Van Ommen, J. G., and Ross, J. R. H. (1990), Appl. Catal., **58**, 131.

Lacy, J.B., Abraham, M.M., Boldu, J. L., Chen, Y., Narayan, J., and Tohver, H.T. (1978), Phys. Rev. B **18**, 4316.

Lapszewicz, J. A. and Jiang, X.-Z. (1992), Catal. Lett., **13**, 103.

Lin, C-H., Wang, J-X., and Lunsford, J.H. (1988), J. Catal, **111**, 302.

Liu, Y-D., Lin, G-D., Zhang, H-B., and Tsai, K. R. (1993), Proc. 3rd Natural Gas Conversion. Sym., 131.

Lunsford, J. H. (1993), Proc. 3rd Natural Gas Conversion. Sym., 1.

Lunsford, J.H., Cisneros, M.D., Hinson, P.G., Tong, Y., and Zhang, H. (1989), Faraday Discuss. Chem. Soc., **87**, 13.

Lunsford, J.H. (1990), Catal. Today, **6**, 235.

Maitra, A. M., Campbell, I., and Tyler, R. J. (1992), Appl. Catal. A: General **85**, 27.

McCarty, J.G., Quinlan, M.A., and Sancier, K.M. (1988), ACS. Div. Fuel Chem. Preps., **33** (3) 363.

Mirodatos, C., Perrichon, V., Durupty, H.C., and Moral, P. (1987), Stud. Surf. Sci. Catal., **34**, 183.

Nelson, P. F., Lukey, C. A., and Cant, N. W. (1989), J. Catal., **120**, 216.

Otsuka, K., Murakami, Y., Wada, Y., Said, A. A., and Morikawa, A. (1990), J. Catal., **121**, 122.

Sinev, M. Yu., Korchak, V. N., and Krylov, O. V. (1986), Kinet. Katal., **27**, 1274.

Sokolovskii, V. D., Aliev, S. M., Buyevskaya, O. V., Davydov, A. A. (1989), Catal. Today, **4**, 293.

Wang, J-X. and Lunsford, J.H. (1986), J. Phys. Chem., **90**, 5883.

Wu, M-C., Truong, C.M., Coultor, K., and Goodman, D.W. (1993), J. Catal., **140**, 344.

Yamashita, H., Machida, Y., and Tomita, A. (1991), Appl. Catal. A: General, **79**, 203.

Yang. T., Feng, L., Hou, R., Shen, S. (1993), Proc. 3rd Natural Gas Conversion. Sym., 281.

Young, D.M. and Crowell, A.D. (1962), Physical Asorption of Gases, London Butterworth, pp 148-150.

CHAPTER 6

DETERMINATION OF ARRHENIUS PARAMETERS FOR DESORPTION OF PHENOL FROM MgO

6.1 Introduction

It is the intent of this Chapter to demonstrate the calculation of kinetic parameters including the pre-exponential factor and activation energy for the desorption of phenol from different surface sites of MgO catalysts. This information has never been reported previously by any research groups.

The temperature at which the maximum desorption appears (T_M) is related to the activation energy of desorption (E_d) and the rate of heating by:

$$2\ln T_M - \ln\beta = E_d/RT_M + \ln(E_d/AR)$$ (Cvetanovic and Amenomiya, 1972) [6.1].

β is the rate of linear temperature increase and A is the pre-exponential factor assumed to be temperature independent. In the present work E_d was determined for MgO (prepared by thermal decomposition of $Mg(OH)_2$ at 600°C and 800°C for 4 h) by measuring the DTG versus temperature trace at ramp rates of 0.5, 2.0, 5.0, 20.0 and 30.0°C/min.

For 1st order desorption, T_M shifts upwards as β is increased. The activation energy will be obtained the slope of a plot of $2\ln T_M - \ln\beta$ versus $1/T_M$ while the pre-exponential factor will be obtained from the intercept, as shown in equation [3.1]. Although in real systems the presence of surface heterogeneity, large surface area and microporosity on catalyst surfaces, will cause deviations from ideal behaviour, each TPD peak represents a group of sites whose energy distribution is continuous in a finite range (Jacobs, 1984).

6.2 Mathematical Formulation

The Arrhenius parameters for desorption were determined using the methodology described by Redhead (1962), and Cvetanovic and Amenomiya (1972). For first order desorption, the peak maximum is dependent only upon the ramp rate. By varying the ramp rate over a sufficiently wide range of about two orders of magnitude (Redhead, 1962), the Arrhenius A-factors and activation energy may be accurately determined. The equations for determining these parameters are derived from the Arrhenius equation for the rate of desorption (k_d) i.e.

$$k_d = -\frac{d\theta}{dt} = A\theta^n \exp(-E_d/RT) \qquad [6.2] \text{ (Redhead,1962)}$$

where θ is the surface coverage, A is frequency factor and E_d is the activation energy. The linear temperature ramp rate,

$$T = T_o + \beta t \qquad [6.3]$$

$$dT = \beta dt \qquad [6.4]$$

where β is the rate of heating in K/s.

From equation [6.2] and [6.4],

$$-\frac{d\theta}{dT} = \frac{A}{\beta}\theta^n \exp(-E_d/RT) \qquad [6.5]$$

$$-\frac{d^2\theta}{dT^2} = \frac{Ad\theta^n}{\beta dT}\exp(-E_d/RT) - \frac{A}{\beta}\frac{E_d}{RT^2}\theta^n \exp(-E_d/RT) \qquad [6.6]$$

if $n = 1$

$$-\frac{d^2\theta}{dT^2} = (\frac{A}{\beta})^2 \theta(\exp(-E_d/RT))^2 - \frac{A}{\beta}\frac{E_d}{RT^2}\theta \exp(-E_d/RT) \qquad [6.7]$$

At maximum rate $\frac{d^2\theta}{dT^2} = 0$

i.e. $$\frac{A}{\beta} \exp(-E_d/RT_M) = E_d/RT^2 \qquad [6.8]$$

$$2\ln T_M - \ln\beta = E_d/RT_M + \ln(E_d/AR) \qquad [6.9]$$

Hencee a plot of $2\ln T_M - \ln\beta$ versus $1/T_M$ will be linear with slope E_d/R and intercept $\ln(E_d/AR)$.

6.3 Experimental and Results

6.3.1 Activation Energy and Arrhenius parameters of phenol desorbed from MgO

The TPD (at a ramp rate of 5°C/min) of the phenol T_M at 280°C (site S_I) observed for MgO calcined at 600°C, and the TPD peak at 308°C (site S_{III}) observed for MgO calcined at 800°C were examined to gain further details about the activation energy and the Arrhenius parameter of the desorption of phenol from the MgO surface. These desorptions were found to be independent of surface coverage and hence were first order processes. At a low coverage of phenol of (60-70%) obtained by adsorbing phenol at about 200°C, purging and then cooling to room temperature before the TPD process, these peaks displayed similar T_M's to those obtained by adsorbing phenol at room temperature which gives 100 % coverage.

By varying the ramp rate of the TPD process the T_M's of these peaks shifted as is shown in Figure 6.1 and Table 6.1.

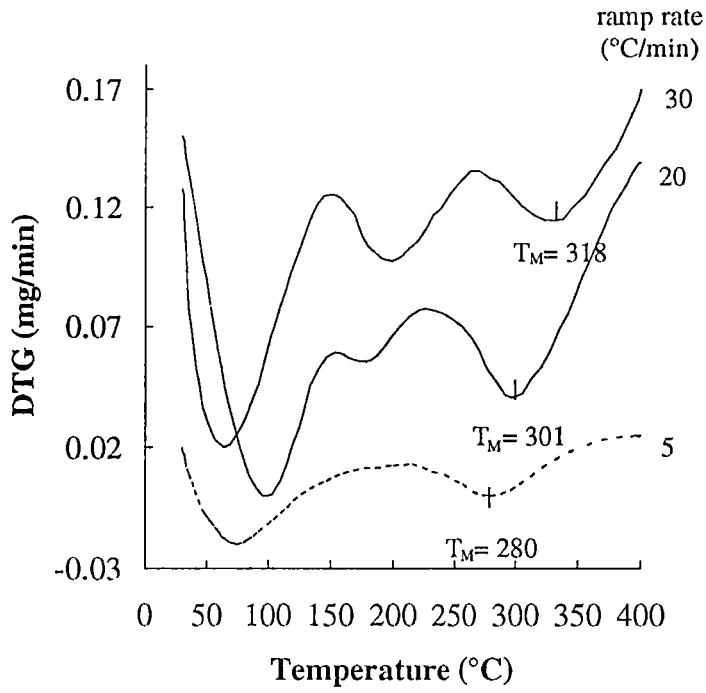

Figure 6.1 The DTG of phenol on MgO (20.1, 20.5 and 19.5 mg) obtained from $Mg(OH)_2$ calcined at 600°C for 4 h, at different ramp rates (30, 20 and 5 °C/min).

Table 6.1 The variation of the T_M's of sites S_I and S_{III} as a function of the temperature ramp rate.

site S_I on MgO calcined at 600°C		site S_{III} on MgO calcined at 800°C	
β (°C/min)	T_M (°C)	β (°C/min)	T_M (°C)
0.5	250 ± 5		
2.0	264 ± 3	2.0	293 ± 7
5.0	280 ± 3	5.0	308 ± 3
20.0	301 ± 5	20.0	329 ± 6
30.0	318 ± 5	30.0	340 ± 6

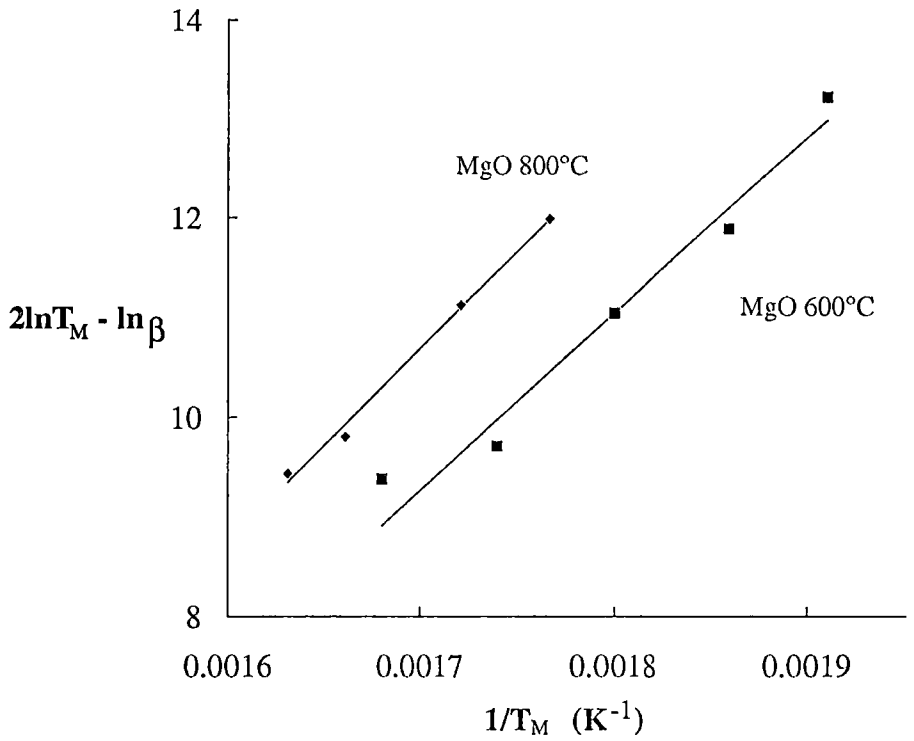

Figure 6.2 The linear relationship between $2\ln T_M - \ln\beta$ and $1/T_M$ of site S_I on MgO calcined at 600°C, and site S_{III} on MgO calcined at 800°C.

The slope (E_d/R) and the intercept ($\ln(E_d/AR)$) of the linear relation for site S_I, assumed to exist on MgO calcined at 600°C (and 400°C), are $1.8 \pm 0.1 \times 10^4$ K and -21 ± 2 respectively. Consequently, the activation energy for the desorption of phenol on MgO at this site is 147 ± 10 kJ/mol and the pre-exponential factor (Arrhenius parameter) is $1.9 \pm 0.3 \times 10^{13}$ s^{-1}. According to Redhead (1962), the activation energy of the other TPD peaks (site S_{II} and site S_{III}) can be estimated by substituting the pre-exponential factor obtained from site S_I into the following relation:

$$E_d/RT_M = \ln(AT_M/\beta) - 3.64 \qquad [6.10] \text{ (Redhead, 1962).}$$

The activation energies for the desorption of phenol on site S_{II} and site S_{III} are 118 ± 10 kJ/mol and 153 ± 12 kJ/mol, calculated using the ramp rate of 5°C/min where the T_M's are 180°C and 308°C respectively.

The activation energy of site S_{III}, observed for MgO calcined at high temperatures, was also estimated using the linear relationship displayed in Figure 6.2, and is 161 ± 9 kJ/mol (derived from a slope of 1.9 ± 0.1 x 10^4 K). The pre-exponential factor found for the desorption from this site is 8.1 ± 0.2 x 10^{13} s^{-1}, derived from the intercept value of -22 ± 2. The activation energy and pre-exponential factor values obtained here are comparable to the values obtained using the Redhead relation [6.10]. It was therefore assumed that the activation energy of site S_{II} could be estimated by the Redhead equation using the pre-exponential factor obtained from the TPD peaks of site S_I or site S_{III}. If the pre-exponential factor obtained from the TPD peak of site S_{III} is used, the activation energy for the desorption of phenol on site S_{II} is 124 ± 10 kJ/mol which is comparable to the value obtained from the TPD peak of site S_I, 118 ± 10 kJ/mol.

In determining the pre-exponential factor for both monoatomic and polyatomic molecules it is assumed that the dynamics of desorption involve the breaking of a single bond between the adsorbed species and the surface. This is analogous to simple bond-fission reactions in homogeneous gas-phase reactions where the pre-exponential factor is generally of the order 10^{15}-10^{18} s^{-1} (Benson, 1976a). According to Ibach et al.(1980), pre-exponential factors of the order of 10^{13} s^{-1} applied only to the desorption of a single atom out of a one dimensional potential where the pre-exponential is kT/h = 6 x 10^{12} T/300 K s^{-1}. For polyatomic molecules the pre-exponential factor is significantly larger (e.g. 10^{15}-10^{16} s^{-1}) because the rotational and vibrational degrees of freedom of the adsorbed molecules are also taken into account (Seebauer et al., 1988).

In this work the pre-exponential factor for phenol desorbed from MgO was of the order of 10^{13} s^{-1}. Continuing the analogy with homogeneous gas-phase reactions, this value corresponds to the pre-exponential factor of cyclic transition states (Benson, 1976b). In terms of transition state theory the magnitude of this value applies to those cases where there is negligible change in entropy when going from reactants to the transition state. This would suggest that the dynamics of phenol desorption may also pass through a cyclic transition state. The most obvious is the four-centre transition state (Figure 6.3) where the phenolate moiety of phenol is adsorbed directly onto a magnesium atom while an adjacent oxygen atom on the MgO substrate has chemisorbed hydrogen. The result is that the transition state consists of the following four atoms: an oxygen and acidic hydrogen from phenol, a magnesium and adjacent oxygen from the substrate.

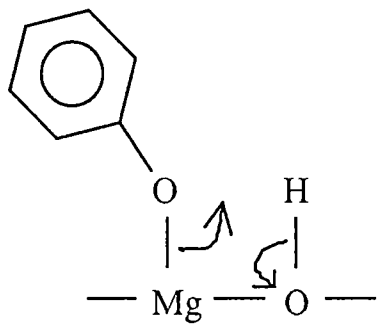

Figure 6.3 The proposed mechanism of the desorption of phenol from MgO.

A number of studies (Redhead, 1962; Cvetanovic and Amenomiya, 1972) have assumed that the pre-exponential factor for the desorption of adsorbate molecules from the surface is about 10^{13} s^{-1}. Soler and Garcia (1983) also noted that there are physical reasons to assign pre-exponential values of about 10^{13}-10^{15} s^{-1}, and it is preferable to accept an uncertainly of two orders magnitude in the pre-exponential factor because this only introduces an error of about 15 % in the activation energy. It

is therefore assumed that the pre-exponential factors and the activation energies of the desorption of phenol from the surface of MgO obtained in the present work are acceptable.

6.3.2 Reactivity comparison of phenol, water, methanol and methane adsorbed on MgO calcined from $Mg(OH)_2$ at 600°C for 4 h

To determine the activation energy of water, methanol and methane desorbed from MgO, the TPD profiles of these desorption studies were displayed again in Figure 6.4.

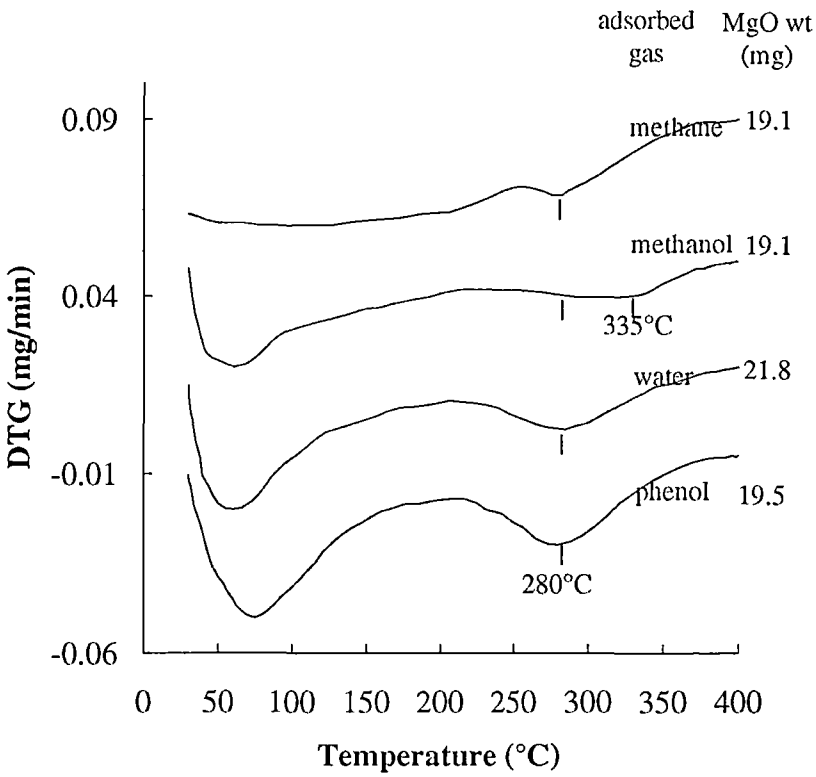

Figure 6.4 TPD-DTG profiles of phenol, water, methane and methanol on MgO.

From Figure 6.4 it can be seen that water, methanol, methane and phenol have the same T_M at 280°C which indicates that these gases have the same activation energy of desorption. As a result of the similar activation energies for the desorption of phenol, water and methane, it is likely that this activation energy corresponds to bond breaking between O^{2-} of the MgO surface and H^+ of the adsorbed species. As mentioned earlier the bond strength between Mg^{2+} (of surface) and anions (of adsorbed species) is assumed to be less than the bond strength between O^{2-} (of surface) and H^+ (of adsorbed species) because surface O^{2-} is a strong basic site while surface Mg^{2+} is a weak acidic site (Tanabe, 1989). Therefore, the anions of the adsorbed species are removed from the Mg^{2+} sites and migrate to form bonds with hydrogen from simultaneous O-H bond breaking. In short it is proposed that water, methanol and methane have the same desorption mechanism as phenol (Figure 6.3).

From the TPD of methanol (Figure 6.4) which showed a broad T_M between 280°C and 335°C, the T_M at 280°C should represent the same mechanism as the other adsorbed gases, while the higher T_M implies a different mechanism of desorption. It is possible that this higher activation energy belongs to bond breaking between O and C of a methoxy group rather than the breaking of bond between O of the methoxy group and Mg on the surface as shown in Figure 6.5. Further explanations were not sought regarding the adsorption of methanol on MgO because phenol was chosen as the probe molecule in the present work for more complete investigation.

(a) (b)

Figure 6.5 The mechanisms of methanol desorbed from MgO surface.

The TPD-DSC of phenol, water, methanol and methane desorbed from MgO were also carried out to determine the heat of desorption of these adsorbed gases. Details of the experiments were described in section 3.3.7. It was found that the desorption of phenol, water, methanol and methane are all endothermic reactions and displayed similar TPD profiles as obtained by the TG technique. The heat of desorption peak at 280°C of phenol, methanol, water and methane from MgO calcined at 600°C were found to be 80 kJ/mol, 42 kJ/mol, 33 kJ/mol and 16 kJ/mol respectively. From the activation energy coupled with the heat of desorption obtained, the kinetic barriers for the desorption/adsorption of the four probe species are displayed in Figure 6.6.

In Figure 6.6 it can be seen that the energy barriers for the desorption of phenol, water and methane are similar, however, the enthalpy change for these desorptions are different. Phenol has the highest enthalpy change, followed by water and methane respectively. As a result the energy barriers for the adsorption of these gases are in the order of phenol (67 kJ/mol) < water (114 kJ/mol) < methane (131 kJ/mol). For methanol, which has the highest activation energy, the energy barrier for adsorption is 111 kJ/mol. From the energy barriers for the adsorption of these gases it can be concluded that phenol is more acidic than methanol which is slightly more acidic than water while methane is less acidic than the others. Such results correspond to that reported by Streitwieser and Heathcock (1981a and b).

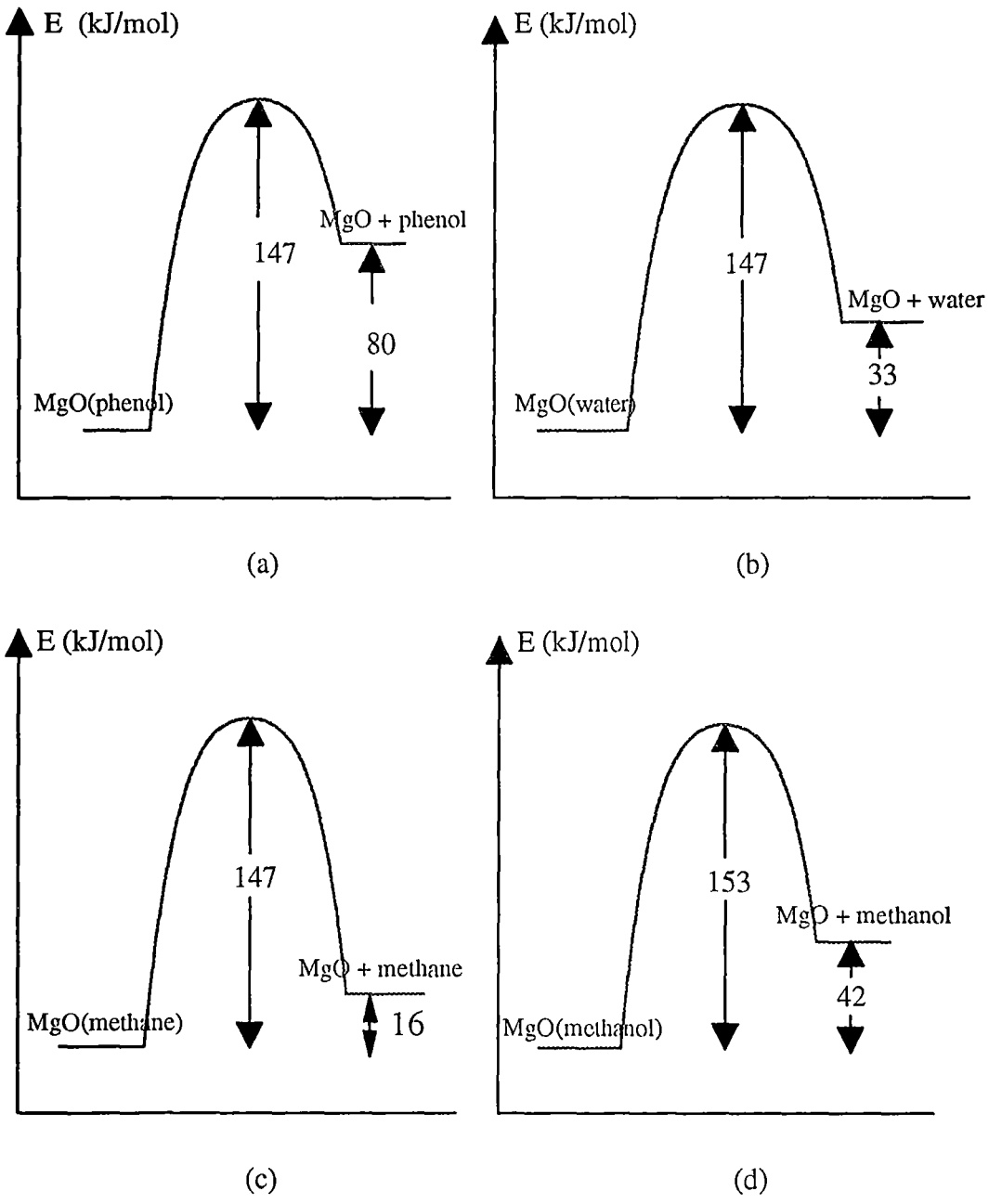

Figure 6.6 Potential energy diagram for the desorption/adsorption of (a) phenol, (b) water, (c) methane and (d) methanol on MgO (calcined from $Mg(OH)_2$ at 600°C 4h).

References

Benson, S. W. (1976a), Thermochemical Kinetics, 2nd, John Wiley & Sons, New York, pp 90-100.

Benson, S. W. (1976b), Thermochemical Kinetics, 2nd, John Wiley & Sons, New York, pp 108-117.

Cvetanovic, R. J. and Amenomiya, Y. (1972) in "Catalysis Reviews", ed Heinemann, H. and Carberry, J. J., **6** (1), p 21, Marcel Dekker, New York.

Ibach, H., Erley, W., and Wagner, H. (1980), Surf. Sci., **92**, 29.

Jacob, P. A. (1984), Characterization of Heterogeneous Catalysts, ed Delannay, F., New York, Marcel Dekker, p 388.

Redhead, P. A. (1962), Vacuum, **12**, 203.

Seebauer, E. G., Kong, A. C. F., and Schmidt, L. D. (1988), Surf. Sci., **193**, 417.

Soler, J. M. and Garcia, N. (1983), Surf. Sci., **124**, 563.

Streitwieser, A. and Heathcock, C. H. (1981a), Introduction to Organic Chemistry, 2nd, Macmillan Publishing Co., Inc., p 238.

Streitwieser, A. and Heathcock, C. H. (1981b), Introduction to Organic Chemistry, 2nd, Macmillan Publishing Co., Inc., p 998.

Tanabe, K. (1989), in " Acid-Base Catalysis", ed Tanabe, K., Hattori, H., Yamaguchi, T., and Tanaka, T., Sapporo, pp 513-527.